**RICE UNIVERSITY**

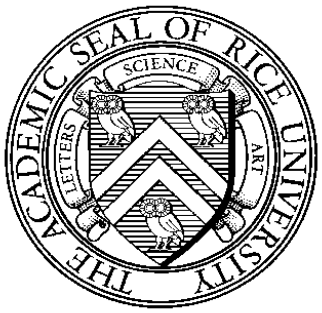


# Alkaline Surfactant Polymer Enhanced Oil Recovery Process

by

**Shunhua Liu**

**DOCTOR OF PHILOSOPHY**

**DECEMBER, 2007**

RICE UNIVERSITY

# Alkaline Surfactant Polymer Enhanced Oil Recovery Process

by

**Shunhua Liu**

A THESIS SUBMITTED
IN PARTIAL FULFILLMENT OF THE
REQUIREMENTS FOR THE DEGREE

**DOCTOR OF PHILOSOPHY**

APPROVED, THESIS COMMITTEE:

_____
Dr. Clarence A. Miller, Louis Calder
Professor of Chemical Engineering, Co-chair

_____
Dr. George J. Hirasaki, A. J. Hartsook
Professor of Chemical Engineering, Co-chair

_____
Dr. Walter G. Chapman, William W. Akers
Professor of Chemical Engineering

_____
Dr. Mason B. Tomson, Professor of Civil and
Environmental Engineering

_____
Maura C. Puerto, Complimentary Visiting
Scholar in Chemical Engineering

HOUSTON, TEXAS

January, 2008

# ABSTRACT


## Alkaline Surfactant Polymer Enhanced Oil Recovery Process

by

Shunhua Liu

This thesis improves the understanding of the Alkaline Surfactant Polymer (ASP) enhanced oil recovery process in order to optimize the ASP operational strategy. The conventional oil recovery methods leave large amounts of oil in the reservoir. ASP process is considered as a promising method for enhanced oil recovery. This dissertation reveals the ASP characteristics by using phase behavior, interfacial tension, surfactant consumption and numerical simulation techniques. The flooding experiments that I performed show that my ASP strategies successfully recover the oil trapped after waterflooding.

The optimal salinity varies when either synthetic surfactant concentration or Water Oil Ratio (WOR) changes in ASP system. In this thesis, these results could be collapsed to a single curve for each synthetic surfactant/crude oil combination in which the optimal salinity depends only on the molar ratio of natural soap to synthetic surfactant, or soap fraction of total soap plus surfactant.

The ASP system studied here has a much wider low IFT region (< 0.01 mN/m) than the system without alkali. In much of the Winsor I region where an oil-in-water microemulsion coexists with excess oil, a second surfactant-containing phase was seen to exist in colloidal form. This colloidal dispersion plays an important role in reaching the ultra-low tension. A new protocol, which significantly reduces the time that is required to

reach equilibrium, is developed to assure that enough of the dispersed material is initially present to achieve low tensions but not so much as to obscure the oil drop during IFT measurements.

Surfactant retention is one of the most significant barriers to the commercial application of ASP. It was found that $Na_2CO_3$ but not NaOH or $Na_2SO_4$, can substantially reduce adsorption of anionic surfactants on carbonate formations, especially at low salinities.

A one-dimensional numerical simulator was developed to model the ASP process. By calculating transport of water, oil, surfactant, soap, salt, alkali and polymer, the simulations show that a gradient in soap-to-surfactant ratio develops with conditions shifting from over-optimum ahead of the displacement front to under-optimum behind the displacement front. This gradient makes the process robust and permits injection at conditions well below optimal salinity of the synthetic surfactant, thereby reducing adsorption and improving compatibility with polymer.

More than 95% of waterflood residual oil was recovered in ASP sand pack experiments at ambient temperature with a slug containing a partially hydrolyzed polyacrylamide polymer and only 0.2 wt% of a particular anionic surfactant blend. The simulator predicts recovery curves in agreement with those found in the flooding experiments.

# ACKNOWLEGEMENTS

I am very grateful as a graduate student at Rice University. I would like to express my sincere appreciation to my two advisors, Professor Clarence A. Miller and Professor George J. Hirasaki for their guidance, inspiration, and assistance. Their wisdom and authoritative knowledge have helped me a lot throughout these years.

I want to give special thanks to Maura C. Puerto for her valuable recommendation, suggestion and help.

I appreciate Professor Mason Tomson and Professor Walter Chapman for serving on my thesis committee.

Many research staffs, graduates and undergraduates have contributed with their experimental work and/or valuable ideas to this thesis. I want to especially thank Leslie Zhang for teaching me phase behavior and IFT experimental skills, Brent Biseda for making a lot of adsorption and IFT measurements, Dick Chronister for repairing old spinning drop machine and other experimental apparatus, Will Knowles for helping me with the BET analysis. I also want to thank to Arjun Kurup, Wei Yan, Busheng Li, Tianmin Jiang, Robert Li, Jie Yu, Nick Parra-Vasque for all their help with the laboratory experiments. Many other students and research staff in Dr. Miller's and Dr. Hirasaki's laboratories have offered me help and their friendships too. I am grateful to this group of people.

I would give many thanks to Dr. Gary Pope and Dr. Mojdeh Delshad, as well as their students at University of Texas at Austin, for those valuable suggestions on DOE

projects. I also thank Dr. Varadarajan Dwarakanath from Chevron, Professor Kishore Mohanty and his student at University of Houston for the discussions.

I acknowledge U.S. DOE and Consortium on Processes in Porous Media at Rice University for the financial support. Thanks to Stepan, Kirk Raney from Shell Chemical for providing surfactant chemicals and SNF Company for polymer.

At the end, I would like to thank my family for their support and encouragement.

# TABLE OF CONTENTS

# LIST OF FIGURES

**Number** **Page**

# LIST OF TABLES

**Number** **Page**

*Chapter 1*

# INTRODUCTION

This chapter provides the general background and motivation of this thesis. The summary of the following chapters is also presented.

## 1.1 General background and motivation

In the near future, there is no economical, abundant substitute for crude oil in the economies of the world. Maintaining the supply to propel these economies requires both developing additional crude oil reserves and improving oil recovery from the present reservoirs. The oil recovery methods that are commonly used include pressure depletion and waterflooding. Oil production by means of pure pressure depletion may result in an oil recovery less than 20% of original oil in place (OOIP), depending on the initial pressure and the compressibility of the fluids (Green and Willhite, 1998). And on average, water flooding whose purpose, in part, is to maintain reservoir pressure to recover more oil, leaves approximately two thirds of the OOIP as unswept and residual oil in reservoir for further recovery (Wardlaw, 1996). In fractured, oil-wet reservoirs, this number might be higher.

Alkaline surfactant polymer (ASP) process is considered as a potential method for enhanced oil recovery (Nelson et al., 1984). Clark et al. (1988) considered four enhanced recovery methods, conventional waterflooding (40% OOIP), polymer-augmented waterflooding (40% OOIP), an alkaline-polymer waterflooding (40% OOIP) and an

alkaline-surfactant-polymer (ASP) flooding (56% OOIP), for the West Kiehl field in USA. They claimed that the ASP process could extend field life and increase ultimate recovery dramatically. Olsen et al. (1990) performed coreflood experiments by using fresh oil-wet, carbonate, Upper Edwards reservoir core material (Central Texas). Their results indicated that alkaline-surfactant-polymer flooding has a much better post-water-flood recovery than alkaline-polymer flooding and polymer flooding. By using a reservoir simulator (UTCHEM) with detailed chemical mechanism modeled, Delshad et al. (1998) predicted oil recovery of the Karamay field, an onshore oil field in China. Among water, alkaline, surfactant-polymer, and alkaline-surfactant-polymer flooding, alkaline-surfactant-polymer flooding provided the best recovery result with 24% of OOIP incremental oil recovery over waterflooding.

The field performance of the alkali surfactant process in the United States has been demonstrated by field tests performed by Shell (Falls et al., 1992) and Surtek (Wyatt et al., 1995). Operators of a Surtek project in Wyoming have reported very low incremental costs of $1.60 to $3.50 per bbl of incremental oil produced.

In recent years, research on alkaline surfactant polymer flooding has attracted more interest (Hirasaki, 2002; Xie, 2004; Seethepalli, 2004). However, alkaline surfactant process is not a simple combination of alkali process and surfactant process. The mechanisms of ASP are not fully understood so that it is difficult to optimize an ASP operational strategy. The goals of this thesis are

(1) Find out the controlling factor for the optimum conditions of alkaline surfactant system by phase behavior and interfacial tension experiments.

(2) Develop and improve the experimental techniques for alkali surfactant systems.

(3) Understand the characteristics of ASP flooding process.

(4) Optimize ASP process.

(5) Confirm the ASP flooding design by 1-D flooding experiments.

## 1.2 Summary of chapters

This thesis is organized into eight chapters, including this introduction chapter.

Chapter 2 describes the extensive background on this thesis. The EOR process and some chemical recovery mechanisms are reviewed, especially for the alkaline surfactant polymer system. The technical information related to ASP process, such as the transport in porous media, phase behavior, is also introduced.

Chapter 3 presents results on phase behavior for alkali surfactant system. The soap to surfactant ratio is introduced to correlate the optimum salinity, water oil ratio and surfactant concentrations. This relation is shown to be very important for understanding the characteristics of alkali surfactant systems.

Chapter 4 investigates the interfacial tension (IFT) properties for brine crude oil system with or without alkaline surfactant. It shows the contamination test should be done for crude oil before further studies. An IFT measurement protocol for alkali surfactant system is developed. Experimental studies show that Huh's correlation can be used to predict IFT by phase behavior tests.

Chapter 5 provides results on the chemical consumption of alkaline surfactant process. The adsorption of anionic surfactants on carbonate media is extensively studied

with both static and dynamic experiments. Nonionic and anionic surfactant adsorption on silica sand is also shown in this chapter. Alkali consumption by gypsum is discussed at the end of this chapter.

Chapter 6 discusses the characteristics of alkali surfactant polymer process by using a one-dimensional ASP simulator developed during this work, which includes the experimental results from previous chapters. The optimized operational area for ASP process is introduced based on this study.

Chapter 7 shows the ASP flooding results with the formulation designed with experimental and simulation results in previous chapters. Good recovery is achieved with the optimized design.

Chapter 8 is devoted to the conclusions of this thesis and recommendations for future research work.

*Chapter* 2

# Concepts and Techniques on Alkaline-Surfactant-Polymer Process

This chapter provides the concepts and techniques background and reviews the previous work related to alkaline-surfactant-polymer process. It begins with general information on enhanced oil recovery (EOR), concepts in alkaline-surfactant-polymer (ASP) process and EOR mechanisms. The general properties and phase behaviors of alkali, surfactant, polymer and oil, which are very important to evaluate an ASP process, are also discussed. Successful numerical simulations, which can describe the ASP process, will help us understand ASP characteristics. This is at the end of this chapter.

## 2.1 Enhanced Oil Recovery

Enhanced oil recovery (EOR), which is also called tertiary recovery, is the oil recovery by injecting a substance that is not present in the reservoir. There are three main categories of EOR: thermal, gas, and chemical methods. Each main category includes some individual processes (Lake, 1989; Green and Willhite, 1998).

Thermal methods, such as injecting steam, recover the oil by introducing heat into the reservoir. Thermal methods rely on several displacement mechanisms to recover oil. The most important mechanism is the reduction of crude viscosity with increasing

temperature. Thermal recovery continues to be an attractive means of maximizing the value and reserves from heavy oil assets (Greaser 2001). However, the viscosity reduction is less for lighter crude oil. Therefore, thermal methods are not nearly so advantageous for light crudes.

Gas methods, particularly carbon dioxide ($CO_2$), recover the oil mainly by injecting gas into the reservoir. Gas methods sometimes are called solvent methods or miscible process. Currently, gas methods account for most EOR production and are very successful especially for the reservoirs with low permeability, high pressure and lighter oil (Lake, 1989; Green and Willhite, 1998). However, gas methods are unattractive if the reservoir has low pressure or if it is difficult to find gas supply.

Chemical methods include polymer methods, surfactant flooding, foam flooding, alkaline flooding etc. The mechanisms of chemical methods vary, depending on the chemical materials added into the reservoir. The chemical methods may provide one or several effects: interfacial tension (IFT) reduction, wettability alteration, emulsification, and mobility control. Thomas (1999) stated that the technical limitations of chemical flooding methods were insufficient understanding of the mechanisms involved and the lack of scale-up criteria. Furthermore, the process should be cost-effective. ASP process is among the chemical methods. It is considered to be the most promising chemical method in recent years because it is possible to achieve interfacial tension reduction, wettability alteration, and mobility control effectively with the combination of alkali, surfactant and polymer. However, the understanding of ASP characteristics is inadequate so that it is difficult to optimize the ASP strategy.

## 2.2 Concepts on Alkaline-surfactant-polymer Process

To describe the mechanisms of ASP process, some principal concepts are discussed below.

### 2.2.1 Darcy's Law

A porous medium consists of a matrix containing void spaces or pores. Typically many of the pores are interconnected, allowing fluid flow to occur. Soils, rocks, sand, etc., are the examples of porous media. We can macroscopically use the phenomenological Darcy Law, which was originally developed by Henry Darcy (chevalier Henri d'Arcy) in 1856, to describe the flow through a porous medium.

Consider a porous medium of absolute permeability $\vec{\vec{k}}$, into which a fluid with viscosity μ is injected by applying a flow potential Φ across the matrix. The superficial flow rate $\vec{u}$ is given by Darcy's equation:

$$\vec{u} = -\frac{\vec{\vec{k}}}{\mu} \cdot \nabla \Phi \tag{2.1}$$

where the permeability $\vec{\vec{k}}$, a quantity only depending on the geometry of the medium, describes the ability of the fluid to flow through the porous medium.

Φ is the flow potential, which is defined as

$$\Phi = p - g \int_{D_0}^{D} \rho dD \tag{2.2}$$

where $\rho$ is the density of the fluid, g is the acceleration of gravity

*D* is depth with respect to some datum such as the mean sea level.

Darcy's equation can be derived from the Navier-Stokes Equation for the Newtonian fluids by neglecting the inertial terms. For the high Reynolds number flow

where the inertial terms in the Navier-Stokes equation will have significant effect, Darcy's equation needs some correction. For ASP applications, the Darcy's equation is accurate enough because low Reynolds number situations are typically found in petroleum reservoirs.

Darcy's equation is a macroscopic equation originally derived for one phase flow. When it is applied to the multi-phase flow, some problems will arise. The capillary pressure between two different phases will cause some differences in their local pressure gradients. Moreover, the permeability of each phase depends on the local saturation of the fluids. To describe the multi-phase flow correctly, we should incorporate these effects into Darcy's equation as:

$$\vec{u}_w = -\frac{\vec{\vec{k}} k_{rw}(S_w)}{\mu_w} \bullet \nabla \Phi_w \tag{2.3}$$

$$\vec{u}_o = -\frac{\vec{\vec{k}} \cdot k_{ro}(S_o)}{\mu_o} \bullet \nabla \Phi_o \tag{2.4}$$

$$P_c = p_o - p_w \tag{2.5}$$

where $k \cdot k_{ri}$ is the effective permeability of the porous medium to phase *i*, which is the product of the intrinsic permeability k and the relative permeability $k_{ri}$.

The relative permeability $k_{ri}$ is a function of fluid saturation $S_i$, it may be a function of other phases in three phase flow.

$P_c$ is the capillary pressure, which is also a function of saturation.

$S_i$ is the saturation of each phase.

The mobility of each phase $\lambda_i$ is defined as

$$\lambda_i = \frac{k \cdot k_{ri}(S_i)}{\mu_i} \tag{2.6}$$

**Mobility ratio** is defined as the ratio of mobility behind and ahead of a displacing front (Lake, 1989). If a mobility ratio greater than unity, it is called an unfavorable ratio because the invading fluid will tend to bypass the displaced fluid. It is called favorable if less than unity and called unit mobility ratio when equal to unity.

### 2.2.2 Interfacial Tension

**Interfacial tension (IFT)** is a force per unit length parallel to the interface, i.e., perpendicular to the local density or concentration gradient (Miller & Neogi, 1985). It is also defined as the excess free energy per unit area in the thermodynamic approach. Both definitions, energy per unit area and force per unit length, are dimensionally equivalent. The qualitative explanation for the interfacial tension comes from the anisotropic tensile stress in the interfacial region. The interfacial tension can be changed by temperature, salinity etc., and surfactants can produce significant interfacial tension decreases.

Equation 2.7 is the Young-Laplace equation that is the basis of measuring interfacial tension by various techniques such as sessile bubble method, pendant bubble method, or spinning drop method

$$p_A - p_B = -2H\sigma \tag{2.7}$$

where $p_A$ and $p_B$ are two bulk phase pressures, $2H$: the mean curvature of interface,

$\sigma$: Interfacial tension between two fluid phases.

### 2.2.3 Wettability

**Wettability** is the preference of one fluid to spread on or adhere to a solid surface in the presence of other immiscible fluids (Craig, 1971). The wettability of a crude oil-

brine-rock system can have a significant impact on flow during oil recovery, and upon the volume and distribution of the residual oil (Morrow, 1990). Wettability depends on the mineral ingredients of the rock, the composition of the oil and water, the initial water saturation, and the temperature. Wettability can be quantified by measuring the contact angle of oil and water on silica or calcite surface or by measuring the characteristics of core plugs with either an Amott imbibition test or a USBM test. Contact angle tests for wettability are widely used. Figure 2.1 illustrates the force balance for contact angle tests. The equilibrium contact angle is defined by equation (2.8).

$$\sigma_{ow}\cos\theta = \sigma_{os} - \sigma_{ws} \tag{2.8}$$

where $\theta$: equilibrium contact angle.

$\sigma_{ow}$: interfacial tension between oil and water phases,

$\sigma_{ws}$: surface energy between water and substrate,

$\sigma_{os}$: surface energy between phase oil and substrate,

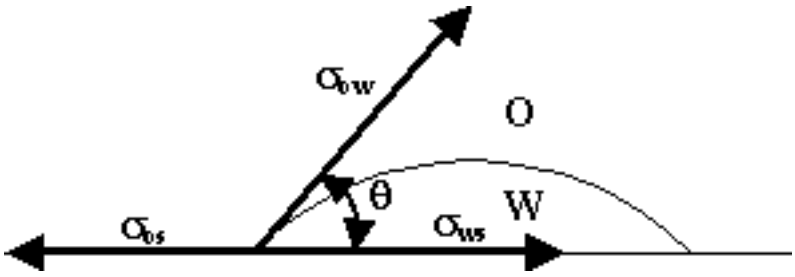


Fig. 2.1 Force balance at three phase contact line

An advancing contact angle is the contact angle measured through water phase when water is the displacing phase. The receding angle is the opposite: it is the contact angle measured through water phase when water is the displaced phase. Wettability of a

rock is usually defined as preferentially water-wet, intermediate-wet, or preferentially oil-wet according to the value of water advancing contact angle (Morrow, 1991).

### 2.2.4 Capillary Pressure

**Capillary pressure** is the most basic rock-fluid characteristic in multiphase flows. It is defined as the difference between the pressures in the non-wetting and wetting phases as the equation (2.9) shows. It is related with the interfacial tension, wettability and the curvature of boundaries between different homogeneous phases. By using the Young-Laplace equation, capillary pressure for a circular tube can be calculated by equation (2.10), assuming a spherical interface:

$$P_c = P_{nw} - P_w \tag{2.9}$$

$$P_c = \frac{2\sigma \cos\theta}{R} \tag{2.10}$$

where $P_c$: capillary pressure,

$P_{nw}$: pressure in the nonwetting phase,

$P_w$: pressure in the wetting phase,

$\sigma$: Interfacial tension between two fluid phases,

$\theta$: Contact angle, measured in wetting phase,

$R$: radius of the tube.

### 2.2.5 Flooding and imbibition

**Flooding** is the technique of increasing oil recovery from a reservoir by injection of water or other liquid, such as alkaline solution, surfactant solution etc., into the

formation to drive the oil to production well. Water flooding is also known as secondary oil recovery. The pressure gradient is the driving force for flooding.

**Imbibition** is a fluid flow process in which the wetting phase saturation increases and the non-wetting phase saturation decreases. It is also defined as the process of increasing wetting phase saturation into a porous media. Spontaneous imbibition refers to imbibition with no external pressure driving the phase into the rock. In a water-wet reservoir, during water-flood, water will spontaneously imbibe into smaller pores to displace oil, but in an oil-wet reservoir, capillary forces inhibit spontaneous imbibition of water.

This thesis focuses on the flooding process. But spontaneous imbibition is still a very useful method when flooding is not effective such as fractured reservoir with low permeability matrix.

## 2.3 Enhanced Oil Recovery Mechanisms

Based on the overall materials balance of the reservoir, the overall oil recovery efficiency can be defined as:

$$E_{ro} = \frac{N_p}{N} = \frac{Amount\ \ of\ \ oil\ \ recovered}{Amount\ \ of\ \ oil\ \ oringinally\ \ in\ \ reservoir} \qquad (2.11)$$

where $N$ is the Original Oil in place,

$N_p$ is the cumulative oil recovered after the recovery process.

The overall efficiency consists of volumetric sweep efficiency $E_{vo}$ and displacement efficiency $E_{do}$ as the equation (2.12) shows.

$$E_{ro} = E_{vo}E_{do} \qquad (2.12)$$

**The volumetric sweep efficiency** $E_{vo}$ is the fraction of the volume swept by the displacing agent to total volume in the reservoir (Lake, 1989). It depends on the selected injection pattern, character and locations of the wells, fractures in the reservoir, position of gas-oil and oil-water contacts, reservoir thickness, heterogeneity, mobility ratio, density difference between the displacing and the displaced fluid, and flow rate etc. Usually, sweep efficiency can be decomposed as the product of areal sweep efficiency and vertical sweep efficiency. Areal sweep efficiency represents the fraction of total formation area swept by the injected displacing agent; vertical sweep efficiency denotes the fraction of the total formation volume in the vertical plane swept by the injected displacing agent. Poor sweep will significantly reduce the total recovery efficiency and increase recovery costs by increasing the volume of displacing agent required. Sweep efficiency can be greatly improved with mobility control methods, such as polymers, foams and WAG process (alternate water and gas injection). The polymer in ASP process could significantly increase the sweep efficiency.

**The displacement efficiency** $E_{do}$ is the ratio of the amount of oil recovered to the oil initially present in the swept volume. It can be expressed in terms of saturation as the equation (2.13).

$$E_{do} = \frac{S_{oi} - S_{or}}{S_{oi}} \tag{2.13}$$

where $S_{oi}$ is the initial oil saturation,

$S_{or}$ is the residual oil saturation after oil recovery process.

The displacement efficiency is a function of time, liquid viscosities, relative permeabilities, interfacial tensions, wettabilities and capillary pressures. Even if all the oil were contacted with injected water during waterflooding, some oil would still remain in

the reservoir. This is due to the trapping of oil droplets by capillary forces due to the high interfacial tension (IFT) between water and oil. The capillary number $N_{vc}$ is a dimensionless ratio of viscous to local capillary forces, often defined as in (2.14). The viscous force will help oil mobilization, while the capillary forces favor oil trapping (Lake, 1989).

$$N_{vc} = \frac{v\mu}{\sigma} \tag{2.14}$$

where $v$ is velocity,

$\mu$ is viscosity

$\sigma$ is interfacial tension.

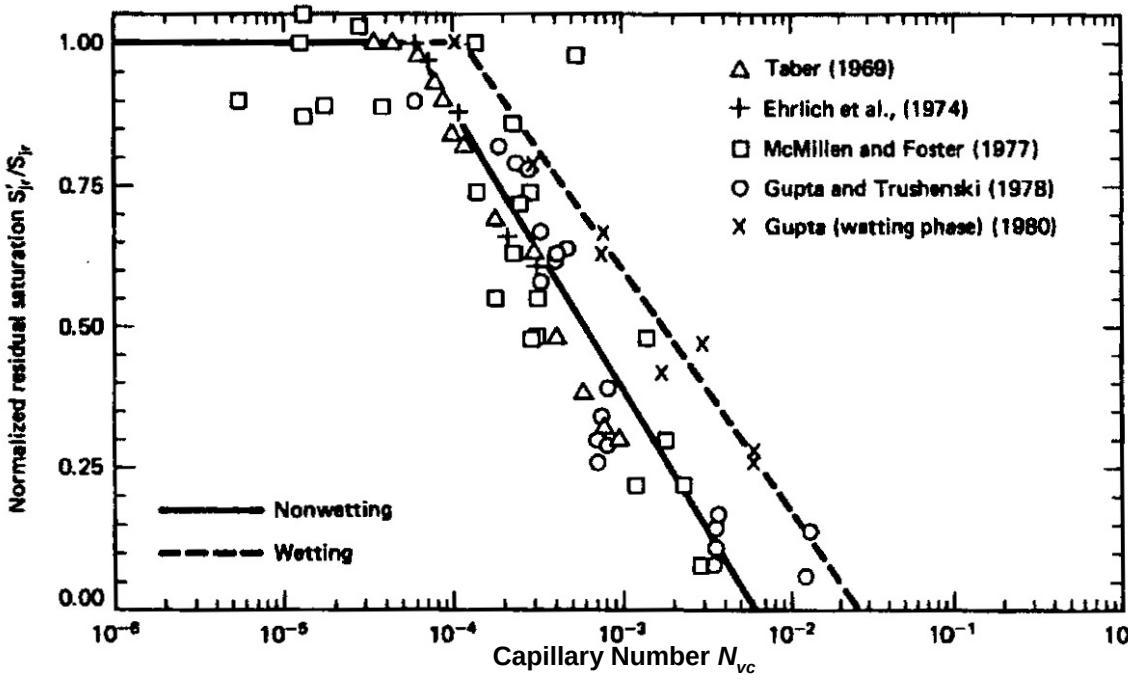


**Figure 2.2 Capillary Desaturation Curves for Sandstone Cores (Delshad, 1986, Lake, 1989)**

Figure 2.2 shows capillary desaturation curves (CDC) that plot residual saturation of oil versus a capillary number on a logarithmic x-axis (Delshad, 1986, Lake, 1989). From figure 2.2, increasing capillary number reduces the residual oil saturation. The

residual oil saturations for both nonwetting and wetting cases are roughly constant at low capillary numbers. Above a certain capillary number, the residual saturation begins to decease. This phenomenon indicates that large capillary number is beneficial to high displacement efficiency because the residual oil fraction becomes smaller. Capillary number must be on the order of $10^{-3}$ in order to reduce the residual oil saturation to near zero. Since it is difficult to increase the fluid viscosity or flow rate by several magnitudes, the most logical way to increase the capillary number is to reduce the IFT. Injection flow rates into a reservoir are often on the order of 1 ft/day and water's viscosity is around 1 cp. Therefore, the IFT should be below $10^{-2}$ mN/m so that capillary number is around $10^{-3}$. The principal objective of the ASP process is to lower the interfacial tension so that the displacement efficiency will be improved. The capillary desaturation curve in figure 2.2 will be used in the simulation in this thesis

If the driving force is gravity force or centrifugal force, Bond number, which is defined as in (2.15.a), is used (Hirasaki et al, 1990). Similar to capillary number, larger Bond number will be beneficial to high oil recovery.

$$N_{Bo} = \frac{kg\Delta\rho}{\sigma}$$

(2.15.a)

where $k$ is permeability

$g$ is the gravity acceleration or centrifuging acceleration

$\Delta\rho$ is the density difference between oleic and aqueous phases

Pope et al. (2000) proposed a trapping number, which essentially combines the effects of capillary number and Bond number. The definition of trapping number is shown in equation 2.15.b.

$$N_T = \frac{\overline{\overline{K}} \cdot (\bar{g}\Delta\rho + \nabla P)}{\sigma}$$

(2.15.b)

where $N_T$ is the trapping number

## 2.4 Alkali Enhanced Oil Recovery

An alkali is a base which produces hydroxide ions ($OH^-$) when dissolved in water or alcohol. The alkali compounds that have been considered for oil recovery can generate high pH and include sodium hydroxide, sodium carbonate, sodium silicate, sodium phosphate, ammonium hydroxide etc.

Oil recovery mechanisms in alkali flooding are complicated and there is a divergence of opinion on the governing principles. There are at least eight postulated recovery mechanisms (deZabala et al., 1982, Ramakrishnan and Wasan, 1983). These include emulsification with entrainment, emulsification with entrapment, emulsification with coalescence, wettability reversal, wettability gradients, oil-phase swelling, disruption of rigid films, and low interfacial tensions. The existence of different mechanisms should be attributed to the chemical character of the crude oil and the reservoir rock. Different crude oils in different reservoir rock can lead to widely disparate behavior when they contact alkali under dissimilar environments such as temperature, salinity, hardness concentration, and pH. However, all the researchers agree on the fact the acidic components in the crude oil are the most important factor for alkali flooding.

The alkali technique can be distinguished from other recovery methods on the basis that the chemicals promoting oil recovery are generated in situ by saponification.

The acid number of a crude oil, which is one of the most important quantities in the alkali flooding, characterizes the amount of natural soap that can be generated by the addition of alkali. **Acid number** is defined as the milligrams of potassium hydroxide (KOH) that is required to neutralize one gram of crude oil (deZabala, 1983). It has long been recognized that carboxylic acids are constituents of most crude oil. Seifert and Howell (1969) isolated numerous aromatic carboxylic acids from the California Midway Sunset crude oil. Farmanian et al (1979) found similar results for other California crudes and suggested that phenolics and porphyrins might act as co-surfactants.

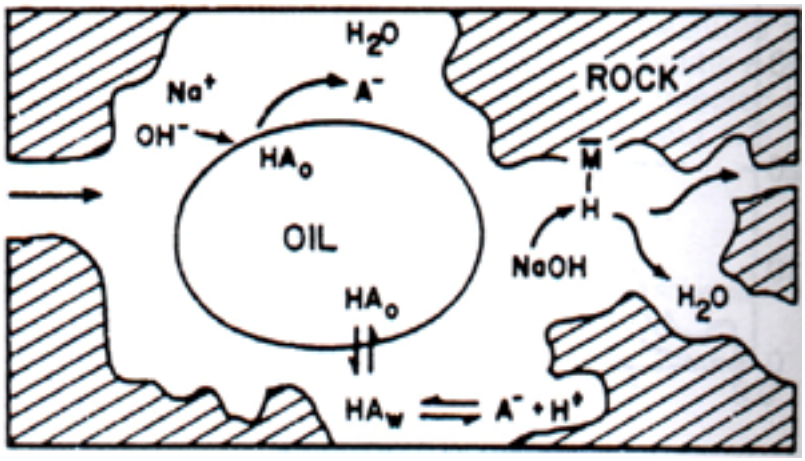


**Figure 2.3 Schematic of alkali recovery process (deZabala, 1982)**

Several investigators have proposed chemical models for the alkali-oil-rock chemistry. Figure 2.3 demonstrates one model by deZabala (deZabala, 1982). In this figure, $HA_o$ denotes the acid in oil phase, and $HA_w$ the acid in aqueous phase. Some experimental results (Ramakrishnan and Wasan, 1983; Borwankar et al., 1985) supported this alkali-oil chemistry model. The deficiency of hydrogen ions, which are consumed by

the hydroxyl ions in the aqueous phase, will promote the generation of the soap ($A_w^-$), which is an anionic surfactant other than synthetic surfactant.

The generated $A_w^-$ ions will adsorb at oil-water interfaces and can lower interfacial tension. Jennings et al (1974) investigated the IFT of a large number of crude oil samples with NaOH solutions of different concentration by using the pendant drop method at ambient temperature. They reported that despite a few oil samples which changed only a little in IFT, many samples showed a very low IFT at only one alkali concentration, while others displayed very low IFT over a broad range of alkali concentrations. Cooke et al. (1974) also found the addition of alkali could lower interfacial tension between oil and water. For many systems with low interfacial tension, IFT value was observed to be smaller than 0.001mN/m. Ramakrishnan and Wasan (1983) found that the IFT between oil and water are sensitive to both NaOH concentration and salinity, and the minimum IFT can be obtained in the concentration range of 0.01-0.1wt% NaOH. Qutubuddin et al. (1984) also found that the ultra-low interfacial tensions were observed with a suitable NaOH concentration which includes the high pH and electrolyte strength. The coexistence of soap and synthetic surfactant (Nelson, 1984) is the key factor of alkaline-surfactant process characteristics, which will be described in detail in this thesis.

Wettability also plays an important role in oil recovery. Wettability reversal will produce fluid redistribution in the pore space, which may be very beneficial for oil recovery (Morrow, 1990). In the original wetting state of the medium, the nonwetting phase occupies large pores, and the wetting phase occupies the small pores. If the wettability of a medium is reversed, the wettabilty of large pores changes from oil wet to

water wet. The phenomenon that high-pH chemicals can alter the wettability has been known for several decades (Wagner and Leach, 1959, Emery et al., 1970, Ehrlich et al., 1977, Olsen et al., 1990). For the oil-wet carbonate reservoirs, imbibition of water occurs only when the wettability changed from oil-wet to water-wet.

Depending on the rock mineralogy, alkali can interact with reservoir rock in several ways, which include surface exchange and hydrolysis, congruent and incongruent dissolution reactions, and insoluble salt formation by reaction with hardness ions in the fluid and those exchanged from rock surface (Somerton and Radke 1983). Among those alkali-rock (clay) interactions, the reversible sodium/hydrogen-base exchange (equation 2.16) is a very important mechanism of alkali consumption and cannot be neglected, as shown in Figure 2.3.

$$\overline{M}H + Na^{+} + OH^{-} \Leftrightarrow \overline{M}Na + H_2O \qquad (2.16)$$

Where $\overline{M}$ denotes a mineral-base exchange site.

Furthermore, alkali can be used as a material to lower surfactant adsorption in alkaline-surfactant recovery process. This adsorption reduction effect will be demonstrated in Chapter 5.

There are many alkali candidates for enhanced oil recovery, which include sodium hydroxide, sodium orthophosphate, sodium carbonate, and sodium silicate. Cheng (1986) made a comparative evaluation of chemical consumption during the alkaline flooding. The comparisons indicated that sodium carbonate might be a good candidate for the alkali flooding. Because of its buffering effect, sodium carbonate had less consumption and shorter alkali breakthrough times than the other alkalis. And

sodium carbonate is more compatible with carbonate formations. Cheng also found that sodium carbonate has less permeability damage compared to hydroxide and silicate. By comparing the sodium carbonate with sodium hydroxide and sodium silicate, Burk (1987) found that sodium carbonate is much less corrosive for sandstone. Compared to other alkalis, sodium carbonate is the least expensive. Also, sodium carbonate suppresses multivalent ion concentration which causes large surfactant consumptions as shown in 2.5.5. In chapter 5, sodium carbonate is shown to reduce the adsorption of anionic surfactant on calcite and dolomite while sodium hydroxide does not have this surfactant adsorption reduction effect. Sodium carbonate also retards the degradation of some anionic surfactant, e.g. sulfates, by increasing the pH. Therefore, sodium carbonate is a good candidate for the alkali flooding in oil recovery and will be chosen as the alkali in this thesis.

As an anionic surfactant, the soap has its own optimum salinity which is usually different from the reservoir salinity. Synthetic surfactant is needed to adjust the optimum salinity. Nelson et al. (1984) first introduced this idea and named it as “Co-Surfactant Enhanced Alkaline Flooding”. In recent years, the combination of alkali and synthetic surfactant is usually called alkaline-surfactant process and almost all alkali processes are now associated with surfactant.

## 2.5 Surfactant Enhanced Oil Recovery

Surface active agents, usually called as surfactants, have at least one hydrophilic and at least one hydrophobic group in the same molecule. Because of this character that can significantly lower the interfacial tensions and alter wetting properties, surfactants are

considered as good enhanced oil recovery agents since 1970s (Healy and Reed, 1974). The cost of surfactant is the major limiting factor and precluded use of surfactant processes when the crude oil price was under $20 per barrel until recent years. Lowering the surfactant consumption is very important for a successful surfactant process.

### 2.5.1 Surfactants

Surfactants are energetically favorable to be located at the interface rather than in the bulk phase (Miller and Neogi, 1985). A surfactant molecule has at least one hydrophilic group and at least one hydrophobic group. The surfactant molecule usually is presented by a “tadpole” symbol. While the hydrophilic portion is usually called head, the hydrophobic portion (usually hydrocarbon chain) is named tail. The hydrophilicity of a surfactant is determined by the structure of the head and tail, e.g. the hydrocarbon chain length, the number of branches in chain etc., and the functional groups, e.g. ethoxylated group or propoxylated group etc. Surfactant molecules prefer to aggregate in solutions to form phases such as micellar solutions, microemulsions, and lyotropic liquid crystals.

According to the charge of the head group, surfactants are categorized into four groups: anionic, cationic, nonionic, and zwitterionic surfactants as Figure 2.4 shows.

Anionic surfactants, which include soap, are negatively charged and the counter ions are usually small cations such as sodium ion, potassium ion, ammonium ion. They are the most used surfactants in the oil recovery process because of their relatively low adsorption in sandstone and clays, stability and relatively cheap price. Anionic surfactant would have high adsorption for carbonate formation as shown in Chapter 5. Zhang et al. (2006) found that sodium carbonate reduces the adsorption of anionic surfactants on

carbonate minerals, so the anionic surfactant consumption will be much less than what is expected without presence of sodium carbonate. Thus, this thesis will focus on anionic surfactant flooding.

Cationic surfactants are positive charged. Because they are highly adsorbed by the anionic surfaces of clays and sand, they are not popular choices for oil recovery in sandstone. However, some research with cationic surfactants has been carried out in recent years for carbonate reservoirs. It will be discussed in Section 2.5.7.

Nonionic surfactants do not form ionic bonds. The ether groups of nonionic surfactants will form hydrogen bonds with water so that nonionic surfactants exhibit surfactant properties. These chemicals derive their polarity from having an oxygen-rich portion of the molecule at one end and a large organic portion at the other end. The oxygen component is usually derived from short polymers of ethylene oxide or propylene oxide. As in water, the oxygen provides a dense electron-rich atom that gives the entire molecule a local negative charge site that makes the whole molecule polar and able to participate in hydrogen bonding with water. In chapter 5, the adsorption of a nonionic surfactant is tested because it may be a good candidate for the $CO_2$ foam oil recovery process.

Amphoteric surfactants may contain both positive and negative charges. These surfactants have not been tested in oil recovery.

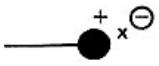

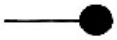

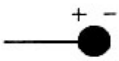

| Anionics | Cationics | Nonionics | Amphoterics |
|---|---|---|---|
| Sulfonates<br>Sulfates<br>Carboxylates<br>Phosphates | Quaternary ammonium organics, pyridinum, imidazolinium, piperidinium, and sulfononium compounds | Alkyl-, Alkyl- aryl-, acyl-, acylamindo-, acyl-aminepolyglycol, and polyol ethers<br>Alkanolamides | Aminocarboxylic acids |

**Figure 2.4 Classification of surfactants and examples (Akstinat, 1981)**

### 2.5.2 Surfactant micelle and microemulsion

At very low concentration, the surfactant molecules in the solution disperse as monomers, so that monomer concentration is equal to surfactant concentration. Due to their surface-active character, the monomers will accumulate and form a monolayer at interface of water and adjacent fluids such as oil or air. The monomers begin to associate among themselves to form micelles when the surfactant concentration increases to a certain value. **Micelle** is an aggregation of molecules which usually consists of 50 or more surfactant molecules. The **Critical Micelle Concentration (CMC)** is defined as the lowest concentration above which monomers cluster to form micelles. Above the CMC, further increasing surfactant concentration will only increase the micelle concentration and not change monomer concentration much. A plot of surfactant monomer concentration versus total surfactant concentration is shown as Figure 2.5. In this plot, the micelles are simplified as spheres. In the actual situation, the structures of the micelles are not static and can take on various forms.

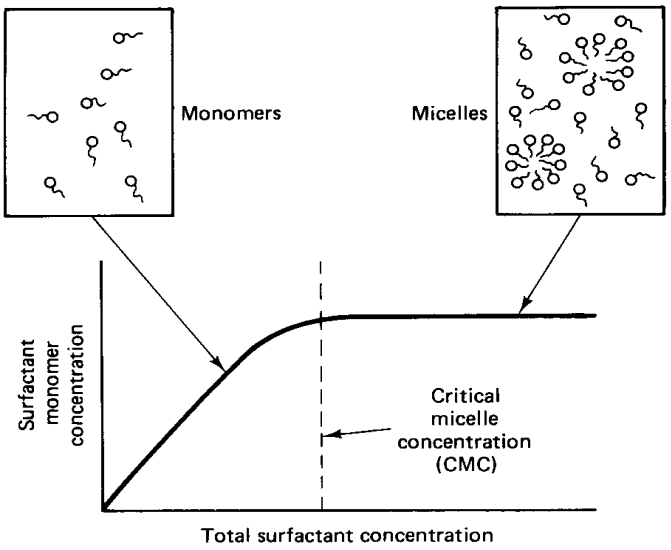


**Fig. 2.5 Schematic definition of the critical micelle concentration (Lake, 1989)**

Critical Micelle Concentration (CMC) is one of the most important quantities for a surfactant solution. The IFT of the aqueous solution of a pure surfactant does not change much beyond the CMC, while it will dramatically decrease with the increase of surfactant concentration below the CMC. As figure 2.6 shows, the sudden change in the slope of the plot is located at CMC. Also it is found that many properties of the bulk solution, e.g., density, solubility, osmotic pressure, electrical resistance, light scattering properties, detergency, etc., will change in the vicinity of CMC. Temperature is also crucial for forming micelle. At very low temperatures, surfactants remain mainly in a crystalline state and are in equilibrium with small amounts of dissolved monomer. CMC can be reached only when the temperature is high enough so that there are enough monomers in the solution. The temperature effect will not be further investigated in this thesis.

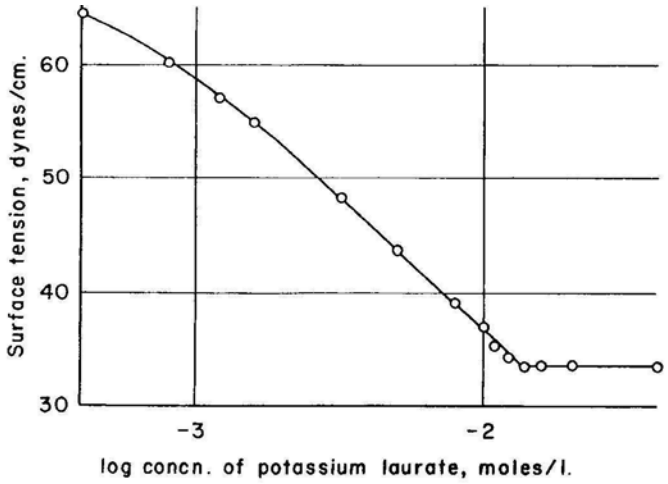


**Figure 2.6 Interfacial Tension as a function of surfactant concentration (Miller and Neogi, 1985)**

If water is the solvent, surfactant solutions with concentrations above CMC can dissolve considerably larger quantities of organic materials than can pure water or surfactant solutions at concentrations below the CMC because the interior of the micelles is capable of solubilizing the organic compounds. Similarly, micelles in a hydrocarbon solvent will solubilize water and enhance the water solubility in the solution significantly. When there is a large amount of solubilized materials, which may be either oil-in-water or water-in-oil, the solution is frequently called a microemulsion. A **microemulsion** is a thermodynamically stable dispersion of oil and water, which contains substantial amounts of both and which is stabilized by surfactant. Microemulsions are typically clear solutions, as the droplet diameter is approximately 100 nanometers or less. The interfacial tension between the microemulsion and excess phase can be extremely low. The final microemulsion state will not depend on order of mixing, and energy input only determines the time it will take to reach the equilibrium state. Figure 2.7 shows schematic diagrams of microemulsions.

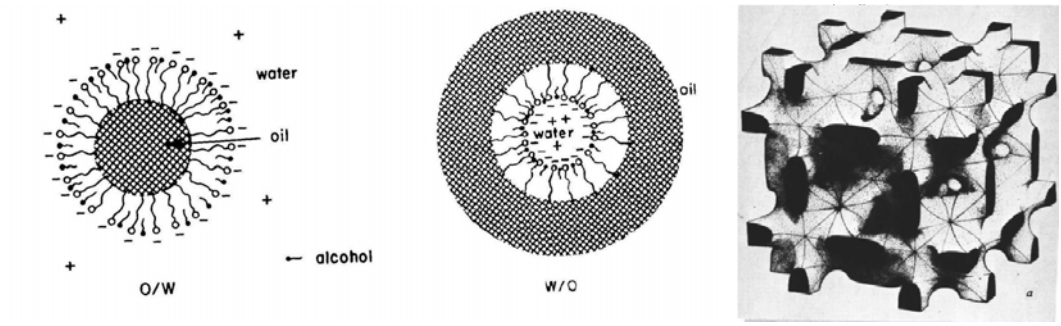


**(a)** **(b)** **(c)**

**Figure 2.7 schematic plots of microemulsions**

**(a) oil-in-water (o/w) microemulsions (Miller and Neogi, 1985)**

**(b) water-in-oil (w/o) microemulsions (Miller and Neogi, 1985)**

**(c) bicontinuous microemulsions (Scriven, 1976)**

**Macroemulsions**, sometimes just called emulsions, are thermodynamically unstable to microemulsions. The suspended droplets will eventually agglomerate and/or coalesce, and the dispersed phase will separate. Macroemulsion droplet sizes are typically much larger, one micron or more, resulting in a cloudy or milky dispersion. The nature of a macroemulsion may depend on the order of mixing of the ingredients and the amount of energy put into the mixing process.

### 2.5.3 Phase Behavior of Microemulsions

The phase behavior of microemulsions is very important to enhanced oil recovery because it can be used as an indicator of ultra-low interfacial tension. Phase behavior screening helps to quickly evaluate favorable surfactant formulations. Winsor (1954) first described the phase behavior of microemulsions for surfactant, oil and brine system. The phase behavior of a microemulsion system is a function of types and concentration of surfactants, cosurfactants, oil, brine, alcohol, temperature, etc. In a particular

microemulsion system containing an ionic surfactant, the concentration of the electrolyte, or the salinity, will be an important impact factor on phase behavior.

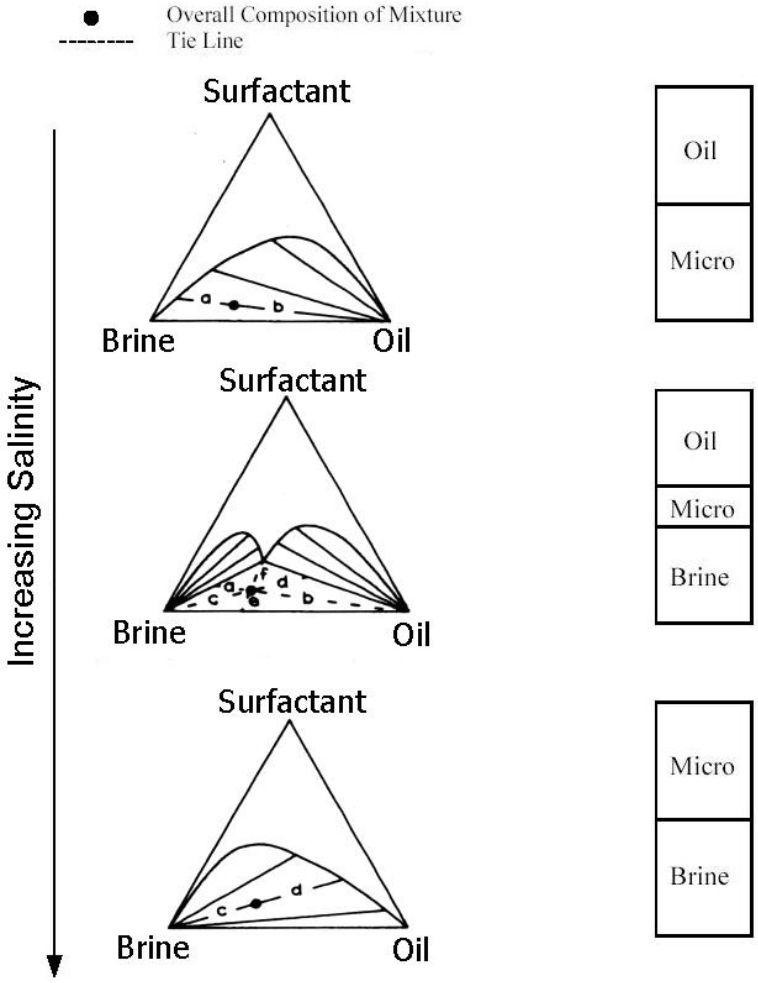


**Figure 2.8 Microemulsion ternary phase diagram for different salinity (Adapted from Healy et al, 1976)**

Ternary phase diagrams, a convenient tool for describing the microemulsion phase behavior (Healy, et al., 1976; Nelson and Pope, 1978), exhibit how salinity changes the phase behavior. With varying salinity, the phase behavior of microemulsions can be divided into three classes, lower-phase microemulsion, upper phase microemulsion and

middle phase microemulsion. Figure 2.8 illustrates the relationship between salinity and phase behavior.

The main mechanism by which salinity affects microemulsion phase behavior with ionic surfactants is the electrostatic forces, for instance those between charged surfactant head groups in surfactant films covering the surfaces of microemulsion drops. These forces will spontaneously change the curvature of the drops, which, in turn, determines the type and solubilization capacity of the microemulsions. At low salinities, the microemulsion is an oil-in-water microemulsion that coexists with nearly pure excess oil. Since the density of this kind of microemulsion is larger than the oil, it is below the oil so that this microemulsion is called **"lower phase" microemulsion**. Also, it is named as **Winsor type I**, or **type II(-)** because the slope of the tie lines of lower phase microemulsion is negative. In this microemulsion, the radius of microemulsion drop will become larger and solubilization of oil will be enhanced with increase of salinity, i.e., the repulsion between the charged head groups decreases.

When the salinities are very high, the electrostatic forces from the electrolytes will change the sign of the drop curvature so that the water-in-oil microemulsion forms. It is called an **"upper phase" microemulsion** because the microemulsion is lighter that the water and above the water phase. The upper phase microemulsion is also named **type II (+)** or **Winsor type II**. Opposite to the "lower phase" microemulsion, the drop size and drop radius decrease with increasing salinity.

At intermediate salinities, three phases are present. A microemulsion is formed in equilibrium with both excess oil and brine. This microemulsion, which is called **"middle phase" microemulsion**, contains almost all the surfactants in the system. Similarly,

middle phase microemulsion is also named **type III**, or **Winsor type III**. This type of microemulsion is of great importance in enhanced oil recovery because of its ultra-low interfacial tension that we will mention in the next section. The middle phase structure is complicated and has attracted many researchers. Scriven (1976) postulated that the middle phase has a bicontinuous structures (see, Figure 2.7 (c)). Theoretical models and some experimental observations were made to develop the bicontinuous microemulsion models (Burauer S. et al., 2003). The bicontinuous structure is similar to a consolidated porous medium where both the solid and pore space are continuous, although, of course much smaller. Since both the oleic phase and aqueous phase are continuous, the interfacial tensions between the middle phase and either excess brine or excess oil are very low.

To visualize the microemulsion change, figure 2.9 shows a typical example of how phase behavior changes with salinity.

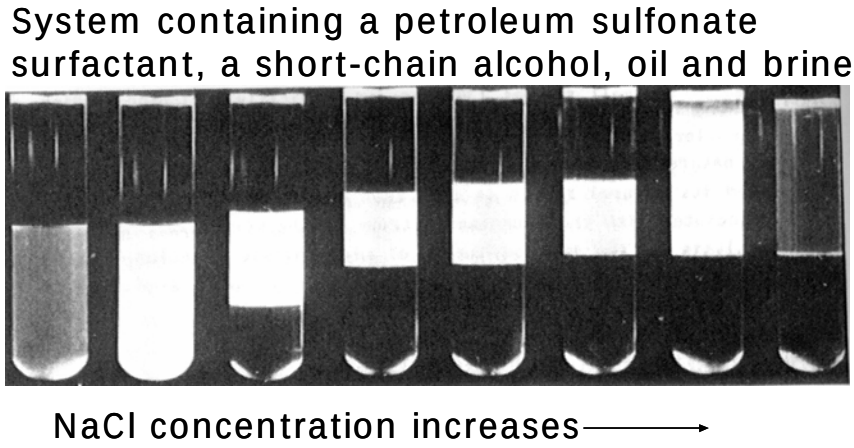


**Figure 2.9 Effect of salinity on microemulsion phase behavior (Miller and Neogi, 1985)**

### 2.5.4 Phase Behavior and Interfacial Tension

Healy and Reed (1974, 1976, and 1977) first developed an empirical correlation between the microemulsion phase behavior and the interfacial tension as figure 2.10 illustrates. Solubilization ratios were introduced to describe the microemulsion phase behavior.

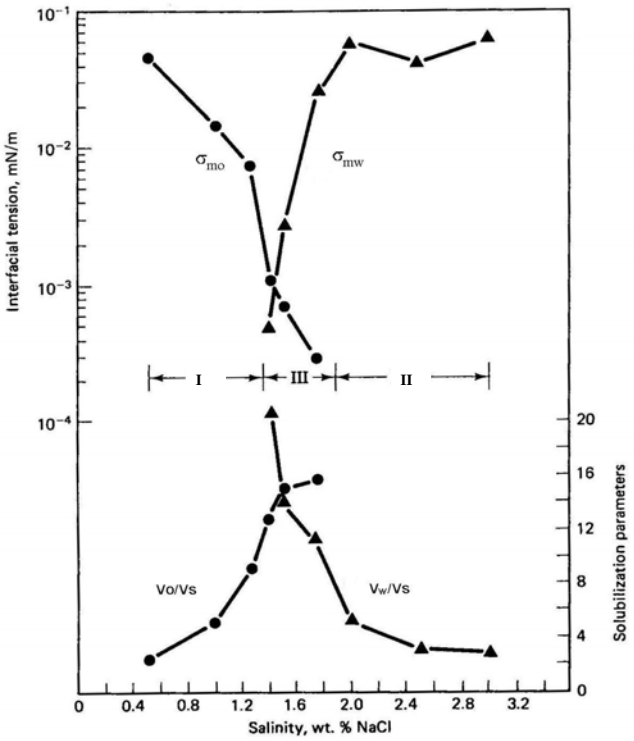


**Figure 2.10 Interfacial tension and solubilization parameter versus salinity (Reed and Healy, 1977)**

Figure 2.10 represents the corresponding behavior of the solubilization parameters and IFT with different salinity. In the upper part this figure, $\sigma_{mo}$ is the IFT between the microemulsion and the excess oil phase, and $\sigma_{mw}$ is the IFT between the microemulsion and water phase. In type I region, $\sigma_{mo}$ is high and $\sigma_{mw}$ does not exist; while in type II region, $\sigma_{mo}$ does not exist and $\sigma_{mw}$ is high. In type III region, $\sigma_{mo}$ and $\sigma_{mw}$ are of the

similar magnitude with very low value. The salinity where the two tensions are equal is called the **optimum salinity**, which is one of the most significant quantities in the surfactant flooding process. As discussed in 2.3, if interfacial tension is small, capillary number will be large enough to let the residual oil saturation goes to zero. This is one of the main mechanisms for enhanced oil recovery with surfactants. Healy and Reed (1977) also confirmed that the optimum salinity was the same as the salinity for maximum oil recovery by core flooding experiments. Clearly, one of the goals of surfactant flooding in enhanced oil recovery is to have the surfactant at the displacement front near optimum conditions.

The solubilization parameter *Vo/Vs* is defined as the volumetric ratio of solubilized oil to surfactant, and *Vw/Vs* is water to surfactant in the microemulsion phase. In the lower part of figure 2.10, *Vo/Vs* increases with salinity, while *Vw/Vs* decreases with salinity. At optimum salinity, the amount of oil and brine solubilized in the surfactant phase are approximately equal. This is also another definition of optimum salinity. Also equal contact angles could be found at the optimum salinity (Reed and Healy, 1984).

Huh (1979) derived a theoretical relationship between solubilization ratio and IFT. Huh's theory predicts that the IFT varies with the inverse square of the solubilization ratio as 2.17. In Huh's equation, C=0.3 is a good approximation for most crude oils and microemulsions. Glinsmann (1979) experimentally validated this relationship. In chapter 4, IFT experimental results substantiate this equation.

$$\sigma = \frac{C}{\left(V_i / V_s\right)^2} \qquad i = \text{water or oil} \qquad (2.17)$$

As shown in chapter 4, the IFT measurement between microemulsion and water and/or crude oil is time consuming and more difficult than the phase behavior observations. Sometimes, it is almost impossible to measure the IFT between some crude oil and its lower phase microemulsion. By using phase behavior observation and measurements of the solubilization ratios, it is much simpler and faster to estimate the IFT of the oil/water/microemulsion system, especially for the surfactant screening. Of course, it is always worth verifying the IFT measurement if a good formulation is identified by phase behavior.

### 2.5.5 Surfactant Retention

To have a successful commercial application of surfactant process, the surfactant retention should be minimized. Surfactants may be retained through these mechanisms: adsorption, precipitation, ion exchange and phase trapping (Green and Willhite, 1998).

#### 2.5.5.1 Surfactant adsorption on mineral surface

Due to the different mineralogy, most solid surfaces, including reservoir rocks, are charged. While silica may be negatively charged, calcite, dolomite and clay may have positive charge on their surfaces at neutral pH. The most important cause of ionic surfactants adsorbing onto a solid is often the electrical interaction between the charged solid surface and surfactant ions, which can be explained by electrical double layer theory (Wesson and Harwell, 2000). Sometimes, surfactant adsorption is presented as the amount of surfactant adsorbed per unit solid weight versus equilibrium surfactant

concentration. It is better to use the amount of surfactant adsorbed per unit of solid surface area to describe the surfactant adsorption. Lake (1989) suggested that the Langmuir-type isotherm of adsorption could describe surfactant adsorption. The surfactant adsorption will not increase when critical micelle concentration (CMC) of the surfactant is reached. The adsorption model of Wesson and Harwell (2000) also supports this Langmuir adsorption except their model is more subtle when the surfactant concentration is less than CMC.

The amount of adsorbed surfactant depends on the surfactant character (the surfactant type, the structure of the chain), the rock properties (surface charge), pH, potential determining ion in solution and salinity. The pH may alter the surface charge to change the adsorption amount; the salinity may change the electrical potential of surface sites for the adsorption. For example, Glover (1978) showed that retention increased linearly with salinity at low salt concentrations and departed from linearity with higher retentions above a critical salinity. Hirasaki and Zhang (2002) found that the potential determining ions ($CO_3^{2-}$) can change the surface charge and reduce the anionic surfactant adsorption on calcite. Grigg and Bai (2005) found that a decreasing order of a surfactant (CD1045) adsorption density (mg/g) onto the five powdered minerals is: montmorillonite, dolomite, kaolinite, silica and calcite. However, the surface area of their mineral was not reported. Chapter 5 will discuss surfactant adsorption further.

#### 2.5.5.2 Surfactant Precipitation

In hard brines, the presence of divalent cations causes surfactant precipitation as equation 2.18 shows.

$$2R^{-} + M^{2+} \rightarrow MR_2 \downarrow \quad (2.18)$$

where $R^-$ is the anionic surfactant;

$MR_2$ is the surfactant-divalent cation complex that has a low solubility in brine.

This reaction leads to retention. Factors that influence the precipitation of anionic surfactants include cation valence, salt concentration, surfactant concentration, alcohol concentration, temperature, etc (Green and Willhite, 1998). When oil is present, it can compete for surfactant; that is, addition of oil can reduce (in some cases completely eliminate) surfactant precipitation. Also the precipitate must compete with the micelles for the surfactants (Somasundaran et al., 1979). Celik (1982) proved that surfactant precipitation increases with surfactant concentration at low concentration. But it will re-dissolve because the micelles will take up multivalent ions, causing redissolution of the precipitation. Addition of alcohol increases the solubility of a surfactant when the alcohol/surfactant ratio is sufficiently high (Green and Willhite, 1998). Also, the ethoxylate (EO) and propoxylate (PO) groups will help the surfactant to have tolerance to divalent cations typically present in reservoir brines. In this thesis, the surfactants considered have EO and PO groups, so that they have high tolerance to divalent cations. Thus, precipitation will not be discussed further in this thesis.

#### 2.5.5.3 Phase Trapping

This form of retention is strongly affected by the phase behavior. Surfactants may exist in the oil phase, and oil phase could be trapped as residual oil (Green and Willhite, 1998). Phase trapping can contribute significantly to surfactant retention and should

always be avoided. Glover et al. (1979) found that the onset of phase trapping with a surfactant-flooding process generally occurred at higher salt concentrations because it would form upper-phase microemulsion so that the surfactant would be trapped in the residual oil. Divalent cations are shown to influence microemulsion phase behavior strongly so that the phase trapping may occur at low divalent ion concentration compared to mono-valent ion concentration.

At lower hardness level, the multivalent cation will react with the anionic surfactant to form a monovalent cation that can chemically exchange with cations originally bound to the reservoir clays (Hill and Lake, 1978) as (2.19) and (2.20).

$$R^- + M^{2+} \rightarrow MR^+ \tag{2.19}$$

$$Na - Clay + MR^+ \rightarrow MR - Clay + Na^+ \tag{2.20}$$

This form of retention is reversible with both $M^{2+}$ and surfactant concentration. Other researchers (Hirasaki, 1982; Hirasaki and Lawson, 1986) found that ion exchange of the cations ($Na^+$, $Ca^{2+}$) with both the clays and the surfactant micelles is much more important for the surfactant retention. A system in which the preflood, slug, and drive have the same sodium and calcium injected concentration can have a significant increase in the calcium concentration in the surfactant bank and a significant decrease in calcium concentration in the drive because of ion exchange. Thus, the salinity of the surfactant flood will be over optimum salinity and form upper-phase microemulsion, i.e. the surfactant will reside in the oil phase and does not move with the flooding front. Krumrine (1982) proposed that the addition of alkali would reduce the concentration of

hardness ions that may cause surfactant retention. Therefore, ASP will have little surfactant retention due to ion exchange.

A trapped, upper-phase microemulsion may be remobilized by flushing with sufficiently lower salinity to cause an in-situ change to a middle- or lower-phase micro-emulsion (Hirasaki et al., 1983). As shown in this thesis, ASP process has a lower-phase region behind the surfactant front, i.e. the surfactant is partition into lower-phase and remobilized again. Thus, ASP process minimizes the retention by phase trapping with the lower-phase microemulsion region after surfactant front.

### 2.5.6 Co-solvents in surfactant process

Co-solvents, normally low molecular weight alcohols, are frequently used in surfactant process. In many surfactant systems, especially at high surfactant or low temperature conditions, high viscosity liquid crystals, emulsions and gels are observed (Healy and Reed 1974; Miller & Neogi, 1985). These phases with large viscosities will be trapped in the porous medium so that the surfactants can not propagate in reservoirs. The most important reason for using alcohols is to inhibit the formation of those high viscosity phases (Sanz and Pope, 1995). There are still some other reasons to use alcohol in surfactant process. The optimum salinity can be adjusted by alcohol. The type and concentration of alcohols change the optimum salinities (Salter, 1978; Lelanne-Cassou et al., 1983). Trushenski (1977) claimed that alcohol can eliminate the polymer-surfactant incompatibility. The presence of alcohol helps to reduce the emulsion coalesce time(Sanz and Pope, 1995).

However, introducing alcohols into surfactant process also has significant negative effects. Alcohols always raise the minimum interfacial tension (IFT) as well as decrease the solubilization ratios. This IFT incremental effect by alcohol is detrimental to oil recovery because IFT reduction is the main mechanism for surfactant enhanced oil recovery. Foam is unstable when alcohol is present (Li, 2006). It is difficult to use foam as mobility control where there is alcohol. Adding alcohol also increases the chemical cost and makes the surfactant process more complicated because of this additional component. Because of these harmful properties, it is better to have an alcohol-free formulation for oil recovery. Sanz and Pope (1995) found that the alcohol could be eliminated in several conditions. This thesis uses the blend of branched alcohol propoxy sulfates and internal olefin sulfonate to avoid the need for alcohol. Although alcohol will not be further discussed in this thesis, we still should remember that alcohols are quite effective to eliminate viscous phases.

### 2.5.7 Cationic Surfactant Flooding

While anionic surfactants are the most used surfactants in oil recovery processes, other surfactants, especially the cationic surfactants, have been considered (Austad and Milter, 1997; Austad et al., 1998; Standnes and Austad, 2000; Standnes et al., 2002, 2003, Strand, 2004). Unlike anionic surfactant flooding, the main mechanism of cationic surfactant flooding is wettability alteration. The mechanism of wettability alteration is the formation of ion-pairs between the positively charged surfactant monomers and negatively charged adsorbed material, mainly carboxylic groups. The resulting desorption makes the rock surface more water-wet, and water will spontaneously imbibe into the

matrix due to capillary effect. The desorbed material may exist in the micelles, or in the oil phase in the form of ion-pairs. Standnes and Austad (2000) also found that cationic surfactant adsorption is low in low-permeable chalk.

## 2.6 Mobility Control in Enhanced Oil Recovery

The purpose of mobility control is to change the mobility ratio to a favorable number so that the injected fluid will not bypass the displaced fluid, i.e. crude oil in reservoir. Because it is not economically practical to change the properties of the crude oil or the permeability of the reservoir, most mobility control methods change the properties of injected fluid. The commonly used mobility control agent is polymer because it can significantly increase the apparent viscosity of the injected fluid. Foam is also a good mobility control method with water, surfactant and gas. Because low surfactant concentrations are used and much of the injected material is gas, the cost of chemical for foam can be much less than the polymer. However, foam is more complicated than the polymer applications and the mechanism of foam transport in porous media is still not fully understood (Yan, 2006). Water-alternating-gas (WAG) is also used to control the mobility in some gas enhanced oil recovery process.

### 2.6.1 Polymer process

Addition of polymer will increase the viscosity of aqueous phase, so that the mobility of aqueous phase decreases. Thus the mobility ratio will be lower with polymer. Unlike the surfactant, the presence of polymer will not decrease residual oil saturation

with a few exceptions (Wang et al., 2000). But it will greatly increase sweep efficiency. If the waterflooding mobility ratio is high, the reservoir heterogeneity is serious, or combination of these two happens, polymer flooding will be useful (Lake 1989). Yang et al. (2006) found that an incremental recovery over water flooding of more than 20% OOIP can be obtained by injection of high molecular weight, high concentration polymer solution in Daqing field.

When polymer is used in surfactant flooding, it can also provide the mobility control at the low IFT front. Otherwise, the front is not stable and will finger and dissipate. Falls et al. (1992) tested an alkaline-surfactant process without using polymer within the White Castle Field, Louisiana. Although this process exhibited a displacement efficiency of virtually 100%, it recovered only 38% of the waterflooding residual oil in the reservoir as true tertiary oil due to the absence of mobility control. This thesis shows that maintaining the mobility is also very important for ASP flooding. Even when the residual oil saturation is zero, the oil recovery will be small without a favorable mobility ratio.

Two types polymers, polyacrylamide and polysaccharide, are commonly used in enhanced oil recovery (Sorbie, 1991). Polyacrylamides used in polymer EOR processes, normally are partially hydrolyzed polyacrylamides (HPAM). Thus, the HPAM is negatively charged, as is the anionic surfactant. Shupe (1981) tested the effect of pH, dissolved oxygen, salinity and hardness on HPAM polymer stability. HPAM has been used in about 95% of the reported polymer tests (Lake, 1989). The commonly used polysaccharide is xanthan gum, which is a bacterial polysaccharide. Compared to HPAM, xanthan gum has a more rigid structure than HPAM and relatively nonionic. These

properties make it relatively insensitive to salinity and hardness. However, it is susceptible to bacterial degradation after it has been injected into the field. In this thesis, only HPAM is used as the polymer.

### 2.6.2 Foam process

Foam is a two-phase system in which a relatively large volume of gas is dispersed in a small volume of liquid (Patton *et al.*, 1983). In porous media, the liquid phase of foam is continuous and at least some part of the gas phase of foam is made discontinuous by thin liquid films (Hirasaki, 1989). The presence of discontinuous gas in foam not only reduces the gas mobility but also reduces the liquid saturation and relative permeability and hence raises liquid phase apparent viscosity. One of the main reason that apparent viscosity of gas phase increases is that an extra force is required to push thin liquid films (lamellae) through pore throats of porous media. Also the viscous shear stresses in the thin films between the pore walls of porous media and gas interface increases the apparent viscosity (Nguyen et al., 2000). Foam can be stabilized by some surfactants. If foam can successfully replace the polymer as the mobility control agent, it may reduce the chemical cost for the surfactant process (Yan, 2006).

## 2.7 Alkaline-Surfactant-Polymer Enhanced Oil Recovery

Currently, alkaline-surfactant-polymer (ASP) is considered as the most promising chemical method in enhanced oil recovery because it integrates the advantages of alkali, surfactant and polymer. In recent years, there have been several field pilot tests using

ASP in USA (Pitts et al., 2006), India (Pratap and Gauma, 2004) and China (Wang et al., 1997; Qiao et al., 2000; Li et al., 2003; Yang 2003; Chang et al., 2006). However, the mechanisms of the alkaline-surfactant flooding are still not fully understood. Most investigators agree that the key issues for the alkaline-surfactant flooding are IFT reduction at low surfactant concentration, wettability alteration, low adsorption of surfactant by alkali, and mobility control.

Like surfactant process, IFT reduction is considered as one of the most important factors in alkaline-surfactant flooding (Falls et al., 1992; Arihara, et al., 1999). Krumrine et al. (1982) found that low IFT could be achieved with several alkaline chemicals and dilute surfactant systems. With the addition of a small amount of surfactant to the alkaline solution, the interfacial tension can become lower than with either surfactant or alkali alone (Schuler et al., 1989). Rudin and Wasan (1992) claimed that the organic acid amount in the oil has significant effect on the IFT reduction of alkaline-surfactant-oil system. They found that at low acid concentrations, the addition of an alkali to the added surfactant solution would only make interfacial tension increase. But at medium to high acid concentrations, the addition of an alkali can produce ultralow interfacial tension. They also observed that the addition of alcohol (isobutanol) could shift the minimum in IFT and reduce the time needed to achieve equilibrium interfacial tension. Nasr-El-Din and Taylor (1992; 1996) found the alkali-surfactant mass ratio changes the time to achieve minimum IFT by using dynamic IFT measurement. Hirasaki and Zhang (2003) found that there were optimum conditions for the IFT reduction by changing the concentration of alkali and surfactants. Seethepalli et al. (2004) identified that some

anionic surfactants could lower the IFT with a West Texas crude oil to very low values ($<10^{-2}$ mN/m).

Many other researchers also found that the ultra-low IFT existed in the alkaline-surfactant systems and would be the main reason for enhanced oil recovery (Nelson et al., 1984; Martin et al., 1985; Olsen et al., 1990; French and Burchfield, 1990; Baviere et al., 1995; Gao et al., 1995, 1996; Al-Hashim et al., 1996; Arihara et al., 1999; Vargo et al., 2000; Hirasaki and Zhang, 2003, Zhang et al. 2006). One of the biggest differences between ASP process and surfactant process is that ASP has two surfactants, synthetic surfactant that is injected and the natural soap created by the alkali in situ. Due to the different hydrophilic properties, they have different optimum salinities. This is one of the crucial factors of the process. This thesis will illustrate this relationship and try to use this characteristic to optimize the ASP process.

In addition to low interfacial tension, wettability alteration is also considered as an important factor for ASP recovery mechanism. As discussed section 2.4, the addition of alkali may result in wettability alteration. ASP process inherits this effect of alkaline flooding. Recent studies showed that alkali with dilute surfactant solution can change the wettability. Some successful imbibition experiments substantiated the results (Xie and Morrow, 2001; Hirasaki, and Zhang, 2003; Adibhatla and Mohanty, 2006). In this thesis, the wettability alteration will not be further discussed. We still should keep in mind that wettability alteration is very important for alkaline-surfactant EOR, especially for the fractured, oil-wet reservoir which spontaneous imbibition might be more suitable than flooding process.

As discussed in 2.5.5, the presence of alkali also reduces the consumption of surfactant. It has long been recognized that alkali can reduce the surfactant adsorption. Many experimental results showed mitigation of the surfactant adsorption by alkali. Polymer in ASP will act as the mobility control agent as shown. With the synergetic effect of alkali, surfactant and polymer, ASP process shows a great potential for enhanced oil recovery.

## 2.8 Numerical Simulation

Numerical simulation is very important to evaluate a process before the actual application because it will save time, cost and effort. And the numbers and complexities of flooding experiments can be minimized with numerical simulation. Thus, it is necessary to build a model to simulate the ASP process besides carrying out the experiments. With a good ASP numerical simulation, it will help the researchers to understand the characteristics of the ASP process.

Pope and Nelson (1978) developed a 1-D numerical simulator for surfactant enhanced oil recovery. Now it has been extended to include other chemical processes and to 3-D as UTCHEM (Delshad et al., 2002; Zerpa et al., 2004; John et al., 2005; Anderson et al., 2006). There are several commercial reservoir simulators, such as ECLIPSE by Schlumberger, VIP® and Nexus® by Halliburton. Several major oil and gas companies develop so called "in-house" packages for themselves, such as CHEARS by Chevron, Empower by ExxonMobil. However, most simulators do not include natural soap which is one of the most important factors in ASP. UTCHEM models the natural soap as an

additional surfactant (Delshad et al., 1998). But it does not distinguish the natural soap from the injected synthetic surfactant. The simulation in this thesis includes soap and its effect on the optimum salinity for ASP. Although it is a simple 1-D model so that it is faster and will not have many numerical convergence problems, it illustrates the characteristics of the ASP process and helps us to understand and optimize the process.

*Chapter* 3

# Phase Behaviors of Alkali-Surfactant System

This chapter presents the phase behavior experiments, also known as emulsion screening test, conducted for this research. The objective of phase behavior studies is to determine the optimum salinity by observing the alkali-surfactant-crude oil samples. Different oil samples are tested to illuminate the alkaline-surfactant phase behaviors.

## 3.1 Materials

### 3.1.1 Surfactant Selection

The surfactants used in the phase behavior experiments are the blends of 4:1 weight ratio (active material) of Neodol 67-7PO sulfate (N67) from Stepan and C15-18 internal olefin sulfonate (IOS) from Shell chemical. In this thesis, this blend is also called NI Blend.

Sulfates are selected because of the low cost of ethoxylated and propoxylated sulfates compared to the corresponding sulfonates. The ethoxy (EO) and propoxy (PO) groups give the possibility to tailor the surfactant molecules for oil recovery (Osterloh, and Jante, 1992; Aoudia et al., 1995; Wu et al., 2005; Levitt et al., 2006). The EO and PO groups can also raise the tolerance to divalent ions (Osterloh, and Jante, 1992). However, sulfate will hydrolyze at high temperature (> 60 °C) with the presence of an ester linkage (Aoudia et al., 1995). In this thesis, all the experiments are at room temperature so that

sulfates can be used. The hydrophobe for this Neodol 67-7PO sulfate is a 16 to 17 chain with an average of 1.5 methyl groups randomly positioned (Annual DOE Report, 2006). The branched chain is introduced to decrease the formation of ordered structure, e.g. liquid crystals. An approximate structure of a $C_{16-17}$ 7PO sulfate molecule generated by a space filling, free-energy minimizing model is shown in Figure 3.1 (a).

Sulfonates have been considered and tested for surfactant EOR process for several decades. Unlike the sulfates, sulfonates are thermally stable at much higher temperatures (Salter, 1986). The sulfonate used in this thesis is $C_{15-18}$ internal olefin sulfonate (IOS). The internal olefin will have an overall size of C15 to C18 and a range of internal, double-bond positions such that sulfonation with $SO_3^{2-}$ will produce a variety of products. This is also expected to minimize the formation of ordered structures such as liquid crystals and gels (Annual DOE Report, 2004). The hydroxyl alkane sulfonate form of a $C_{15-18}$ IOS is shown in Figure 3.1 (b).

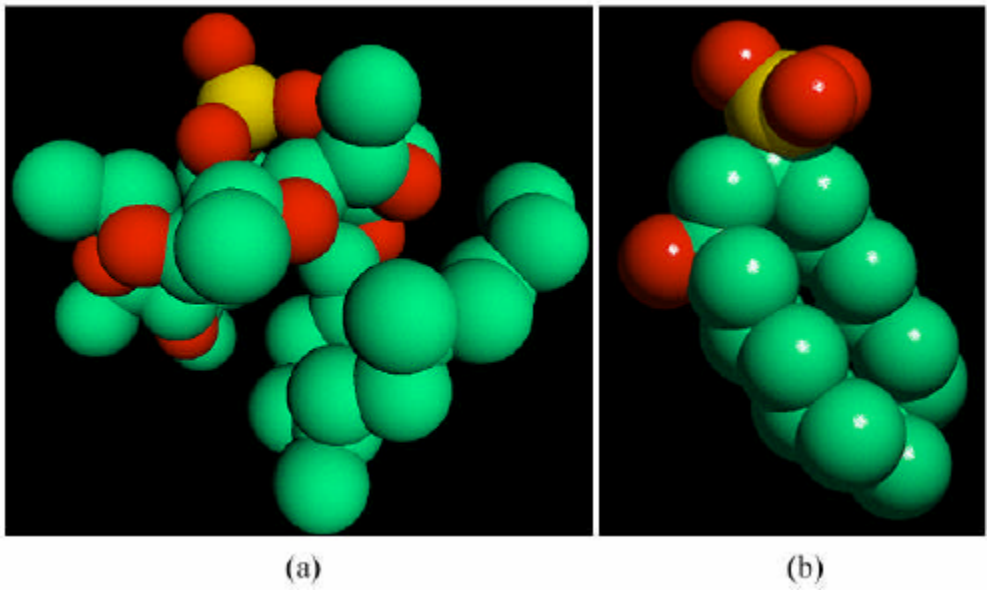


**Figure 3.1 Possible structures of (a) $C_{16-17}$-$(PO)_7$-$SO_4$ (b) $C_{15-18}$ Internal Olefin Sulfonate (IOS) (Annual DOE Report, 2006)**

The NI blend is selected because it exhibited the most promising performance with Yates and Midland Farm oils (Annual DOE Report, 2006; Zhang et al., 2006; Levitt et al., 2006). This blend has good solubility behavior without forming liquid crystals or gels. Another reason to choose the NI blend is that NI blend can be injected as a single phase solution at ambient temperature at high salinities as shown in figure 3.2. It is very important to keep the ASP solution as one phase to avoid highly viscous phases. Figure 3.2 shows that NI blend has much higher salt tolerance than IOS or N67 by itself. Liu et al. (2006) also reported that the surfactant blend will increase the calcium tolerance for surfactant.

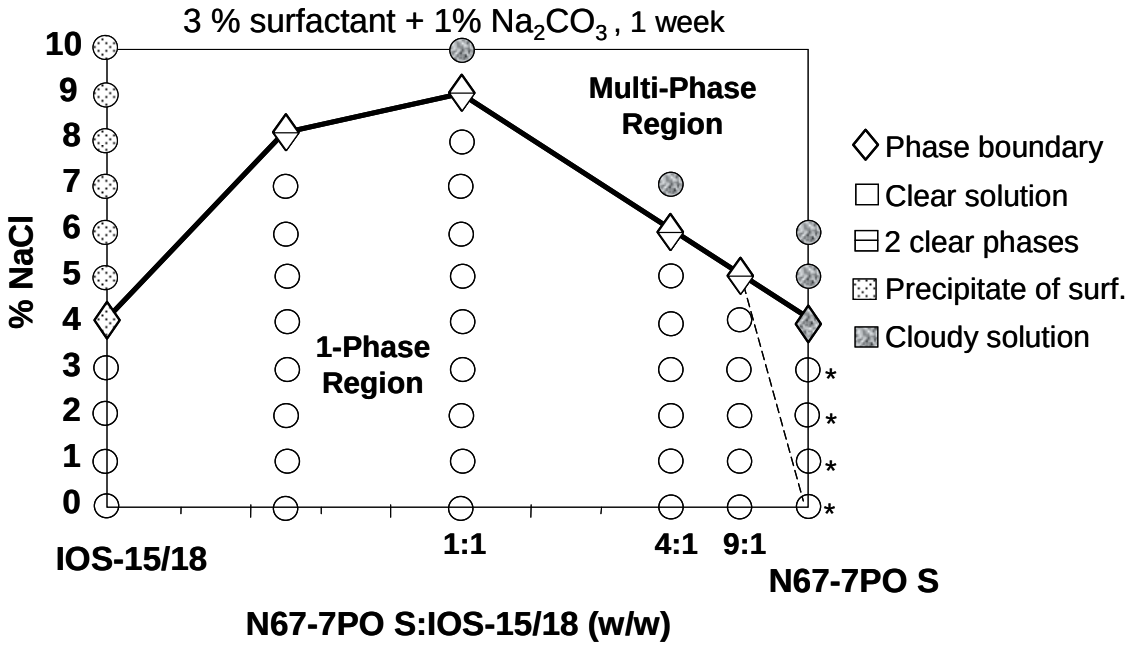


**Figure 3.2 Effect of added NaCl on phase behavior of 3 wt% solutions of N67/IOS mixtures containing 1 wt% $Na_2CO_3$. (Liu et al., 2006)**

### 3.1.2 Crude Oils

Yates crude (MY) oil and PBB crude oil have been extensively investigated in this chapter. MY represents the crude oil with low acid number (0.2 mg KOH/gram oil by Fan and Buckley, 2006) and moderate viscosity (19 cp at ambient temperature); PBB is the oil with much higher acid number (4 mg KOH/gram oil) and high viscosity (266 cp at ambient temperature). A few samples with Shell White Castle Q-sand (SWCQ) oil (1.5 mg KOH/gram oil and 2.8 cp) and synthetic oils (octane, decane, dodecane) were also tested. The synthetic oils are from Sigma-Aldrich.

### 3.1.3 Other Chemicals

*Deionized (DI) water*: Deionized (DI) water with conductivity of 4-7 μS/cm was used for all experimental solutions.

*Sodium carbonate*: Sodium carbonate from Fisher, is ≥99.8% pure with less than 0.005% calcium. Sometimes, the sodium carbonate solution has to be filtered because of a very small amount of precipitation.

*Sodium chloride*: Sodium chloride, which adjusts the electrolyte strength, is a Fisher product. It is enzyme grade with ≥99.9% sodium chloride.

*Sodium hydroxide*: Sodium hydroxide, which is used in soap extraction, is also a Fisher product with 98.5% sodium hydroxide.

*Isopropyl alcohol*: Isopropyl alcohol (IPA), which is used in soap extraction, is a Fisher product with ≥99% IPA.

## 3.2 Soap Extraction for crude oils

As discussed in Chapter 2, natural soap, which is an anionic surfactant, will be generated by the saponification of the acidic components in the crude oil with alkali. Thus, the soap amount, or the natural surfactant concentration, is a very important value for phase behavior study. Usually, acid number determined by non-aqueous phase titration (Fan and Buckley, 2006) is used to estimate the soap amount (Zhang & Hirasaki, 2006). However, short chain acids, which also react with alkali, may not behave like surfactant because they are too hydrophilic. Also phenolics and porphyrins in crude oil will consume alkali and will not change the interfacial properties as much as surfactant. Asphaltenes and/or resins may have carboxylate functional groups but not be extracted into the aqueous phase. Total acid number determined by non-aqueous phase titration could not distinguish the acids that can generate natural soap and those that can consume alkali without producing surfactant. Therefore, another method that can obtain the soap amount is introduced.

Since the anionic surfactant can be accurately determined by potentiometric titration (See Appendix A) with Benzethonium Chloride (hyamine 1622), it is reasonable to use this method to find the natural soap amount. Since this potentiometric titration is for aqueous phase, the soap should be extracted into aqueous phase as the first step. As an anionic surfactant, the natural soap may stay in the oleic phase and form upper-phase microemulsion when the electrolyte strength is high. To extract the soap into aqueous phase, NaOH was used to keep the pH high with low electrolyte strength. Also isopropyl alcohol was added to make the system hydrophilic so that soap will partition into aqueous phase. The extraction procedure is shown as below:

1. Mix crude oil, 0.1 M NaOH solution and isopropyl alcohol (IPA) together. The weight ratio is 1 (oil): 3 (NaOH): 0.44 (IPA). This ratio was chosen because it assures the NaOH is enough to react with the acid in the oil and still keep pH around 13.
2. Shake the sample well by hand for 1 or 2 minutes and keep on shaking sample by a rotating shaker for 24 hours.
3. Settle the sample until the water oil interface does not change.
4. Sample the aqueous phase and determine the aqueous phase surfactant concentration by potentiometric titration with hyamine. (for PBB, the sample is never settled, and entire emulsion was used for titration)
5. Use mass balance to calculate the acid number.

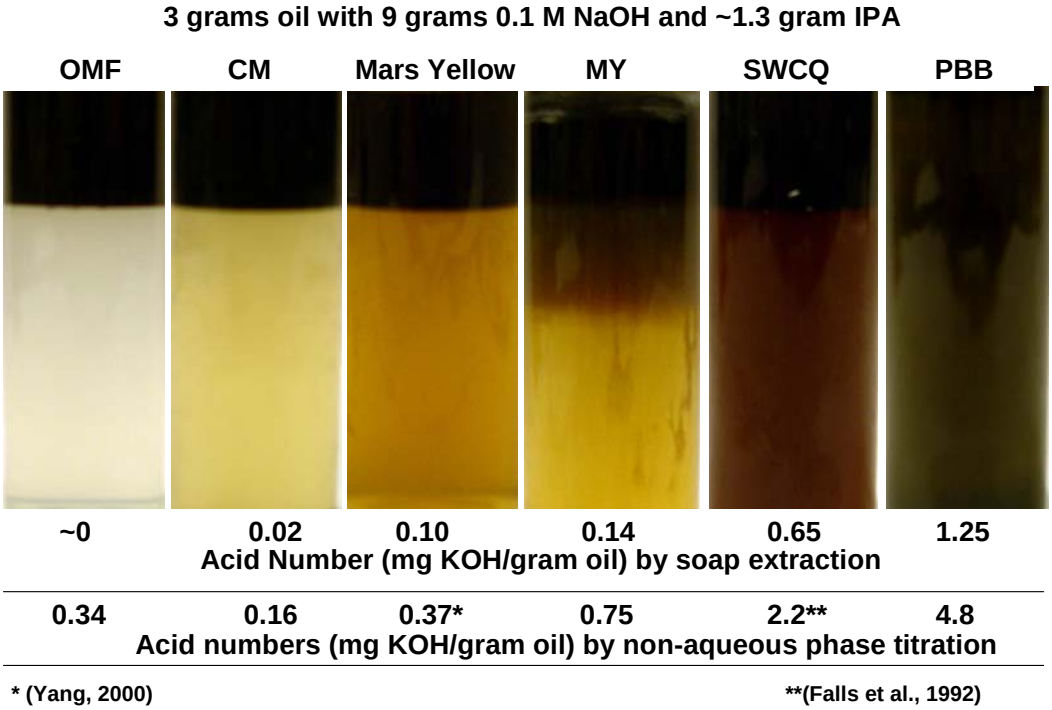


**Figure 3.3 Soap extraction behaviors and acid numbers by soap extraction and non-aqueous phase titration.**

Figure 3.3 shows the photos of soap extraction and compares the acid number determined by soap extraction and non-aqueous phase titration. Six different crude oils were tested. Since those acids that can not generate soap will not detected by the potentiometric titration, the acid numbers obtained by the soap extraction are less than the acid numbers determined by non-aqueous phase titration as expected. There is no general ratio between those two acid numbers, i.e., the natural soap amount of an oil can not be determined just by non-aqueous phase titration. Oils with high acid number by non-aqueous phase titration usually have high soap content. But it is not always true. For example, the higher acid number of Midland Farm by non-aqueous phase titration is 0.34 mg KOH/ g, which is higher than Minas oil (0.16 mg KOH/g) and close to Mars (0.37 mg KOH/g). But no soap can be found by soap extraction for Midland Farm, while the Minas is 0.02 mg KOH/g and Mars is 0.10 mg KOH/g by the soap extraction. The other interesting observation is that the color of the aqueous phase indicates how much soap has been extracted. Darker aqueous phase indicates higher extracted soap. This is reasonable because naphthenic acids are colored and also higher soap concentration will help dissolve more oil into the aqueous phase so that the aqueous phase will be darker.

## 3.3 Phase behavior Experimental Procedure

The concentrated stock solutions of surfactant, sodium carbonate and sodium chloride were prepared before mixing them together. All solutions were made by weight percentage. By mixing the stock solutions and DI water in different ratios, the solutions over a range of salinities were made. The solutions should be made in this order:

1. Sodium chloride and sodium carbonate stock(s)
2. De-ionized water
3. Surfactant stock(s) which has been mixed as NI blend

This order was chosen because the surfactant solution will precipitate or have phase separation problems at high salinity. The tips of 5 ml glass pipettes from Fisher Brand® or similar pipettes were sealed by acetylene and oxygen flame with VICTOR® torch. Then, the surfactant solutions and crude oils were mixed at a specific Water Oil Ratio (WOR) into these pipettes. After the mixing procedure, the other ends of the pipettes were sealed so that water and volatiles in crude oil will stay in the samples. Afterwards, the samples were shaken well by hand for 1 or 2 minutes and put on a rotating shaker for 24 hours to provide adequate mixing. Finally, they were arranged on the racks to settle in an upright position. Photos were taken to record the phase behaviors which would be used to calculate the solubilization ratios. The oil water interface changes with settling time. The equilibrium phase behavior was usually achieved after 7 days because no further changes were observed in the interface positions, i.e. phase volumes. In the next section about phase behavior results, all the phase behavior results are equilibrium.

## 3.4 Phase behavior Results

### 3.4.1 Phase Behavior of PBB and NI Blend

Fig. 3.4 (b) illustrates variation of phase behavior with NaCl concentration for alcohol-free solutions containing 0.2 wt% (active) NI blend and 1 wt% $Na_2CO_3$ mixed

with PBB crude oil at a water-to-oil (WOR) ratio of 24 and stored at ambient temperature for 40 days. Hereafter, all the surfactant, sodium carbonate and sodium chloride concentrations are based on aqueous solutions. The concentration of $Na_2CO_3$ was chosen as 1% because this concentration will assure the low surfactant adsorption even with the consumption of surfactant by acid in crude oil as shown in Chapter 5. The photos for those samples were taken after 40 days because such a long time assures that the equilibrium is achieved. In fact, no further changes for the interfaces of those samples were observed after 10 days. At 4.8 % NaCl, it is lower phase microemulsion (Winsor I) because the aqueous phase volume is greater than its initial volume. As discussed in Chapter 2, the incremental volume in the lower phase is due to the solubilization of oil by the surfactant in aqueous phase. When the salinity is at 5.2% NaCl, it is upper phase microemulsion (Winsor II) because the swelled oleic phase indicates that surfactant is in oleic phase and solubilizes water. It is difficult to observe the classical Winsor type III region for crude oil system with such a low surfactant concentration (0.2%). Phase behavior with crude oil and low surfactant concentration often changes from Winsor I to Winsor II directly. Therefore, the optimum salinity is located as the salinity between the highest Winsor I salinity and the lowest Winsor II salinity. Therefore, the optimum salinity of Figure 3.4 (b) is around 5.0% NaCl. Optimum salinities for other samples were similarly determined as shown in figure 3.4(a) and 3.4(c).

Figure 3.4 also represents that optimum salinity is a function of both surfactant concentration and WOR for PBB and NI blend. Fig 3.4 (a) is around 3.2 % NaCl at 0.05 % surfactant concentration with all the other conditions identical to Figure 3.4 (b). And

the optimum salinity is between 2.4 and 3.0% with WOR at 3 with all the other conditions identical to Figure 3.4 (b).

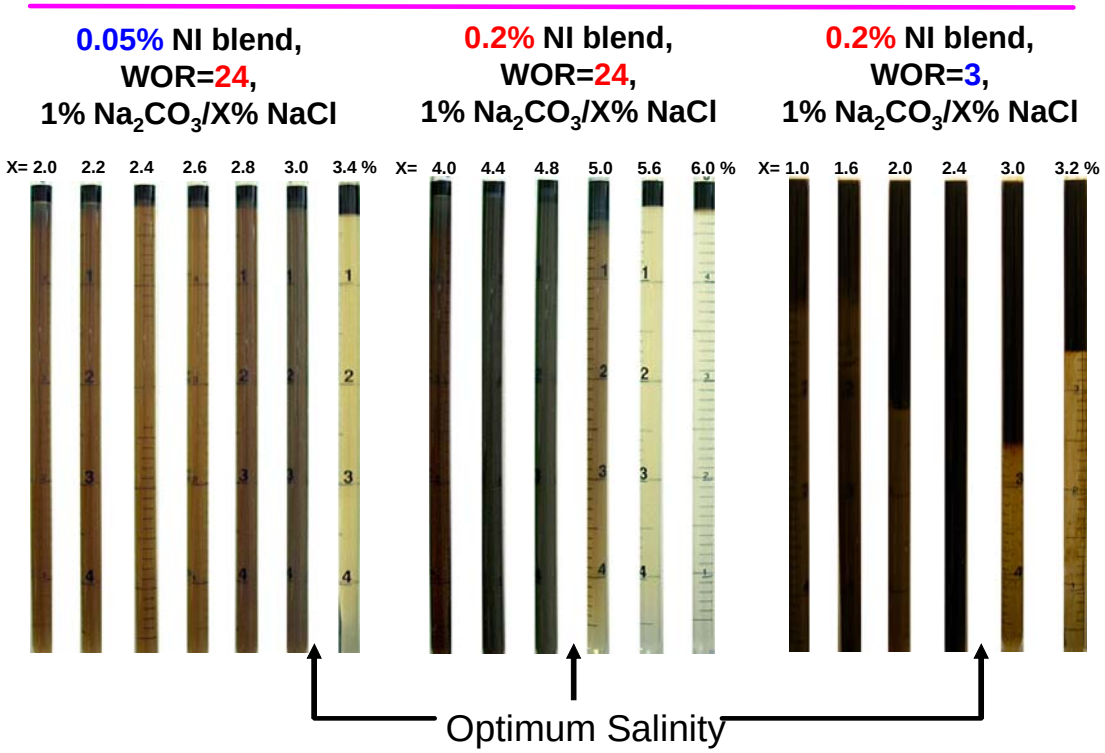


**Figure 3.4 Phase behavior is a function of WOR and surfactant concentration for PBB and NI blend at ambient temperature.**

The optimum salinities for other surfactant concentrations and WORs are also plotted in Figure 3.5. The point with 0% surfactant concentration in figure 3.5 indicates that the optimum salinity for soap is around 0.8% NaCl. And optimum salinity for PBB and NI blend without any $Na_2CO_3$ is around 7.5 % NaCl. It is consistent with figure 3.5 that the optimum salinity increases to above 6% NaCl with presence of 1% $Na_2CO_3$ when both surfactant concentration and WOR are high. From figure 3.5, the optimum salinity can be increased by raising either the surfactant concentration or WOR. The similarity between raising the surfactant concentration and increasing WOR is that the ratio of natural soap to synthetic surfactant deceases. It is reasonable that the soap to surfactant

ratio is the parameter that determines the optimum salinity. Figure 3.6 shows that the dependence of optimum salinity on surfactant concentration and WOR can be correlated with natural soap/synthetic surfactant mole ratio. The three curves with different WORs in figure 3.4 collapse into one curve as shown in figure 3.5. The soap amount is based on the soap extraction. When soap to surfactant ratio is low, i.e., surfactant is dominant, the optimum salinity goes to the optimum salinity of the surfactant (~6.5% NaCl + 1% $Na_2CO_3$); while when the ratio is high, i.e., soap is dominant, the optimum salinity is close to the optimum salinity of soap (~0.8% NaCl + 1% $Na_2CO_3$). The fact that optimum salinity is a function only of the soap/surfactant ratio is a very important property for the alkali surfactant crude oil system. And this property is very beneficial to design a successful ASP process, as will be shown in Chapter 6.

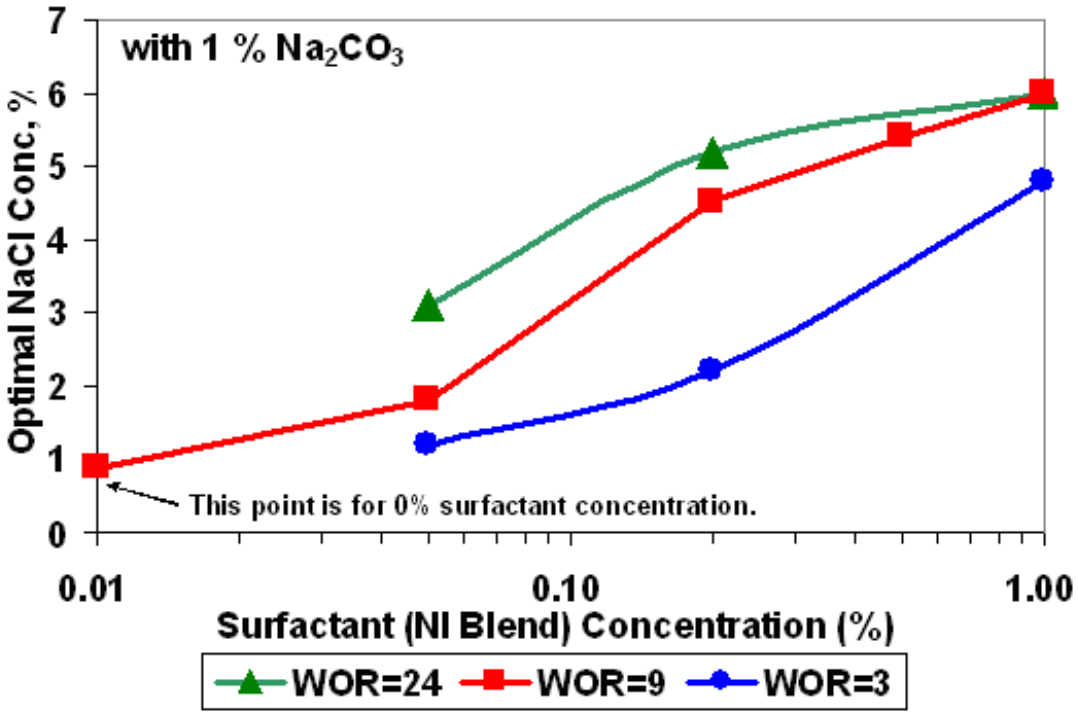


**Figure 3.5 Optimum salinity of NI blend as a function of WOR and surfactant concentration for PBB oil.**

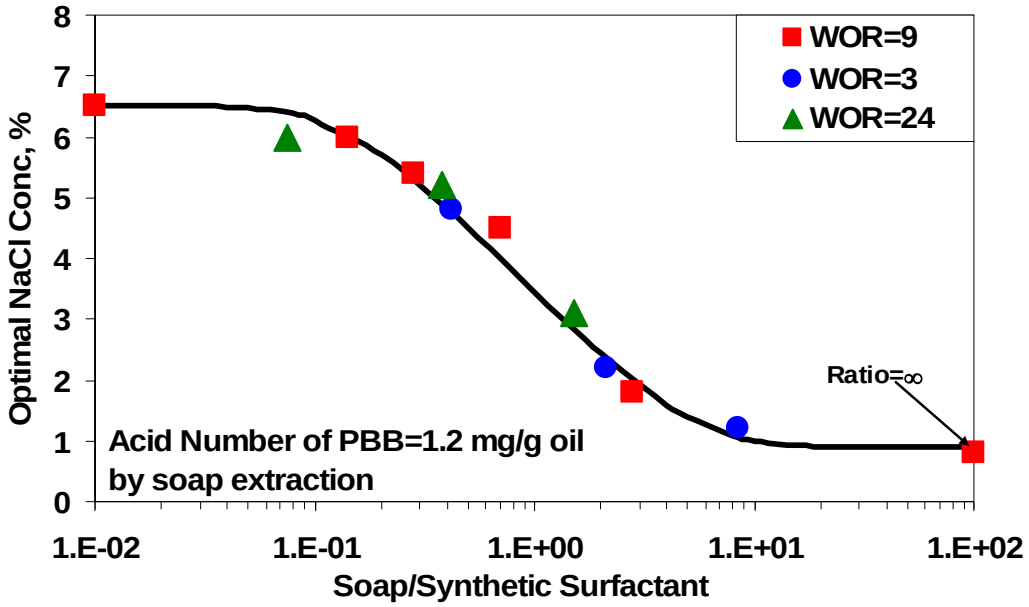


**Figure 3.6 Optimum salinity of NI blend as a function of natural soap/synthetic surfactant mole ratio for PBB oil.**

Since soap amount can be determined by either soap extraction or non-aqueous phase titration, it is a question which number should be chosen to calculate the soap amount. It is known that optimum salinity of orthoxylene sulfonate mixtures can be characterized by a mixing rule (Bourrel and Schechter, 1988) as shown in equation (3.1). Some experimental results show that this relationship fits the experimental data quite well (Puerto and Gale, 1977). UTCHEM also used this equation as a mixing rule for all the anionic surfactants.

$$\log(Opt_{mix}) = \sum_i X_i \log(Opt_i) \qquad (3.1)$$

where $X_i$ is the mole fraction of surfactant $i$.

$Opt_{mix}$ is the optimum salinity of surfactant mixture

$Opt_i$ is the optimum salinity of surfactant i

Since soap is also an anionic surfactant, it is reasonable to assume that the blend of soap and synthetic anionic surfactant might follow the same mixing rule. For alkali surfactant system, equation (3.1) can be simplified as:

$$\log(Opt) = Xsoap * \log(Opt_{soap}) + (1 - Xsoap) * \log(Opt_{surfactant}) \qquad (3.2)$$

where $X_{soap}$ is the mole fraction of natural soap.

$$Xsoap = \frac{Soap}{Soap + Surfactant}$$

The straight lines in figure 3.7(a) and 3.7(b) present equation (3.2). Both figures show the relationship of optimum salinity and soap mole fraction. Figure 3.7(a) uses the number from non-aqueous phase titration to calculate soap fraction, while figure 3.7(b) gets the soap fraction by soap extraction. The acid number from soap extraction gives a much better agreement between the theoretical mixing rule and experimental data. Thus, acid number from the soap extraction is the better choice to evaluate the optimum salinity of alkaline surfactant systems.

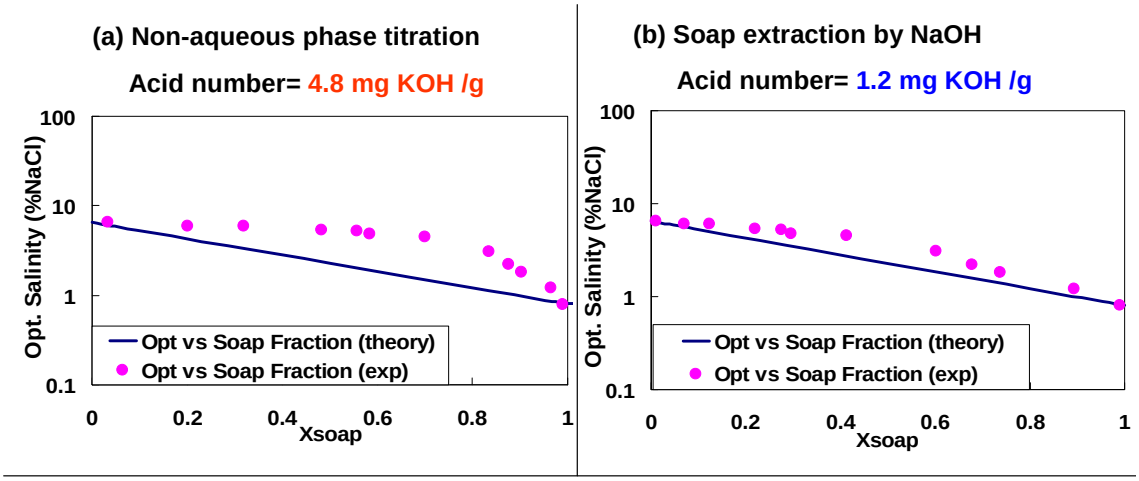


**Figure 3.7 Relationship of optimum salinity and soap mole fraction by difference acid number for NI Blend and PBB oil.**

### 3.4.2 Phase Behavior of Yates and NI Blend

Compared to PBB, the Yates crude oil is lower acid number oil (0.75mg KOH/gram oil from non-aqueous phase titration). The phase behavior samples of 0.2% NI blend/1% $Na_2CO_3$/ x% NaCl at WOR of 3:1 are shown in figure 3.8. In this series, the optimum salinity is between 3.2% NaCl and 3.6% NaCl with presence of 1% $Na_2CO_3$. In the lower phase microemulsion region, the color of Yates lower phase is much lighter than the PBB sample because the soap in Yates is much less than that in PBB.

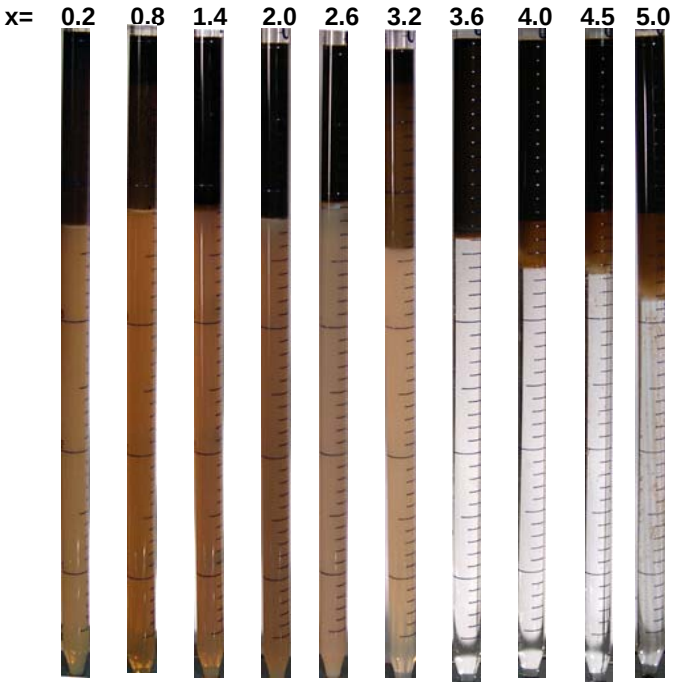


**Figure 3.8 Salinity scan for 0.2% NI blend, 1% $Na_2CO_3$ with MY4 crude oil for WOR=3 at ambient temperature. x = wt.% NaCl.**

Optimum salinity of NI blend for Yates oil is still a function of WOR and surfactant concentration as shown in figure 3.9. Similar to PBB, raising either surfactant concentration or WOR will increase the optimum salinity.

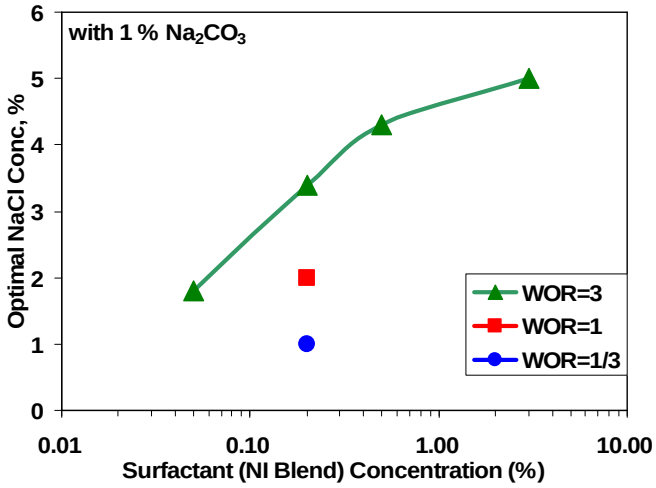


**Figure 3.9 Optimum salinity of NI blend as a function of WOR and surfactant concentration for Yates oil.**

Figure 3.10 illustrates the correlation of optimum salinity of NI blend as a function of soap to synthetic surfactant ratio. The optimum salinity depends only on the soap to surfactant ratio like the PBB oil. The gray curve in figure 3.10 shows the optimum salinity curve of TC blend and Yates oil (Zhang et al. 2006). TC blend is 1:1 (wt) blend of TDA-4PO (iso-tridecyl 4 propoxylate sulfate from Stepan) and CS-330 (dodecyl 3 ethoxylated sulfate from Stepan). For Yates oil, NI blend is better than TC blend because the optimum salinity of NI blend is much closer to the formation brine salinity than TC blend.

From figures 3.6 and 3.10, the optimum salinities of NI blend for PBB and Yates without soap are different, as are the soap optimum salinities for PBB and Yates. As shown in figure 3.10, different surfactants for the same oil have different optimum curves. However for a given surfactant and crude oil, the optimum salinity depends only on soap to surfactant ratio. This is very useful because the researchers don't need hundreds scans to determine the optimum salinities of different surfactant concentrations and WORs.

With only with a few salinity scans, the optimum salinities of arbitrary surfactant concentration and WOR samples can be predicted by the optimum salinity curves such as those of figure 3.6 and figure 3.10.

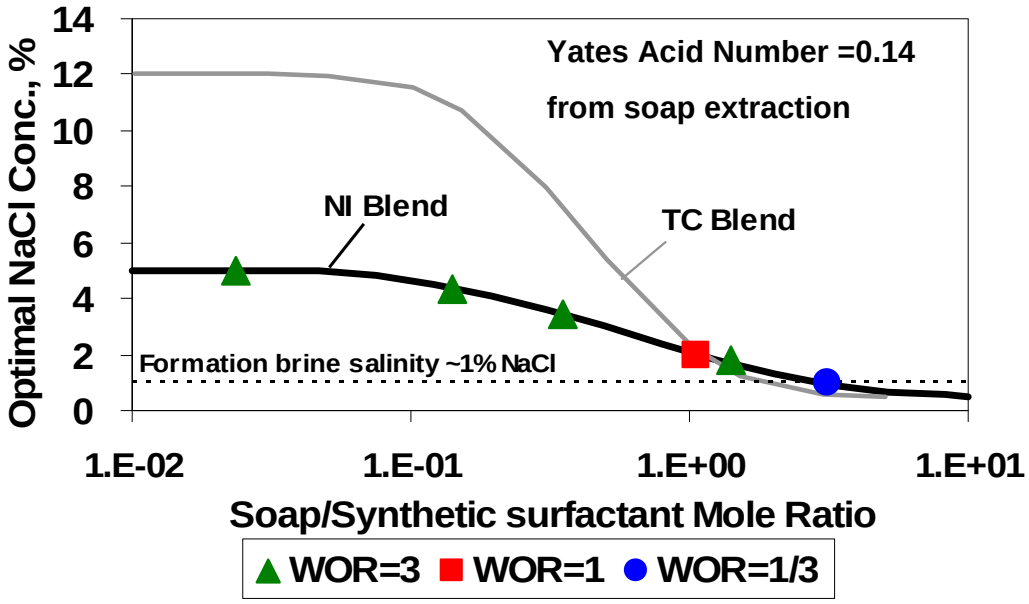


**Figure 3.10 Optimum salinity of NI blend as a function of natural soap/synthetic surfactant mole ratio for Yates oil.**

For NI blend and Yates system, the acid number from soap extraction has a better agreement with the mixing rule as figure 3.11 shows. By using the soap amount estimated from soap extraction, all the data for NI blend and Yates oil follow the mixing rule correlation used in previous work on surfactant EOR. The NI blend and Yates system, as well as the NI blend and PBB oil shown in figure 3.7, demonstrates again that it is better to use the acid number from the soap extraction to correlate the optimum salinity of alkaline surfactant systems.

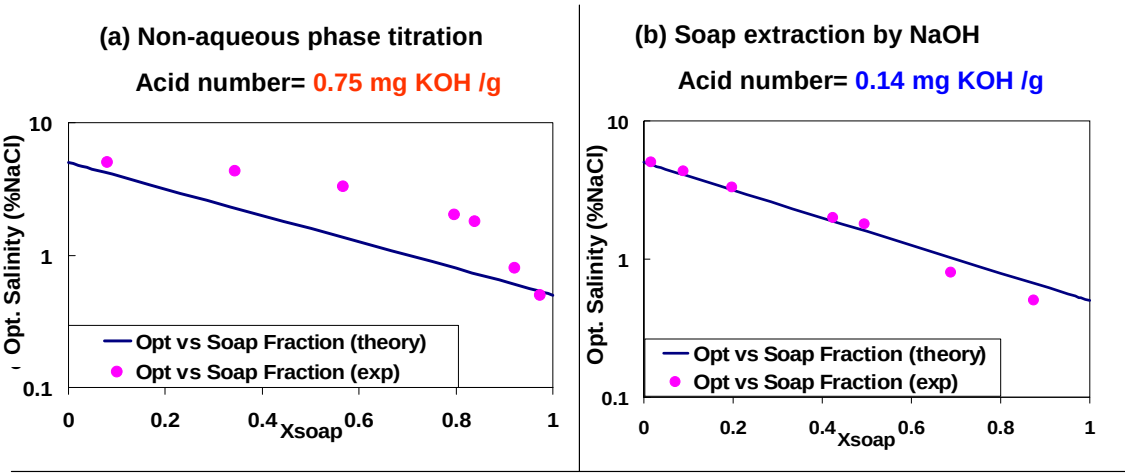


**Figure 3.11 Relationship of optimum salinity and soap mole fraction by difference acid number for NI Blend and Yates oil.**

All the previous phase behavior scans are conducted by changing salinity with fixing WOR. If salinity is fixed and WOR is changed, it is expected that there is an optimum WOR for a specific salinity.

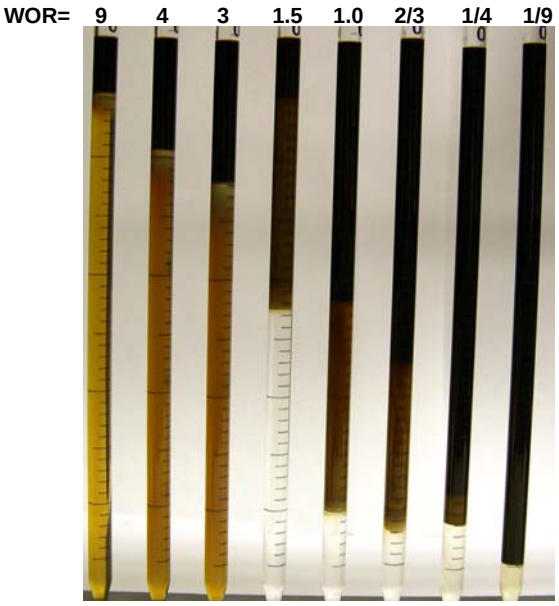


**Figure 3.12 WOR scan for 0.2% NI blend/ 1% $Na_2CO_3$/ 2% NaCl with Yates crude oil at ambient temperature.**

Figure 3.12 shows the WOR ratio scan for 0.2% NI blend/1% $Na_2CO_3$/ 2.0 % NaCl and Yates oil. It seems that the optimum WOR for this condition is between 1.5 and 3.0. This optimum WOR also can be predicted from figure 3.10 through the soap to surfactant ratio. The predicted WOR value by figure 3.10 is around 1.5. This result is consistent with the conclusion that the optimum salinity for alkali surfactant crude oil system depends only on the soap to surfactant ratio.

### 3.4.3 Phase Behavior of SWCQ and NI Blend

Crude oils other than Yates, such as SWCQ and OMF were also investigated with the NI blend. Figure 3.13 shows the White Castle system with WOR = 9. It is found that the sample (2.0%NaCl) forms a middle layer as the traditional Winsor III region after 40 days settling unlike the PBB and Yates.

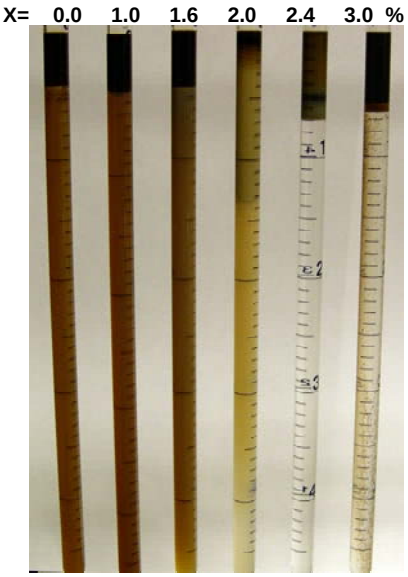


**Figure 3.13 Salinity scan for 0.2% NI blend, 1% $Na_2CO_3$ with SWCQ crude oil for WOR=9 at ambient temperature. x = wt. % NaCl.**

Like the Yates and PBB, reducing the WOR decreases the optimum salinity. When the WOR is 3 and all the other conditions remain the same, no middle phase was observed. But from the color of lower phase, the optimum salinity decreases to 0.9% NaCl. No more SWCQ oil scans were made because of the lack of SWCQ oil. Figure 3.14 plots the two SWCQ optimum salinity points the same way of figure 3.10. The soap amount of this system can be calculated by the acid number (0.65mg KOH/g oil). The black curve in figure 3.14 is the optimum salinity vs soap/surfactant ratio curve for Yates crude oil. Figure 3.14 indicates that the White Castle oil and NI blend system does not follow the curve of Yates and NI blend.

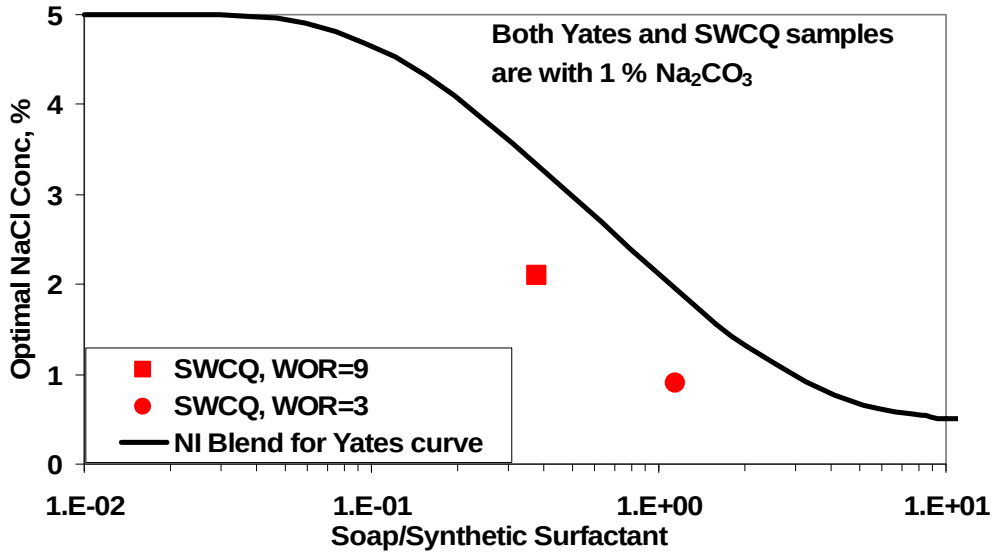


**Figure 3.14 Optimum Salinity vs soap/ surfactant ratio for Yates and SWCQ**

### 3.4.4 Phase Behavior of Pure Hydrocarbons and NI Blend

Three alkanes, octane, decane and dodecane, were tested with 1.0% NI blend / 1% $Na_2CO_3$ / x% NaCl. The phase behavior of octane samples is shown in figure 3.15. The

optimum salinity is around 3.4% NaCl. The optimum salinities for decane and dodecane are 5.2% and 7.0% NaCl respectively. Figure 3.16 shows the optimum salinity versus the carbon number of the refined oil for NI surfactant with 1 % $Na_2CO_3$. This result may explain why the optimum salinity of NI blend for Yates and PBB are different. The Yates oil has optimum salinity near that of decane and PBB oil near that of dodecane.

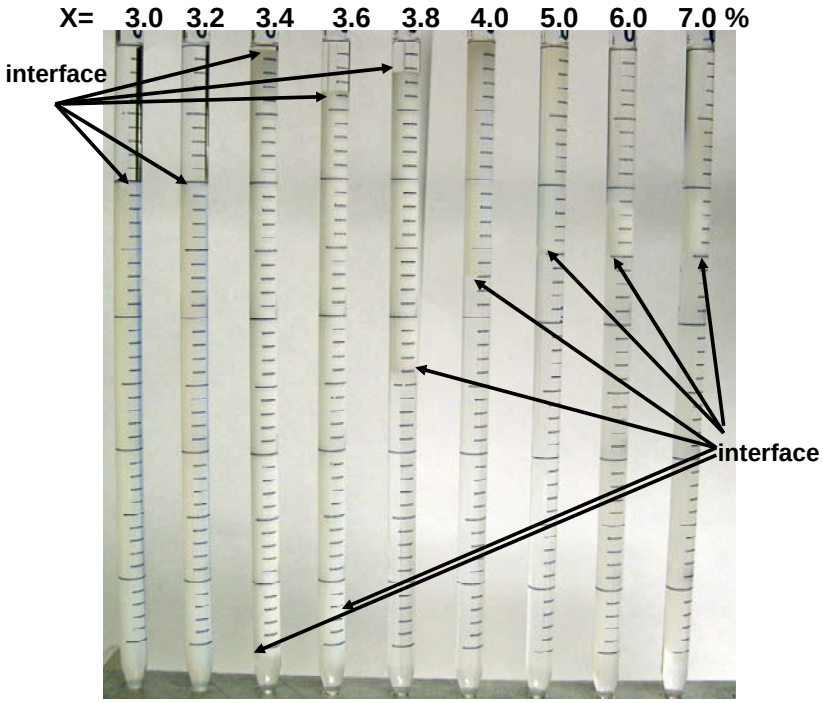


**Figure 3.15 Phase behavior of Octane with 1.0% NI blend / 1% $Na_2CO_3$ / x% NaCl, WOR=3**

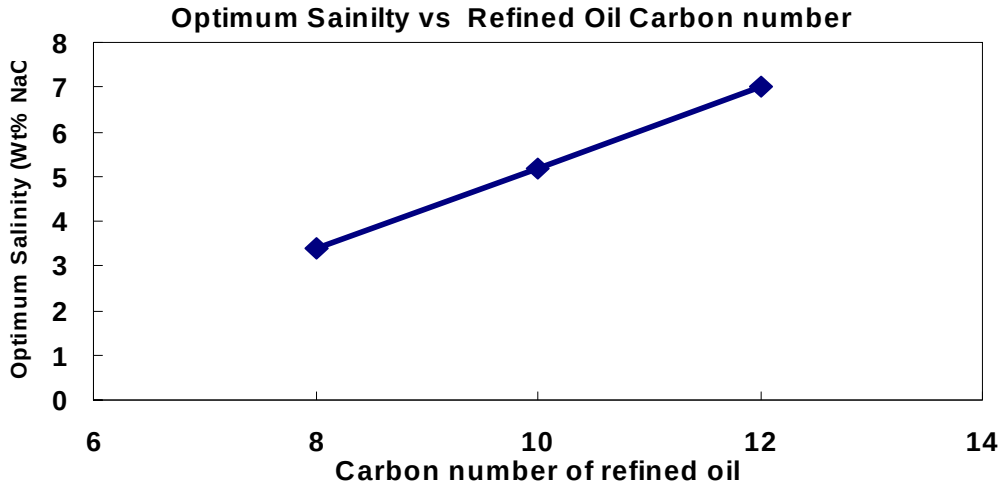


**Figure 3.16 Optimum salinity vs the carbon number of the refined oil for NI surfactant with 1 % $Na_2CO_3$**

Introducing alcohol can significantly change the optimum salinity as figure 3.17 shows. These octane samples are with 3.4% NaCl, which is the optimum salinity for octane and with large volume middle layer. If the middle layer at the optimum salinity is emulsion, the introduction of SBA will let the emulsion settle and coalesce. Several Secondary Butanol Alcohol (SBA) concentrations were tested. The middle layer keeps opaque until the SBA concentration reaches 2%. However, it seems the presence of SBA lowers the optimum salinity. With 2.0% SBA and 4.0% SBA, the samples are clearly over-optimum. Figure 3.18 shows the same scan as figure 3.15 except with 4.0% SBA added. The optimum salinity goes down from 3.4% NaCl to 2.4% NaCl. Figure 3.19 shows the effect on optimum salinity of different SBA concentration.

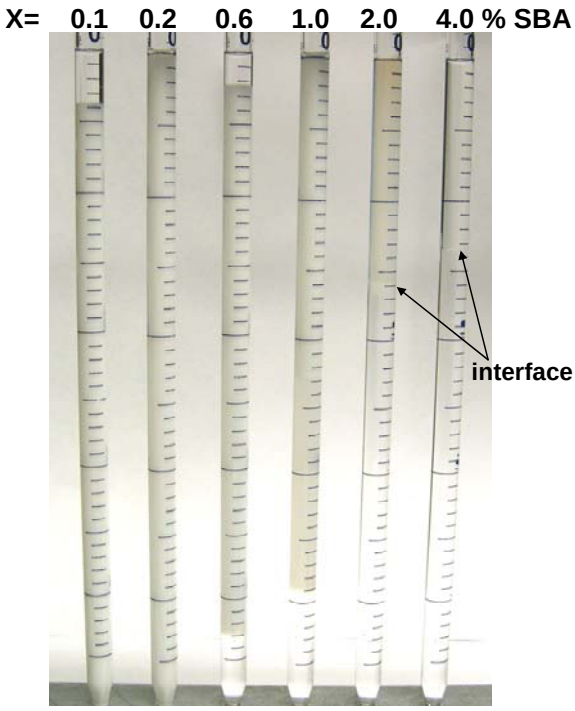


**Figure 3.17 Phase behavior of Octane with 1.0% NI blend / 1% $Na_2CO_3$ / 3.4% NaCl/ x % SBA, WOR=3**

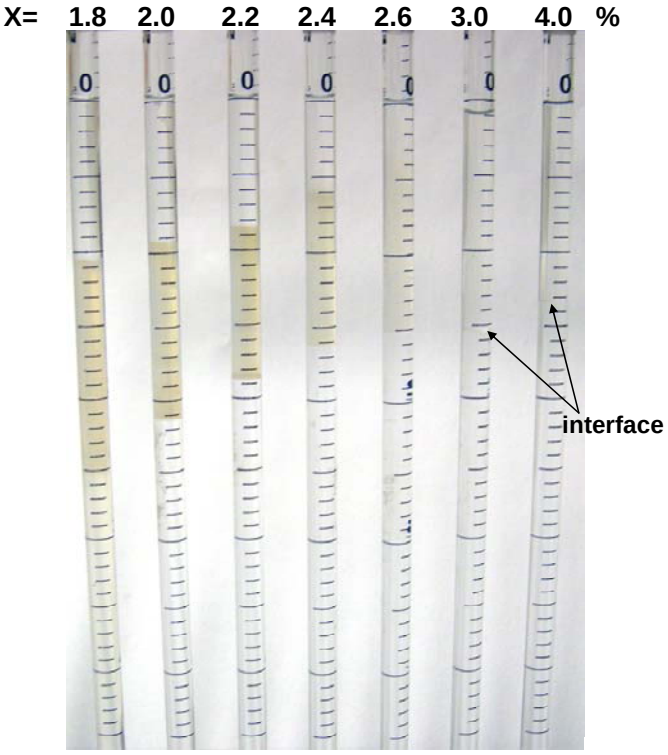


**Figure 3.18 Phase behavior of Octane with 1.0% NI blend / 1% $Na_2CO_3$ / x % NaCl/ 4% SBA, WOR=3**

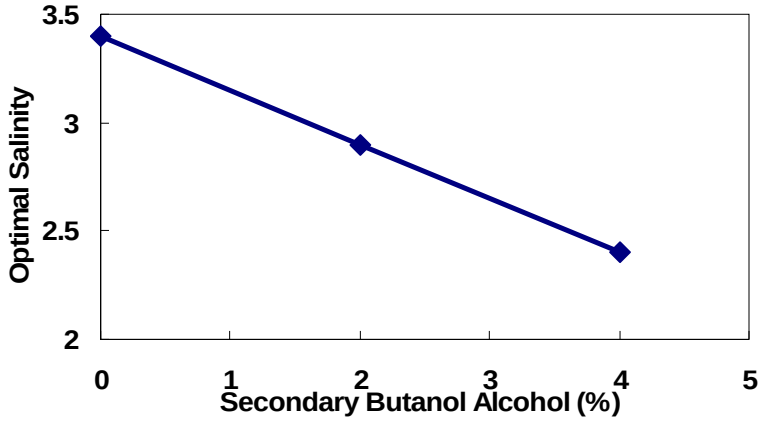


**Figure 3.19 Optimum salinity vs SBA amount for 1.0% NI blend / 1% $Na_2CO_3$ / Octane /WOR=3**

### 3.4.5 Birefringence of MY4-NI Blend system

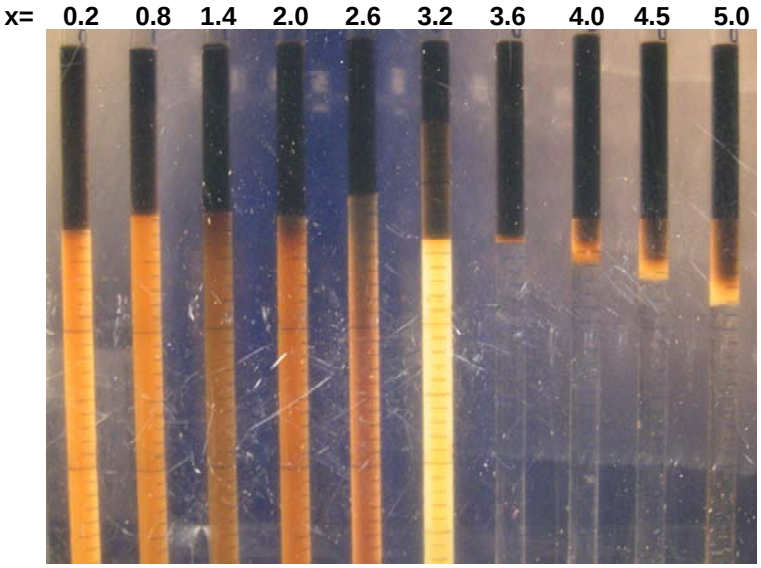


**Figure 3.20 Appearance of 0.2% NI blend / 1% $Na_2CO_3$ / x% NaCl, WOR=3:1,**

Birefringence was observed in the 0.2% NI blend salinity scan at 1% $Na_2CO_3$, WOR=3, as shown in figure 3.20. There is strong birefringence for the sample with 3.2 %

NaCl, which is close to the optimum condition. Birefringence might indicate that liquid crystalline material is present. The lamellar liquid crystalline phase might be expected near optimum salinity where spontaneous curvature of the surfactant films is near zero. Some liquid crystalline phases are very viscous and may not propagate through porous media. Several experiments were done using different viscometers. With both the Brookfield Couette viscometer and the RDA III cone and plate rheometer, the viscosities of the birefringent lower phase at 3.2% NaCl for different shear rates were measured. Figure 3.21 indicates that this birefringent solution is a Newtonian fluid with roughly the viscosity of water. The viscosity is 1.07 cP ± 0.07 at shear rates of 100-1000 $s^{-1}$. For lower shear rates (< 60 $sec^{-1}$) uncertainty in viscosity increases owing to less accuracy in measuring torques, but it never exceeds ±20%. Thus, the sample with strong birefringence is not highly viscous. It may be that liquid crystalline material is dispersed (perhaps along with some oil drops) in the lower phase microemulsion. But it won't affect the viscosity. No birefringence was observed for PBB oil and SWCQ oil probably because the phases were so dark in those systems that it could be observed.

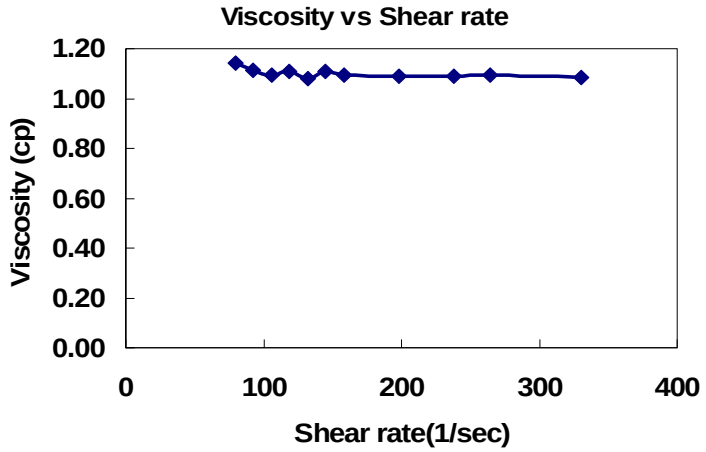


**Figure 3.21 Viscosities of 0.2% NI / 1% $Na_2CO_3$/ 3.2% NaCl at varied shear rates**

*Chapter* 4

# Interfacial Tension Properties of Alkaline Surfactant System

This chapter shows the IFT properties of alkaline surfactant system. An equilibrium spinning drop IFT measurement protocol for alkaline surfactant system is provided. Experimental results show that there is much wider low IFT region in alkali surfactant system than in the system without alkali. The correlation of IFT and phase behavior is also discussed in this chapter.

## 4.1 IFT Measurement Methods

There are many IFT measurement methods, such as capillary rise, Wilhelmy plate, Du Noüy Ring method, spinning drop, pendant/sessile drop, maximum bubble pressure method, etc. (Miller and Neogi, 1985; Holmberg, 2001). In this thesis, pendant drop is used for measuring relatively high tension samples (above 1 mN/m); spinning drop is for the low tension samples.

### 4.1.1 Pendant Drop Method

The pendant drop method, which is based on geometric analysis of the interface of the drop, is performed on a drop of liquid surrounded by the other phase. This method is widely used in determining the relatively high IFT system because the pendant drop is

not stable at ultra-low tension. Lin and Hwang (1994) tried to measure ultra-low tensions with pendant drop method, but it is still very difficult to measure the tension that is less than $10^{-2}$ mN/m. A typical crude oil/brine interfacial tension is around 20-30 mN/m. Pendant drop method is very accurate in this tension area. Therefore, it is chosen to measure the measure crude oil/brine interfacial tensions.

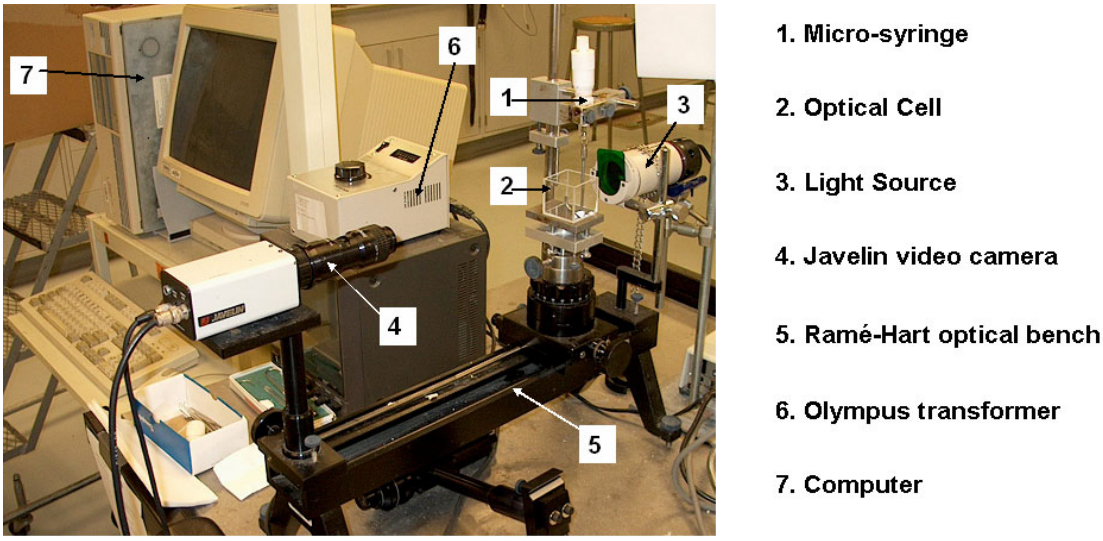


**Figure 4.1 Pendant drop apparatus**

Figure 4.1 is the pendant drop apparatus. The micro-syringe, optical cell and a Javelin video camera sit on a Ramé-Hart optical bench. During the pendant drop measurement, the syringe is filled with the crude oil and the optical cell is filled with brine. A U-shaped needle is connected to the micro syringe and is submerged by the brine. The volume of oil drop can be controlled by manipulating the micro syringe. The size of oil drop affects the measurement accuracy. Larger size will give more accurate result. However, it is difficult to hold larger size drop for longer duration. Thus, a compromise drop size should be selected. The other factor that influences the experiments' accuracy is the needle size. It should be chosen to be approximately equal

to the capillary constant $a$ (Adamson, 1976) in equation (4.1). The needle diameter should be as close as possible to match the capillary constant so that a more accurate IFT can be measured.

$$a = \sqrt{\frac{\sigma}{(\Delta\rho)g}} \tag{4.1}$$

where $\sigma$ is the interfacial tension between oil and brine

$\Delta\rho$ represents the density difference between the two fluids.

The light source behind the optical cell provides the illumination. The light intensity is adjusted by the Olympus transformer. The Javelin camera takes the pictures of the pendant drop, which are transferred to the computer. Figure 4.2 is a typical pendant drop image acquired by the camera. The software in the computer digitizes the picture and fits the interface curve with Young-Laplace equation. Finally, the IFTs are computed based on the curve-fitting.

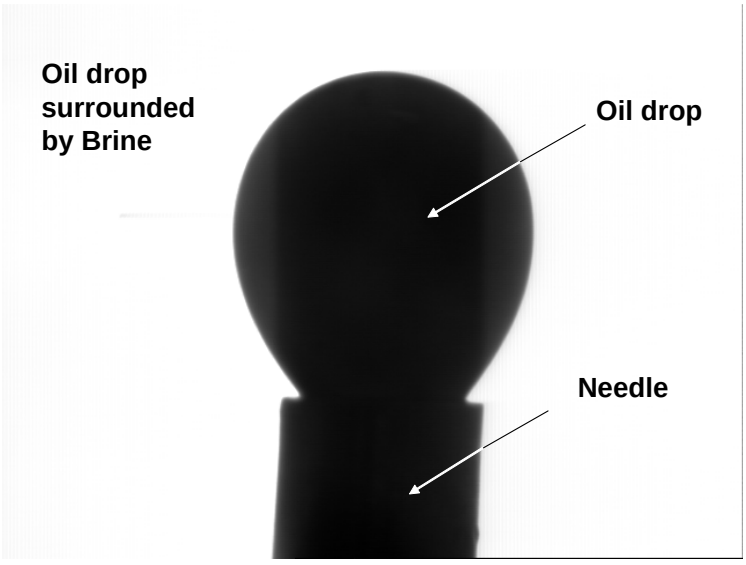


**Figure 4.2 A typical pendant drop image acquired by camera**

### 4.1.2 Spinning Drop Method

Spinning drop method is generally known as a good IFT measurement for ultra-low tension system. In this method, two immiscible fluids are placed in a capillary tube, which is rotated, as shown in figure 4.3. Fluid A is the less dense fluid, while fluid B is more dense fluid. The centrifugal field generated by rotation forces the less dense fluid to stay in the center of the capillary tube to form an elongated drop. The configuration of the drop is determined by the balance of the centrifugal force and interfacial tension force. The centrifugal force elongates the drop, while the IFT suppresses this elongation to minimize the interfacial area. For a cylindrical drop whose length is at least four times greater than its radius, the following expression is often used to calculate IFT

$$\sigma = \frac{\Delta\rho\omega^2 r^3}{4} \qquad \text{(Miller and Neogi, 1985)} \qquad (4.2)$$

where $\sigma$: interfacial tension,

$\Delta\rho$: density difference of the two fluids,

ω: rotation rate,

$r$: the radius of the less dense drop.

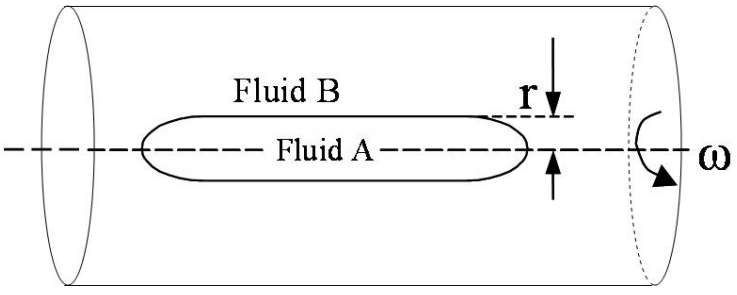


**Figure 4.3 Schematic of the spinning drop method (Adapted form Miller and Neogi, 1985)**

Figure 4.4 shows the spinning drop apparatus. During the spinning drop measurement, the capillary tube with two fluids is located in the spinning tube holder, which can provide temperature control. A Motormatic® motor, which is controlled by the Model 300 Tensiometer, Model 300, rotates the capillary tube. The rotating speed can be manipulated and read by the tensiometer. With the synchronous light source, a Javelin video camera acquires the image of the spinning drop and transfers it to the monitor. The diameter of the spinning drop can be read on the monitor and the pictures of spinning drop can be recorded by the recorder. The diameter read on the monitor is not the exact diameter of the spinning drop because of the refraction of light by more dense fluid. By measuring the refractive index of more dense fluid, usually the aqueous phase, the actual diameter of the spinning drop can be calculated by dividing the value read on the monitor by the refractive index. With the densities of the two fluids, the IFT can be calculated by equation (4.2)

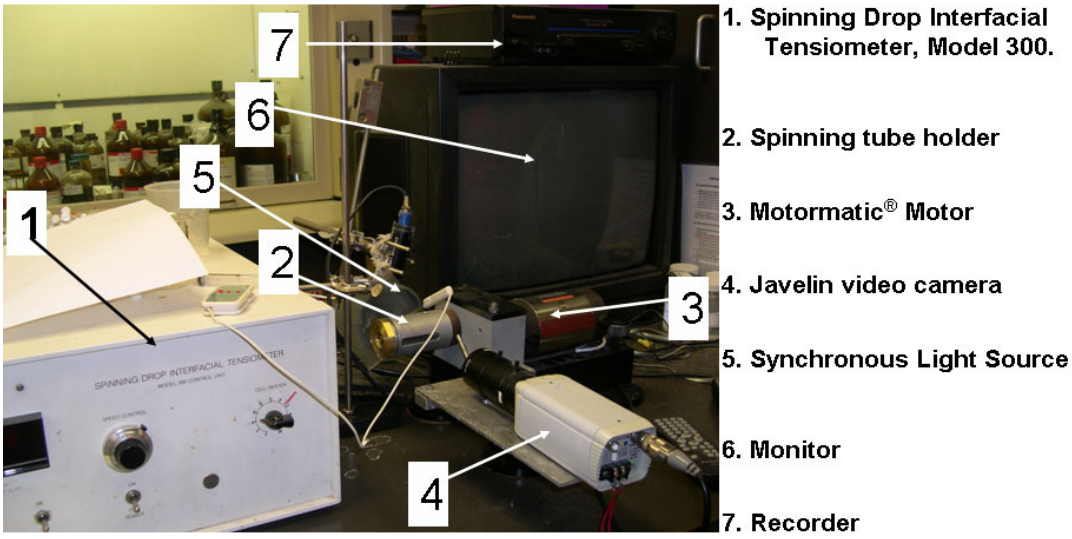


**Figure 4.4 Spinning drop apparatus**

## 4.2 Interfacial Tension of Crude Oil and Brine

To investigate the interfacial properties of crude oil and brine, the crude oil sample should be representative without any contamination, such as emulsion breaker, scale inhibitor, or rust inhibitor. It is necessary to test oil contamination as the first step. Measuring transient interfacial tension at crude oil and brine interface by pendant drop method is a simple way to test for contamination.

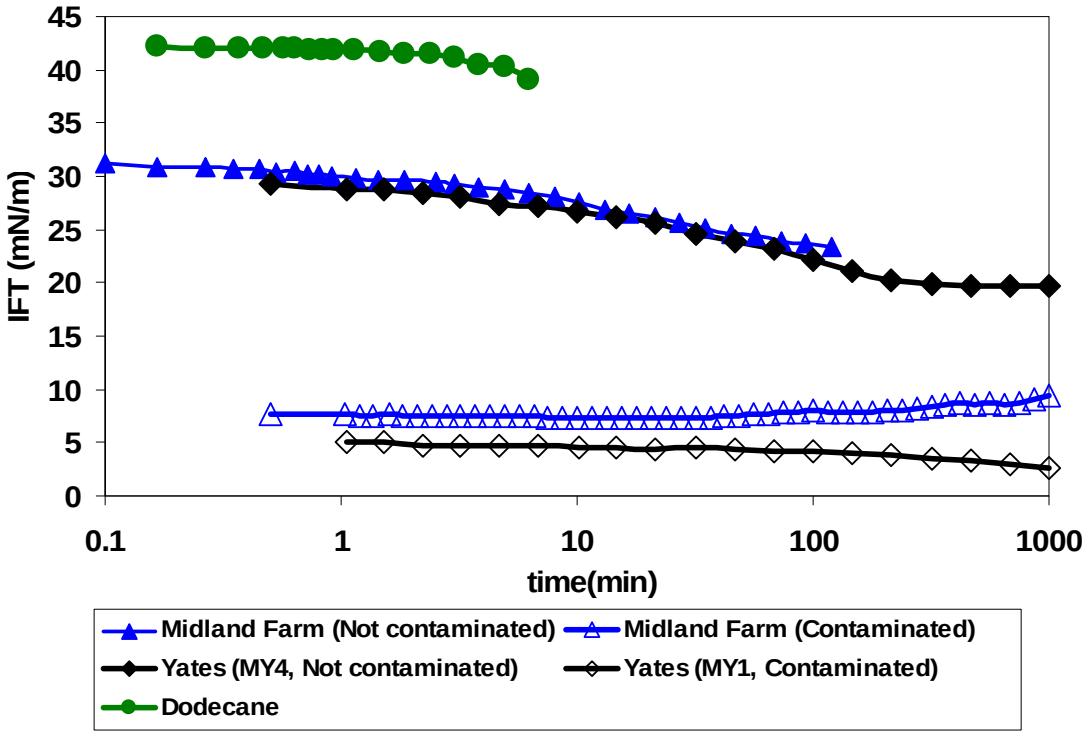


**Figure 4.5 Transient crude oil/brine IFT**

Four crude oil samples and one synthetic oil sample were tested at ambient temperature. The measured dodecane (99 %+) and brine sample value is around 43 mN/m, which is close to the literature value 50 mN/m (Zeppieri et al. 2001). The difference of the experimental value and literature value may come from the impurities in

the oil. The contaminated crude oil samples have much lower IFT than those that were not contaminated. The IFT of contaminated Yates oil is 5 mN/m; while the value of uncontaminated sample is around 25 mN/m. Midland Farm oil has similar result. Contaminated oil IFT is 7 mN/m, while the uncontaminated IFT is the same magnitude as uncontaminated Yates oil. Because impurities significantly change the IFT and other properties, it is very important to test the oil for contamination before further studying it.

## 4.3 Interfacial Tension of Alkali Surfactant Systems

### 4.3.1 Interfacial Tension and Colloidal Dispersion of Alkali Surfactant System

As discussed in Chapter 2, achieving ultra-low tension is the main mechanism to recover the oil. To optimize an alkali surfactant process, it is very important to study the IFT properties of the system.

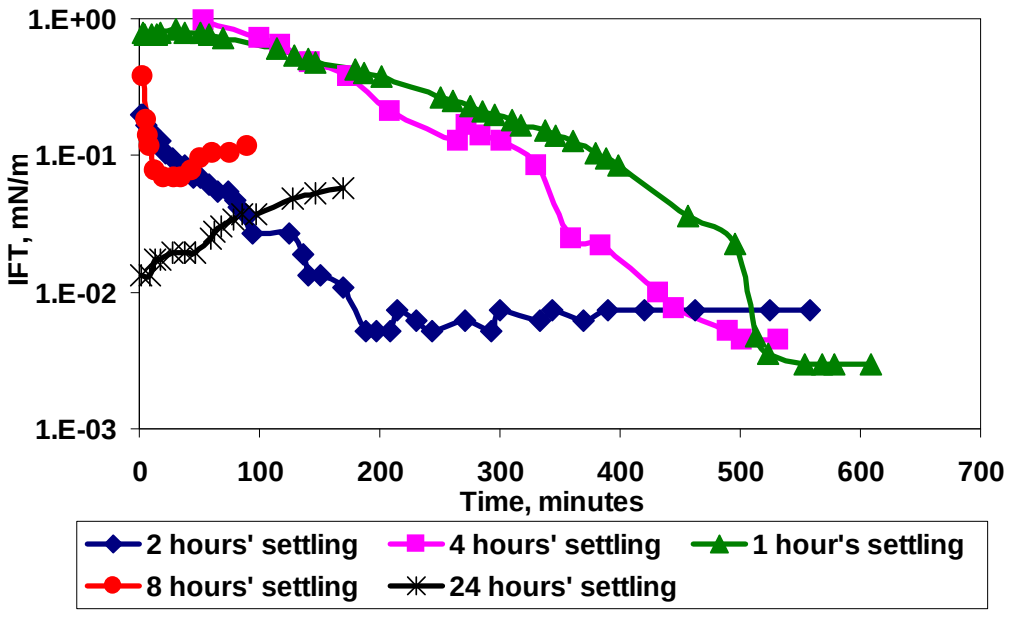


**Figure 4.6 Dependence of IFT on settling time of 0.2 wt% NI blend / 1% $Na_2CO_3$ / 2.0% NaCl.**

For the phase behavior scan of 0.2 wt% NI blend / 1% $Na_2CO_3$ / x% NaCl (see figure 3.6), it was found that below optimal salinity, measured tensions between the lower phase and excess oil depended on the settling time between the end of the mixing process and the sampling of the lower phase (well below the interface) and excess oil as figure 4.6 illustrates. From this figure, low tensions below 0.01 mN/m could be achieved only for settling times of about four hours or less. Similar phenomena were observed in TC blend and Yates oil system (Zhang, 2006). IFT went up more than an order of magnitude when settling time is increased.

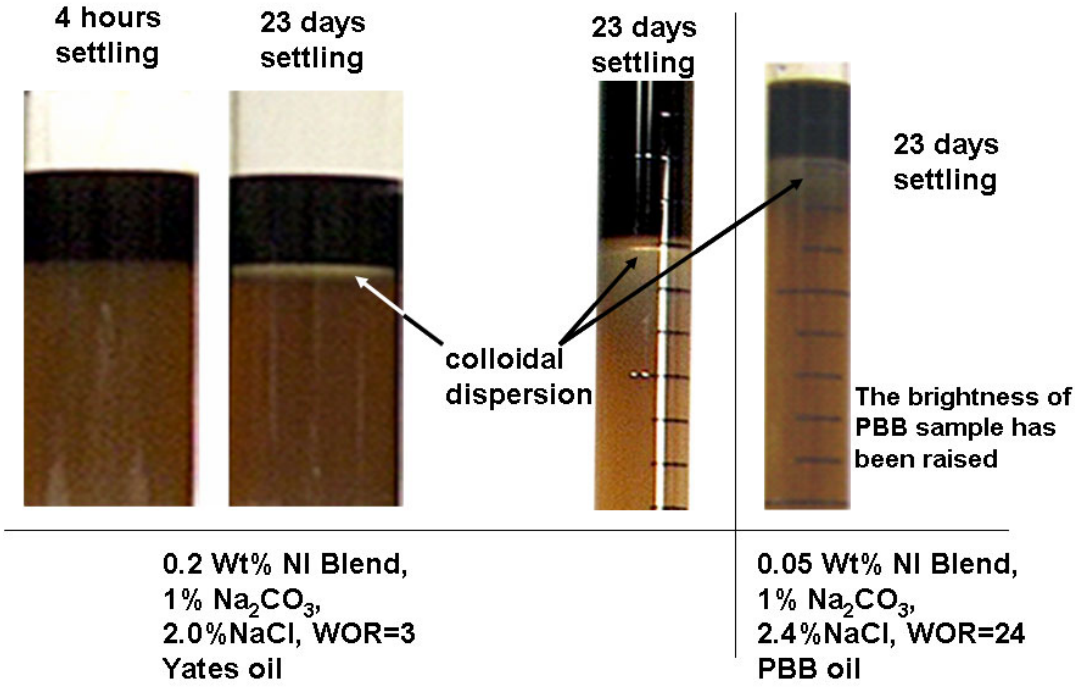


**Figure 4.7 View of dispersion region near interface for sample from Yates oil and PBB oil.**

Observation of those Yates oil samples with different settling times reveals that there is a thin layer of a colloidal dispersion formed with longer settling time as shown in the left part of figure 4.7. After 4 hours settling, no colloidal dispersion was observed; while after 23 days settling, a layer settled between the excess oil and lower phase

microemulsion. The colloidal dispersion is not simply a collection of drops with the same composition as the crude oil that have not yet coalesced with the excess oil phase because the colloidal dispersion will not coalesced either by much longer settling time (>12 months) or by centrifuging. More important, the presence of colloidal dispersion affects IFT, so its composition must be different from oil. The colloidal dispersion might be a microemulsion phase with higher ratio of oil to brine than the lower phase. For the same surfactant concentration, the volume of colloidal dispersion was significantly greater at WOR=1, which contained more soap and less surfactant. This result implies that the amount of colloidal dispersed material is related to the soap amount. Not only the Yates oil, but the PBB oil samples also have similar colloidal dispersion as the right part of figure 4.7 shows. The brightness of the PBB sample has been raised so that the colloidal dispersion can be distinguished from the lower phase. The colloidal dispersion was also observed in the lower phase region of SWCQ oil as well. The colloidal dispersion can also be observed during spinning drop interfacial tension measurements for samples with Yates oil whose settling time is no longer than 4 hours. Figure 4.8 shows that during spinning drop tension measurement of 0.2 % NI blend/1% $Na_2CO_3$ /2% NaCl after 4 hours settling time, there are three regions: aqueous phase, middle layer (colloidal dispersion) and oil. For the samples with longer settling time, the low tensions could be achieved if the colloidal dispersion was added into the system. This also indicates that the colloidal dispersion is necessary for reaching ultra-low tensions at under-optimum conditions.

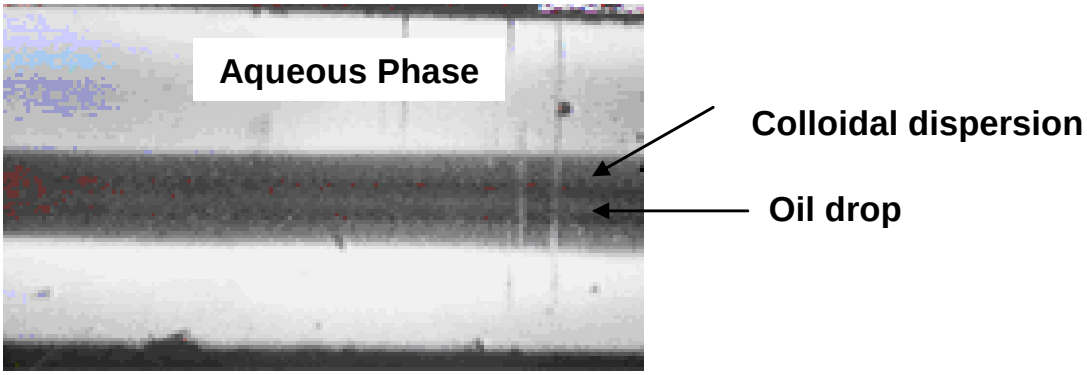


**Figure 4.8 Colloidal dispersion in spinning drop measurement after 2 hours spinning (0.2 % NI /1% $Na_2CO_3$/2% NaCl/Yates oil, 4 hours' settling sample).**

The microstructures of colloidal dispersion and lower phase microemulsion are different as figure 4.9 shows. The sample was the alkaline/surfactant solution which contained 0.2% NI blend, 1% $Na_2CO_3$ and 2% NaCl mixed with Yates oil (WOR=3). After 24 hours mixing, the lower phase was sampled by syringe and put into spinning tube to centrifuge. The colloidal dispersion and clear lower phase separated after centrifuging in the tensiometer. These two regions were sampled and sealed into different capillary chambers. The photos were taken under the microscope. In the colloidal dispersion, the concentration of dispersed drops is much more than that in clear lower phase. The sizes of most drops in colloidal dispersion are around 1 micron. In the clear lower phase, there are a few vesicles. Those vesicles are not oil drops because they did not settle after centrifuging.

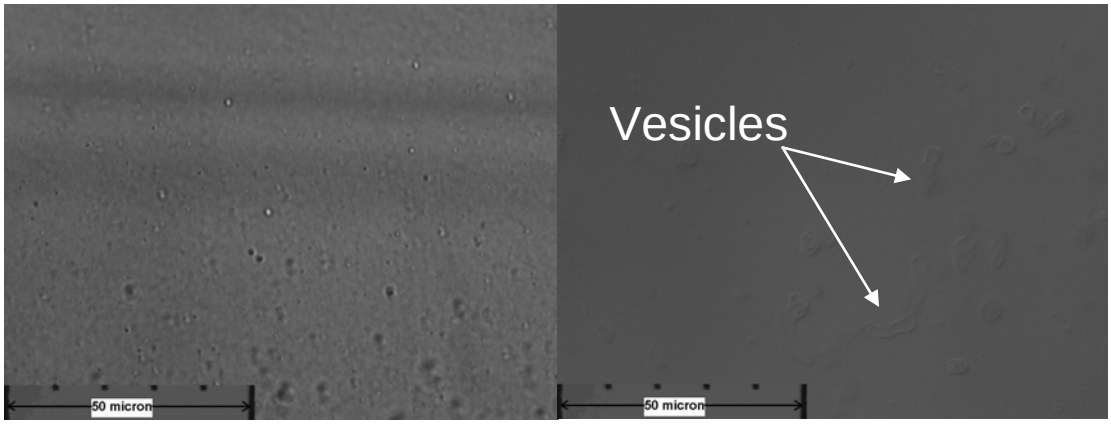


Colloidal Dispersion Lower phase microemulsion

**Figure 4.9 Microstructure of colloidal dispersion and lower phase microemulsion (0.2 % NI blend/1% $Na_2CO_3$/2% NaCl/Yates oil)**

Figure 4.10 shows how the drop diameter changes during the spinning drop measurement, which indicates that IFT changes. It is also evidence that colloidal dispersion has the key role for low tension. When colloidal dispersion covers the oil drop, the low tension is reached. However, too much colloidal dispersion will obscure the oil drop during the spinning drop measurement. An example of the this obscuring effect is shown in Figure 4.11, where the oil drop at the far left is almost invisible in the colloidal dispersion cloud.

Based on this relationship of colloidal dispersion and interfacial tension, a protocol given in the next section was developed to assure that enough of the colloidal dispersion was initially present in the lower phase sample to achieve low tensions but not so much as to obscure the oil drop during the spinning drop measurement.

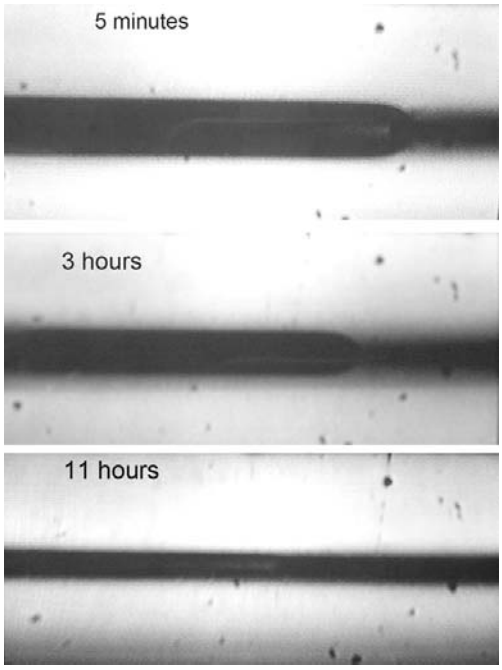


**Figure 4.10 Photos of spinning drop of IFT of 0.2% NI blend / 1% $Na_2CO_3$ / 2% NaCl/Yates oil/WOR=3 at different time**

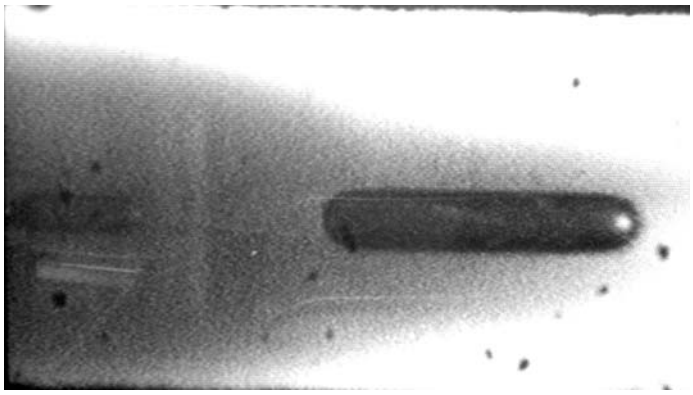

**Figure 4.11 View of cloud of dispersed material nearly obscuring drop at far left but not that at right during spinning drop experiment**

### 4.3.2 Spinning Drop IFT Experimental Protocol for Alkali Surfactant Crude System

The results in previous section show that colloidal dispersion is very important for the IFT measurement. And the spinning oil drop cannot be seen if the colloidal dispersion surrounds the oil drop and extends to the end of the tube. The oil drops in figures 4.10

and 4.11 can be seen because the amount of colloidal dispersion is no more than the amount of oil drop. The colloidal dispersion needs time to coalesce with and occupy the oil-water interface. It's better to let the oil drop and the colloidal dispersion settle in the spinning tube for some time before the spinning experiments. Otherwise, a longer spinning time is needed to reach equilibrium IFT.

A standard protocol, which can quickly provide reproducible equilibrium IFT values, is introduced. Some aspects of the protocol such as the rotation, settling, and pre-equilibration times of steps 2, 3, and 6 are specific for the NI blend and Yates oil system, but the basic procedure should be useful in other systems with similar behavior. The spinning drop IFT experiments should be conducted as follows:

1. Mix the crude oil with the alkaline surfactant solutions containing 0.2% NI blend, 1% $Na_2CO_3$ and varied salinities at WOR = 3.

2. Rotate the mixture for 24 hours to reach equilibrium.

3. After letting the mixture settle for 4 hours, take samples of oleic and aqueous phases into different syringes.

4. Since these samples may continue to settle and the settling time in the two syringes may be different, shake them before the IFT spinning drop measurement, so that they can be considered as the same sample that was obtained after 4 hours settling.

5. Put some of the aqueous phase (but no oil) into the capillary tube for the spinning drop device and centrifuge it in the device. Remove some of the colloidal dispersion from the central portion of the capillary tube because the sample will be too dark if too much colloidal dispersion is left. The remaining colloidal dispersion should

have slightly less volume than the volume of the excess oil drop that is added into the spinning drop tube.

6. Inject an equilibrated excess oil drop into the vertically oriented tube and let it settle for some time (~12 hours), so that the colloidal dispersion can equilibrate with the oil and the lower phase microemulsion.

7. Begin the spinning drop IFT measurement.

Step 5 is to make sure that the colloidal dispersion is enough to achieve low tension without obscuring the oil drop. Step 6 is to reduce the time that is needed to reach the equilibrium low tension as shown in figure 4.12. Without step 6, it took at least 3 hours (0% NaCl) to reach the equilibrium IFT. By applying step 6, less than 30 minutes was needed to reach the equilibrium.

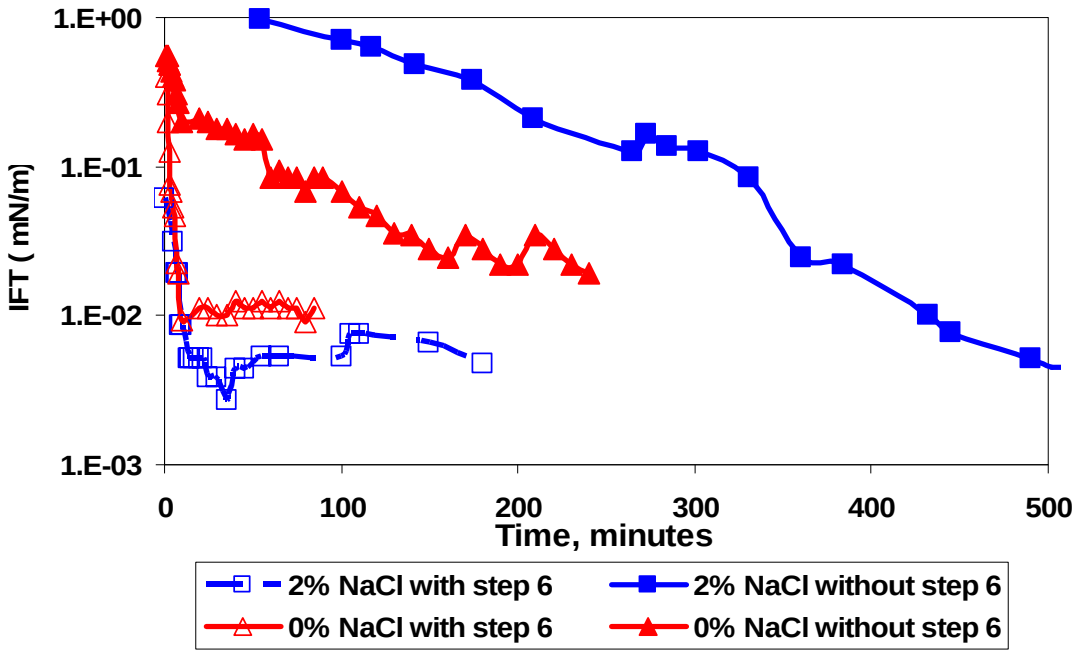


**Figure 4.12 Step 6 in protocol reduces the time to reach the equilibrium for 0.2 % NI blend/1% $Na_2CO_3$/Yates oil/x% NaCl/WOR=3**

Figure 4.13 just shows again that low tensions are not seen if the colloidal dispersion is absent due either to long settling times or to the complete removal after centrifuging the aqueous phase and concentrating the colloidal dispersion in the spinning drop device before adding an oil drop. The two lower curves indicate that step 6 of the protocol that is the pre-equilibration of oil drop and aqueous phase in the spinning drop tube before spinning will not affect the equilibrium IFT value. This step just can significantly reduce the time to reach equilibrium as in Figure 4.12.

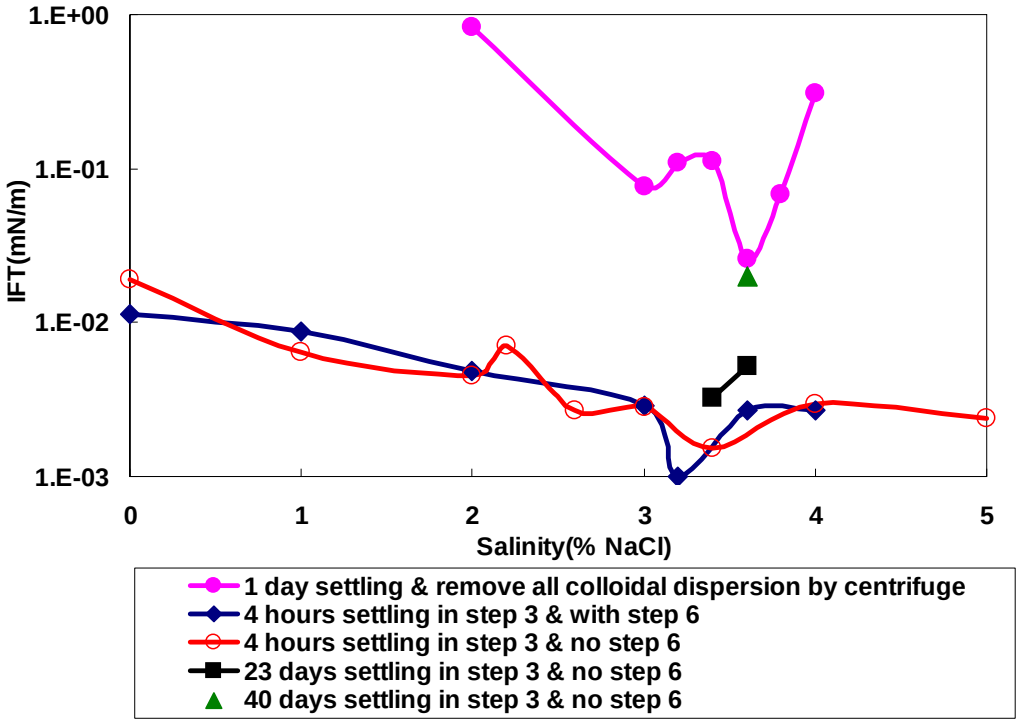


**Figure 4.13 IFT for salinity scan of 0.2% NI blend/1% $Na_2CO_3$/Yates/x% NaCl /WOR=3 with different settling times and procedures.**

### 4.3.3 Width of Low IFT Region of Alkali Surfactant System

The generation of soap will significantly change the width of low tension region as figure 4.14 shows. IFT values without presence of $Na_2CO_3$ were below 0.01 mN/m

over a much narrower range of NaCl concentrations than those with $Na_2CO_3$. This result indicates that the wide range of low tensions with alkali present is a consequence of formation of naphthenic soaps. Levitt et al. (2006) also claimed similar result for Midland Farms oil from their phase behavior evaluation although they did not measure the exact IFT value. Their results show that the salinity region with high solubilization ratios is wider when $Na_2CO_3$ is added into the system. In Chapter 6, it is shown that the wider low tension region is beneficial to oil recovery in ASP system.

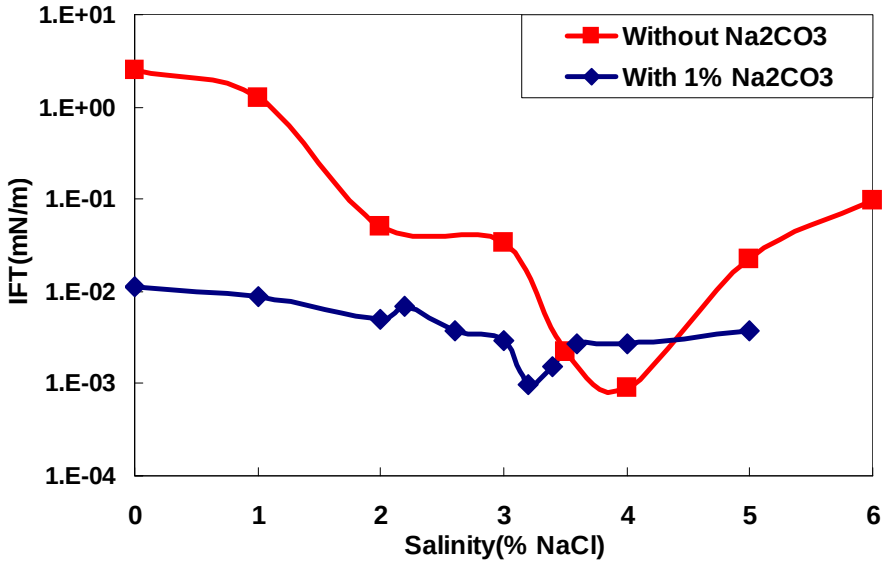


**Figure 4.14 IFT for 0.2% NI blend/Yates oil/WOR=3 with and without $Na_2CO_3$.**

### 4.3.4 Correlation between Phase Behavior and IFT

As already discussed in Chapter 2, IFT is related to the solubilization ratio that can be described by equation (4.3).

$$\sigma = \frac{C}{(V_i / V_s)^2} \quad \text{(Huh, 1979)} \qquad (4.3)$$

where $\sigma$: Interfacial tension (IFT)

$V_i/V_s$: Solubilization ratio

$C$: A constant with a typical value of 0.3.

The solubilization ratio ($V_o/V_s$) is the ratio of solubilized oil volume to surfactant volume present (excluding soap) for the under-optimum samples. The volume of solubilized oil can be measured by the difference between the volume of the initial oil in the sample and that of the excess oil phase after equilibration. It represents a composite value for the combined lower or middle phase microemulsion and colloidal dispersion phase. As figure 4.15 shows for the salinity scan of 0.2% NI blend//1% $Na_2CO_3$/Yates oil/WOR=3, solubilization ratio ($V_o/V_s$) increases from about 7 at 2% NaCl to about 20 at 3.4% NaCl, just below optimal salinity. For over-optimal samples, a similar calculation can be made to obtain the value ($V_w/V_s$). Similar values were found for a scan with 0.5 wt% NI blend except that the salinities were higher with optimal salinity approximately 4.5% NaCl because the soap-to-surfactant ratio was smaller (Liu et al., 2006).

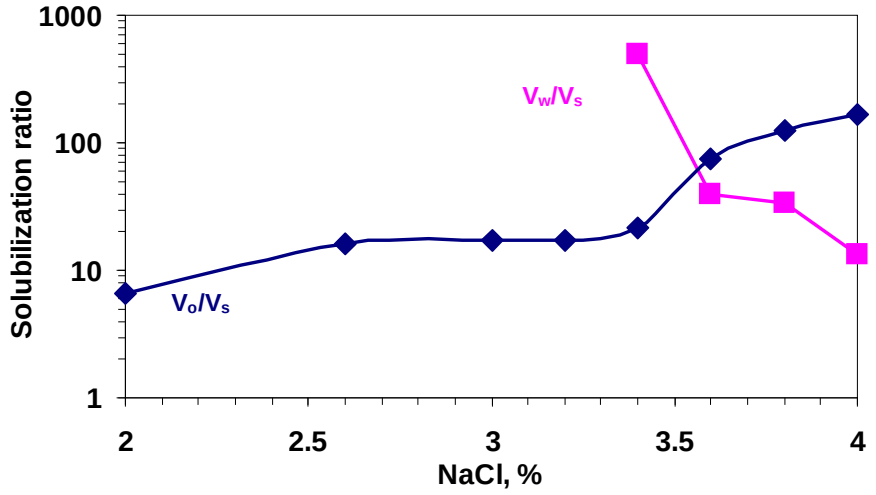


**Figure 4.15 Solubilization ratios for 0.2% NI blend//1% $Na_2CO_3$/Yates oil/WOR=3**

In Huh's correlation, ($V_o/V_s$) is used for calculating the IFT between microemulsion and excess phase when the salinities are below the optimum condition and ($V_w/V_s$) is used as the solubilization ratio when the salinities are above the optimum condition. With the solubilization ratios and Huh's correlation, the predicted IFT values are shown in figure 4.16. The experimental IFT values are in good agreement with the predicted values from solubilization ratios except at 3.6%-3.8% NaCl where the measured value is higher. However, the measured value is ultra-low (around $10^{-3}$ mN/m) and can mobilize oil.

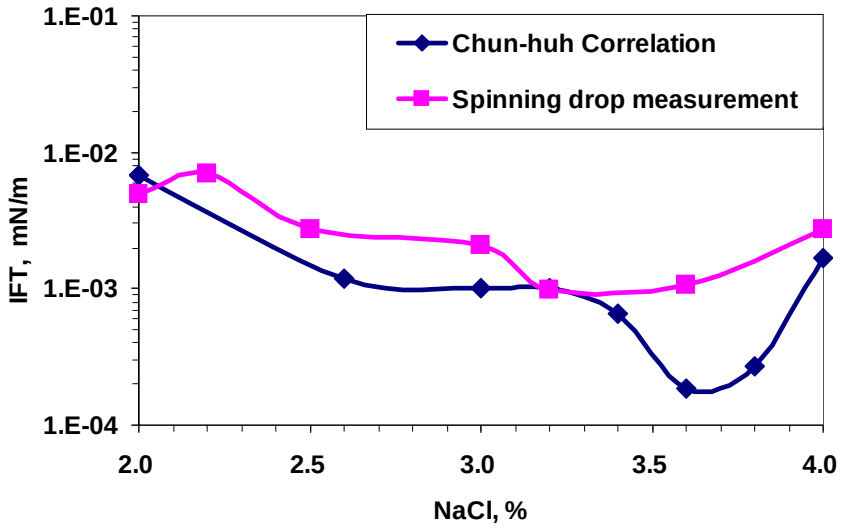


**Figure 4.16 Comparison the IFT predicted from solubilization ratios and measured IFT for 0.2% NI blend//1% $Na_2CO_3$/Yates oil/WOR=3**

The solubilization ratios of 0.2% NI blend/1% $Na_2CO_3$/Midland Farm oil and WOR=3 samples were also measured by phase behavior scan as shown in figure 4.17. And the predicted IFT values and measured IFT values are shown in figure 4.18. Similar to Yates oil, IFT from the solubilization ratios and the measured IFT are very close to each other.

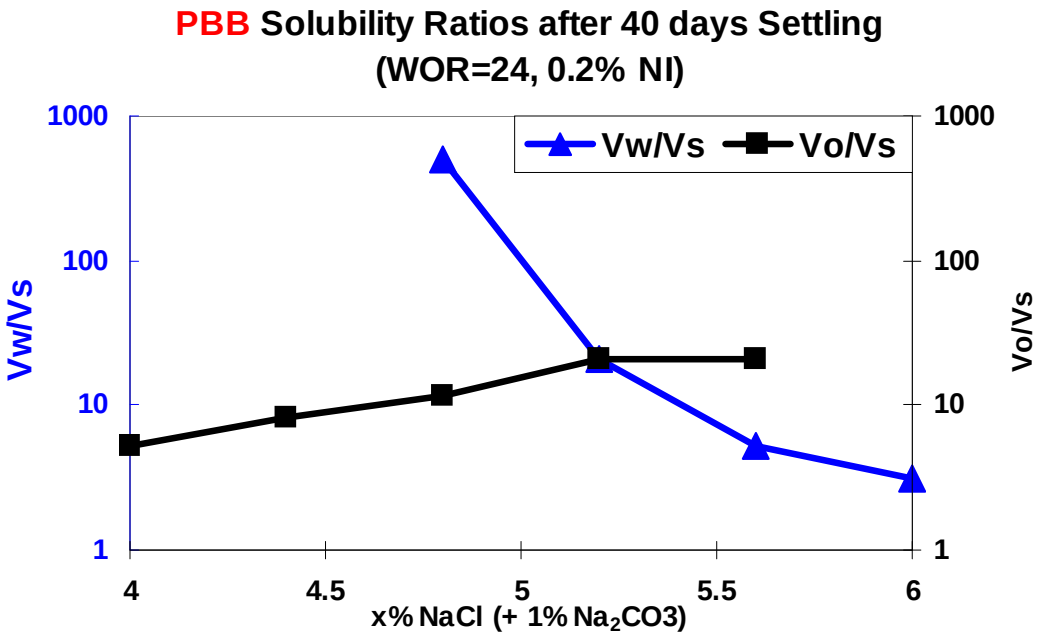


**Figure 4.17 Solubilization ratios for 0.2% NI blend//1% $Na_2CO_3$/Midland Farm oil/WOR=3**

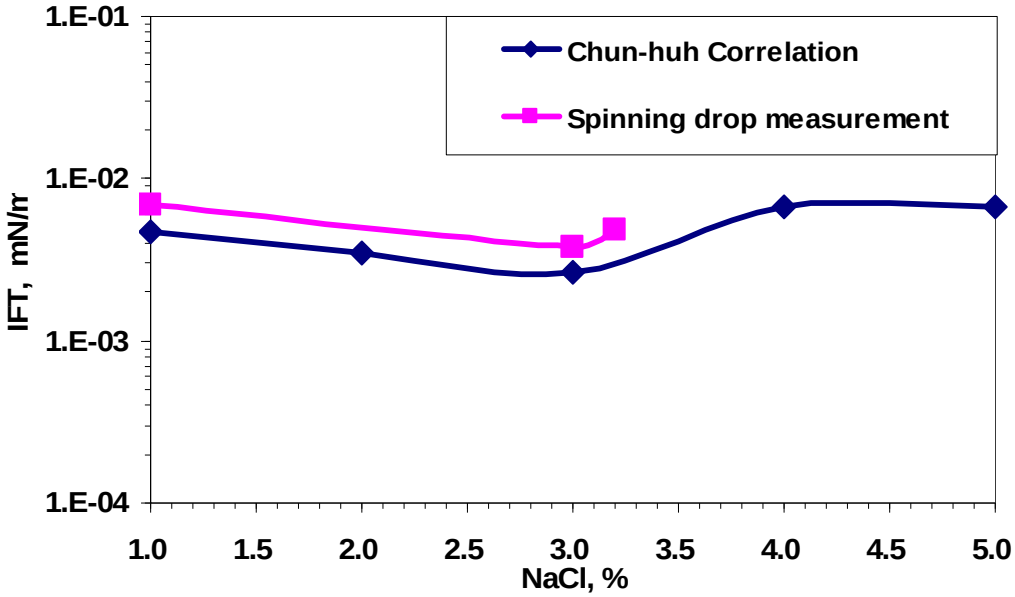


**Figure 4.18 Comparison the IFT predicted from solubilization ratios and measured IFT for 0.2% NI blend//1% $Na_2CO_3$/Midland Farm/WOR=3**

The results for Yates and Midland Farm oil indicate that IFT can be estimated by measuring the solubilization ratios with phase behavior samples. For the PBB oil sample,

the lower phases for under-optimum region are too dark to see through in the spinning drop instrument. As a result, the oil drop diameter could not be measured because the drop is obscured. Then, an alternative method to get the IFT value is with solubilization ratios by observing the phase behavior samples. Also, it is much faster to obtain IFT by using solubilization ratios than by spinning drop measurement. Figure 4.19 shows the solubilization ratios of 0.2% NI blend/1% $Na_2CO_3$/PBB oil and WOR=24. Figure 4.20 is the estimated IFT values from by the solubilization ratios in figure 4.19. The width of the low tension region is from 4.0% NaCl to 5.5% NaCl. Because of the difficulties in accurately measuring the phase volume with such a high WOR (24), salinities lower than 4.0% NaCl or higher than 6.0% NaCl were not included in figure 4.19. The lowest IFT value at optimum condition is still around $10^{-3}$ mN/m. This result suggests that NI blend is also a good IFT reduction agent for PBB oil.

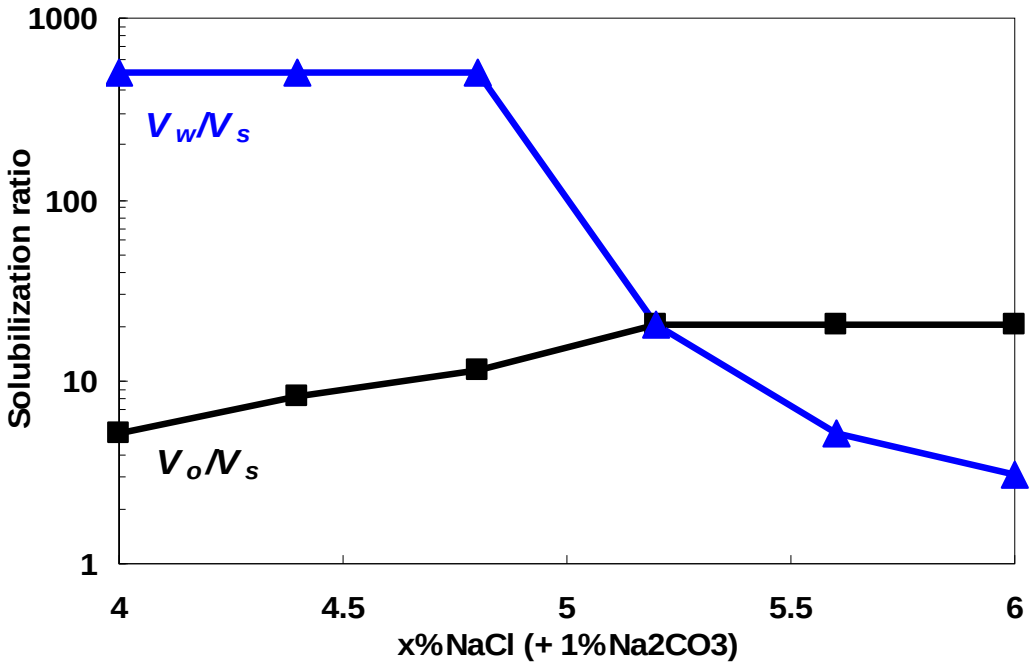


**Figure 4.19 Solubilization ratios for 0.2% NI blend//1% $Na_2CO_3$/PBB oil/WOR=24**

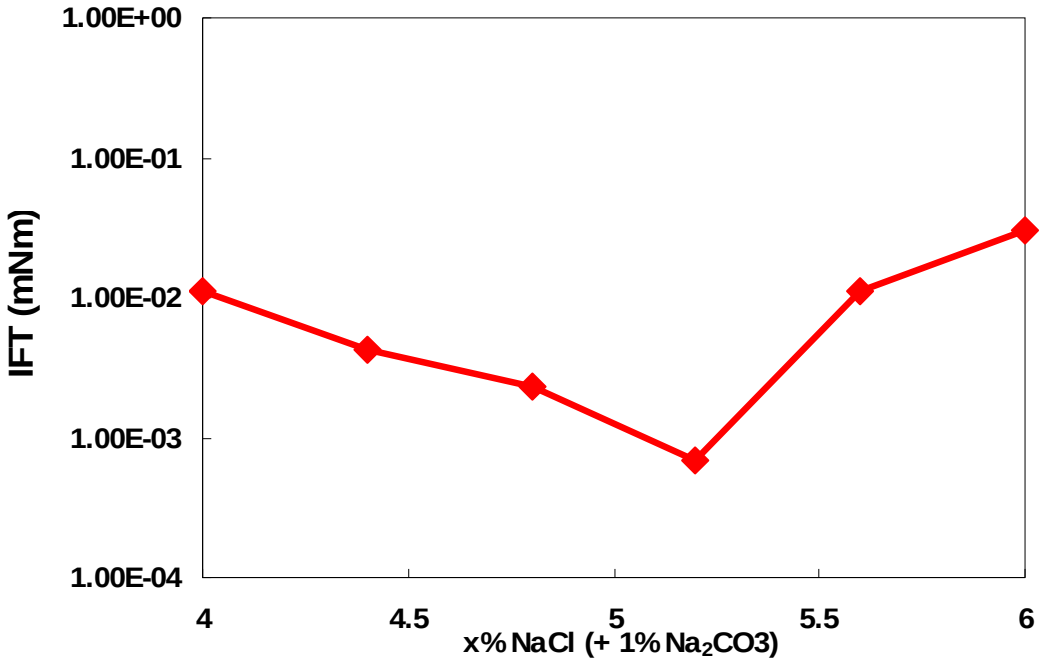


**Figure 4.20 IFT predicted from solubilization ratios for 0.2% NI blend//1% $Na_2CO_3$/PBB oil/WOR=24**

### 4.3.5 Dynamic IFT and equilibrium IFT

All the previous IFT measurements are equilibrium IFT measurements, i.e., the surfactant solution and crude oil has been mixed and reached equilibrium before the spinning drop measurement. However, many researchers have used dynamic IFT measurement, in which a fresh crude oil drop is directly injected into spinning tube with the alkali surfactant solution. If dynamic IFT is for surfactant system without alkali, it might be possibly correct because the optimum condition is not a function of water oil ratio for pure surfactant system. However, it is not suitable for alkali surfactant system because optimum salinity is a function of water oil ratio, as discussed in the previous chapter. If dynamic method is used, it is applicable only for very high water oil ratio because the system consists of only a single oil drop and a whole tube of alkali surfactant

solution. Furthermore, the natural soap is generated at the oil water interface due to the reaction of alkali and naphthenic acid in the oil drop, and the soap and surfactant will transfer to aqueous phase or stay in oleic phase depending on the phase behavior. In many cases, this effect will cause a transient ultra-low tension because soap and surfactant will be at the interface for some time and then desorbed. Figure 4.21 shows an example for dynamic IFT. A fresh oil drop was injected into a spinning tube full of 0.2% NI Blend, 1% $Na_2CO_3$ and 1% NaCl solution at ambient temperature. In this case, it is under-optimum phase behavior because water oil ratio is very high so that the soap to surfactant ratio is very low. The soap is generated at oil water interface and transfers to the aqueous phase. At 20 minutes, most soap was at interface so that an ultra-low tension was observed. When soap left the interface and went to the aqueous phase, the IFT bounced up by approximately two orders of magnitude. IFT will be low at equilibrium only when the aqueous solution is near optimum conditions for the surfactant.

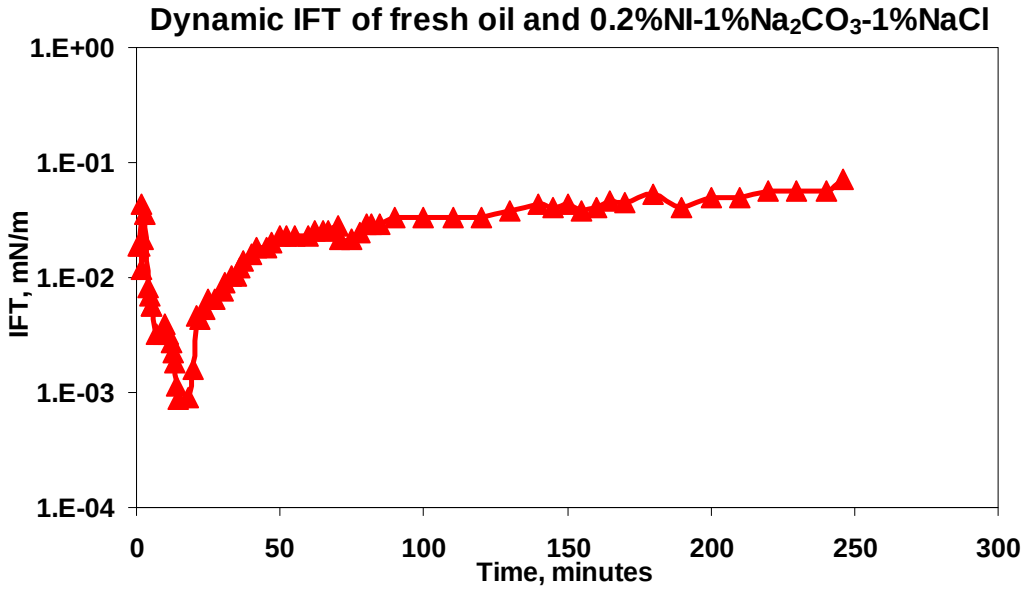


**Figure 4.21 Dynamic IFT of fresh Yates oil and 0.2% NI Blend / 1% $Na_2CO_3$ / 1% NaCl**

In some papers, existence of a transient ultra-low IFT was reported to be an adequate criterion for a good surfactant formulation. As figure 4.21 shows, it is not correct because the real equilibrium IFT might be much higher. In the reservoir, it is not a transient minimal IFT but the equilibrium IFT that generates high capillary number because of the time scale of flooding process. It takes years to finish a flooding process. Therefore, equilibrium IFT as discussed in the previous sections should be used for designing alkali surfactant processes.

*Chapter 5*

# Chemical Consumptions of Alkali Surfactant Process

An ASP process is feasible only when the cost of chemical consumptions is small. It is very crucial to limit the chemical consumptions, such as surfactant adsorption, alkali precipitation. This chapter shows how to measure and control the chemical consumptions.

As discussed in Chapter 2, surfactant adsorption is very important for the surfactant consumption. In this section, both static and dynamic experiments are performed to evaluate the adsorption of surfactant on dolomite. The static test is the bottle test for surfactant adsorption on porous media by shaking and settling. The dynamic experiments are the flow experiments where the breakthrough of the surfactants is compared with that of a non-adsorbing tracer, which is chloride ion determined by conductivity measurement in this research.

## 5.1 Static Adsorption of Surfactant

### 5.1.1 Static Adsorption Experimental Procedure

The static adsorption experiments were performed in the following procedure. The initial surfactant solution has a fixed concentration that can be accurately determined by Potentiometric titration (See Appendix A) with Benzethonium Chloride (hyamine

1622). Then the surfactant solution was mixed with the porous medium, such as calcite powder or dolomite powder, at varied weight ratios in centrifuge tubes. If the powder amount is large so that the powder agglomerates, the Branson® Sonifier 450 can be used to sonicate the powder and solution mixture for at least 1 minute. After the powder was well dispersed in the solution, the samples were put on a rotating shaker and shaken for at least 24 hours. Afterwards, the samples were centrifuged at 3000 rpm for at least 30 minutes. Finally, the equilibrium surfactant concentrations of the liquid phase were determined again by potentiometric titration. By comparing the initial and equilibrium surfactant concentration, the amount of surfactant adsorbed on the surface can be obtained. Because the porous media surface area can be determined by BET adsorption, surfactant adsorption density was calculated. Three carbonate porous medium samples with different surface areas were tested. The three samples are calcite powder (SOCAL31® from Solvay Performance Chemicals, BET area: 17.9 $m^2$/gram), dolomite powder (Carpool® from Earth Safe Organics, BET area: 1.7 $m^2$/gram) and dolomite sand (from Unimin corporation, BET area: 0.3 $m^2$/gram).

### 5.1.2 Static Adsorption Results for Anionic surfactant

Two surfactant formulations, NI blend and TC blend, which have been introduced in Chapter 3, are used to test anionic surfactant adsorption on carbonate.

#### 5.1.2.1 TC Blend

The adsorption of TC blend on dolomite with or without sodium carbonate is shown in Figure 5.1. The initial surfactant concentration was fixed at either 0.05% or 0.1% (active material). The specific surface area of dolomite powder determined by the

BET adsorption is 1.7$m^2$/gram dolomite powder. The adsorption isotherm in the absence of sodium carbonate is similar to a Langmuir adsorption isotherm with a plateau adsorption of about 0.002 mmol/$m^2$ or 1.2 mg (surfactant)/gram (dolomite). Addition of 0.2-0.4 M sodium carbonate reduced the adsorption by a factor of 10 and the saturation plateau is about $2\times10^{-4}$ mmol/$m^2$ or around 0.1 mg (surfactant)/gram (dolomite). This result is consistent with previous results in the adsorption of TC blend on calcite powder, which show sodium carbonate can significantly reduce the adsorption (Hirasaki and Zhang, 2002). The reduction of adsorption may be attributed to change surface charge to negative charge by the addition of carbonate ion, which is a constituent ion of carbonate formation and is a potential determining ion.

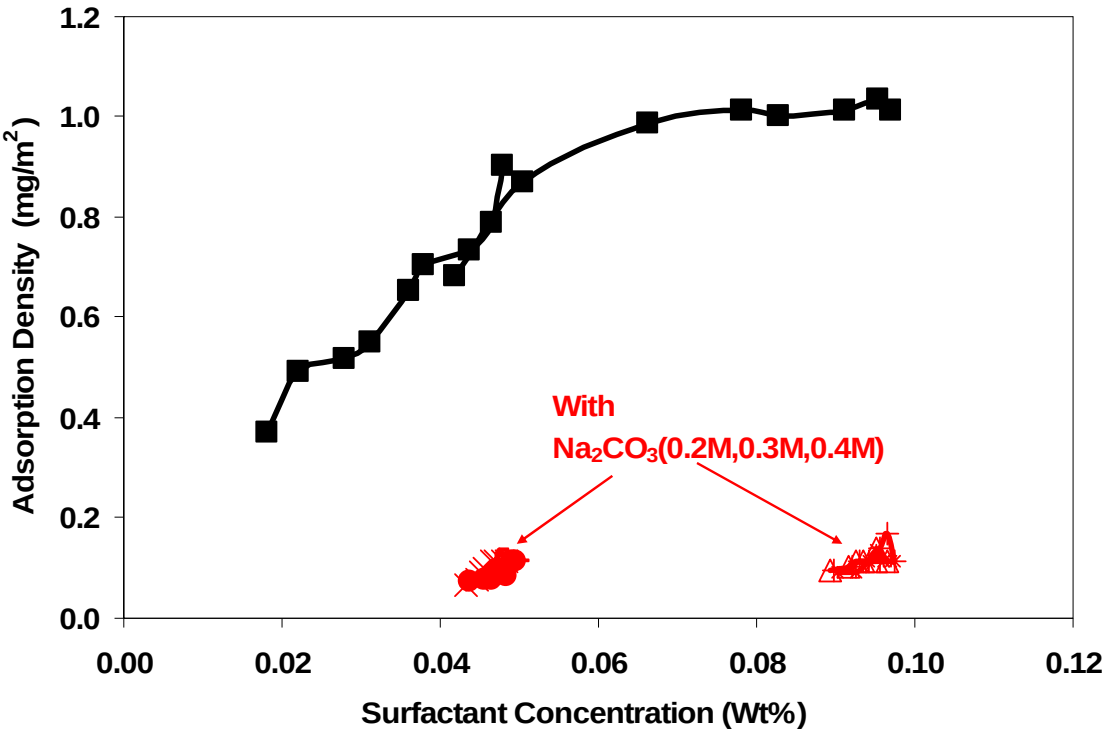


**Figure 5.1 Adsorption on powdered dolomite of TC blend with/without $Na_2CO_3$**

### 5.1.2.2 Test of Other Potential Determining Ions

Other potential determining ions were tested for the adsorption of TC blend on the same dolomite powder (BET 1.7$m^2$/gram). Hydroxyl ion can change the zeta potential of the carbonate/brine interface from positive charge to negative charge by raising the pH (Thompson and Pownall, 1989).

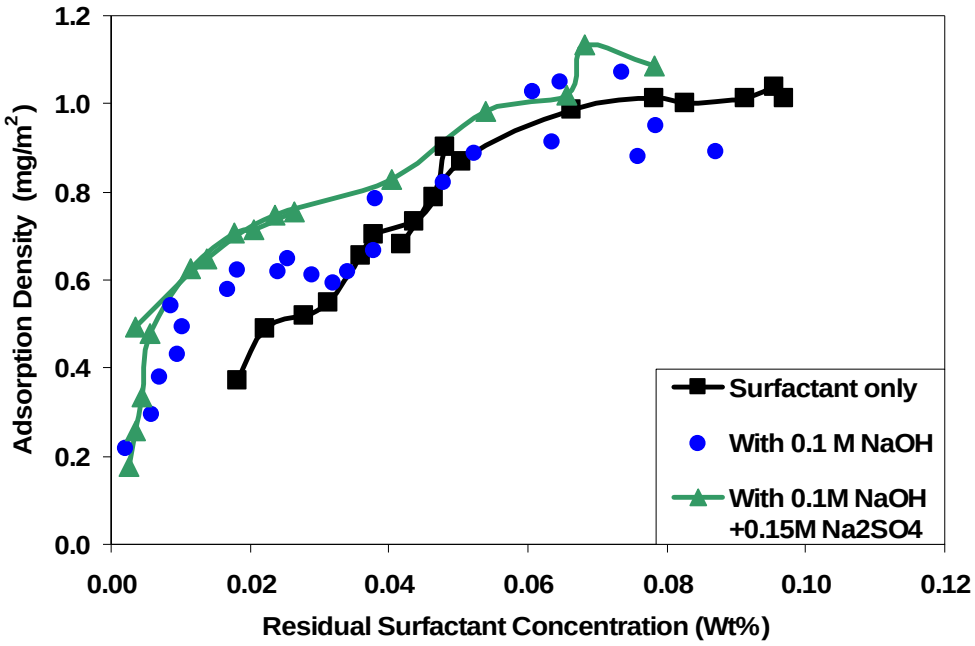


**Figure 5.2 Adsorption of TC blend on dolomite with hydroxyl ion and sulfate ion**

Hydroxyl ion can change the pH so that the zeta potential of the carbonate/brine interface changes from positive charge to negative charge (Thompson and Pownall, 1989). In a fractured chalk formation, Austad and Strand et al. (2005) used sulfate ion to alter the surface potential of chalk surface. However, either hydroxyl ion or sulfate ion could not decrease the surfactant adsorption on dolomite surface. As figures 5.2 shows, the adsorption amount on dolomite surface with these ions is the same as those without any

potential determining ion. It seems that between carbonate, hydroxyl and sulfate ions, only carbonate ion can reduce the adsorption on the dolomite surface.

#### 5.1.2.3 Surfactant Adsorption on Different Surface Area

Surface area of the porous media has remarkable effect on the surfactant adsorption. As mentioned in the previous part, three carbonate porous medium samples with different surface areas were tested. They are calcite powder (17.9 $m^2$/gram), dolomite powder (1.7 $m^2$/gram) and dolomite sand (0.3 $m^2$/gram). Figure 5.3 shows that the adsorptions of TC blend on the three samples are close to each other if the adsorption is calculated by using surfactant adsorption amount per porous media surface area. However, if the adsorption is calculated by using surfactant adsorption amount per porous media weight as in figure 5.4, the adsorptions on the three samples are very different, even though the mineralogy of the three samples is similar. These results imply that it is the surface area, not the weight, of the porous media that should be used to compare the adsorption. For static adsorption experiments, samples with larger surface areas will adsorb more surfactant, so that it is more accurate for adsorption measurement because the difference between the residual surfactant concentration after the surfactant and solid mixing and initial surfactant concentration is significant. Thus, the calcite powder was used in the static adsorption experiments hereafter.

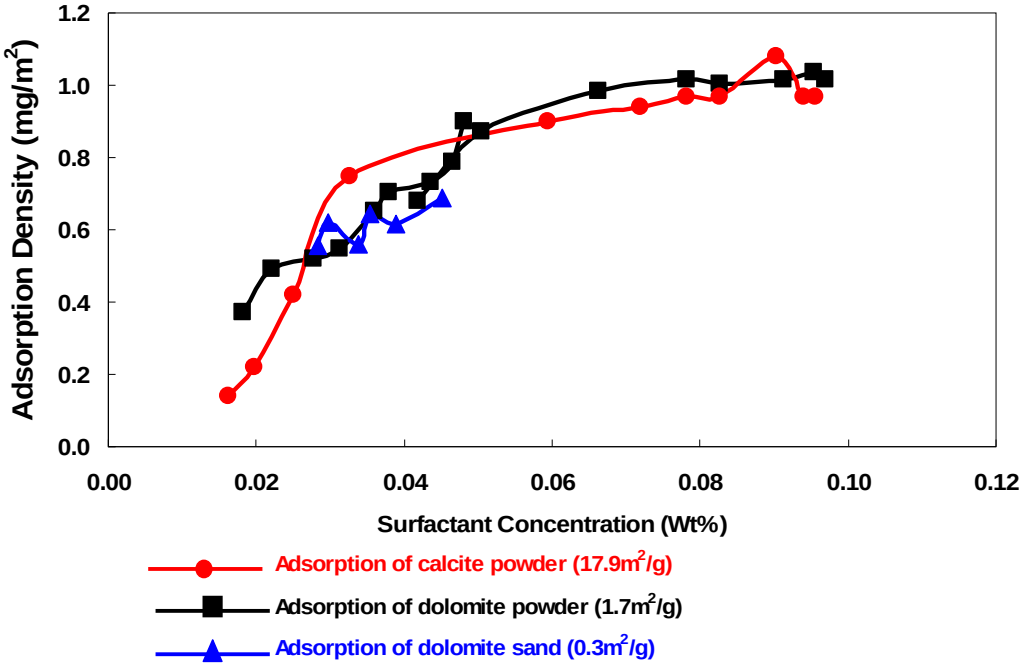


**Figure 5.3 Adsorption of TC blend on different samples per surface area**

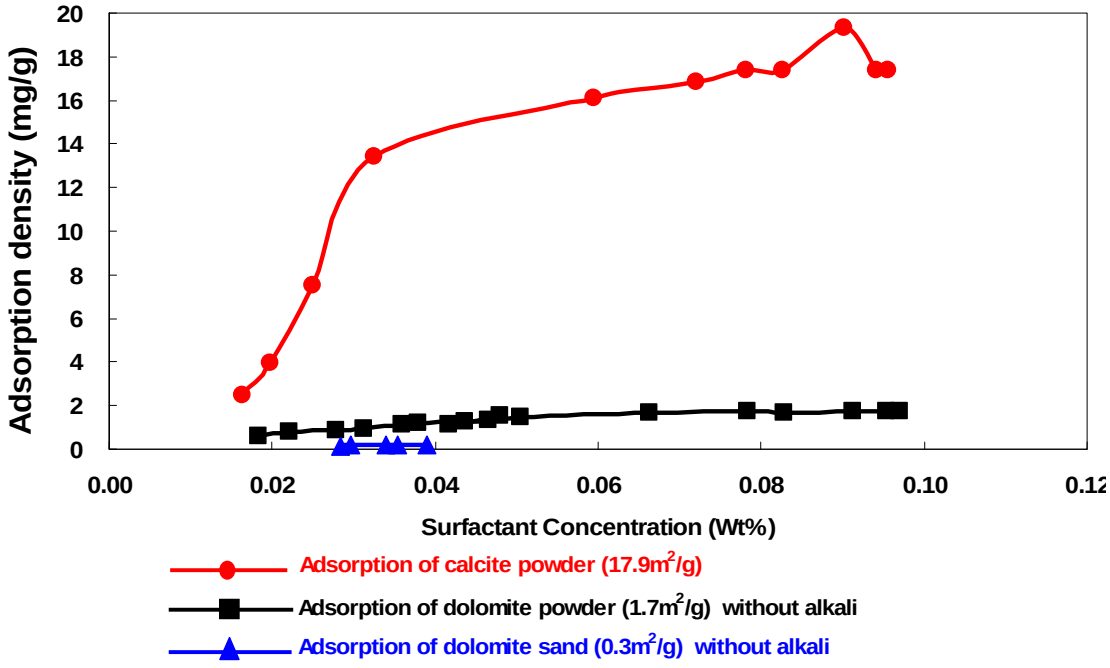


**Figure 5.4 Adsorption of TC blend on different samples by using weight of porous media**

### 5.1.2.4 NI Blend

As introduced in Chapter 3, NI blend is a mixture of N67 and IOS. The adsorption isotherms of N67 and IOS on calcite powder for solutions containing no NaCl and either 0% or 1% $Na_2CO_3$ are shown in figure 5.5 and 5.6. Similar to TC blend, the adsorptions of both N67 and IOS were greatly reduced around an order of magnitude by addition of $Na_2CO_3$ because carbonate ions reverse the charge of the calcite surface from positive to negative so that anionic surfactant ions are repulsed (Zhang et al, 2005).

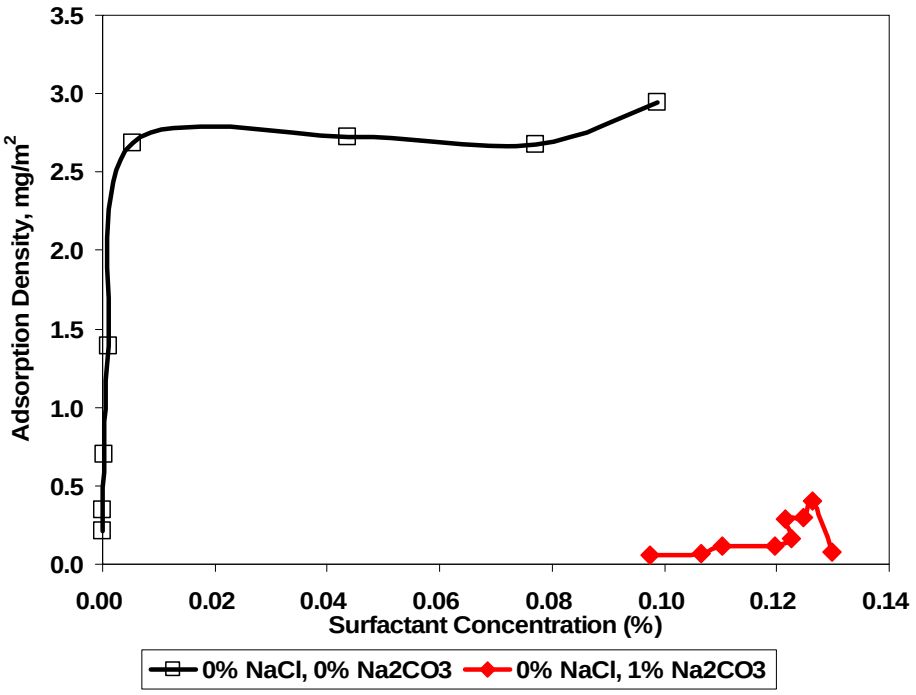


**Figure 5.5 Adsorption of N67 on calcite powder (17.9 $m^2/g$) with or without 1 % $Na_2CO_3$ and with no NaCl.**

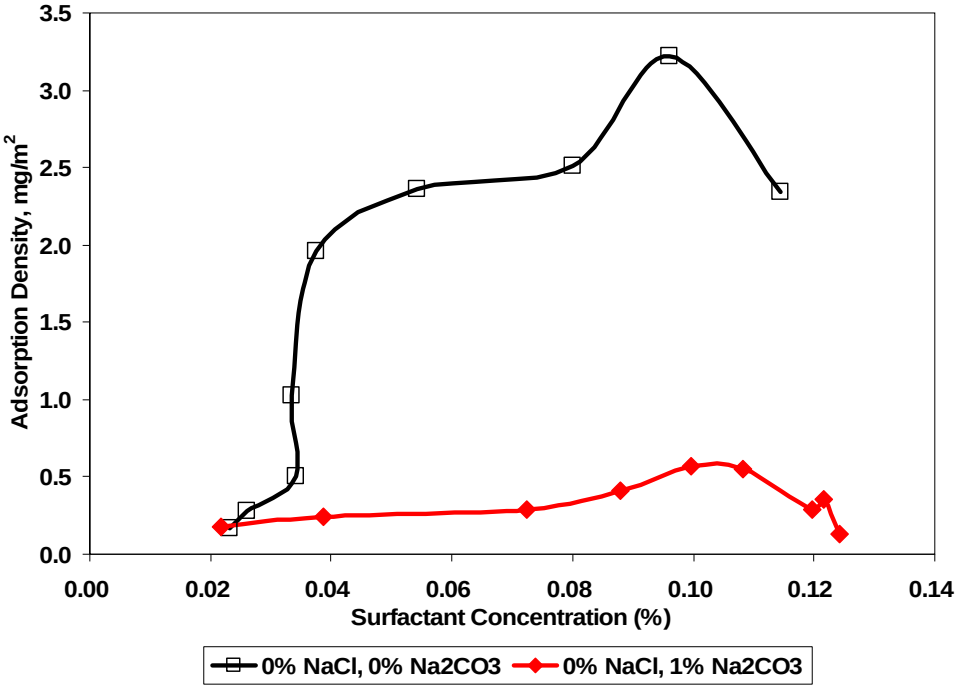


**Figure 5.6 Adsorption of IOS on calcite powder (17.9 $m^2/g$) with or without 1 % $Na_2CO_3$ and with no NaCl.**

Adsorption is approximately 2.8 and 3.0 $mg/m^2$ in the plateau regions for the respective surfactants in the absence of $Na_2CO_3$, corresponding to 0.47 and 0.23 $nm^2$/molecule, assuming a uniform monolayer. The latter number (for IOS) is close to the area of a single straight hydrocarbon chain. Since this surfactant consists of a mixture of molecules with the sulfonate group located at various places along the hydrocarbon chain, the adsorbed molecules are twin-tailed. As a result, their area per molecule should be about twice that of a single chain, and it seems likely that an adsorbed bilayer exists in the plateau region. Bilayers often form for adsorption of surfactant ions on surfaces of opposite charge at concentrations near and above the critical micelle concentration (CMC). This is because bilayers expose a polar surface, which has a low free energy with the aqueous phase. The arrangement of adsorbed molecules for N67 is not clear.

Figure 5.7 shows adsorption isotherms of the NI blend on calcite powder at different NaCl concentrations with and without 1 wt% $Na_2CO_3$. In the absence of NaCl adsorption is comparable to that of N67 or IOS alone. As NaCl concentration increases, the beneficial effect of $Na_2CO_3$ is reduced, presumably because the screening effect of the additional electrolyte decreases electrostatic repulsion between surfactant ions in solution and the calcite surface. Nevertheless, $Na_2CO_3$ reduces adsorption by more than a factor of three for 3 wt% NaCl.

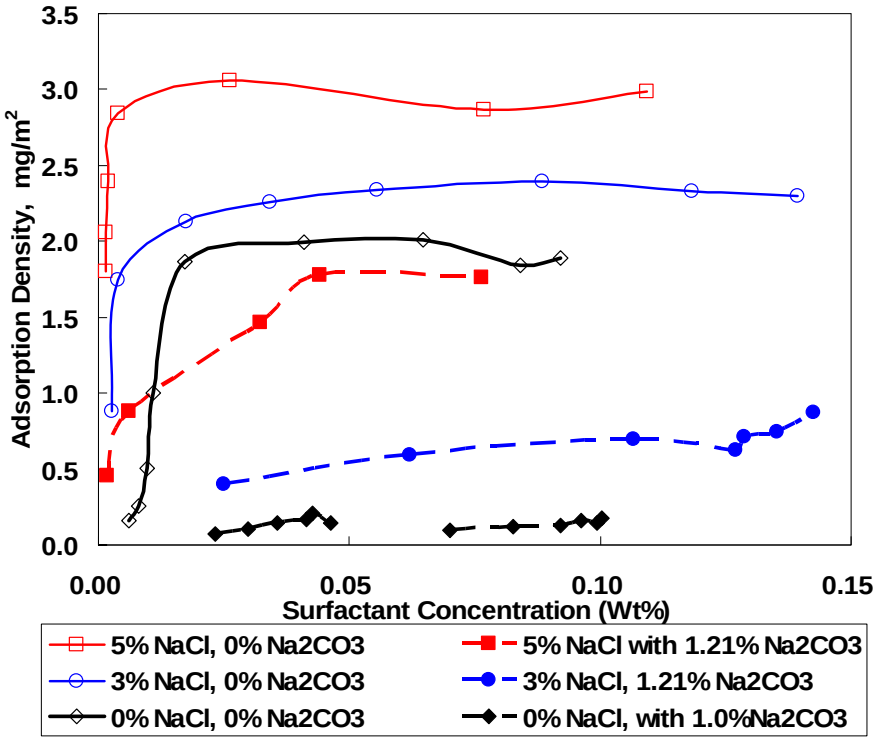


**Figure 5.7 Adsorption of NI blend on calcite as a function of NaCl content with and without 1 wt% $Na_2CO_3$.**

In the previous static adsorption experiments, approximately 1% $Na_2CO_3$ was used as adsorption reduction agent. It is also important to know how much $Na_2CO_3$ is needed to have this adsorption reduction effect. The threshold of $Na_2CO_3$ concentration at which the adsorption reduction effect occurs is shown as figure 5.8. The initial surfactant

concentration is fixed at 0.06% without any NaCl, but the $Na_2CO_3$ concentration is varied. The ratio of calcite powder and surfactant solution was also fixed and the two were mixed. Then the residual surfactant concentration after mixing was measured. It is found that the adsorption changes with the $Na_2CO_3$ concentration as shown by figure 5.8. The adsorption reduction effect seemed the same when the $Na_2CO_3$ concentration was higher than 0.1 %, i.e., further increasing the $Na_2CO_3$ concentration does not further decrease the surfactant adsorption. However, the adsorption will increase as the $Na_2CO_3$ concentration deceases when it is lower than 0.1%. From this result, the lowest alkali concentration for lowering the surfactant adsorption on calcite should be higher than 0.1% $Na_2CO_3$. Figure 5.9 indicates that with 5% NaCl, increasing the $Na_2CO_3$ concentration more than 0.18% will not further decrease the surfactant adsorption. However, the threshold concentration could be lower since data were not obtained between 0 and 0.18% $Na_2CO_3$.

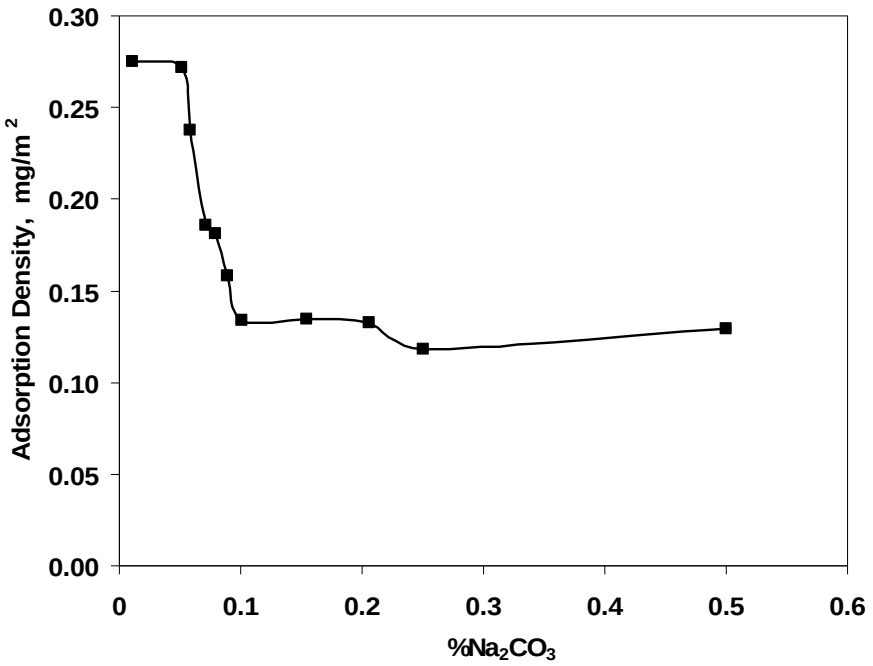


**Figure 5.8 Test of threshold concentration of $Na_2CO_3$ for the adsorption.**

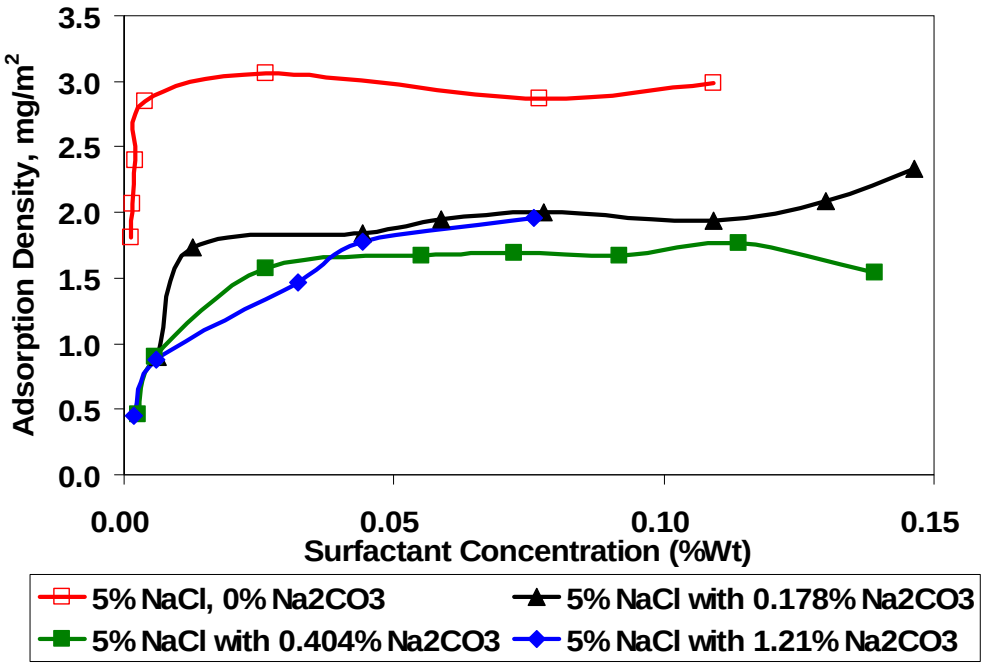


**Figure 5.9 Adsorption of NI blend on calcite at 5% NaCl with different $Na_2CO_3$.**

By summarizing those data in figures 5.7 to 5.9 and additional experiments with different NaCl and $Na_2CO_3$ concentrations, the contours of plateau adsorption for NI blend are plotted as Figure 5.10. This plot shows that the domain with surfactant adsorption less than 1 mg/m$^2$ is: [$Na_2CO_3$]>0.2% and [NaCl] <3%. Hence, it's better to perform the alkali-surfactant process with this anionic surfactant (NI blend) in this concentration range for low surfactant adsorption.

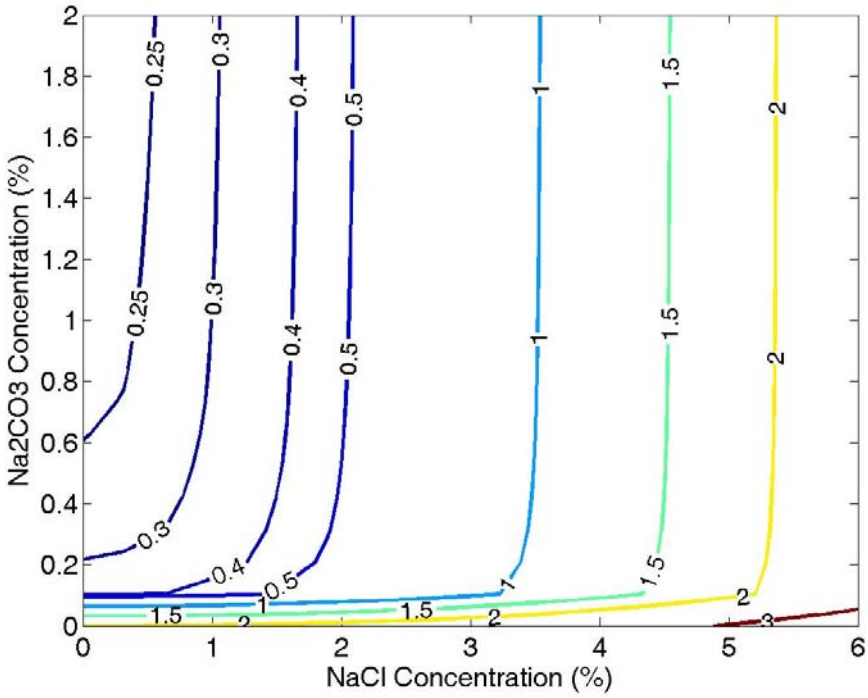


**Figure 5.10 Contour of Plateau Adsorption (mg/m$^2$) for NI Blend on calcite.**

### 5.1.2.5 Adsorption of Nonionic Surfactant and Anionic Surfactant

Nonionic surfactant is not generally considered as a candidate for surfactant EOR process because its adsorption on sandstone formation is very large comparing to anionic surfactant. A nonionic surfactant, Nonylphenol-12EO-3PO (from Harcros Chem), was tested in the same static procedure as the anionic surfactant except the UV-vis spectrum was used to determine the nonionic surfactant concentration. The UV (ultra-violet) absorbent peak of this surfactant is at 277nm. There is a linear relationship between the absorbency at 277 nm and surfactant concentration when the concentration is less than 0.2 wt% so that the surfactant concentration can be accurately measured.

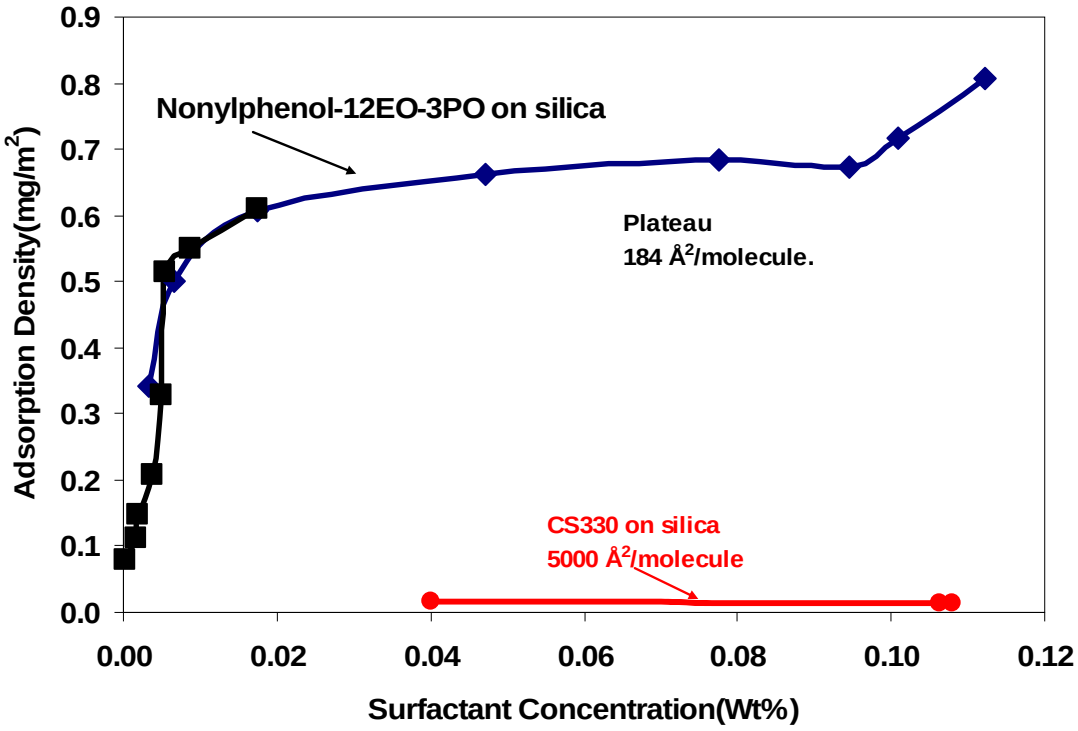


**Figure 5.11 Comparison the adsorption on silica sand between nonionic surfactant and anionic surfactant**

Figure 5.11 shows that this nonionic surfactant has much higher adsorption on silica sand (from US Silica®, BET area: 3.6mg/gram) than the anionic surfactant (CS330) as expected. The high nonionic surfactant adsorption on silica surface is because the hydrogen bond between the nonionic surfactant and silica surface will help the nonionic surfactant attach the surface of silica because silica surface also has hydroxyl group. However, on dolomite surface, hydrogen bond between the carbonate surface and nonionic surfactant is not expected. Thus carbonate surface will not attract the nonionic surfactant. As figure 5.12 illustrates, the adsorption of nonionic surfactant is much lower than that of anionic surfactant in the absence of $Na_2CO_3$ and is in the same magnitude of

that of anionic surfactant with presence of $Na_2CO_3$. This result indicates that the nonionic surfactant is also a candidate for carbonate formations from the adsorption point of view.

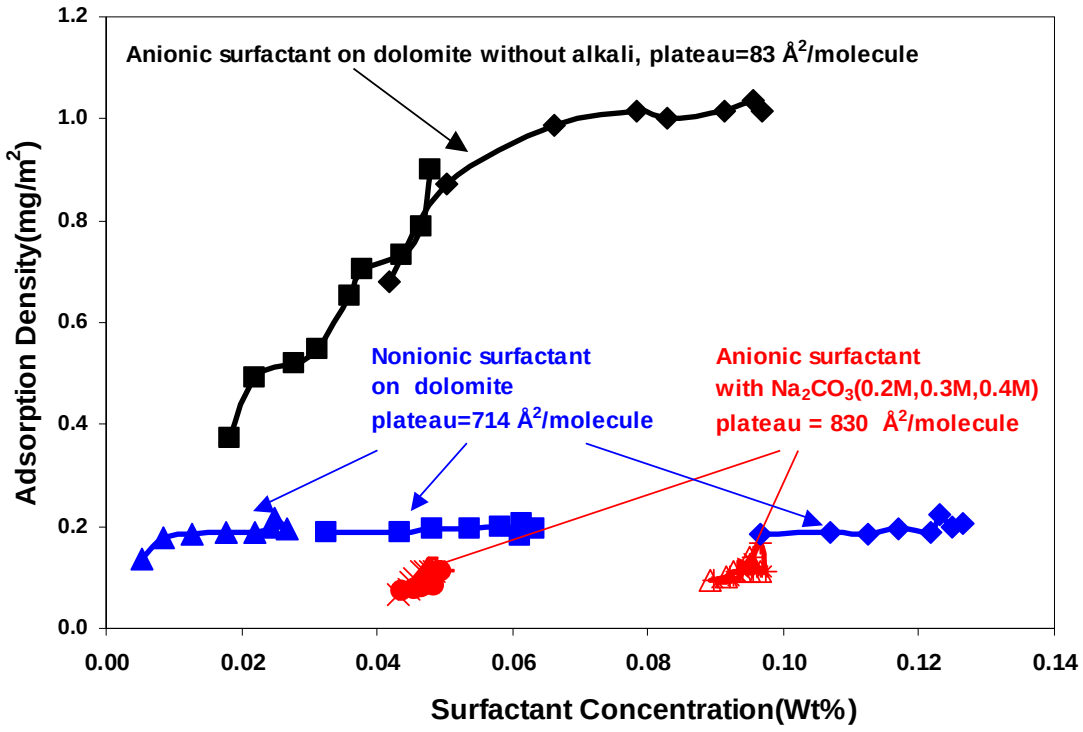


**Figure 5.12 Comparison the adsorption on dolomite powder between nonionic surfactant and anionic surfactant.**

## 5.2 Dynamic Adsorption of Surfactant

Dynamic adsorption experiment measures the surfactant adsorption by surfactant flooding in one dimensional sand pack or core. By comparing the breakthrough history of surfactant and non-adsorbing tracer, the adsorption can be determined. Although the dynamic method is much more complicated and takes much longer time than the static adsorption method, it is still widely used to estimate the surfactant consumption because it is analogous to the actual surfactant flooding process (Griggs and Bai, 2005).

Furthermore, the dynamic method can provide the information about the kinetic effects of adsorption.

### 5.2.1 Dynamic Adsorption Experimental Procedure

Dynamic adsorption experiments on the silica sand, dolomite sand and dolomite cores were performed in a one-foot column packed with sand. The experimental apparatus diagram is shown in figure 5.13.

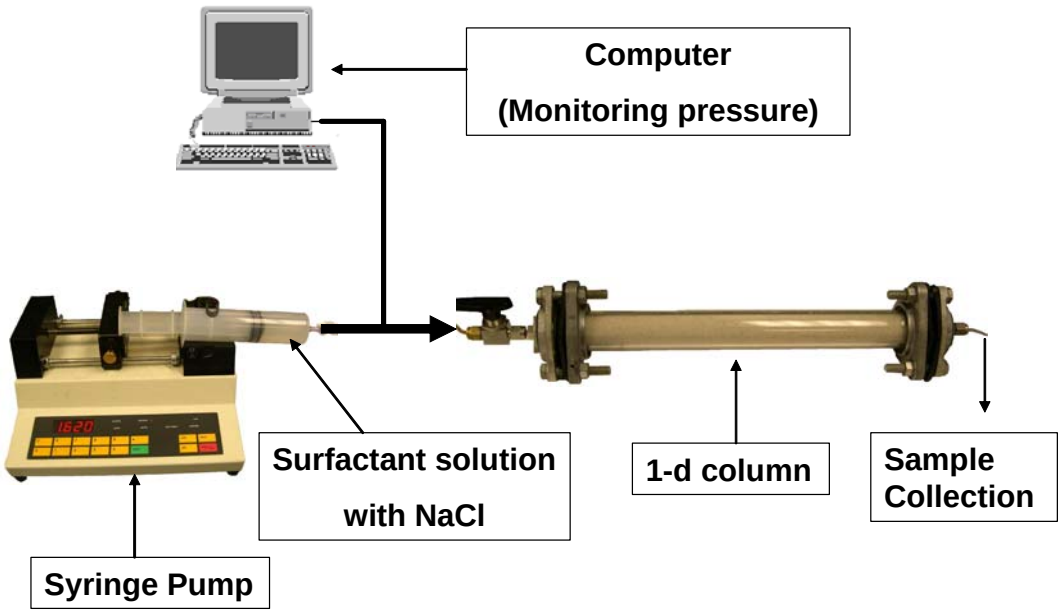


**Figure 5.13 Schematic Experimental Apparatus**

The experimental procedure is:

1. Fill the column with formation brine.

2. Inject the surfactant solution into the column by the pump; the solution also contains sodium chloride as a non-absorbing tracer.

3. Collect the effluent at different times and measure the concentration of the surfactant and sodium chloride to obtain the breakthrough curves of the two components

4. For the silica sand pack, isobutyl alcohol and de-ionized water are used to wash the column for the next experiment. For dolomite sand pack or dolomite cores, the column is repacked with fresh dolomite sand for the next experiment because the adsorbed surfactant could not be totally removed by the washing process.

In the experiment, the conductivity of the solution was used to measure the NaCl concentration, and potentiometric titration was used to measure the surfactant concentration as in the static experiments. Because the ionic surfactant may affect the conductivity of the water, an auxiliary experiment was performed to determine whether this effect would introduce error in measuring the NaCl for the surfactant and NaCl concentration used here. The results showed that there was not a significant error induced by the ionic surfactants. Furthermore, equations (5.1) for NaCl concentration less than 0.5 wt%, which were obtained from the experiments, can be used to calculate the NaCl concentration. In the dynamic experiments, the NaCl concentration can be obtained by measuring the diluted effluent.

$$\textbf{[Conductivity]= 16905*[NaCl Wt\%]+ 30}\pm\textbf{140.}$$
$$\text{or } \textbf{[NaCl Wt\%]= 5.92*10}^{-5}\textbf{*[Conductivity]- 2*10}^{-3}\pm\textbf{8*10}^{-3} \qquad (5.1)$$

### 5.2.2 Dynamic Adsorption Model

In order to obtain the adsorption by analyzing the breakthrough history, a dynamic adsorption model is introduced in this section. Below is a brief description of the one dimensional adsorption model. The major assumptions of the model are:

1. No velocity in the r and θ directions, i.e., one-dimensional flow

2. The adsorption isotherm can be approximated with a constant slope over the range of concentration studied, i.e., the adsorption is linear with the local concentration. The actual adsorption is a Langmuir type isotherm as shown in those static adsorption isotherms, e.g. figure 5.7. This assumption is made so that an analytical solution can be obtained.

3. The physical properties, such as viscosities and densities etc., do not change with any component concentration of the solute.

4. The dispersion coefficient $K_l$ is assumed to be proportional to velocity and the velocity is constant, i.e. the dispersion is constant.

5. The medium is homogeneous.

With these assumptions, the mass conservation equation with adsorption is as follows:

$$\phi(1+\beta)\frac{\partial c}{\partial t} + u\frac{\partial c}{\partial x} = \phi K_l \frac{\partial^2 c}{\partial x^2} \qquad \text{x>0, t>0} \qquad (5.2)$$

where $\phi$ is the porosity.

$K_l$ is the dispersion coefficient.

The cord slope of the adsorption isotherm with respect to the reduced concentration is denoted by $\beta$. $\beta$ can be calculated from the static adsorption isotherm by using the equation (5.3). Because the actual surfactant adsorption isotherm is not a linear isotherm, the chord on the isotherm between zero and local concentration was used as the $\beta$.

$$\beta = \frac{c_s}{c} = \frac{(1-\phi)}{\phi}\rho S k_{iso} \qquad (5.3)$$

where $\phi$ is the porosity of the porous medium

$\rho_{dolomite}$ is the density of the porous medium

$S$ is the BET surface area of the porous medium

$k_{iso}$ is the cord slope of the isotherm plot from static adsorption isotherms

The concentration is transformed to a reduced concentration that has a range between 0 and 1. Hereafter, the concentration used here is the dimensionless concentration. Thus the boundary conditions and the initial conditions are:

$c\ (x,\ 0) = c_{IC} = 0,\ x > 0$

$c\ (0,\ t) = c_{BC} = 1,\ t > 0$

$$\frac{\partial c}{\partial x}(\infty, t) = 0\ ,\ t > 0$$

By using interstitial velocity $v = u/\phi$, the differential equation can be translated to:

$$\frac{\partial c}{\partial t} + \frac{v}{(1+\beta)}\frac{\partial c}{\partial x} = \frac{K_l}{(1+\beta)}\frac{\partial^2 c}{\partial x^2} \tag{5.4}$$

In the absence of dispersion, the analytical solution to this differential equation is an indifferent step wave with a velocity equal to $v/(1+\beta)$. Thus the cord slope of the adsorption isotherm describes the retardation of the concentration wave. By transforming the variables, this partial difference equation (PDE) can be reduced into an ordinary difference equation (ODE).

$$\frac{\mathrm{d}^2 \mathrm{C}}{\mathrm{d}\eta^2} + 2\eta\frac{\mathrm{dC}}{\mathrm{d}\eta} = 0 \qquad \text{where} \qquad \eta = \frac{x - \dfrac{vt}{1+\beta}}{\sqrt{\dfrac{4K_l t}{1+\beta}}} \tag{5.5}$$

By integrating the ODE, the solution obtained is:

$$C = \frac{1}{2}\left[1 - \frac{2}{\sqrt{\pi}}\int_0^{\eta} e^{-\eta^2}\, d\eta\right] = \frac{1}{2}\mathrm{erfc}(\eta) \tag{5.6}$$

With the characteristic system length L, the distance variable will be made dimensionless with respect to L. Thus the non-dimensional variable η is:

$$\eta = \frac{x_D - \frac{t_D}{(1+\beta)}}{2\sqrt{\frac{t_D}{Pe(1+\beta)}}} \tag{5.7}$$

where $x_D = x/L$, $t_D = uAt/\phi AL$ and $Pe = Lv/K_l$.

The effluent history, i.e., the concentration history at $x_D$=1 can be obtained. And the retardation of the break-through curve can be expressed as $\beta$. If the nonabsorbent tracer and adsorbing solute break-through curves coincide, then $\beta$=0, that is no adsorption occurred for the component measured.

Since the data obtained are the effluent history, the value of β and Peclet number (*Pe*) can be calculated by following manipulation. From the relation of the complementary error function to the cumulative Gaussian probability distribution, the slope of adsorption isotherm and the Peclet number can be estimated by the mean and standard deviation of a Gaussian distribution. The cumulative Gaussian probability distribution is given by the following formula:

$$P\{y\} = \frac{1}{2}\left[1 + erf\left(\frac{u}{\sqrt{2}}\right)\right] \tag{5.8}$$

$$u = \frac{y-\mu}{\sigma} \tag{5.9}$$

$$y = \mu + \sigma u \tag{5.10}$$

where $\mu$ and $\sigma$ are the mean and standard deviation of the Gaussian distribution.

Recall that the effluent concentration is given by equation (5.6) as.

$$C = \frac{1}{2} erfc(\eta) = \frac{1}{2}\left[1 - erf(\eta)\right] \qquad \text{where } \eta = \frac{1 - \frac{t_D}{(1+\beta)}}{2\sqrt{\frac{t_D}{Pe(1+\beta)}}} \tag{5.11}$$

Next the variables are transformed such that the transformed variables are a cumulative Gaussian distribution. First, transform C such that it has the same dependence on the error function as the Gaussian distribution.

$$\frac{1}{2}\left[1 + erf(\eta)\right] = 1 - C \Rightarrow P \tag{5.12}$$

The argument of the error function should map the independent variables:

$$\eta(x_D = 1) = \frac{1 - \frac{t_D}{(1+\beta)}}{2\sqrt{\frac{t_D}{Pe(1+\beta)}}} = \frac{1 + \beta - t_D}{2\sqrt{\frac{t_D(1+\beta)}{Pe}}} \Rightarrow \frac{u}{\sqrt{2}} \quad \text{and} \quad \frac{1 - t_D}{\sqrt{t_D}} \Rightarrow y$$

Finally, the expressions for μ and σ are: $\mu = -\beta$ and $\sigma \approx \sqrt{2}\sqrt{\frac{1+\beta}{Pe}}$.

From the experimental data *c* and the $t_D$, *Pe*, *y* and $\eta$ can be calculated. With *y* and $\eta$, $\mu$ and $\sigma$ can be calculated by linear regression. Then $\beta$ and *Pe* are obtained.

Since the exact porosities of the sand packs or cores are unknown, they should be determined first. The fact that there is no adsorption for NaCl in the sand or the dolomite can be used to estimate the porosity. For the NaCl data, a pore volume is guessed at first, and then the μ and σ are calculated based on the guessed pore volume. Because β equals zero for no adsorption case, the porosity for which $\beta$=0 would be the actual porosity. The porosity (0.34) calculated by this method is close to the porosity that comes from the weight method (0.35). With the calculated porosity, we can obtain the $\beta$ and Peclet

Number by using the linear regression for the surfactant data. The simulation curve also can be plotted with the calculated $\beta$ and Peclet Number.

### 5.2.3 Dynamic Adsorption of Anionic Surfactant

Figure 5.14 shows the break-through curve and simulation curve of TC blend in silica sand.

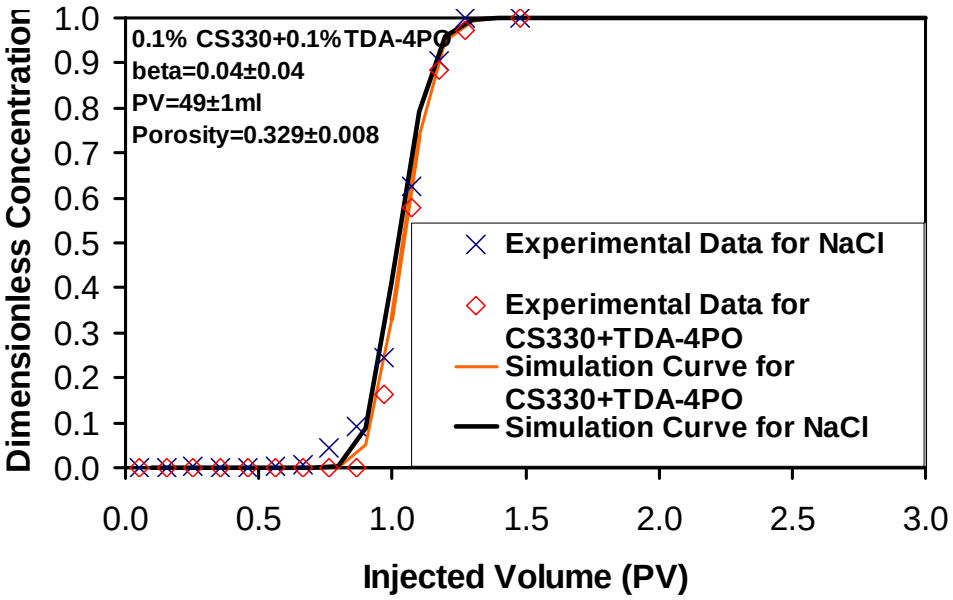


**Figure 5.14 Dynamic Adsorption of TC Blend in silica sand column**

From this plot, no significant adsorption for TC blend is found in the silica sand (From US Silica® BET: 0.25 mg/g) packed column because the break-through curves of the two components (NaCl and surfactant) superimpose each other. Also this one-dimensional model can simulate this displacement experiment very well. The value of $\beta$ is only 0.04, which also indicates that the adsorption amount is very small. The two components of TC blend, TDA-4PO and CS330, were also tested by the dynamic method

respectively. Both $\beta$ values of these two surfactants are 0.02, which is also quite small. The reason that the adsorption of anionic surfactant is negligible on the silica surface is due to the negatively charged interface of brine/silica, which repels the negatively charged surfactant by electrostatic forces.

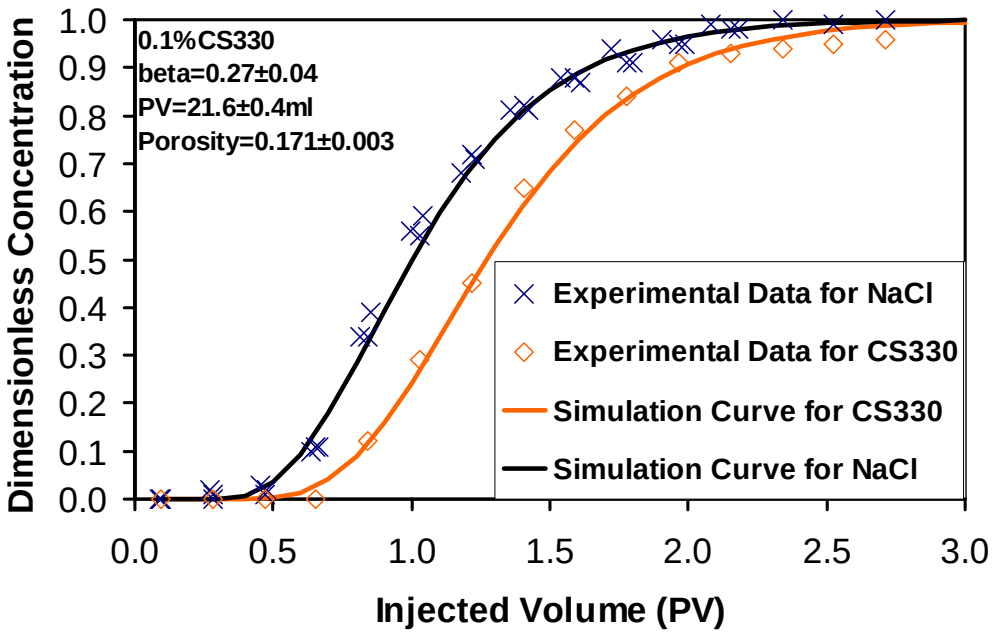


**Figure 5.15 Dynamic Adsorption of CS 330 in dolomite core**

On dolomite surface, the dynamic adsorption of the anionic surfactant is much greater. Figure 5.15 shows the break-through curve and the simulation curve of CS330 and NaCl in the dolomite core from Yates (permeability is 122~284 md; porosity is 0.171±0.003). The break-through curve for CS330 has some lag compared with the break-through of NaCl. This means the dolomite core adsorbs a certain amount of surfactant so that it breaks through later. From the simulation result, $\beta$ is estimated as β=0.27±0.04, which is much larger than that in the silica sand pack. Because the core samples are not identical and the BET surface area of the core could not be measured,

crushed dolomite sand will be used as an alternative carbonate media for the remaining dynamic adsorption experiments.

As mentioned in previous section, the surface area of crushed dolomite sand that was determined by the BET adsorption is 0.3 $m^2$/gram sand. With the porosity and dolomite density, $\beta$ can be calculated by using equation (5.3), assuming the adsorption density, i.e., the adsorption amount per active surface area is not changed. Then, the adsorption from the static method and dynamic method can be compared as shown in figure 5.16. The break-through curve and the simulation curve of the surfactant mixture and NaCl for dolomite sand pack column (porosity is 0.34) are plotted in Figure 5.16.

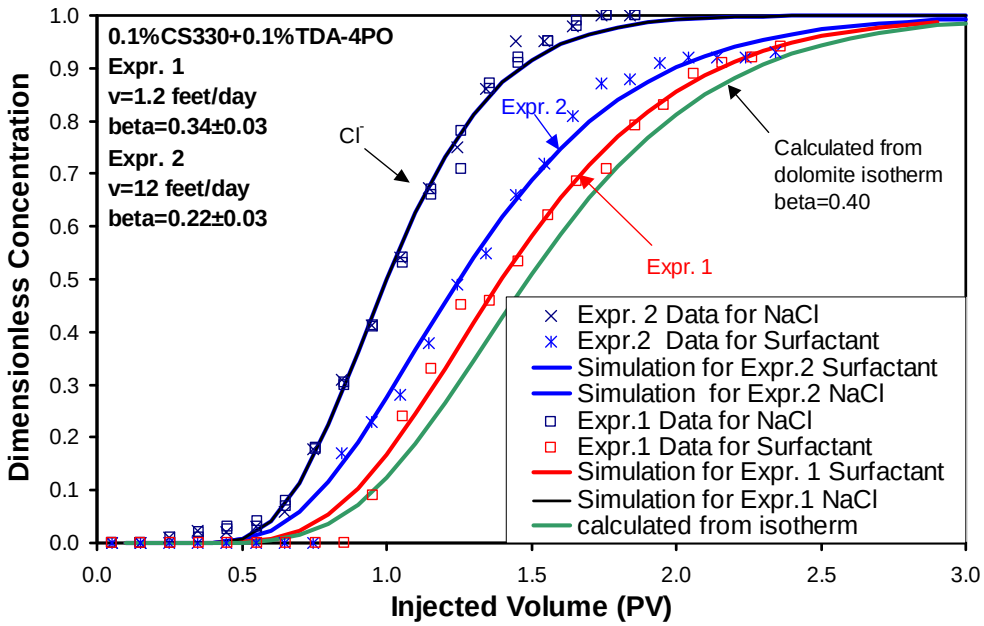


**Figure 5.16 Adsorption of TC blend in dolomite sand column without $Na_2CO_3$**

Figure 5.16 points out that the adsorption of surfactant on dolomite sand is significant. It also demonstrates that the adsorption of surfactants is not an instantaneous process and depends on the flow rate. At a high interstitial velocity of 12 feet/day

($\beta$=0.22), the retardation is much smaller than that at 1.2 feet/day ($\beta$=0.34). Even at the lower flow rate, $\beta$ is less than that calculated from the static adsorption isotherm ($\beta$=0.40).

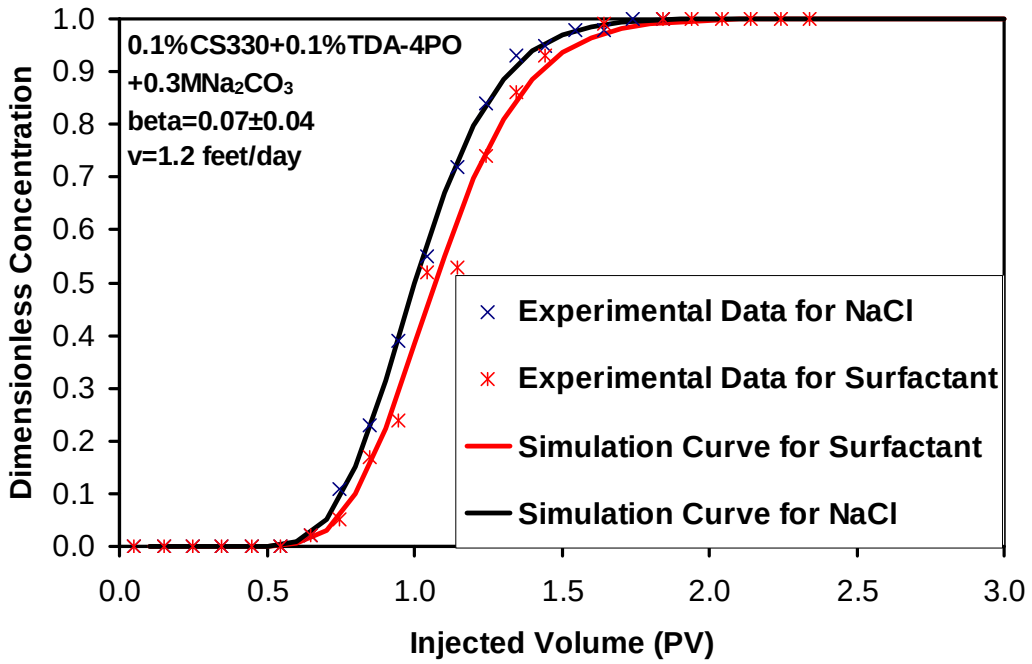


**Figure 5.17 Adsorption of TC blend in dolomite sand column with $Na_2CO_3$**

Similar to what was found in static adsorption, the addition of sodium carbonate can significantly reduce surfactant adsorption, as shown in Figure 5.17. At the same slow flow rate, β is reduced from 0.34 to 0.07 by adding 0.3 M $Na_2CO_3$.

Table 5.1 summarizes the dynamic adsorption results.

| Porous Media | From | Permeability | Porosity | Pore volume | Inject Surfactant | Flow rate | Retardation β |
|---|---|---|---|---|---|---|---|
| Silica sand (BET: 0.2$m^2$/g) | US Silica Ottawa Foundry | ~120 darcy | 0.329 ±0.008 | 49±1ml | CS330 (0.1%) | 8 feet/day | 0.02 ±0.03 |
| Silica sand (BET: 0.2$m^2$/g) | US Silica Ottawa Foundry | ~120 darcy | 0.329 ±0.008 | 49±1ml | TDA-4PO (0.1%) | 8 feet/day | 0.02 ±0.03 |
| Silica sand (BET: 0.2$m^2$/g) | US Silica Ottawa Foundry | ~120 darcy | 0.329 ±0.008 | 49±1ml | TC Blend (0.2%) | 8 feet/day | 0.04 ±0.04 |
| Dolomite core | Marathon Oil Company | 122~284 md | 0.171 ±0.003 | 21.6±0.4 ml | CS330 (0.1%) | 5 feet/day | 0.27 ±0.03 |
| Dolomite sand BET: 0.3$m^2$/g | Unimin corporation | ~40 darcy | 0.335 ±0.008 | 50±1ml | TC Blend (0.2%) | 1.2 feet/day | 0.34 ±0.03 |
| Dolomite sand (BET: 0.3$m^2$/g | Unimin corporation | ~40 darcy | 0.338 ±0.008 | 50±1ml | TC Blend (0.2%) | 12 feet/day | 0.22 ±0.03 |
| Dolomite sand (BET: 0.2$m^2$/g) | Unimin corporation | ~40 darcy | 0.337 ±0.008 | 50±1ml | TC Blend (0.2%) $Na_2CO_3$ (0.3M) | 1.2 feet/day | 0.07 ±0.04 |

**Table 5.1 Summarization of dynamic adsorption experiments' condition and results.**

## 5.3 Sodium carbonate consumption by gypsum

Pure calcite does not consume much alkali. However, the consumption of alkali in carbonate reservoir may be a crucial problem because of the precipitation reaction of alkali with gypsum or anhydrite. Because the solubility products of $CaCO_3$ and $CaSO_4$ are $4.96*10^{-9}$ and $7.10*10^{-5}$ respectively (CRC Handbook, 68th Edition), it is a serious problem to apply $Na_2CO_3$ as the alkali candidate in the presence of gypsum or anhydrite because of the precipitation reaction shown as equation (5.13).

$$CO_3^{2-} + CaSO_4 \rightarrow CaCO_3 \downarrow + SO_4^{2-} \qquad (5.13)$$

By using the same analysis as in dynamic surfactant adsorption, figure 5.18 shows the retardation for a porous medium with porosity 0.3. It illustrates that the retardation is significant. For a 0.1M (~1%) $Na_2CO_3$, the concentration usually being considered for oil recovery processes, the retardation is around 0.7 PV for the condition that 0.1% of the porous medium is $CaSO_4$. Although the propagation velocity of sodium carbonate can be increased by raising the injection alkali concentration, the total amount of alkali consumption will not change. It is impractical to solve this problem by increasing the sulfate ion concentration through adding $Na_2SO_4$ because of the tremendous difference between the two solubility products. Although this calculation is approximate because they are based on room temperature value of solubility products and neglect activity coefficients, the point made here is that other alkali should be considered when gypsum is present.

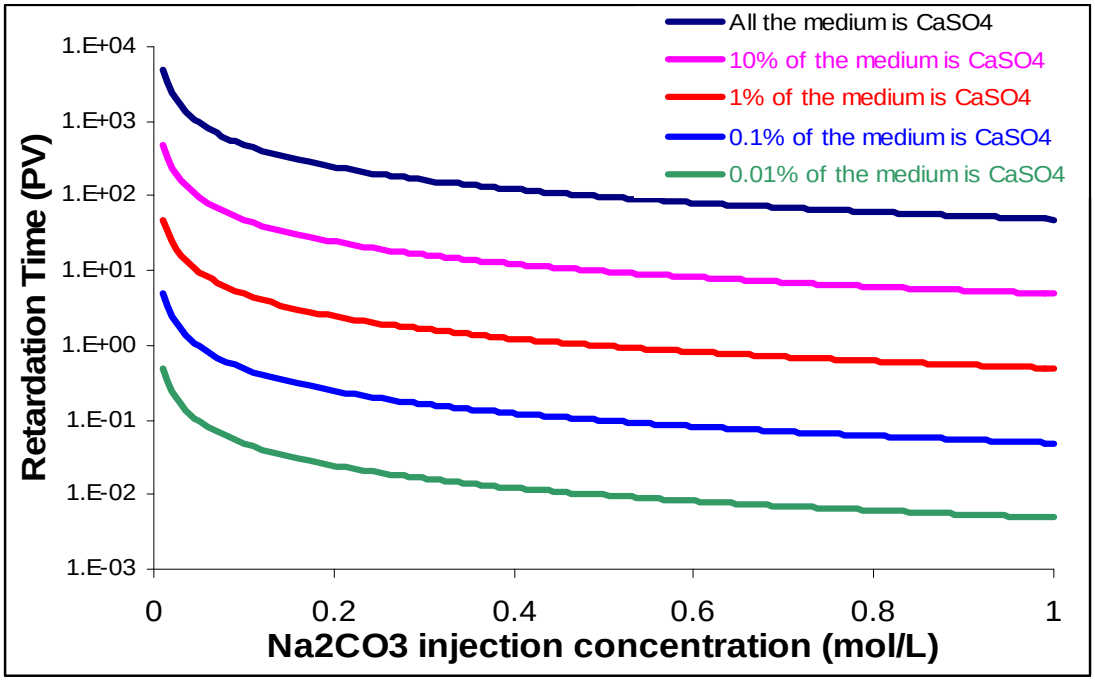


**Figure 5.18 Relationships between retardation and $CaSO_4$ fraction in porous medium (porosity=0.3)**

$NaHCO_3$ with $Na_2SO_4$ may be a potential choice for the situation with $CaSO_4$. $NaHCO_3$ has much lower carbonate ion concentration and additional sulfate ions can decrease calcium ion concentration in the solution. However, this method is not applicable again. The concentration of $CO_3^{2-}$ is around the one hundredth the concentration of $NaHCO_3$ for a $NaHCO_3$ solution so that large amount $Na_2SO_4$ is needed to avoid precipitation of $CaCO_3$. For a 0.1M $NaHCO_3$ solution, the carbonate ion concentration is around $1.0*10^{-3}$ M, and we need 14 M $Na_2SO_4$ to prevent the precipitation of $CaCO_3$.

The other alkali candidate is NaOH with $Na_2SO_4$ since the solubility product of $Ca(OH)_2$ is $4.68*10^{-6}$. The reaction between NaOH with $Na_2SO_4$ is shown as equation (5.14). The minimum $Na_2SO_4$ concentration that restrains the $Ca(OH)_2$ precipitation can be calculated by equation (5.15). For a 0.1 M NaOH solution, 0.15 M $Na_2SO_4$ is needed to suppress the calcium ion concentration so that no $Ca(OH)_2$ will precipitate. Higher $Na_2SO_4$ is necessary with higher NaOH concentration. However, the adsorption of anionic surfactant will not decreased by NaOH formulation.

$$2NaOH + CaSO_4 \Leftrightarrow Ca(OH)_2 + Na_2SO_4 \tag{5.14}$$

$$[SO_4^{2-}] = [OH^-]^2 \frac{K_{spCaSO_4}}{K_{spCa(OH)_2}} = 15 * [OH^-]^2 \tag{5.15}$$

Some organic alkalis, such as sodium citrate, sodium metaborate, might be the alternate choices when gypsum is present because calcium citrate or calcium metaborate has larger solubility product than calcium sulfate. Further studies should be done in this area.

*Chapter 6*

# Simulation and Optimization of Alkaline Surfactant Polymer Process

A one-dimensional simulator was developed and used in this chapter to show characteristics of ASP process with the IFT properties of alkali–surfactant system shown in previous chapters.

## 6.1 One-dimensional Simulator

The synergic effect of synthetic surfactant and soap are very important for the success of ASP process as shown in the phase behavior and interfacial tension results in Chapters 3 and 4. However, because current reservoir simulators do not include soap component, they do not have the capacity to evaluate the characteristics of the ASP process. In order to understand the ASP process, a one-dimensional, two phase, multi-componential simulator was developed to calculate the profiles and oil recovery as a function of process variables. In this simulator, the main relationships are as follows:

(1) Phase behavior and interfacial tension are functions of alkali , electrolyte (NaCl), surfactant and natural soap concentrations,

(2) Fractional flow curves are functions of interfacial tension, phase saturation and viscosity of each phase,

(3) Surfactant adsorption is a function of surfactant concentration in aqueous phase, alkali concentration and salinity,

(4) Natural soap is generated from the naphthenic acids contacted by the alkali,

(5) Physical dispersion is described by convective dispersion, i.e, proportional to velocity

(6) Aqueous phase viscosity is a function of electrolyte (NaCl) and polymer concentration,

(7) A single parameter is used to describe the alkali consumptions, such as the precipitation reaction between injected $Na_2CO_3$, $CaSO_4$ that resides in the reservoir and the calcium ions in the formation brine, reaction between alkali and clays etc.

### 6.1.1 Assumptions and Models

The basic assumptions of the model are as follows:

1. The system is one-dimensional and homogeneous in permeability and porosity.

2. Local equilibrium exists everywhere.

3. Capillary pressure is negligible.

4. The system is one-dimensional and horizontal. Thus there is no gravity effect.

5. The system has eight components. They are water (1), oil (2), synthetic surfactant (3), natural soap (4), electrolyte (NaCl) (5), alkali ($Na_2CO_3$) (6), polymer(7), naphthenic acid (8). The numbers behind the chemicals are the indices that were used in the simulator and will be used for the future discussion in the thesis.

6. Two mobile phases are: aqueous phase (1), oleic phase (2). For example, $c_{ij}$ is the concentration of component $i$ in phase $j$.

7. All the chemicals except water and oil are assumed to occupy negligible volume and are treated as tracers.

Additional assumptions also required for this simulator are discussed below.

#### 6.1.1.1 Surfactant and Soap Partitioning

Since this simulator is a two-phase model, there must be a partitioning of chemicals between the oleic and aqueous phases. The partition coefficient of the component *i* is defined as equation (6.1).

$$K_{Ci} = \frac{c_{i2}}{c_{i1}} \tag{6.1}$$

where $c_{i1}$ is the concentration in aqueous phase for component *i*

$c_{i2}$ is the concentration in oleic phase for component *i*

In the simulator, electrolyte (NaCl), alkali and polymer are assumed to be totally in the aqueous phase, i.e. $K_{Ci} = 0$, when *i*=5, 6 or 7. The undissociated naphthenic acid is assumed to be totally in oleic phase, i.e., $K_{C8} = 0$. Naphthenic acid changes to soap when it contacts alkali.

The partitioning for the surfactant and soap is not that simple and depends on the phase behavior, which is a function of the salinity (concentration of electrolyte) and the soap/surfactant mole ratio. The partition of soap and surfactant is unity at the optimum condition. For over-optimum conditions, most of the surfactant and soap are in the oleic phase so that the partition coefficients of soap and surfactant are larger than unity for over-optimum conditions. Similarly when phase behavior is under-optimum, the partition coefficients of soap and surfactant are less than the unity. The optimum curve at which

the partition of soap and surfactant is unity is given in figure 3.10. It shows dependence of optimum salinity on soap/surfactant ratio for the NI blend and Yates oil as discussed in Chapter 3. The partition coefficients $K_{C3}$ and $K_{C4}$ between oil and aqueous phases for the soap and surfactant are assumed to be same and are calculated by the following empirical equations (6.2-a) and (6.2-b). Hereafter, $K_{Part}$ is used as either $K_{C3}$ or $K_{C4}$.

Above optimum salinity: $$K_{part} = 10^{2*(Sal/Sal_{opt}-1)} \quad (6.2\text{-a})$$

Below optimum salinity: $$K_{part} = 10^{2*(1-Sal/Sal_{opt})} \quad (6.2\text{-b})$$

where *Sal* is the local salinity,

$Sal_{opt}$ is the optimum salinity based on local soap to surfactant ratio. It is calculated as (6.3) as discussed in Chapter 3.

$$\log(Sal_{opt}) = Xsoap * \log(Soap\_Opt) + (1 - Xsoap) * \log(Surfactant\_Opt) \quad (6.3)$$

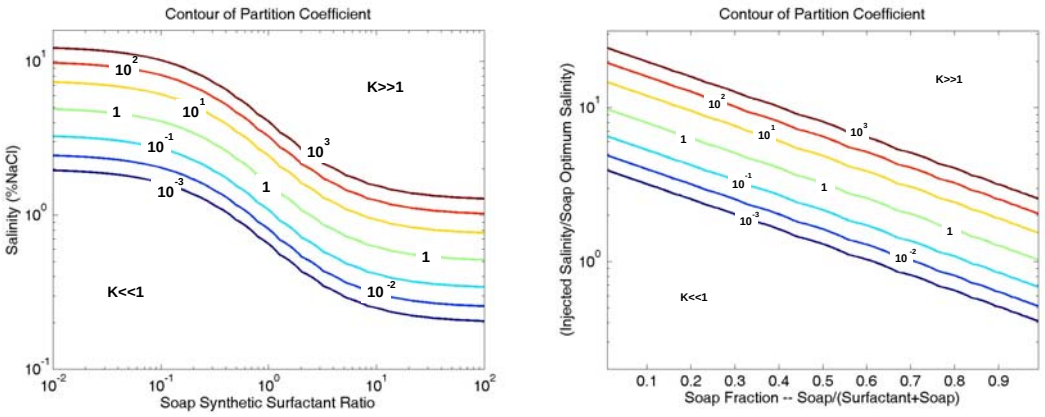


**(a)** **(b)**

**(a) Salinity (%NaCl) vs Soap to surfactant ratio**
**(b) (Injected Salinity/Soap Optimum Salinity) vs Soap Fraction**

**Figure 6.1 Contour of Partition Coefficient**

$K_{part}$ is unity at optimal salinity. Recovery predicted by the simulator was found to be relatively insensitive to the detailed expression for calculating $K_{Part}$ except that numerical instabilities were encountered if $K_{Part}$ varied too rapidly near optimum conditions. Figures in 6.1 are the contour plots for partition coefficient $K_{Part}$. Figures 6.1(a) and 6.1(b) are actually equivalent with different axis.

### 6.1.1.2 Interfacial Tension

The interfacial tension is a crucial factor for ASP process. To calculate the IFT at different conditions, IFT contour plots as shown in figures 6.2 are constructed as follows. Figures 6.2(a) and 6.2(b) are equivalent with different axis. Based on the lowest measured IFT shown figure 4.13 in Chapter 4, IFT was taken to be 0.001 mN/m along the entire optimum curve which is the same optimum curve when surfactant and soap partition coefficient equals unity, i.e., equation (6.3).

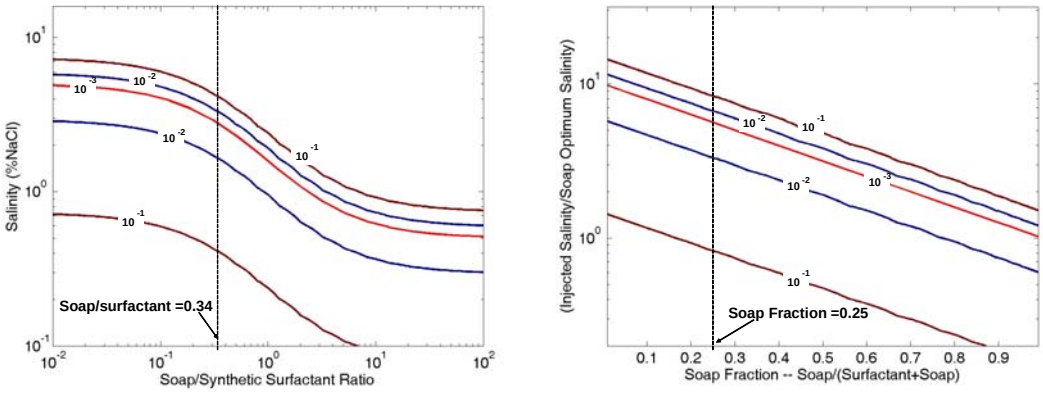


**(a)** **(b)**

**(a) Salinity (%NaCl) vs Soap to surfactant ratio**
**(b) (Injected Salinity/Soap Optimum Salinity) vs Soap Fraction**

**Figure 6.2 IFT Contour used in simulation based on measured IFTs (mN/m) for NI blend and Yates**

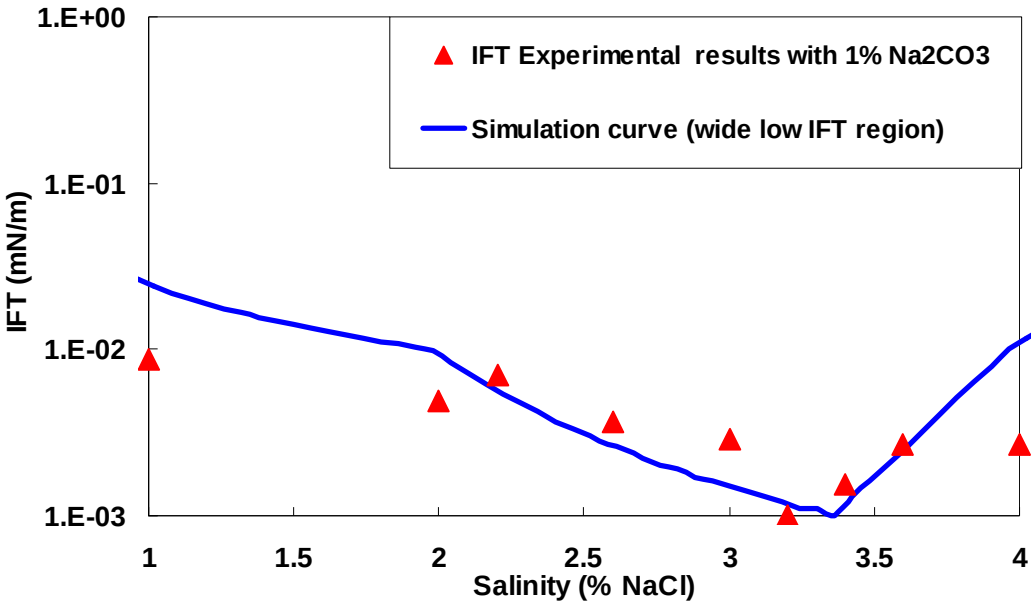


**Figure 6.3 Comparison between simulation and experimental IFT**

For a soap to surfactant ratio of 0.34 or soap fraction of 0.25, where optimal salinity is approximately 3.5% NaCl, the point in the under-optimum region on the IFT contour for 0.01 mN/m was estimated to be at 2.0% NaCl, using experimental data in Chapter 4. This choice is conservative because IFT values near 0.01 mN/m were seen at even lower salinities, according to figure 4.13. However, emulsions present at these low salinities prevented confirmation of the low tensions by solubilization ratio measurements. In the over-optimum region IFT was taken to be 0.01 mN/m at 4.0% NaCl for the same soap/surfactant ratio. Here too the choice is conservative because measured IFT values were near 0.01 mN/m at higher salinities, but emulsions precluded estimates of solubilization parameter. For the same soap/surfactant ratio IFT was taken to be 0.1 mN/m at 0.5% and 5.0% NaCl. These choices are also conservative. Simulation results were insensitive to the exact location of the 0.1 mN/m IFT contours. Points on the IFT contours for other soap/surfactant ratios were located by assuming that a particular IFT, e.g., 0.01 mN/m, was the same percentage below (or above) the optimal

value as when the ratio was 0.35. The equations used to calculate IFT are shown in the Appendix C, FindIFT.m. The comparison between the IFT curve used in simulation and experimental IFT is shown in figure 6.3.

#### 6.1.1.3 Surfactant Adsorption

The assumption for surfactant adsorption is Langmuir-type adsorption with two parameters ($c_{max}$, $H$) as equation (6.4).

$$C_{3ads} = \frac{c_{\max} c_{31}}{\frac{c_{\max}}{H} + c_{31}} \tag{6.4}$$

where $c_{max}$ is the maximal adsorption amount (adsorption plateau),

$H$ is the initial slope of the isotherm, i.e., Henry's law coefficient. In the simulation, $H = 4$ is used.

$c_{max}$ is a function of the concentrations of NaCl ($c_{51}$) and $Na_2CO_3$ ($c_{61}$) as discussed in Chapter 5. The contour map in figure 5.9 in Chapter 5 is used for calculate $c_{max}$.

#### 6.1.1.4 Aqueous Phase Viscosity

The viscosity of aqueous phase determines the mobility ratio, which is very important for a successful ASP process. The aqueous phase viscosity is adjusted by changing the polymer concentration. As a non-Newtonian, shear thinning fluid, the polymer solution viscosity decreases with increasing rate of shear. As reported in Annual DOE Report 2005, the polymer (Flopaam 3330) is only mildly shear thinning at the

salinity of interest. When shear rate is below 100 $sec^{-1}$, the viscosity is almost constant. Thus, the viscosity at 69.5 $sec^{-1}$ is used as a benchmark value for the simulation. Experimental results (DOE Report 2005) show that the viscosity of polymer solution at 69.5 $sec^{-1}$ is a function of polymer concentration and salinity as figure 6.4 shows.

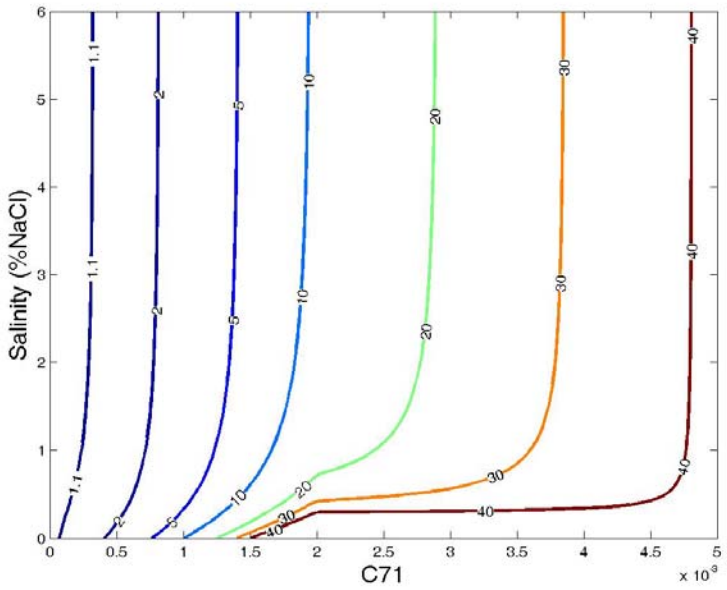


**Figure 6.4 Contour of aqueous phase viscosity (for Flopaam 3330 shear rate 69.5 $sec^{-1}$) (DOE Report 2005)**

In this figure, $c_{71}$ represents the concentration of polymer. When the salinity is less than 1% NaCl, lower salinity leads to higher viscosity: but when the salinity is larger than 1% NaCl, there is not much change on the viscosity by further increasing salinity. Aqueous phase viscosity will be calculated according to figure 6.4. The calculation equations are shown in appendix C, FindVis.m.

### 6.1.1.5 Fractional flow

The fractional flow curve is a function of residual oil saturations and relative permeabilities, which are determined by IFT. Residual saturation is calculated by equations 6.5, which is similar to the approach used by Pope and Nelson (1978).

$$\begin{cases} S_{1r}=0,\ S_{2r}=0 & \text{when IFT}<0.005\ \text{mN/m} \\ \begin{matrix} S_{1r}=0.3*\left[1+\left(\log_{10}(IFT)/2.3\right)\right] \\ S_{2r}=0.3*\left[1+\left(\log_{10}(IFT)/2.3\right)\right] \end{matrix} & \text{when } 0.005\text{dyne/cm}<\text{IFT}<1\ \text{mN/m} \\ S_{1r}=0.3,\ S_{2r}=0.3 & \text{when IFT}>1\ \text{mN/m} \end{cases} \quad (6.5)$$

where $S_{1r}$ is the residual saturation of aqueous phase and $S_{2r}$ is the residual saturation of oleic phase.

The relative permeabilities are calculated as follows:

$$S_{jR}=\frac{\left(S_j-S_{jr}\right)}{\left(1-S_{1r}-S_{2r}\right)} \qquad j=1,2 \qquad (6.6)$$

$$k_{rj}=k_{rj}^{o}S_{jR}^{Ej} \qquad j=1,2 \qquad (6.7)$$

$$k_{r1}^{o}=k_{rw}^{o}+(1-k_{rw}^{o})(0.3-S_{2r})/0.3 \qquad (6.8\text{-a})$$

$$k_{r2}^{o}=k_{ro}^{o}+(1-k_{ro}^{o})(0.3-S_{1r})/0.3 \qquad (6.8\text{-b})$$

where $k_{rw}^{o}$ is end point permeability of water, $k_{ro}^{o}$ is end point permeability of oil.

$$\begin{cases} Ej=1.0 & \text{when IFT}<0.005\ \text{mN/m} \\ Ej=1.5+1/6*\log_{10}(IFT) & \text{when } 0.005\ \text{mN/m}<\text{IFT}<1\ \text{mN/m} \\ Ej=1.5 & \text{when IFT}>1\ \text{mN/m} \end{cases} \quad (6.9)$$

With these equations, the fractional flow curve can be calculated as (6.10)

$$f_1 = \frac{k_{r1}/\mu_1}{k_{r1}/\mu_1 + k_{r2}/\mu_2} \tag{6.10}$$

where $\mu_i$ is the viscosity of phase *i*,

At high IFT, the above parameters are for a water-wet system. Figure 6.5 shows the fractional flow changes with saturation at different IFT by assuming aqueous phase and oleic phase have same viscosity.

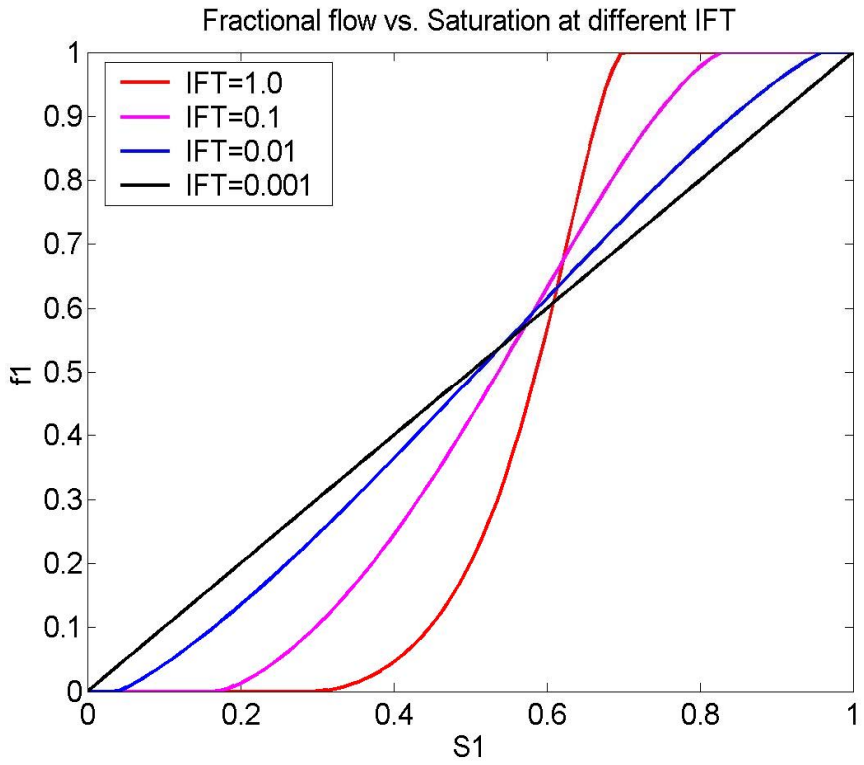


**Figure 6.5 Fractional flow changes with saturation at different IFT (Aqueous phase viscosity = Oleic phase viscosity)**

### 6.1.2 Equations and Calculation Procedure

Given the above assumptions, the continuity equations for each component *i* (Pope and Nelson, 1978) are:

$$\frac{\partial(C_i + C_{iads})}{\partial t} + \frac{q}{A\phi}\frac{\partial F_i}{\partial x} = K_l \frac{\partial^2 C_i}{\partial x^2} \tag{6.11}$$

Dimensionless equations (6.15) can be derived from equation (6.11) by using dimensionless variables (6.12-6.14).

$$x_D = \frac{x}{L} \tag{6.12}$$

$$t_D = \frac{q}{A\phi L}t \tag{6.13}$$

$$Pe = \frac{Lq}{K_l A\phi} = \frac{L}{\alpha_l}$$ Peclet Number (6.14)

$$\frac{\partial(C_i + C_{iads})}{\partial t_D} + \frac{\partial F_i}{\partial x_D} = \frac{1}{Pe}\frac{\partial^2 C_i}{\partial x_D{}^2} \tag{6.15}$$

where $C_i$ is the overall concentration of component *i*. $C_i = c_{i1} * S_1 + c_{i2} * S_2$

$C_{iads}$ is the adsorbed concentration of component *i*

$F_i$ is the overall fractional flow of component *i*. $F_i = c_{i1} * f_1 + c_{i2} * f_2$

Equations (6.15) are solved numerically by explicit finite difference with upstream weighting of fractional flow. The computational procedure is as follows:

1. For a given $C_1$(water saturation), $C_2$(oil saturation, i.e., 1- $C_1$) and other compositions $C_i$, $c_{ij}$ in each grid block can be calculated by partition calculation if the component *i* is not adsorbed. For adsorbing component, it is solved by Newton-Raphson iteration with the relationships of partition and adsorption. For the first time step, it starts with initial conditions.
2. Optimum salinity is determined from the local soap fraction. Thus, IFT of each grid block is calculated with $c_{ij}$ calculated in step 1.
3. The residual saturation and relative permeability are solved with IFT calculated in

step 2. Thus the overall fractional flow $F_i$ is calculated.

4. Equations (6.15) are used to calculate the overall concentration of each component with overall fractional flow $F_i$ for the next time step.

5. Steps 1 to 5 are repeated until the simulation is done.

## 6.2 Characteristics of Alkali-Surfactant-Polymer process

### 6.2.1 Concentration Profiles and Soap to Surfactant Gradient with Large Slug

An example of ASP process is presented with the parameters in table 6.1. In this base case, surfactant concentration is 0.2% NI Blend, the surfactant slug size is 0.5 pore volume, and the initial reservoir salinity as well as all injection fluids are at 2% NaCl. This simulation example is an illustration of oil recovery by injecting alkali, surfactant and polymer slugs. The initial condition of this example is after waterflooding, i.e., the oil saturation is the residual oil saturation after water flooding. The value of *dt/dx* of 0.05 was used. This value is the largest value where stability could be maintained during the finite difference calculations. For *dt/dx* = 0.1, sometimes there was an instability problem. Similarly the choice of 100 grid blocks reflects the smallest number for which the solution does not change significantly with increasing number of grid blocks. The dynamic surfactant adsorption breakthrough curve shown in Chapter 5 shows the dispersion of the 1-D sand pack. When the simulator was used to match the results, a Peclet number of 500 was obtained. Other parameters are chosen based on the values of the sand pack displacement experiments which will be shown in the next chapter.

| Initial Oil Saturation | Formation Brine | Acid No. of Crude oil | Injection $Na_2CO_3$ concentration | Injection Salinity |
|---|---|---|---|---|
| 0.3 | 2.0% NaCl | 0.2 mg KOH/g | 1.0% | 2.0% NaCl |
| | | | | |
| Surfactant concentration | Surfactant Slug Size | Injection Polymer Conc. (Flopaam 3330S) | Injection solution viscosity: | Crude Oil viscosity |
| 0.2% (NI blend) | 0.5 PV | 5000 ppm | 40 cp | 19.7 cp |
| | | | | |
| Polymer adsorption | Surfactant Adsorption | Surfactant retardation due to adsorption $\beta_1$ * | Polymer retardation due to adsorption $\beta_2$ * | Peclet No |
| 20 μg/g | 0.2 mg/g | 0.03 | 0.01 | 500 |
| | | | | |
| Optimum salinity of pure soap | Optimum salinity of pure surfactant | IFT assumption | NX (Grid block No.) | dt/dx |
| 0.5% NaCl | 5.0% NaCl | Wide low IFT region | 100 | 0.05 |

**Table 6.1 Simulation parameters of the example case**

Figure 6.6 shows the concentration profiles of the example case after 0.5 pore volume. From this plot, the soap front is ahead of the surfactant because the surfactant propagation rate is slower than the alkali due to surfactant adsorption and the soap propagation in the oil phase ahead of the surfactant front. Thus ahead of alkali and surfactant front, there is the type II (over-optimum) region because soap is dominant and local salinity is higher than the optimum salinity of soap. In this region, the soap to surfactant ratio is very high. Well behind the surfactant front, there is a type I (under-optimum) region because surfactant is dominant when little or no natural soap resides in this region. Here the local salinity is lower than the optimum salinity of surfactant. In the type I region, the soap to surfactant ratio is very small. Thus, a soap/surfactant ratio gradient is generated. This soap/surfactant ratio gradient has following merits: (1) It assures that the process passes through the optimum region; (2) It retards surfactant that moves into the soap-dominant region ahead of the major surfactant bank because this surfactant partitions into the oil phase, (3) Surfactant will not be phase trapped behind the surfactant bank since the surfactant is in the aqueous phase. To achieve such a gradient, the electrolyte strength of the injected fluids needs to be between the optimum salinities

of natural soap and synthetic surfactant so that the process passes from over-optimum condition ahead of the front, to optimal at the displacement front, and under-optimum behind the front.

Figure 6.7 shows the IFT and soap to surfactant ratio profiles at 0.5 PV. The soap to surfactant ratio gradient is shown in this plot as discussed. The minimum low tension is found at the location where the soap to surfactant ratio is the optimal value when salinity is 2% NaCl.

Figure 6.8 shows the oil saturation profile at 0.5 PV for the same example case. In this figure, the initial oil saturation is the waterflood residual oil saturation (30%). The residual oil saturation after ASP was close to zero and an oil bank is generated.

Figure 6.9 shows the effluent histories of surfactant and soap. Figure 6.10 shows the effluent history of oil. Figures 6.9 indicates that soap breaks through earlier than the surfactant as expected because of the soap to surfactant ratio gradient. Oil bank breaks through even ahead of the soap, which is desirable because the oil produced before soap breaks through is clean and free of emulsion problems. The final recovery efficiency of the example case is 96%, i.e., nearly all the oil has been recovered.

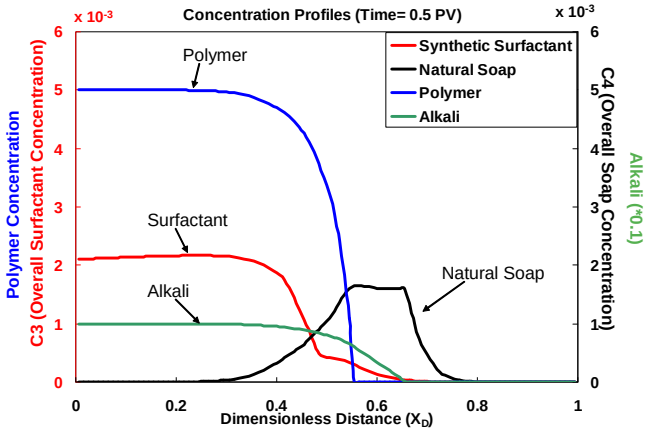


**Figure 6.6 Concentration profiles of example case (0.5 PV)**

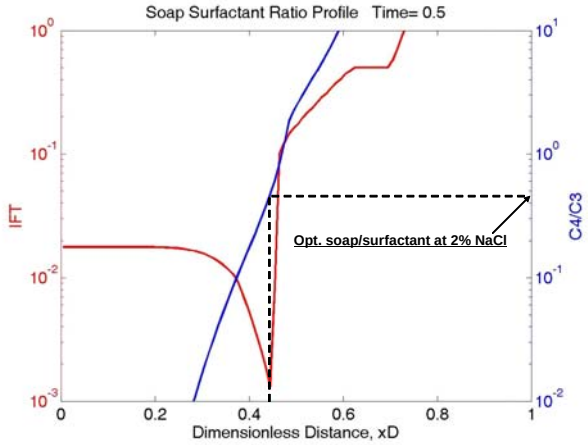


**Figure 6.7 IFT and soap to surfactant ratio profiles of example case (0.5 PV)**

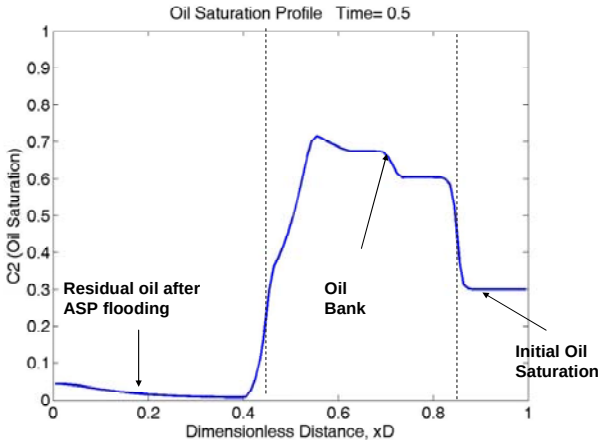


**Figure 6.8 Oil Saturation Profile of example case (0.5 PV)**

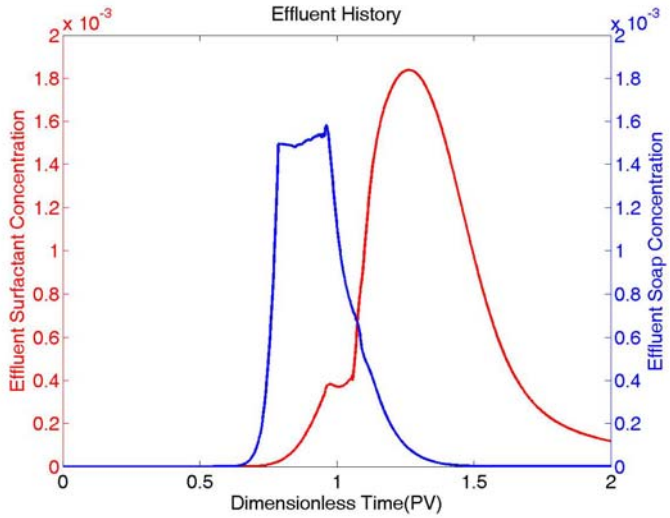


**Figure 6.9 Soap and surfactant effluent history of example case**

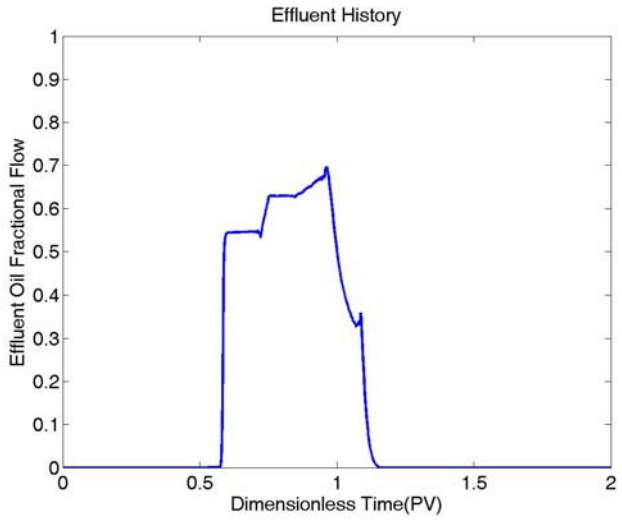


**Figure 6.10 Oil effluent history of example case**

### 6.2.2 Width of Ultra-low Tension Region

As discussed in Chapter 4, the alkali-surfactant-crude oil system studied has wider ultra-low IFT region than is usually observed in the synthetic surfactant systems in the absence of naphthenic soaps. Simulations with different low IFT regions are conducted in this section. A medium width IFT example whose contour is shown as figure 6.11(a) is

based on the IFT curve with no sodium carbonate in the same system, i.e., conventional surfactant polymer flood. As shown in figure 4.14 of Chapter 4, the low IFT region is narrower if no sodium carbonate is present. The narrow width IFT assumption is shown as figure 6.11 (b). In this case, the narrow IFT region is much narrower than the figures 6.2 and 6.11(a) as to illustrate the effect of width of ultra-low tension region for oil recovery. Other major parameters are the same and are shown in Table 6.1. Hereafter, the IFT assumption based on NI blend with $Na_2CO_3$ is called wide low IFT region assumption (contour figure 6.2); the IFT assumption based on NI blend without $Na_2CO_3$ is called medium low IFT region assumption (contour figure 6.11(a)); the extremely narrow IFT is called narrow IFT region assumption (contour figure 6.11(b)).

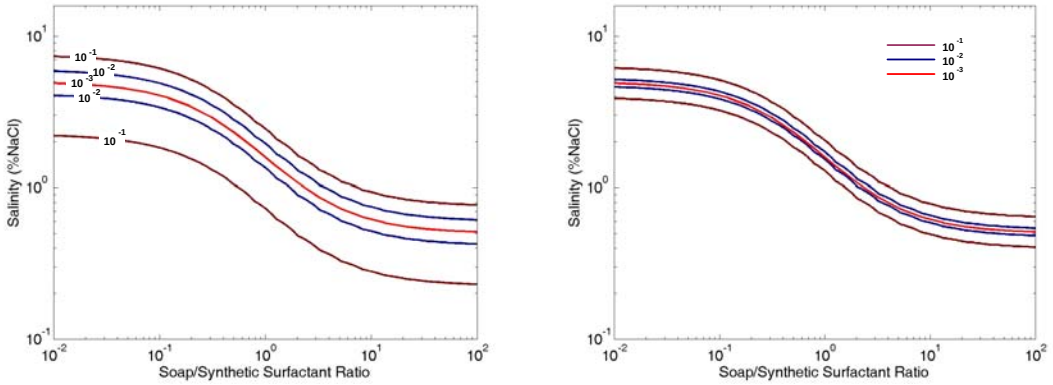


**(a)Medium low IFT region assumption (b) Narrow low IFT assumption**

**Figure 6.11 IFT Contour of two suppositional low IFT region assumptions**

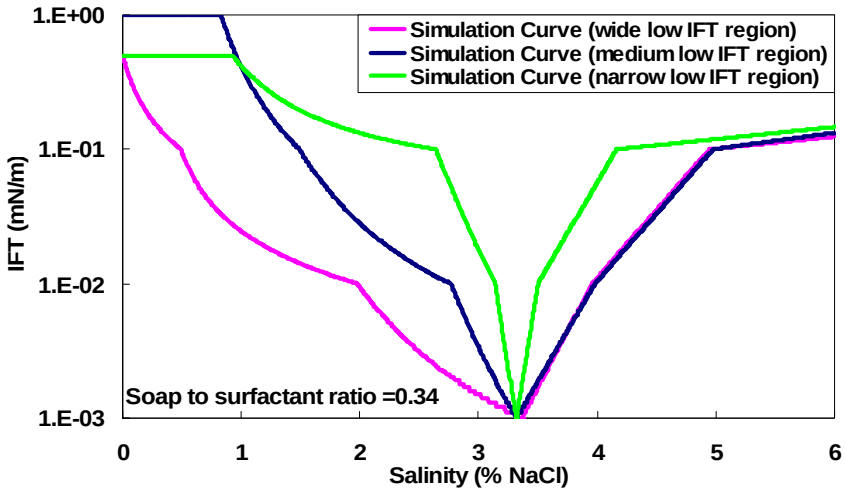


**Figure 6.12 IFT simulation curves with different low IFT regions**

Figure 6.12 shows the IFT versus salinity with different low IFT assumptions when soap to surfactant ratio is 0.34. The minimum IFT value, i.e., the IFT values at optimum are the same ($10^{-3}$ mN/m). But the widths of low IFT region with different assumptions are different.

The simulation results show that the recovery was 96% with wide low IFT region and only 84% and 72% with medium and narrow low IFT region respectively. This result can be explained by figure 6.13. The plots at left show the surfactant, soap, IFT, soap to surfactant ratio and oil saturation profiles respectively for the wide low IFT region when the dimensionless time equals 0.5 PV. The plots in the middle and at right show the same profiles at same time but with medium and narrow IFT region. The width of the low tension region ($<10^{-2}$ mN/m) in the left profile is around 0.1 dimensionless distance, while that of the low tension region in the right profile is only 0.03 dimensionless distance. The oil saturation in the left profile is much less than that in the right profile. Narrow low IFT region will have less recovery because oil is trapped when the IFT increases. When the low IFT region is wide, less oil is trapped after the low tension

region. Thus, with the wide low IFT region in the alkali-surfactant system, higher oil recovery can be achieved for a larger range of salinities. High salinities can cause polymer-surfactant phase separation and lead to high surfactant and/or polymer retention. With the wide low tension region and soap to surfactant gradient, high recovery can be achieved by injecting at salinities well below the optimal value for the synthetic surfactant such that the surfactant and polymer will coexist in the same phase.

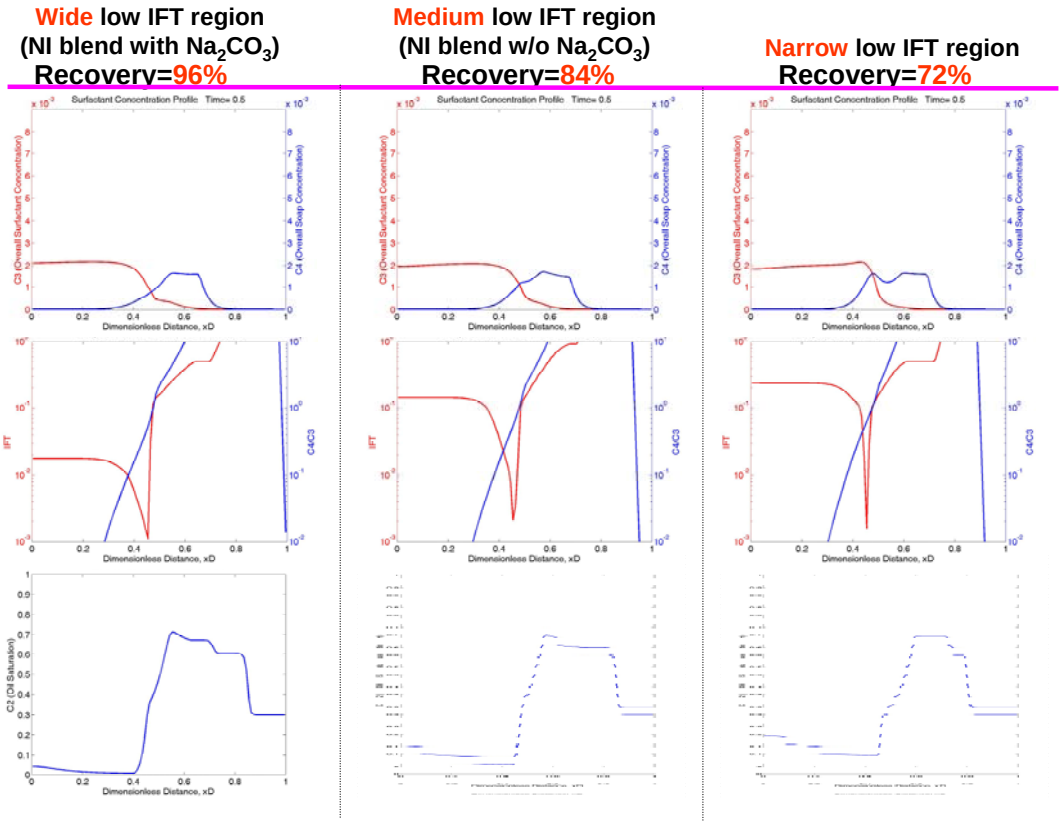


**Figure 6.13 Comparison of profiles between different low IFT region assumptions**

Another interesting phenomenon is the soap and surfactant concentration peak at surfactant front when the IFT region is narrow. The generation of this peak is due to the soap to surfactant gradient. As discussed in the previous section, soap and surfactant ahead of low IFT region are retarded, while soap and surfactant behind the low IFT

region move forward with the velocity of aqueous phase. The accumulation of soap and surfactant makes this peak. This effect is more significant when there is more trapped oil, e.g., the narrow IFT case. Therefore, the displacement front of the ASP is a self-sharpening process similar to the salinity gradient (Hirasaki et al., 1983). However, the back of the surfactant slug can be a spreading wave.

### 6.2.3 Injection Solution Viscosity

Another factor for ASP is the injection solution viscosity. As figure 6.14 shows, the injection solution viscosity can change the oil recovery significantly. The wide low tension region was used in the two cases of figure 6.14. All major parameters except the injection solution viscosity are the same as shown in Table 6.1. The plots in 6.14 show the surfactant, soap, IFT, soap to surfactant ratio and oil saturation profiles respectively when the dimensionless time equals 0.5 PV as in figure 6.13. The difference between these plots is that the left plots are calculated by using 40 cp as the injection solution viscosity, while the right plots use 24 cp as the injection solution viscosity.

The IFT profiles of these two conditions are similar to each other. However, the oil saturation profiles are different, thus the oil recoveries are different. The injection solution viscosity has a significant effect on recovery because it is related to mobility ratio. Because the oil fractional flow increases with increasing aqueous phase viscosity, the oil in the low tension region can be displaced in less distance before the IFT increases.

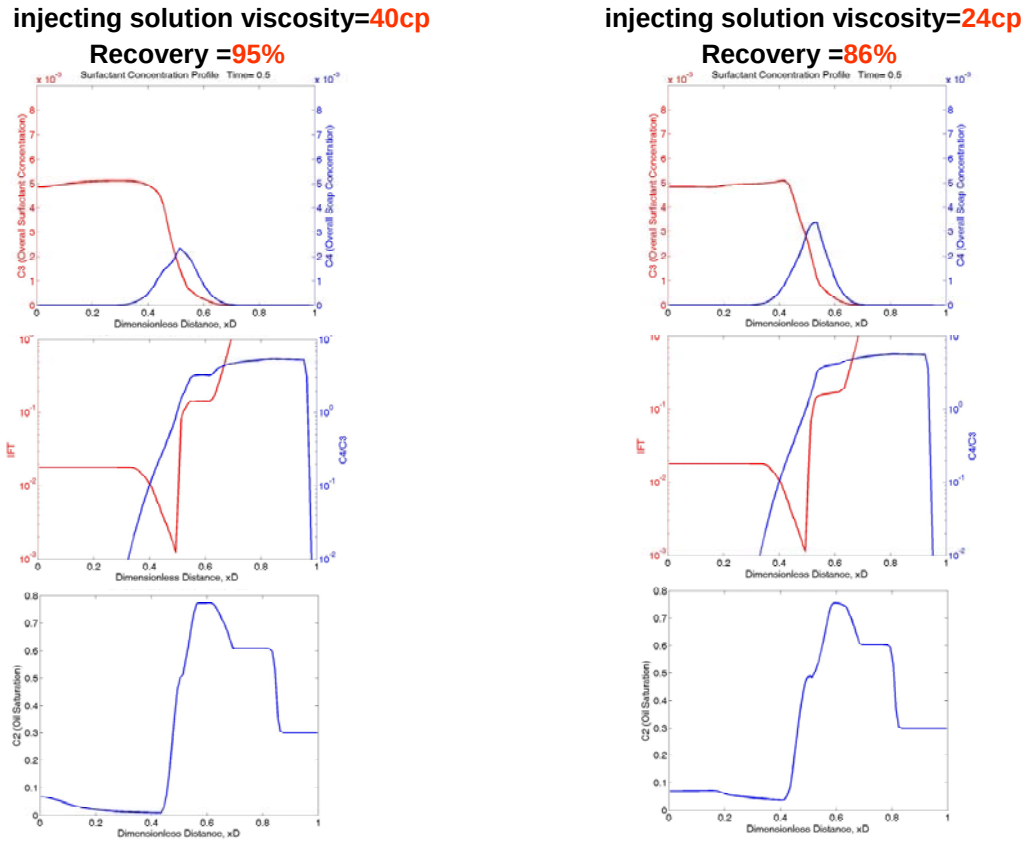


**Figure 6.14 Comparison of profiles between varied injecting solution viscosities**

Figure 6.15 illustrates this effect. Lower aqueous phase viscosity, i.e., higher mobility ratio, has lower oil recovery even with wide low IFT region because it takes a greater distance to displace the oil before the IFT increases. Thus, the injection solution viscosity should be high enough to obtain high oil recovery. The fractional flow curve in Figure 6.15 indicates that the displacement front should be a shock. However, the simulation model includes dispersion. A self-sharping wave in the presence of dispersion is not a shock but rather a wave of constant width (Pope, Lake and Helfferich, 1978)

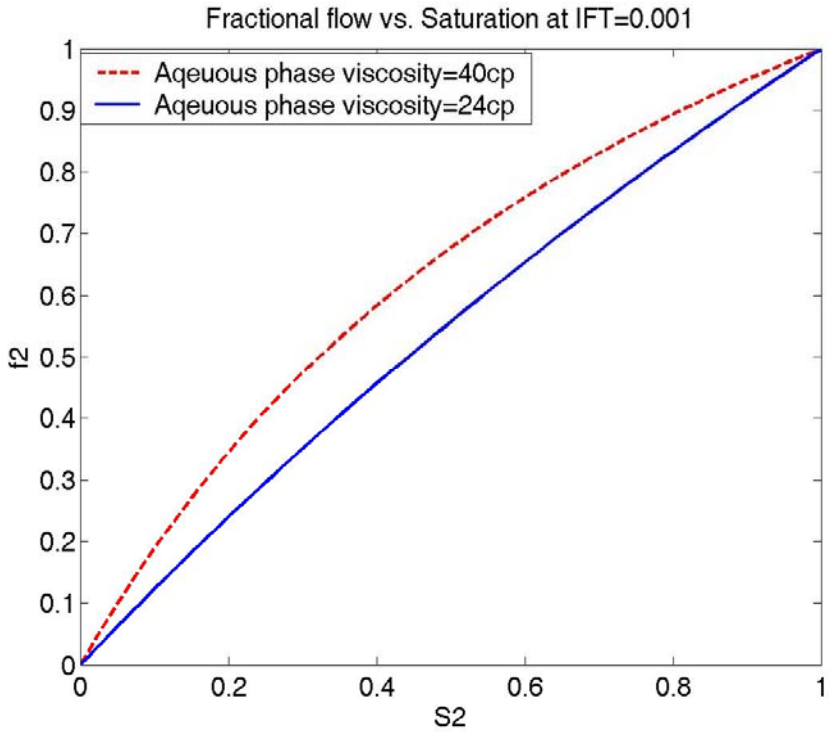


**Figure 6.15 Oil Fractional Flow vs. Saturation at IFT=0.001dyne/cm (Oil viscosity =19.7 cp)**

### 6.2.4 Effect of Dispersion

In the previous section, a Peclet number of 500 was chosen by matching the 1-D sand pack adsorption experiments. However, the dispersion can be much larger, i.e., the Peclet number can be much smaller, in the field due to the reservoir heterogeneity than the 1-D sand experiments. Figure 6.16 shows the effect of dispersion for large surfactant slug size.

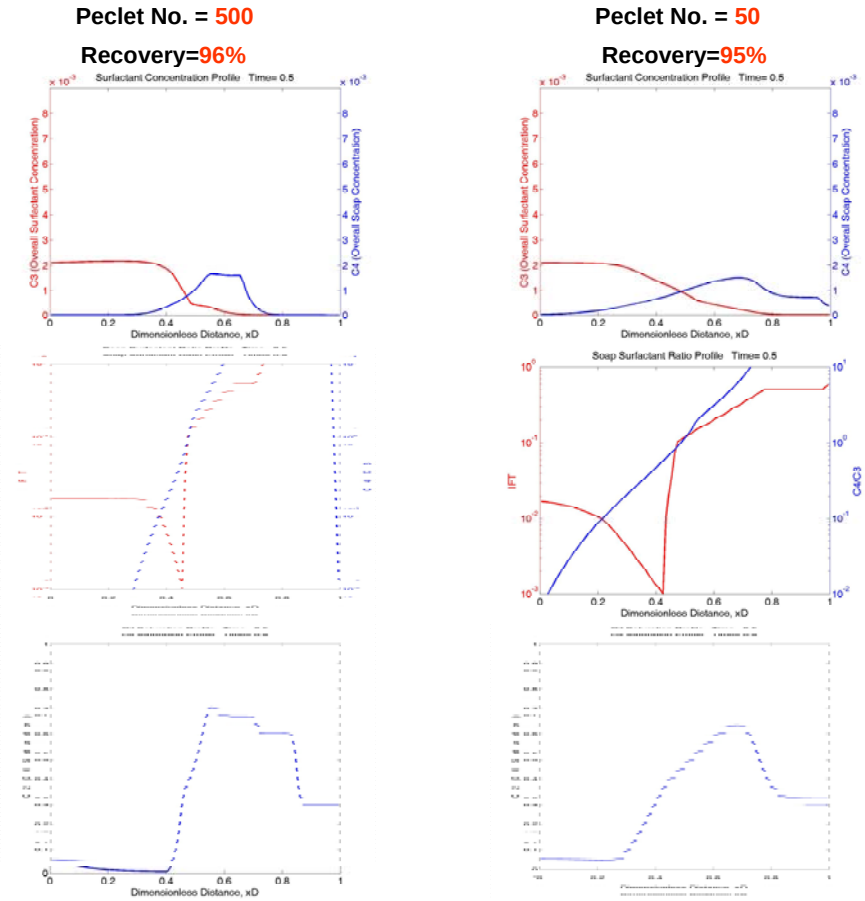


**Figure 6.16 Comparison of profiles between dispersions after 0.5 PV with large surfactant slug (0.5PV)**

The plots in 6.16 show the surfactant, soap, IFT, soap to surfactant ratio and oil saturation profiles respectively when the dimensionless time equals 0.5 PV as in figure 6.13. The difference between these plots is that the left figures are calculated with Peclet number 500, while the right figures use Peclet number 50. Peclet number 50 is chosen because it represents the field scale dispersion for a distance of 1 km (Lake, 1989). Because of the larger dispersion, the concentration profiles of the case with Peclet number 50 change more gradually than the profiles of the case with Peclet number 500. The surfactant front travels even faster and there is a longer soap concentration tail after the surfactant front due to the high dispersion. This effect causes the soap to surfactant

ratio to change more gradually, so that the low IFT area in the profiles is even wider even though the same low tension versus salinity relationship was used in both simulations. This counteracts the effect of larger dispersion which may be expected to reduce the oil recovery. The two cases have similar oil recovery. Therefore, the self-sharpening effect of ASP helps to counteract the unfavorable larger dispersion when surfactant slug size is large.

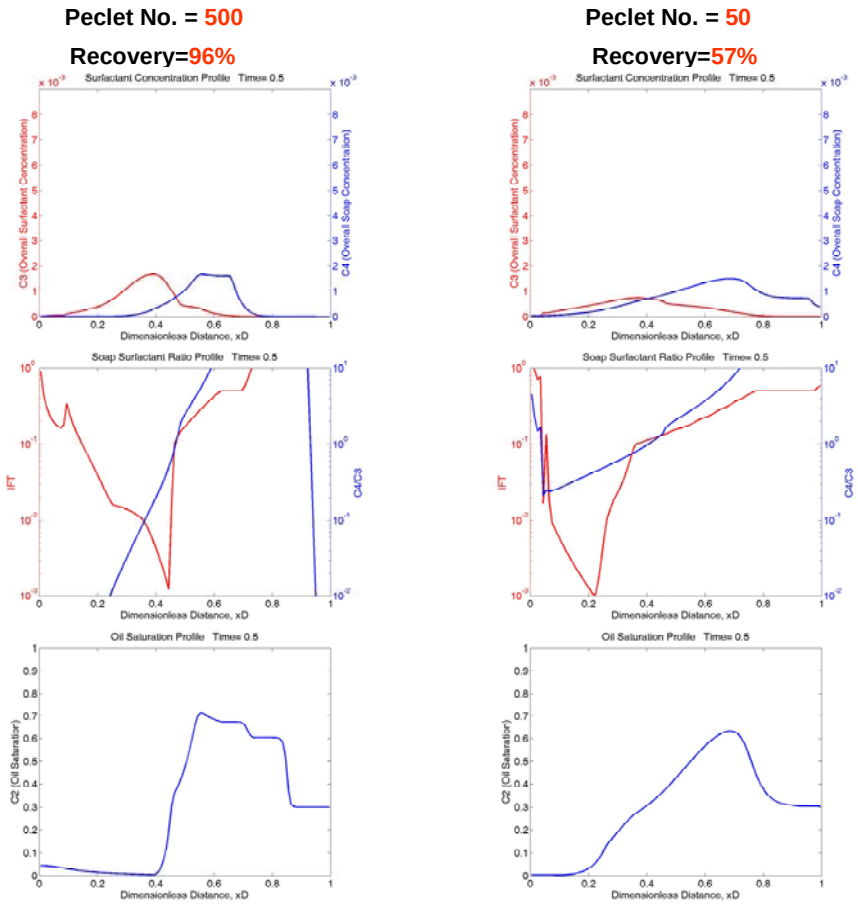


**Figure 6.17 Comparison of profiles between dispersions with small surfactant slug (0.2PV)**

As shown in figure 6.17, the recovery factor changes much with dispersion when the surfactant slug size is as small as 0.2 PV. From 6.17, the displacement front travels slower when dispersion is large. Figure 6.18 is the distance-time diagram that illustrates

the difference between large and small surfactant slug. When surfactant slug size is large (0.5 PV), the displacement front propagates at similar velocities with different dispersion. However, when surfactant slug is small (0.2 PV), the displacement front seems not to propagates any more after 0.3 PV with large dispersion. It is because the surfactant concentration in the surfactant slug decreases significantly with large dispersion and small surfactant slug. This makes the local soap to surfactant ratio larger so that more surfactant partitions into the oleic phase and is retarded. In the section 6.2.6, the recovery can be significantly improved by using salinity gradient.

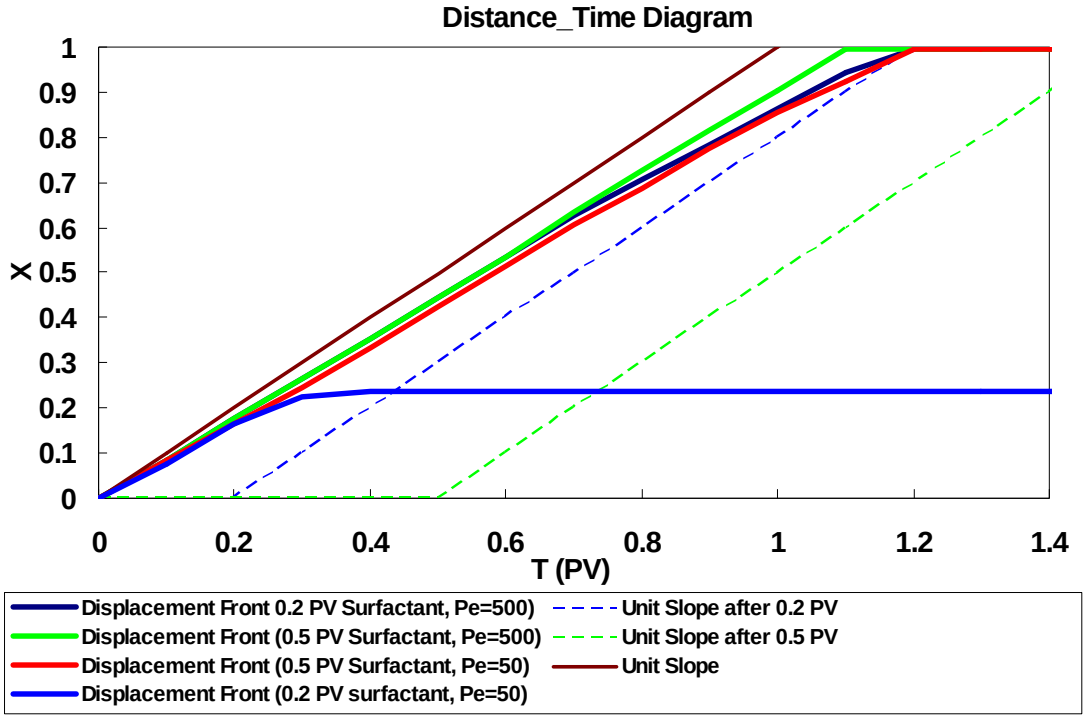


**Figure 6.18 Distance Time Diagram for different surfactant slug and dispersion**

### 6.2.5 Optimum Operational Region

As shown in the previous section, the soap to surfactant ratio gradient in ASP process assures that the process passes the optimum condition at the displacement front if

the injection salinity is between that of soap and surfactant. But that does not mean high recovery can be achieved by injecting at any salinity between optimum salinity of soap and surfactant for any conditions. A number of simulations were conducted with different naphthenic soap concentrations, injected surfactant concentrations and salinity (Appendix B). As figure 6.19 shows, the percent recovery of the waterflood residual oil was contour plotted as a function of a characteristic soap fraction at the surfactant front as abscissa and the injected dimensionless salinity as the ordinate. To make the contour plot consistent, the recovery efficiency is the oil recovery at 2.0 pore volumes. The soap fraction at the surfactant front and dimensionless salinity are defined as equation (6.16) and (6.17). The soap fraction is volume of soap in an element of pore volume at initial $S_{or}$ as a fraction of surfactant plus soap if the initial brine is replaced by surfactant solution to be injected.

$$Soap\_Fraction = \frac{C_{soap} * S_{or}}{C_{soap} * S_{or} + C_{surfactant} * (1 - S_{or})} \tag{6.16}$$

where $C_{soap}$ is the soap molar concentration. $C_{soap} = Acid\_No./MW\_KOH$

$S_{or}$ is initial oil saturation,

$C_{surfactant}$ is injection surfactant molar concentration,

$$Dimensionless\_Salinity = \frac{Salinity}{Optimum\_Salinity\_of\_Soap} \tag{6.17}$$

Since the optimum salinity of pure soap in this case is 0.5% NaCl, the value of dimensionless optimum salinity of pure surfactant is 10 because optimum salinity of pure surfactant is 5% NaCl.

### 6.2.5.2 Wide low tension assumption with 0.5 Pore Volume Surfactant Slug

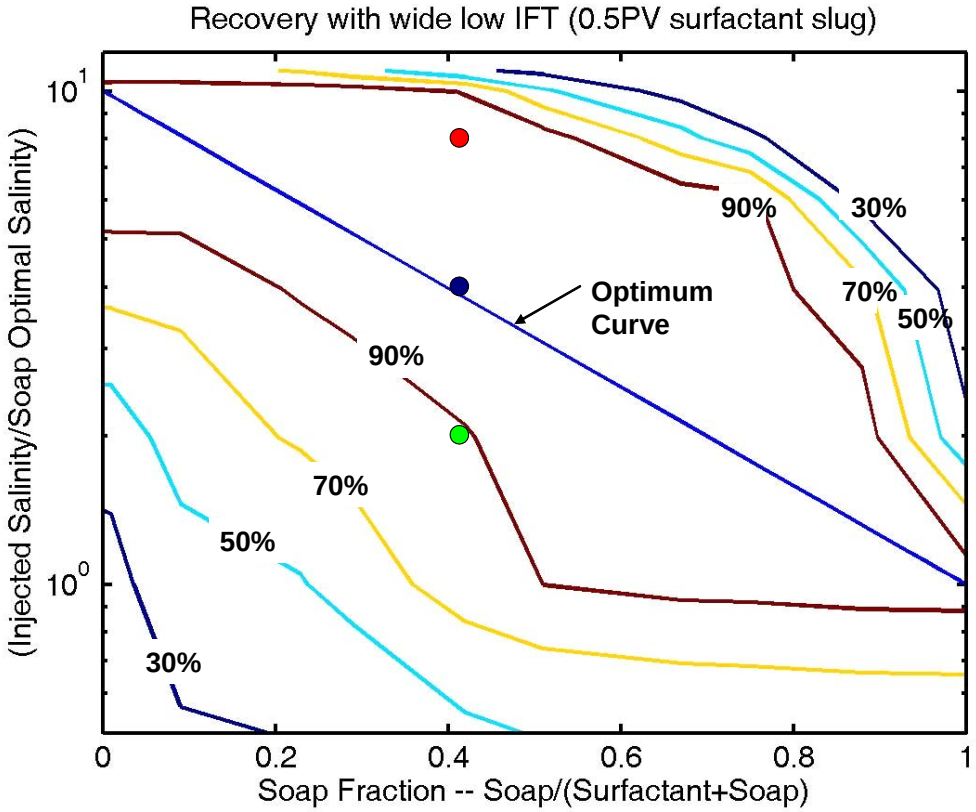


**Figure 6.19 Contour of recovery factor at 2.0 PV with 0.5 PV surfactant slug size (wide low IFT assumption)**

From figure 6.19 in which the surfactant slug size is 0.5 pore volume with wide low IFT assumption, high oil recovery can be achieved by following the optimum curve which is determined by the phase behavior experiments. The optimum salinity line on the plot is that for characteristic soap fraction based on figure 3.10 that gives optimum conditions. When the injected salinity is more than the calculated optimum salinity, the recovery factor will drop off very quickly when the salinity reaches a certain high value. This is because of surfactant retardation and retention with over-optimum conditions.

Nearly all the surfactant is trapped in the oil phase and will not propagate any more. The recovery efficiency falls off more gradually when the injected salinity is less than the calculated optimum salinity.

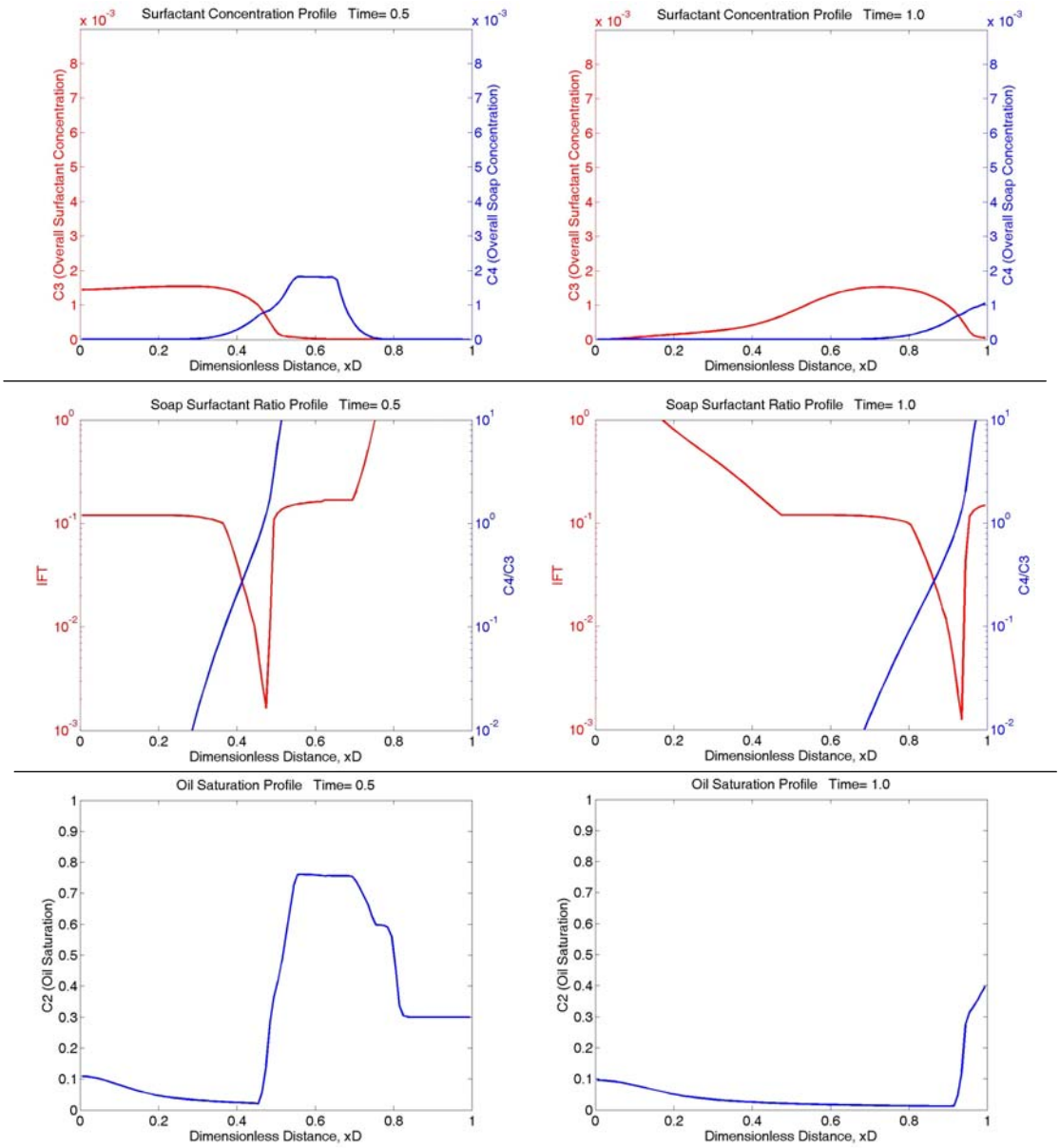


**Figure 6.20 Profiles for an under-optimum case with <u>0.5 PV</u> surfactant slug size <u>wide low tension</u> assumption (Acid No.=0.2mg/g, surfactant concentration=0.14%, injection salinity=<u>1.0%</u>)**

Figure 6.20 shows the typical profiles for the *<u>under-optimum</u>* case at time 0.5 and 1.0 pore volume after initial injection for a 0.5 PV surfactant slug size with wide low IFT

assumption. This case is with 0.2 mg/g acid number, 0.14% surfactant so that the soap fraction for this case is 0.42, for which the dimensionless optimum salinity is 3.8, or the optimum salinity is 1.9 % NaCl. The injection salinity for figure 6.20 is 1.0 % NaCl so that it is an under-optimum case as shown as the green point in figure 6.19. The recovery efficiency for this condition is 89.5%.

Similar to the base case profiles, the soap front is ahead of the surfactant, and a soap to surfactant gradient is generated during this ASP process in figure 6.20. The IFT value is high at the soap front (where soap is generated) because of the over-optimum condition; it is also very high at the rear of the surfactant slug because it is under-optimum. There is a low IFT optimum region which displaces the oil. The lowest tension is located at the optimum soap to surfactant ratio when salinity is 1% NaCl. The profiles in figure 6.20 indicate that 0.5 PV surfactant slug size is larger than needed. The surfactant profile shows that there is still a lot of surfactant present behind the IFT minimum. However, IFT in this region is too high to displace the oil remaining there.

Figure 6.21 shows the same case as that in figure 6.20 except the injection salinity is 2.0% NaCl which is *near the optimum* curve. The recovery efficiency for this condition is 98.1%. The concentration and IFT profiles are similar to the under-optimum case, and the slug again is much larger than needed. The IFT value (~0.02 mN/m) in the surfactant slug in this case is lower than that (0.1mN/m) in under-optimum cases. The reason that optimum condition has a higher recovery is because it has moderately low IFT at the injection point ($X_D$=0). Figures 6.20 and 6.21 show that the recovery efficiency does not change much in going from optimum to under-optimum conditions.

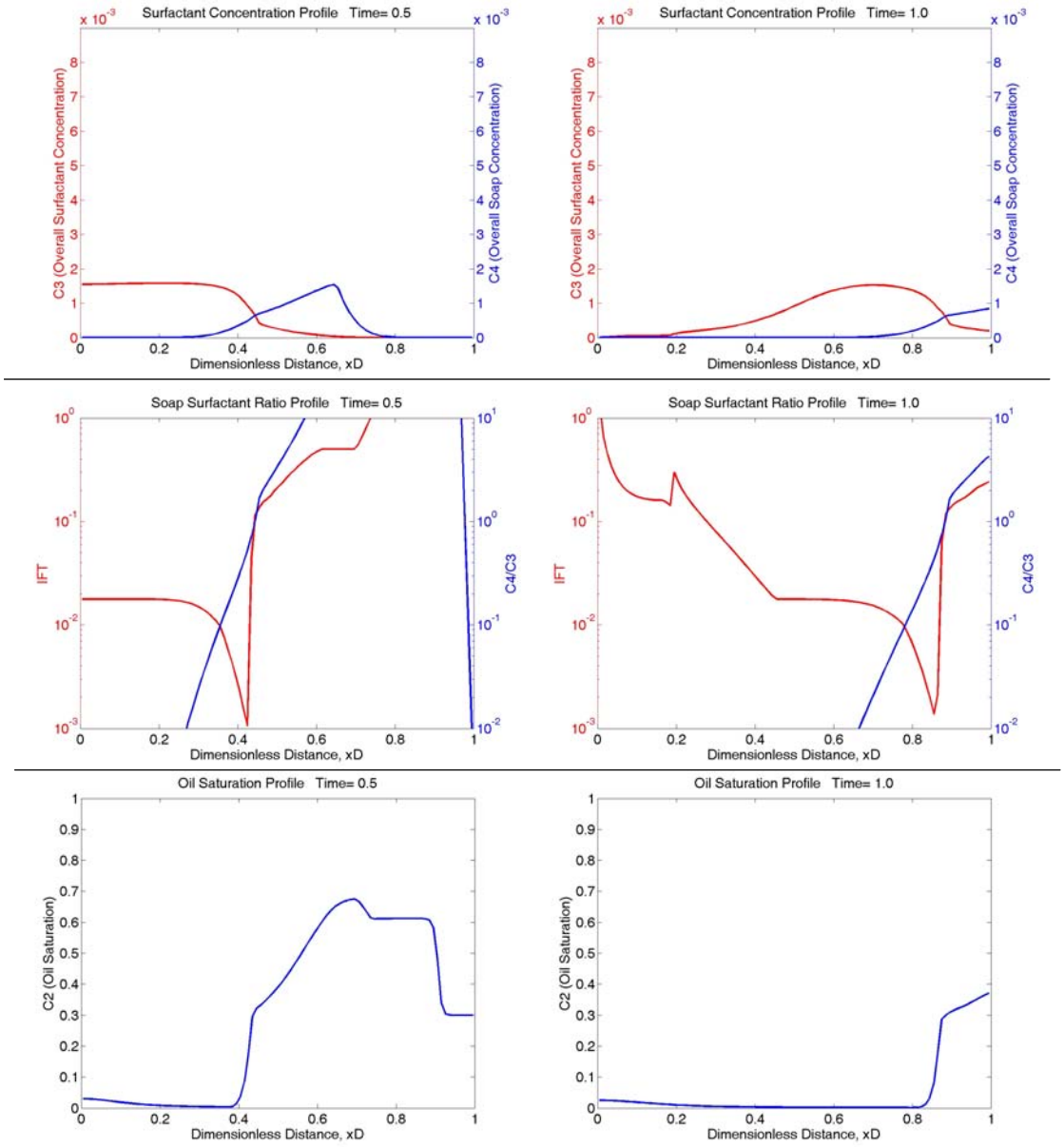


**Figure 6.21 Profiles for an optimum case with <u>0.5 PV</u> slug size and <u>wide low tension assumption</u> (Acid No.=0.2mg/g, surfactant concentration=0.14%, injection salinity=<u>2.0%</u>)**

Figure 6.22 shows the *<u>over-optimum</u>* case with injection salinity 4.0 % NaCl. The recovery efficiency is 100% after 2.0 PV. The low propagation velocity of low tension region is because the higher salinity results in higher partition coefficient and thus slower surfactant propagation. This is typically seen in the over-optimum surfactant flood (Nelson, 1978). Although it shows higher recovery in this case, it may not desirable due

to large surfactant slug required (0.5 PV). When the surfactant slug becomes less, the recovery will drop significantly, (see small slug results in the next section). The effect of surfactant-polymer phase separation was not modeled. This effect could have made the over-optimum case much worse.

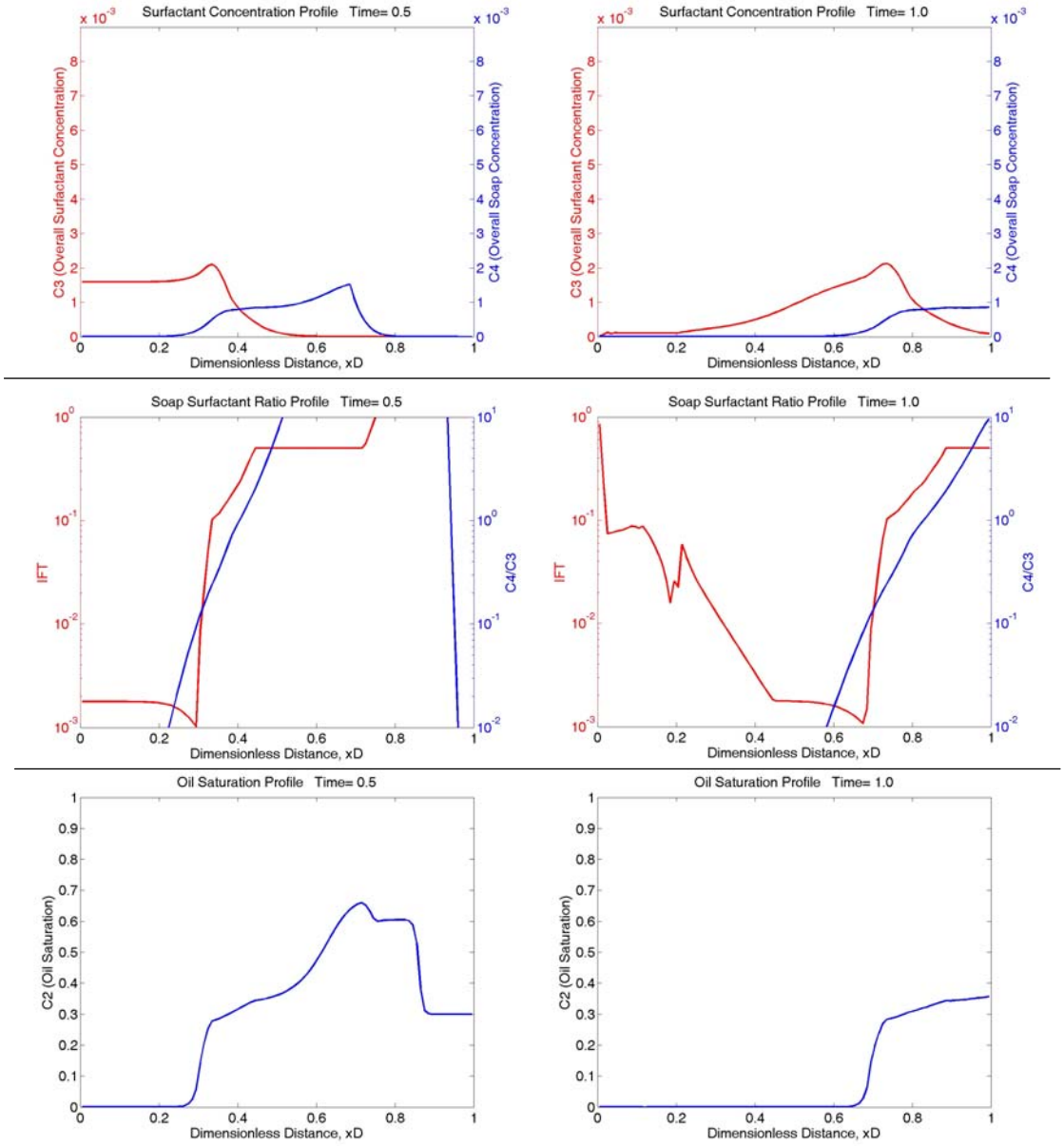


**Figure 6.22 Profiles for an over-optimum case with <u>0.5 PV</u> slug size and <u>wide low tension assumption</u> (Acid No.=0.2mg/g, surfactant concentration=0.14%, injection salinity=<u>4.0%</u>)**

### 6.2.5.2 Wide low tension assumption with 0.2 Pore Volume Surfactant Slug

If the surfactant slug size is reduced to 0.2 pore volumes, the recovery contour plot is shown as figure 6.23. Compared to figure 6.19, the contour shape in the under-optimum part does not change much but that in the over-optimum part changes a lot. This effect can be explained by figures 6.24, 6.25 and 6.26, which are the counterparts of figures 6.20 to figure 6.22 but with smaller slug size`.

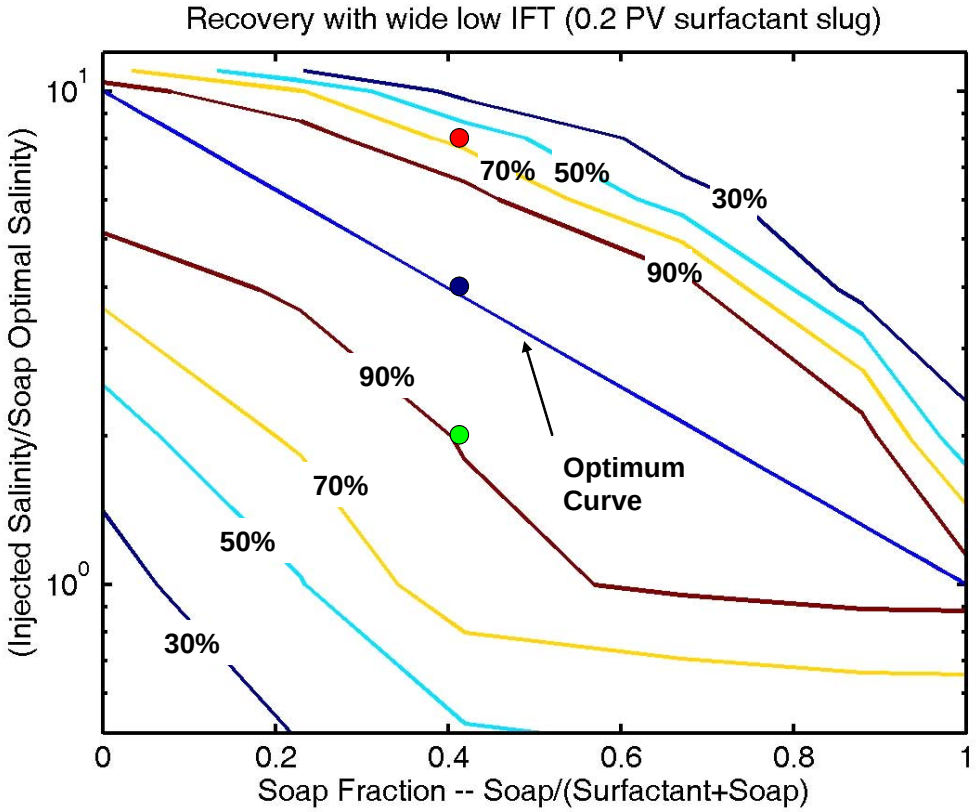


**Figure 6.23 Contour of recovery factor at 2.0 PV with 0.2 PV surfactant slug size (wide low tension assumption)**

The *under-optimum* conditions in figure 6.24 are the same as that of figure 6.20 except the surfactant slug size is 0.2 pore volume. The recovery factor for this condition

is 91% which is very close to that of figure 6.20 (90%). The profiles are also similar except for the surfactant slug size in figure 6.24 is less than that in figure 6.20. The recovery and oil saturation profiles are also close in figures 6.20 and 6.24.

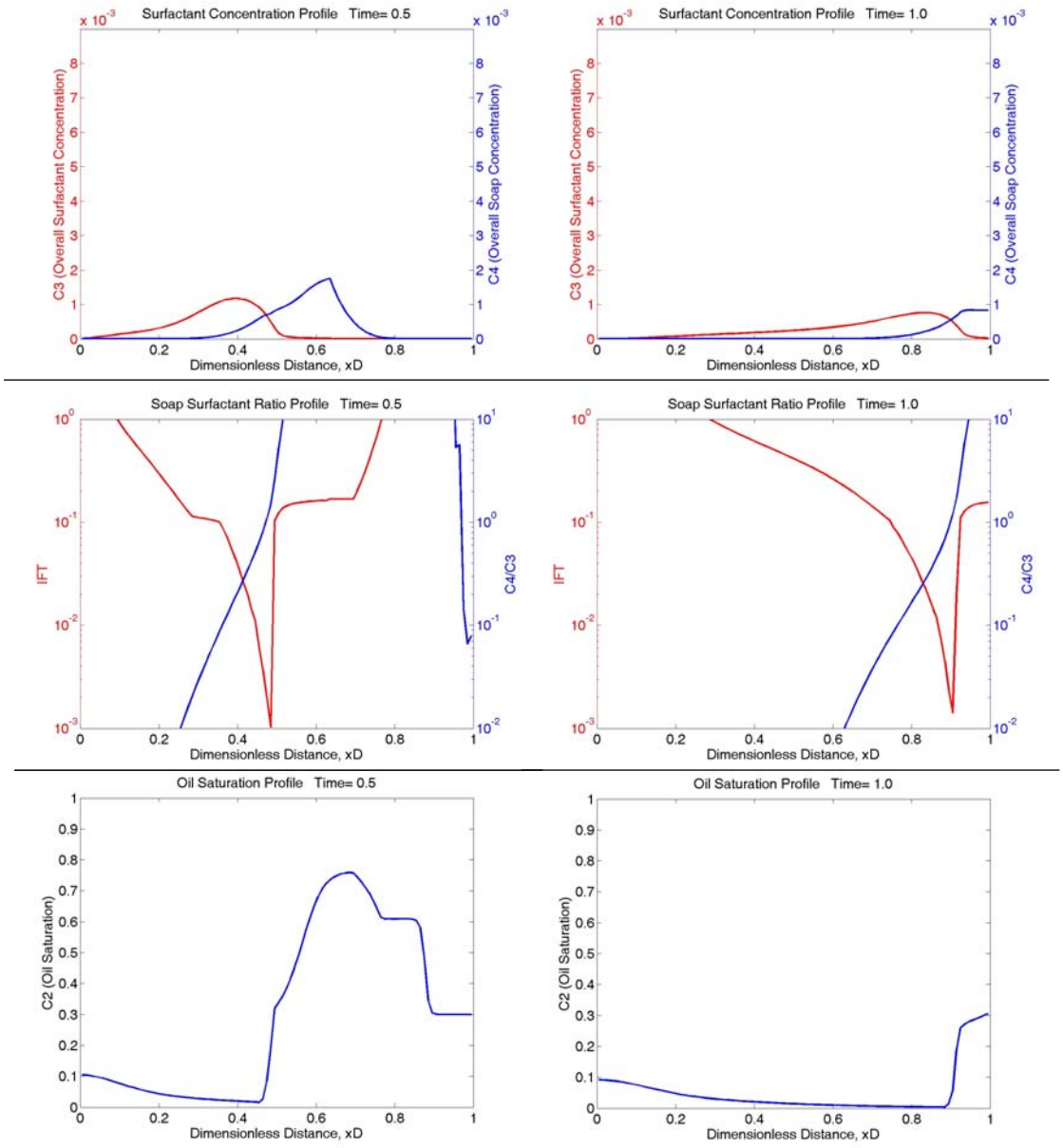


**Figure 6.24 Profiles for an under-optimum case with <u>0.2 PV</u> surfactant slug size <u>wide low tension</u> assumption (Acid No.=0.2mg/g, surfactant concentration=0.14%, injection salinity=<u>1.0%</u>)**

Figure 6.25 with 0.2 PV surfactant slug *near optimum* is the counterpart to figure 6.21 with 0.5 PV surfactant slug for the optimum condition (2% NaCl). The recovery factor for figure 6.25 is 98.4% while that for figure 6.20 is 98.1%. Similar to the under-optimum cases, the slug size does not change the recovery much.

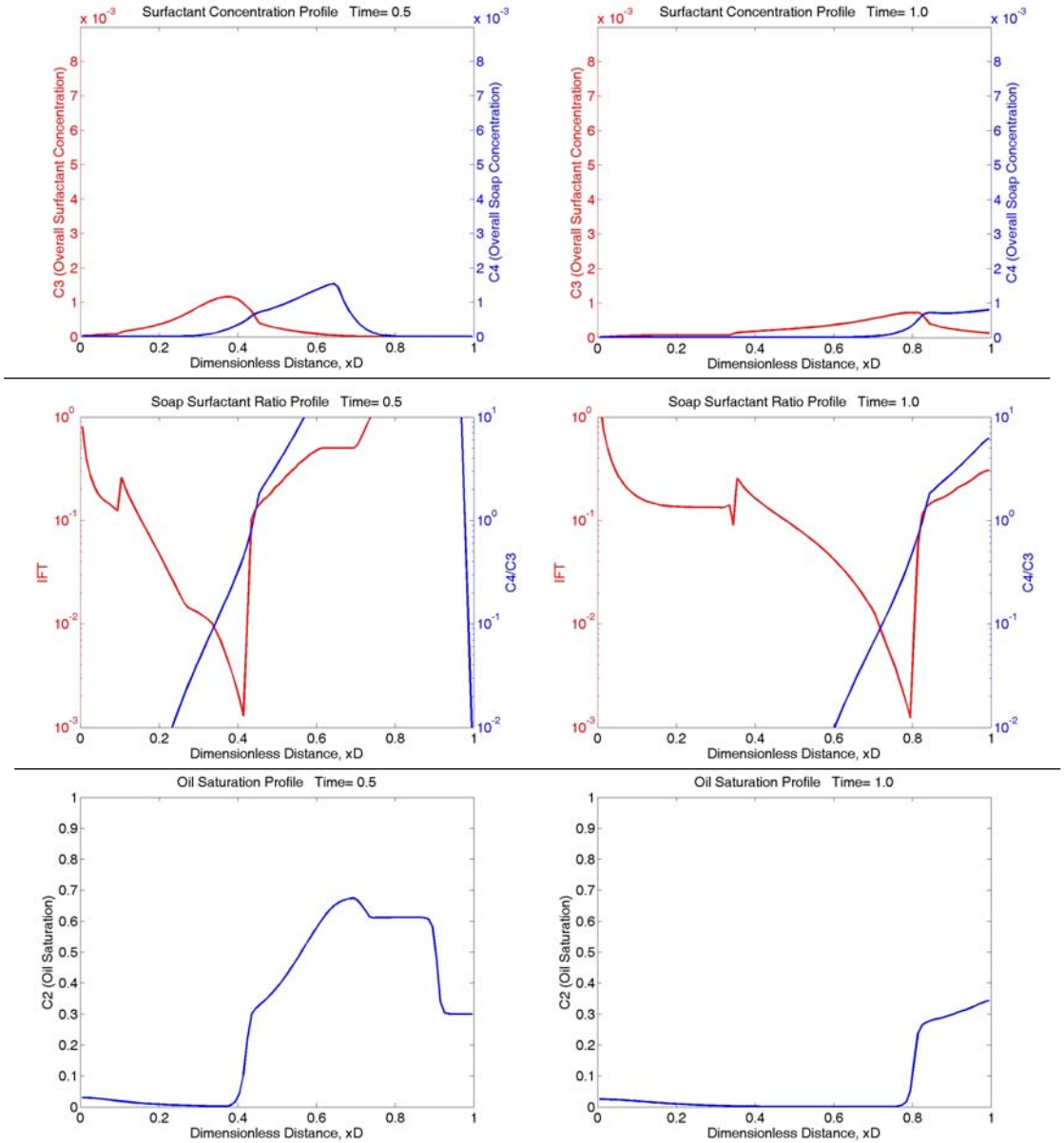


**Figure 6.25 Profiles for a near optimum case with <u>0.2 PV</u> slug size and <u>wide low tension assumption</u> (Acid No.=0.2mg/g, surfactant concentration=0.14%, injection salinity=2.0%)**

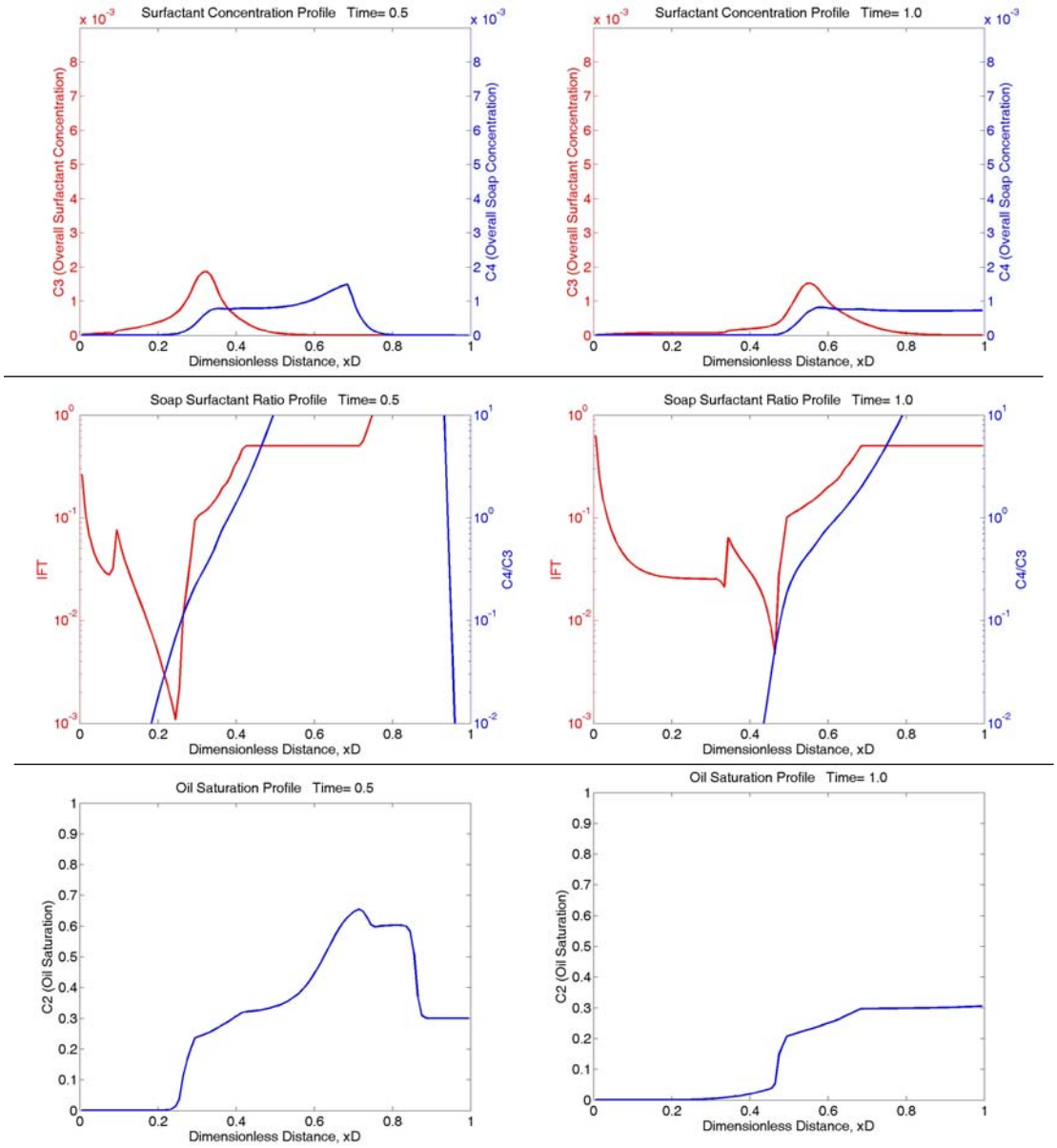


**Figure 6.26 Profiles for an over-optimum case with <u>0.2 PV</u> slug size and <u>wide low tension assumption</u> (Acid No.=0.2mg/g, surfactant concentration=0.14%, injection salinity=<u>4.0%</u>)**

For *<u>over-optimum case</u>* with 4% NaCl, the recovery changes much as shown in Fig. 6.26. The case with 0.2 pore volume surfactant slug shown in figure 6.26 has only 62.6% oil recovery. Compared to figure 6.22, the surfactant travels much slower with 0.2 PV surfactant slug than with 0.5 PV slug. At time equals 1.0 pore volume after injection, the surfactant front is only at $X_D$=0.5, while in 0.5 PV surfactant slug case, the surfactant

front is at $X_D$=0.7. This is because soap and surfactant is trapped in the oil phase when at over-optimum case and with a small slug, there is not enough surfactant to lower the soap to surfactant ratio enough to transfer the soap and surfactant into the aqueous phase. With a small slug and constant salinity, it's better to operate the ASP process at or slightly below the optimum salinity as calculated by the soap fraction. Below optimum condition, surfactant retardation and retention is less a problem and interfacial tension remains moderately low valued in the Winsor I conditions because of the presence of naphthenic soap. As a result, the recovery will stay high and change more gradually with salinity. If the salinity is not constant, i.e. a salinity gradient is used, the recovery can be improved. This will be further discussed in section 6.26.

It is possible for someone to design with over-optimum conditions if a large water/oil ratio is used to determine optimum salinity. The results here suggest that the injection salinity should be designed using water/oil ratio corresponding to $(1-S_{or})/S_{or}$.

#### 6.2.5.3 Narrow low tension assumption with 0.5 & 0.2 Pore Volume Surfactant Slug

As discussed in section 6.2.2, the width of low tension region changes the recovery significantly. However, the wide low tension might not be general; at least it is not valid for zero soap condition. Figure 6.27 and figure 6.28 plot the recovery contours for the case with narrow low tension assumption for 0.5 pore volume and 0.2 pore volume surfactant slug respectively.

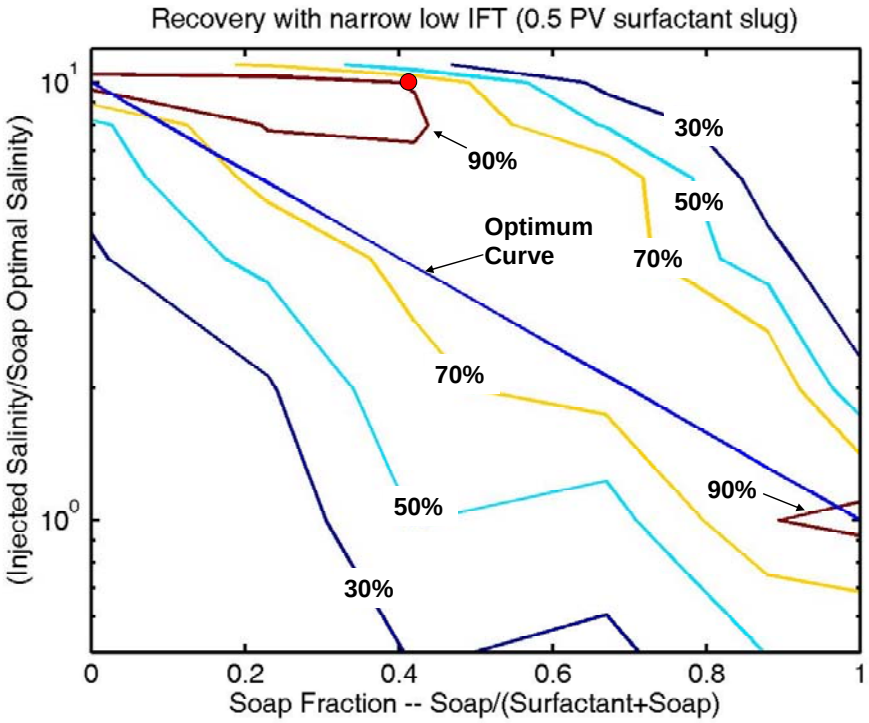


**Figure 6.27 Contour of recovery factor at 2.0 PV with 0.5 PV surfactant slug size (narrow low tension assumption)**

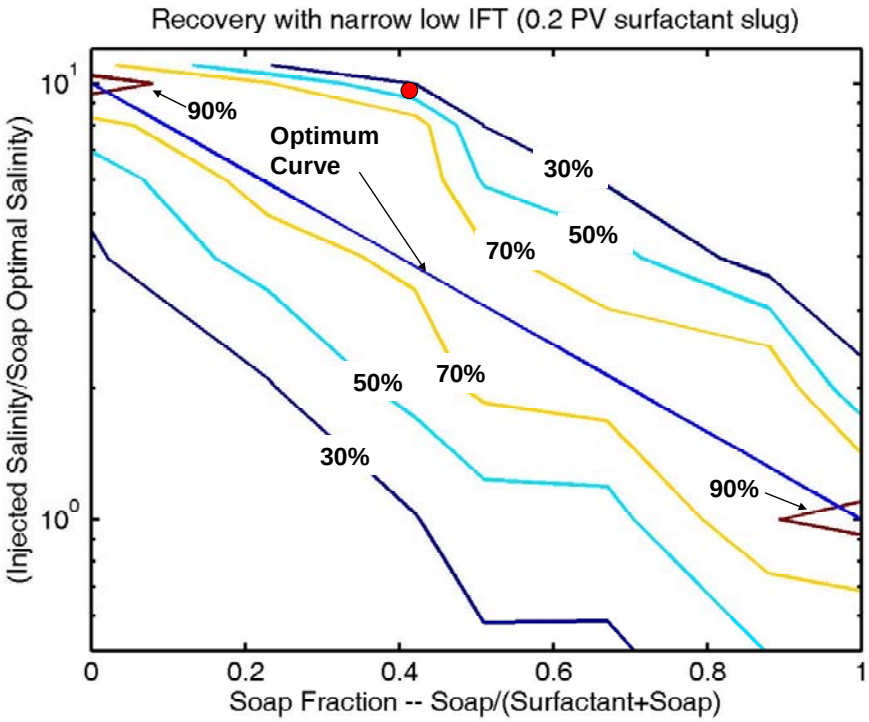


**Figure 6.28 Contour of recovery factor at 2.0 PV with 0.2 PV surfactant slug size (narrow low tension assumption)**

It seems that high recovery is reached at optimum salinity of soap with pure soap or at optimum salinity or surfactant with pure surfactant. These results are reasonable because they are either alkali flood (soap fraction=1.0) or surfactant flood (soap fraction=0) at their exact optimum condition. In the other area, moderately high recovery (>70%) can be achieved by following the optimum curve line. Higher recovery can be achieved by increasing the injection fluid viscosity as discussed in section 6.2.3 because it allows more oil to be displaced by highly viscous water before the IFT increases. However, it will increase the cost and reduce the injectivity for the reservoir applications.

From figure 6.27, high recovery can also be achieved at salinity close to the optimum salinity of surfactant by using 0.5 pore volume surfactant slug size with low soap fraction number. This can be explained by figure 6.29, which compares the profiles with 0.2 and 0.5 pore volume surfactant slug sizes. Other conditions, such as acid number and surfactant concentration, salinity, are the same. The injection salinity is exactly at optimum salinity of surfactant (5.0% NaCl). From figure 6.28, the ultra low tension can be achieved when soap is displaced and surfactant is dominant. In this case, the width of low tension region will not affect the low tension width in the reservoir since the reservoir salinity is at the optimum salinity of surfactant. The upper right region with 90% oil recovery in contour figure 6.29 can be regarded as the transition area from surfactant process to ASP process. For the ASP process with very low acid component or very high surfactant concentration, it is similar to traditional surfactant process and should be operated at the optimum condition of surfactant if salinity is to be maintained constant as in this study. But if the ASP process is operated at this condition, operator

should aware that the surfactant propagation rate is very slow and it works only with large surfactant slug.

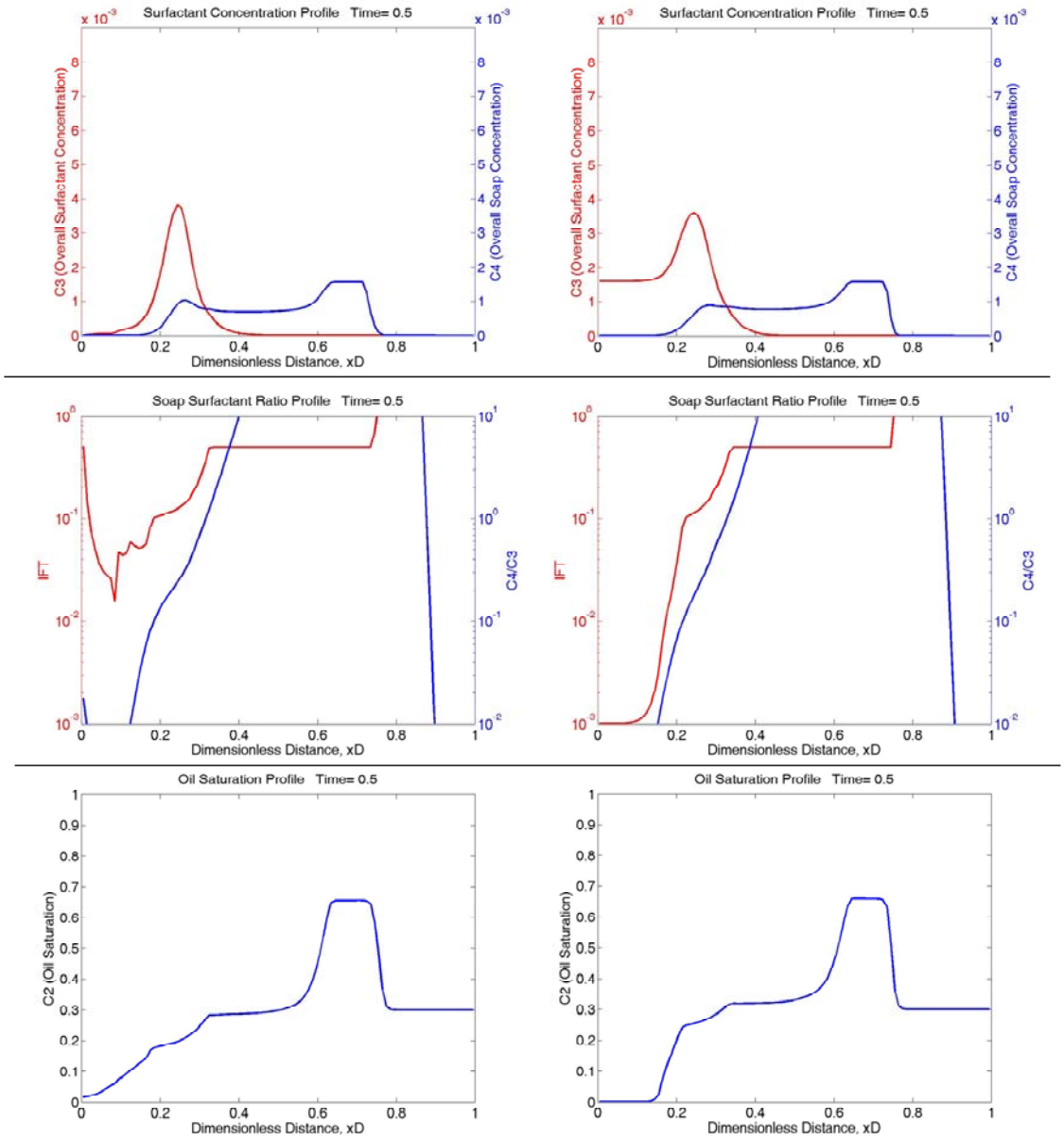


0.2 PV surfactant slug (recovery=30%) 0.5 PV surfactant slug (recovery=88%)

**Figure 6.29 Comparison of slug size with narrow low tension assumption (Acid No.=0.2mg/g, surfactant concentration=0.14%, injection salinity=5.0%)**

### 6.2.6 Salinity Gradient in ASP

Previous sections in this chapter show the constant salinity cases. In this section, the benefit of the salinity gradient will be shown.

#### 6.2.6.1 Salinity Gradient for Large Dispersion and Small Surfactant Slug

As discussed in section 6.2.4, large dispersion and small surfactant slug causes low recovery with constant salinity. As shown in figure 6.17 and 6.18, the displacement front of large dispersion and small surfactant slug is significantly retarded so that the recovery is poor. To improve the recovery, a salinity gradient is applied. In this salinity gradient case, the initial salinity is 4% NaCl, the salinity in the 0.2 PV surfactant slug is 2% and the drive salinity is 1% NaCl. It is found that the recovery of the salinity gradient case is 98% even with large dispersion ($Pe$=50), while the recovery of constant salinity is only 57% with large dispersion. Figure 6.30 compares the profiles of the constant salinity (2% NaCl) and this salinity gradient design with large dispersion. Although the surfactant and soap profiles look similar, the displacement front of the salinity gradient case is faster than that of the constant salinity. This is because more soap and surfactant partition into aqueous phase with low salinity at the same soap to surfactant ratio. In addition to the soap to surfactant ratio gradient, the salinity gradient further improves the recovery.

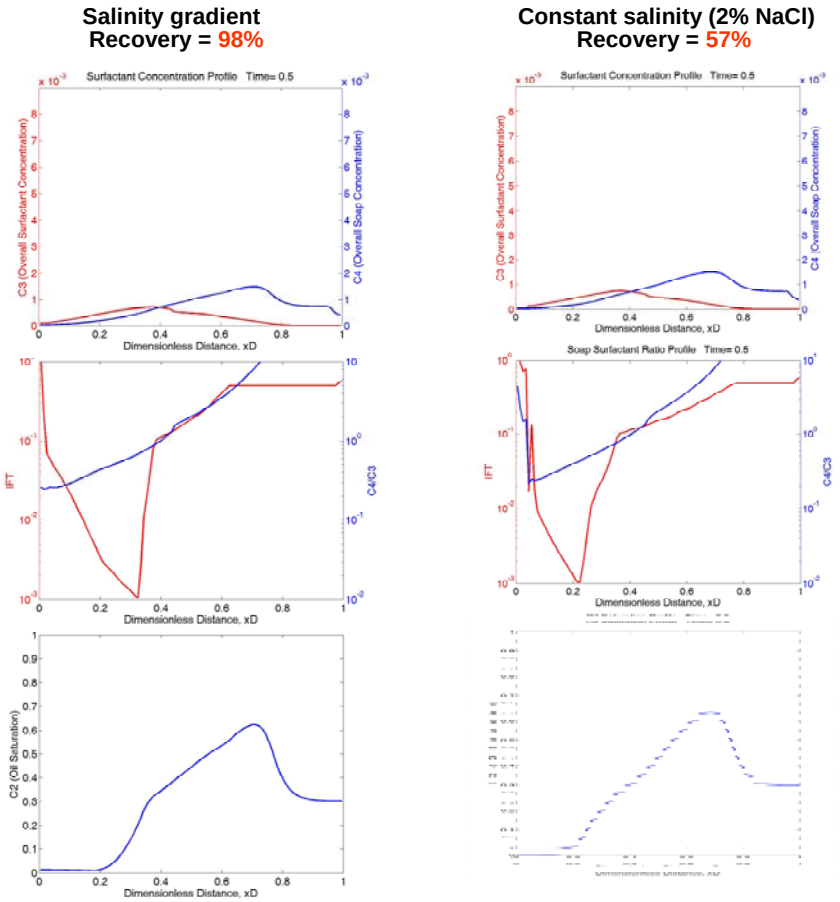


**Figure 6.30 Comparison of salinity gradient and constant salinity with large dispersion**

Figure 6.31 is the distance-time diagram for the salinity gradient case and constant salinity case. Figure 6.31 shows that the displacement front sweeps the whole area and recovers almost all the oil with the salinity gradient, while the displacement front of constant salinity stops propagating after 0.3 PV such that the recovery is poor.

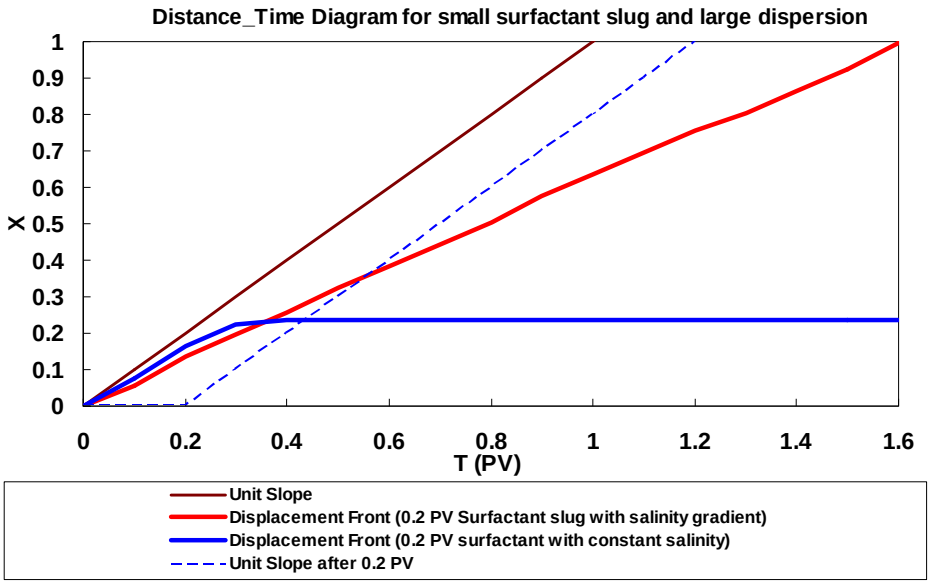


**Figure 6.31 Distance-time diagrams of salinity gradient and constant salinity with large dispersion (Pe=50)**

### 6.2.6.2 Salinity Gradient for Over-optimum 0.2 PV surfactant with Small Dispersion

The poor recovery of the over-optimum case shown in figure 6.26 can also improved by this salinity gradient. For the over-optimum case with constant 4% NaCl, the recovery is only 63%. If a low salinity (1% NaCl) drive, rather than the 4% NaCl, is injected. The recovery is improved to 99.5%. The profiles of the constant salinity over-optimum case and the salinity gradient case are shown in figure 6.32. Figure 6.33 is the distance time diagrams. Figure 6.33 shows that salinity gradient makes the displacement front travel fast so that it can propagates through the reservoir, while the displacement front of constant salinity of over-optimum case is retarded and stops propagation after 1 PV. Figure 6.33 also shows the reason that large surfactant slug of over-optimum case can give the good recovery. It is because large surfactant slug keeps the drive front away from the displacement front so that the displacement front can sweep the whole reservoir.

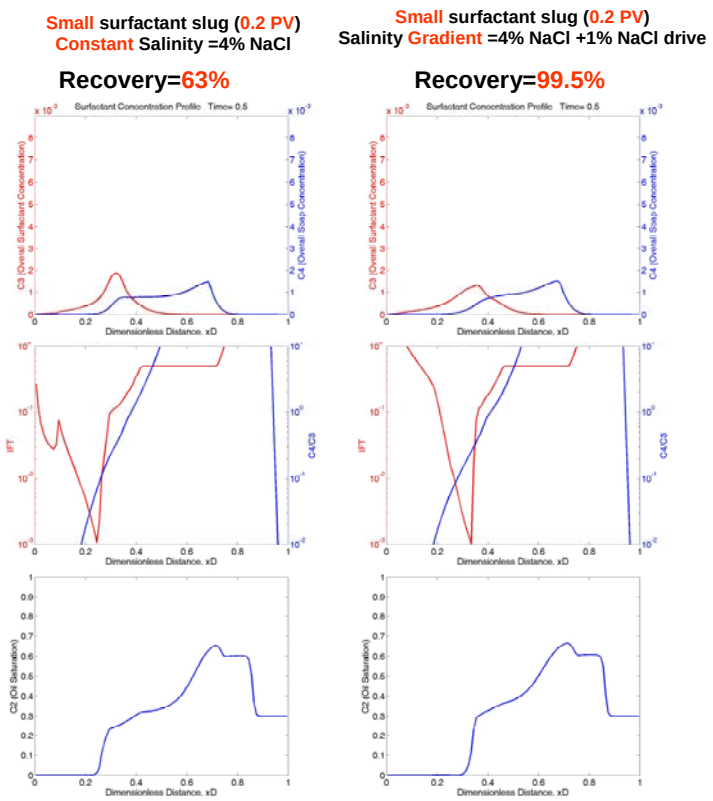


**Figure 6.32 Comparison of salinity gradient and constant salinity for small surfactant slug at over-optimum condition (small dispersion)**

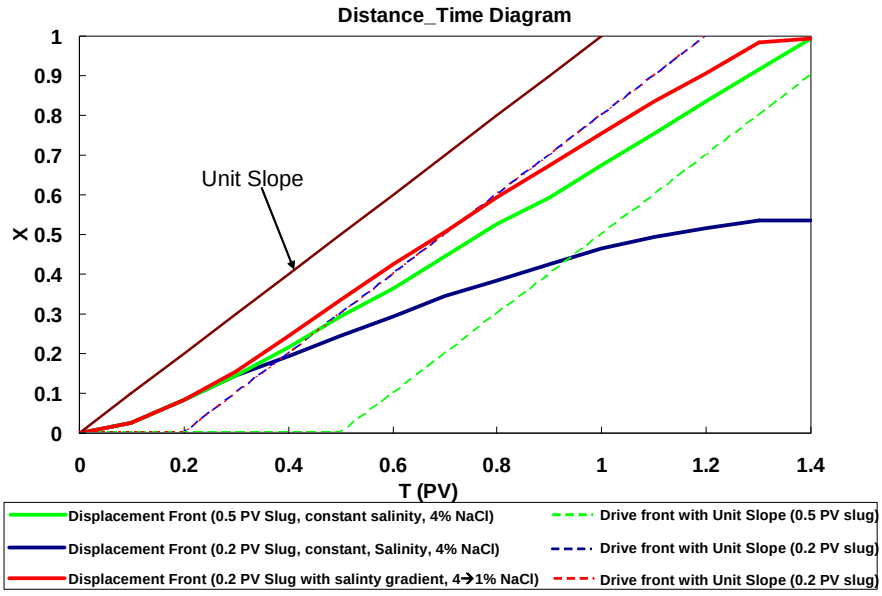


**Figure 6.33 Distance-time diagrams of salinity gradient and constant salinity for over-optimum conditions (small dispersion)**

### 6.2.7 Summary of Simulations

The simulation shows a soap to surfactant ratio gradient is generated in the ASP process. This gradient not only assures the profile of passing through the optimal condition where the low IFT is achieved, but also makes ASP a robust process because surfactant that moves ahead into the soap-dominant region ahead of the major surfactant bank is retarded and surfactant behind the displacement front travels at the velocity close to the aqueous phase.

Narrow low IFT region will have less recovery because oil will be trapped again when the IFT increases. When the low IFT region is as wide as the experimental values for Yates oil and NI blend, less oil will be trapped after the low tension region. Thus, it is favorable to have the ASP formulation with wide low IFT region.

The injection solution viscosity has significant effect on recovery. Lower aqueous phase viscosity, i.e., higher mobility ratio, has lower oil recovery even with wide low IFT region. It is because oil fractional flow is less even in the low IFT region where the residual oil saturation is zero. Oil will be trapped again after the low tension region.

There is an optimum operation region for ASP process, which can be determined if the initial natural soap content is known. For a certain surfactant concentration, good recovery can be achieved in a certain range of salinity which follows the relationship of optimum salinity and soap to surfactant ratio.

With significant dispersion, the recovery for small surfactant slug may be significantly less than that for the large surfactant slug, even at optimum conditions.

With salinity gradient, ASP process could work well with small surfactant slug and large dispersion.

*Chapter* 7

# Alkali Surfactant Polymer Flooding

Based on the phase behavior, IFT, adsorption and simulation results, ASP flooding experiments were designed. Results are presented in this chapter. The flooding experiments can be used to demonstrate those important mechanisms that have been identified and incorporated in the simulator in previous chapters and provide the directions for the real field test.

## 7.1 Flooding Experimental Procedure

The ASP solution used in the flooding experiments is the NI blend and the polymer (polyacrylamide, CS 3330® from SNF Inc.). The general mixing procedure for ASP solution is as follows:

1. Mix sodium chloride and sodium carbonate with DI water
2. Add surfactant into solution before adding polymer.
3. Using the magnetic stirrer, establish a vortex in the surfactant solution in step 2 that just reaches the stir bar. Sprinkle the desiccated polymer powder on the shoulder of the vortex just slowly enough to prevent clumping of the polymer. Adding the polymer too fast will form gel which is very difficult to dissolve.

4. Continue stirring the polymer solution until all polymer particles appear to be fully hydrated and dissolved. This may take 30-60 minutes. Visual examination should show that no turbity exists. Continue stirring for an additional 30 minutes to let the solution hydrate.

The flooding experimental apparatus shown in figure 7.1 is similar to what is used in dynamic surfactant adsorption experiments except the pump is the HPLC pump (ISCO® Model 2350) because high injection pressure is needed due to the high viscosity fluids. The other difference is that the one foot long sand pack is vertical so that the gravity will help to stabilize the oil-brine interface.

The ASP flooding experiments were conducted by the following procedure:

1. $CO_2$ was injected into the sand pack so that it was saturated with $CO_2$ with no air left.
2. Brine with 2% NaCl was injected at the velocity 0.5 ml/min (interstitial velocity = 14 ft/day) until the column was saturated by the brine. The objectives of step 1 and 2 is to eliminate the air that will be trapped in the column
3. Crude oil was injected at the velocity 0.5 ml/min (interstitial velocity = 14 ft/day) until the oil broke through.
4. The oil-saturated column was placed into a 60 °C oven for 60 hours. The purpose of this aging procedure was to change the wettabilty of the substrate (dolomite) to mixed-wet.
5. After aging, brine with 2 % NaCl was pumped into the column at velocity 0.5 ml/min (interstitial velocity = 14 ft/day) until there was no oil in the effluent.
6. The ASP solution is injected at velocity around 1 ft/day.

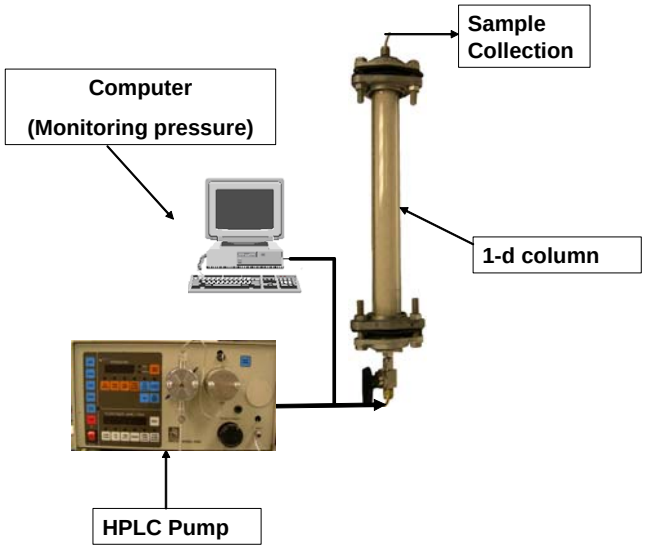


**Figure 7.1 Schematic Experimental Apparatus for flooding**

## 7.2 Alkaline Surfactant Polymer Flooding for Yates Oil

The ASP flooding for Yates oil was performed on a 35 darcy dolomite sand (from Unimin Corp.) pack. Figure 7.2 shows the photos for Yates oil flooding and water flooding before the ASP flooding. the left one in figure 7.2 is the oil flooding after 0.1 Pore Volume (PV). The oil cut was 100% immediately after breakthrough. The oil saturation after the oil flooding was 0.98. The right five photos illustrate the water flooding at different pore volumes injected. The cumulative oil recovery and the fractional flow of oil at the outlet are shown in figure 7.3. In this figure, the oil saturation is 0.177 (Sor=0.177) after 3.2PV was injected. Further injection of water would not be expected to recover much more oil.

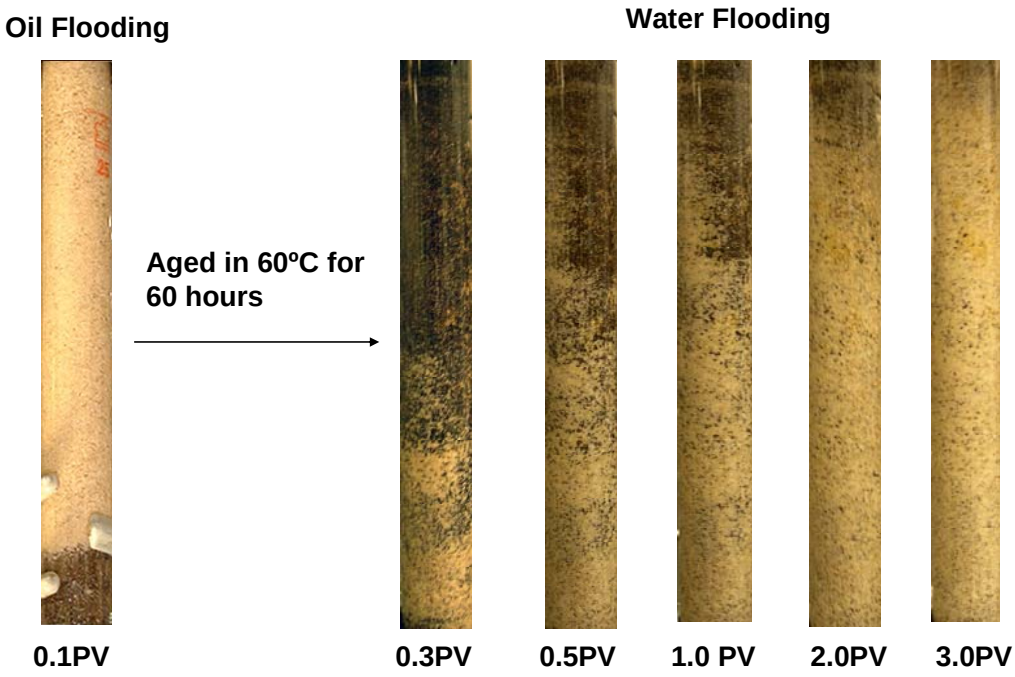


**Figure 7.2 Oil flooding and water flooding for Yates oil**

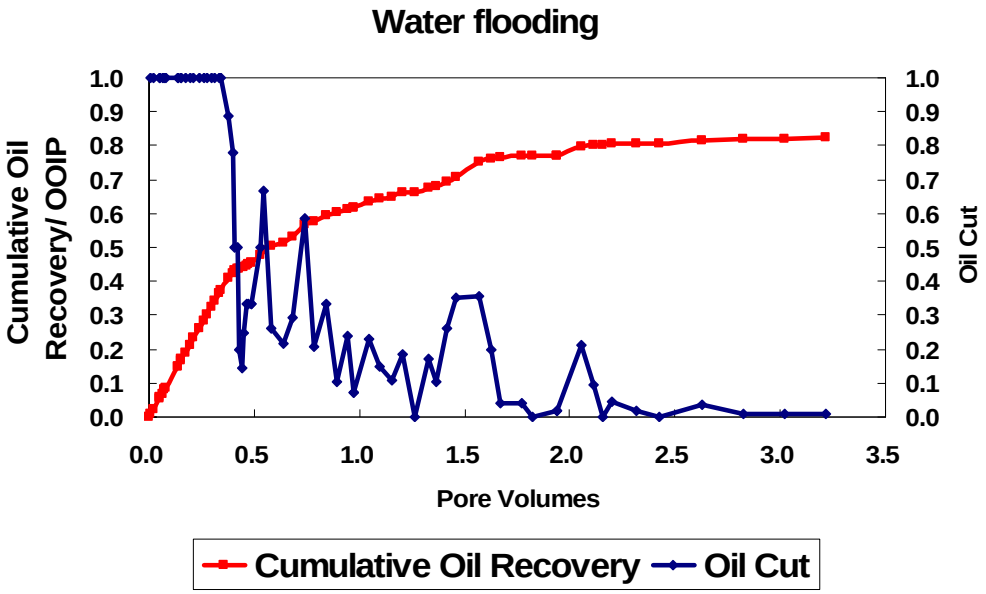


**Figure 7.3 Oil Recovery of Water Flooding in Dolomite Sand Pack (OOIP: Original Oil in Place)**

After water-flooding, ASP process was implemented on the dolomite sand pack. A 0.50 PV slug of ASP solution was injected into the sand pack followed by a 1.0 PV

polymer drive. The formulation of alkaline-surfactant-polymer solution is shown in Table 7.1. The viscosity of ASP solution was 45.1 cp at the shear rate of 66 $sec^{-1}$. The reason that such high viscosity was used is that the crude oil viscosity was 19.4 cp. The polymer drive consists of 5000 ppm polymer and 2.0% NaCl.

| Chemicals | Concentration |
|---|---|
| Alkali ($Na_2CO_3$) | 1.0 % |
| NaCl | 2.0% |
| Surfactant (NI Blend ) | 0.2% |
| Polymer (Flopaam 3330) | 5000ppm |

**Table 7.1 Formulation for ASP solution for Yates oil flooding**

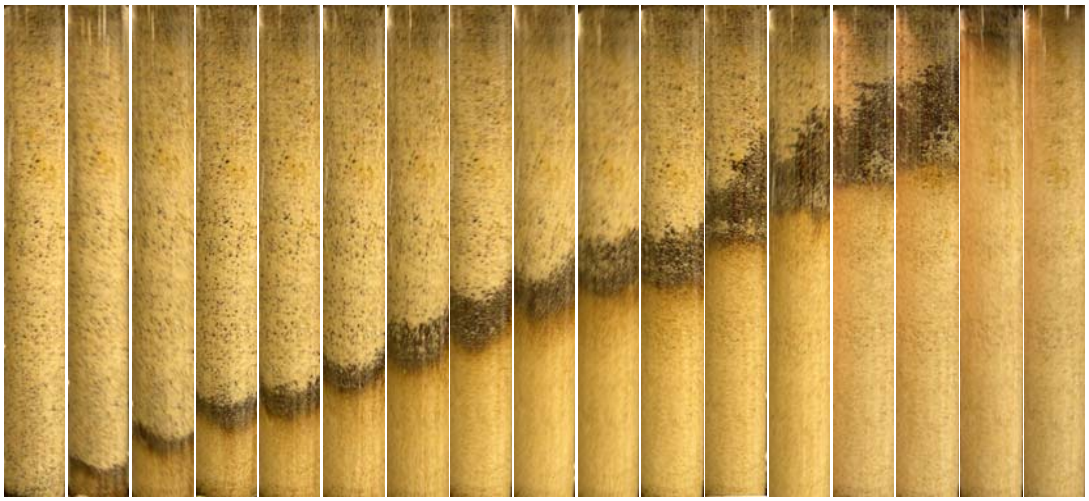


**Figure 7.4 Photos of ASP flooding for Yates in dolomite pack at different injecting pore volumes**

The photos in figure 7.4 represent how the oil bank forms and propagates during the ASP process. Figure 7.5 shows the cumulative oil recovery and the fractional flow of produced oil. And the effluent of the flooding at different pore volumes is shown in figure 7.6. The oil bank breaks though at 0.8 PV. The surfactant breaks through at around

0.99 PV because lower phase micro-emulsion can be found at that time. The incremental oil recovery is 98.1% and the oil recovery without emulsion is 61.3%. There may be some oil in the aqueous phase because the color of the aqueous phase of some effluent is brown.

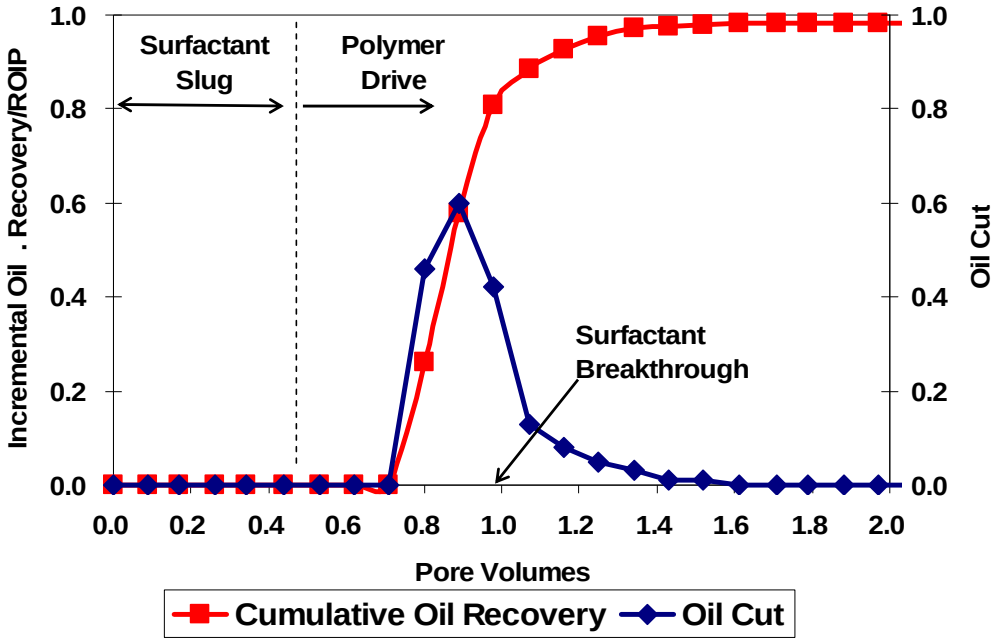


**Figure 7.5 Oil Recovery of ASP Flooding for Yates oil in Dolomite Sand Pack (ROIP: Residual Oil in place)**

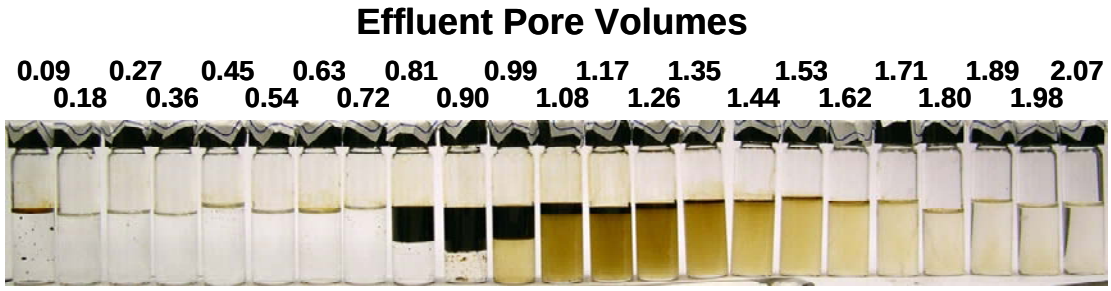


**Figure 7.6 Effluent of ASP Flooding in Dolomite Sand Pack**

The history of pressure drop is shown in figure 7.7. The pressure increases with the injection because the surfactant slug and polymer drive were designed to have a

favorable mobility ratio. The pressure became stable and did not increase any more after the surfactant broke through because the whole column was occupied by the surfactant slug and polymer drive which have nearly identical viscosities. Further injecting polymer solution did not change the apparent viscosity of the system.

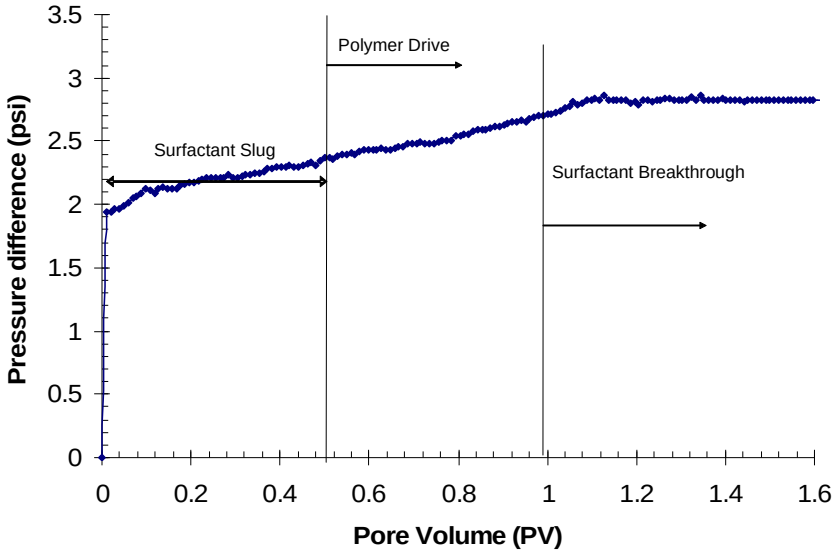


**Figure 7.7 Pressure drop during ASP flood for Yates oil in dolomite sand pack.**

The one-dimensional simulator described in Chapter 6 was used to simulate this experiment. Figure 7.8 compares the simulation results and the experimental results. This plot shows the simulation result matches the experimental results quite well.

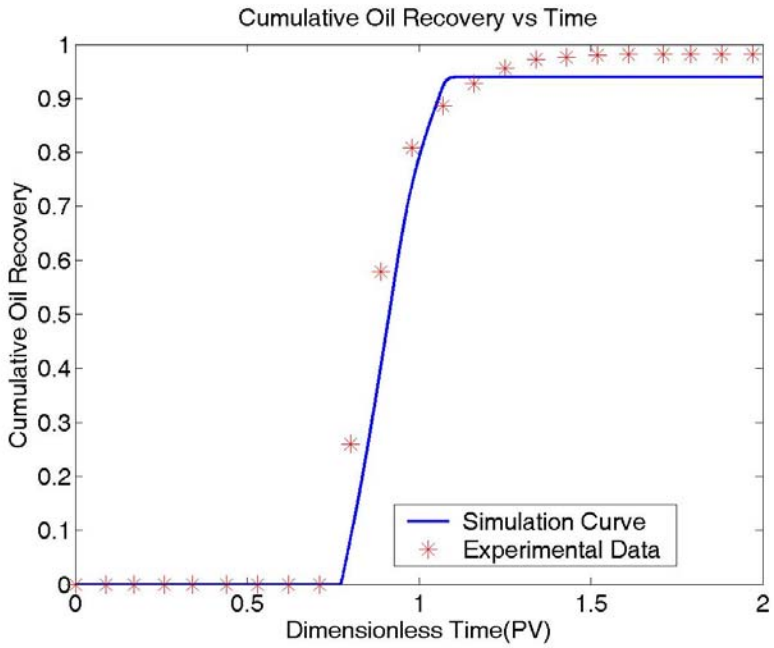


**Figure 7.8 Effluent of ASP Flooding for Yates oil in Dolomite Sand Pack**

Similar ASP flooding was also performed in a 40 darcy silica sand pack with same ASP formulation in Table 7.1 except that the surfactant concentration was 0.5% and the injection solution viscosity was 43 cp at the shear rate of 66 $sec^{-1}$. The waterflood remaining oil saturation after 2 pore volumes was 0.25. Photos in figure 7.9 illustrate how the oil bank forms and propagates in the silica pack. From figure 7.10, it took about 1.3 pore volumes to get an incremental recovery of 98% of the remaining oil after waterflooding.


**Figure 7.9 Photos of ASP flooding for Yates oil in silica pack at different injecting pore volumes**

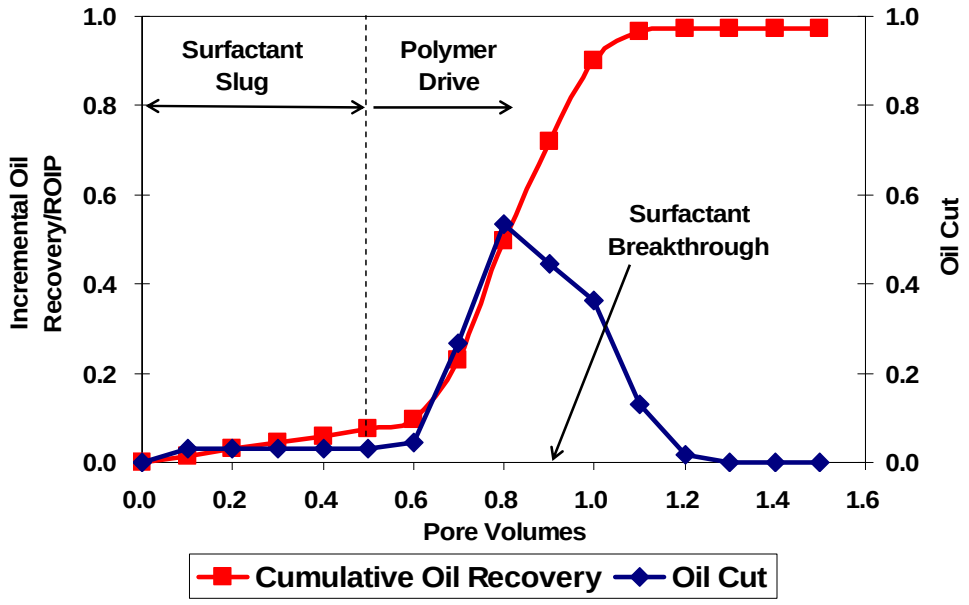


**Figure 7.10 Oil Recovery of ASP Flooding for Yates oil in Silica Sand Pack (ROIP: Residual Oil in place)**

The pressure drop history is shown as figure 7.11, in which the final pressure drop is close to that of figure 7.7. Figure 7.12 also shows that the simulation result matches the

experimental results with the exception of the early oil production. The early oil breakthrough in this experiment is because the remaining oil saturation after waterflooding is slightly greater than the residual oil saturation after water flooding.

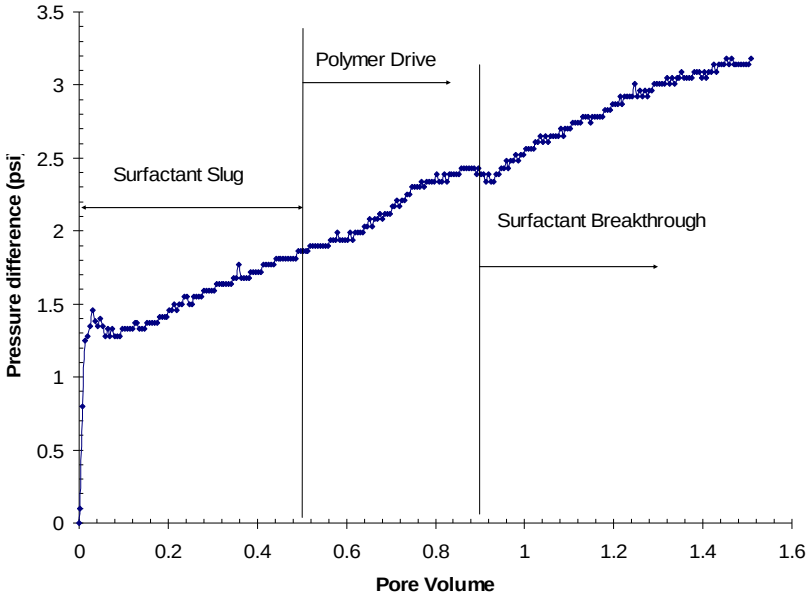


**Figure 7.11 Pressure drop during ASP flood for Yates oil in silica sand pack.**

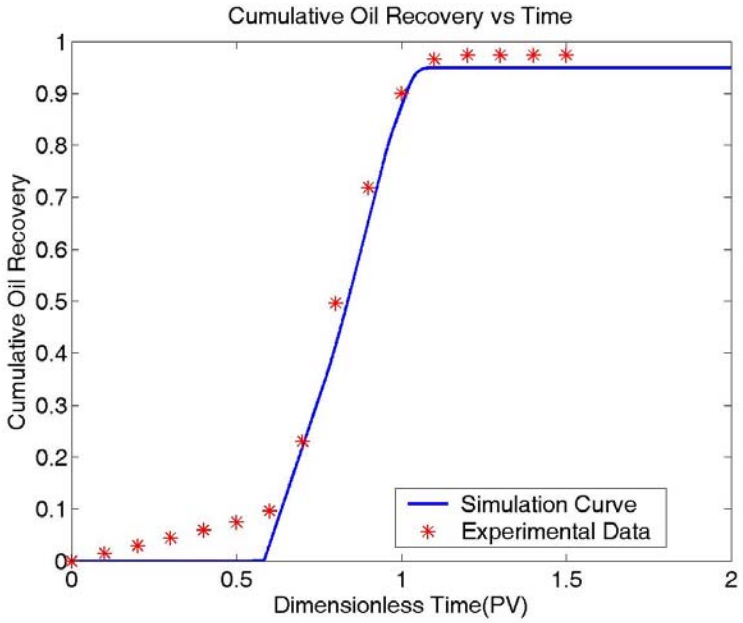


**Figure 7.12 Effluent of ASP Flooding for Yates oil in silica sand pack**

## 7.3 The Problem of Phase Separation of Injection Solution

The phase behavior experiments of NI blend and Yates oil show that the optimal salinity for NI blend and Yates is around 5% NaCl with 1% $Na_2CO_3$ without the presence of soap. If an experiment was run at salinity close to the optimal salinity of NI blend itself, the recovery might be even better than with the previous 2% NaCl, according to the phase behavior experiments without presence of polymer.

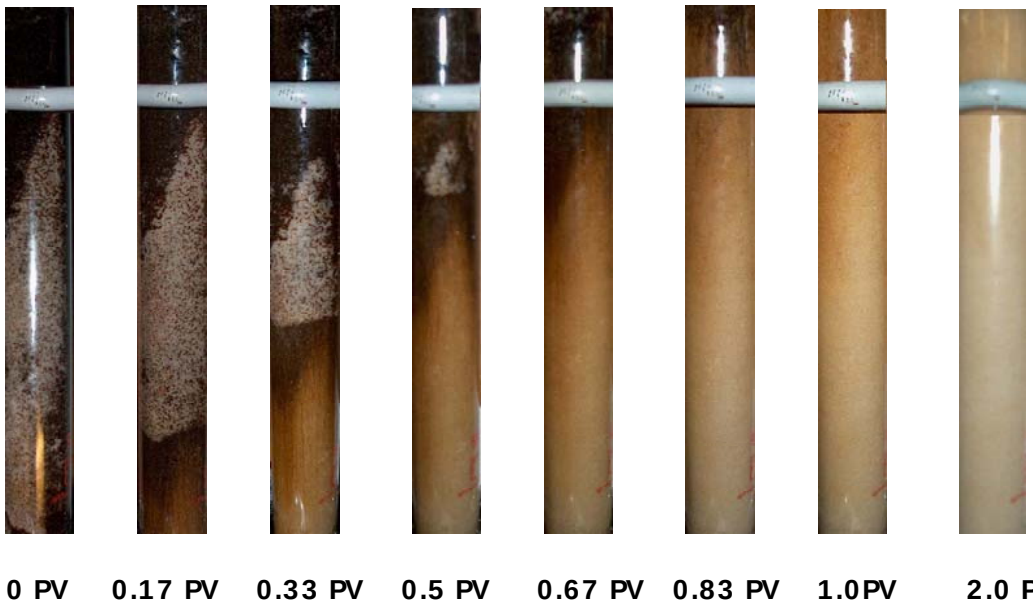


**Figure 7.13 Photos showing behavior during unsuccessful ASP flood of silica sand pack where phase separation due to polymer has occurred.**

Another ASP flooding was done at the same condition as in figure 7.9 except the injection salinity was 4.0% NaCl. Before injection, the ASP solution with 4% NaCl looked a bit turbid while the 2% NaCl ASP solution was clear. As figure 7.13 shows, no distinct oil bank was found after injection. There is significant amount of oil that propagated behind surfactant front. The mobilized oil appears to be behind the surfactant front as if there was lack of mobility control.

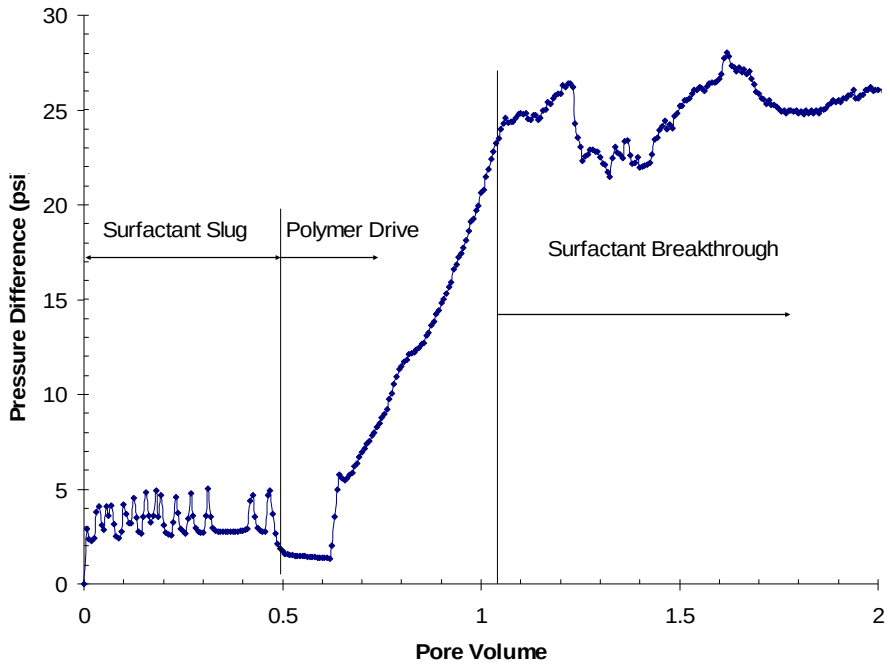


**Figure 7.14 Pressure drop during ASP flood in silica sand pack where phase separation due to polymer has occurred.**

Moreover, the pressure drop shown in figure 7.14 indicates that the pressure drop rose to 25 psi, which was around 10 times of that in figure 7.11. This implies that there is a more viscous phase in the experiment of figure 7.13 since the flow rates were same in both experiments. After one week settling of the ASP solutions with different salinities, phase separation can be observed in the sample with 4% NaCl, as seen in the right figure in Figure 7.15. There is a separated layer in that sample. This separated layer must be a highly viscous polymer-rich phase that caused the high pressure drop. Before the polymer drive was injected, the highly viscous polymer-rich phase might adhere at the sand pack entrance. The polymer-lean phase of newly injected ASP solution might have to break past the polymer-rich gel so that the pressure drop sharply oscillated. After the polymer drive was injected, the pressure drop significantly increased because the highly viscous polymer-rich phase dissolve in the polymer drive due to absence of surfactant. Thus, the

injected solution should be a clear, one-phase system in ASP flooding system. Otherwise, phase separation may occur during the flooding process. Lowering injection salinity would be a good way to avoid the phase separation. This is one of the benefits of ASP process. The flooding salinity does not need to be at the exact optimum salinity of synthetic surfactant.

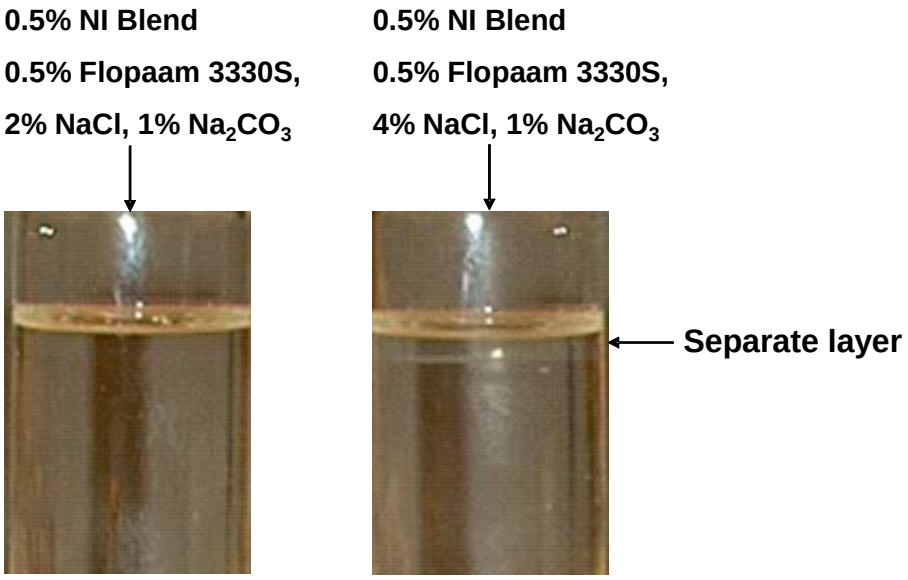


**Figure 7.15 Phase separation caused by increasing NaCl content for aqueous solution of 0.5 wt% NI blend, 1 wt% Na2CO3 and 0.5 wt% polymer.**

## 7.4 Alkali Surfactant Flooding Process for High Viscosity Oil

It is very difficult to maintain a favorable mobility ratio for high viscosity oil, e.g., PBB oil (266cp). According to the simulation for highly viscous oil, the oil recovery will be only around 40% even with 5000 ppm polymer. To recover this highly viscous oil, mobility control method other than the polymer should be considered. An ASP

experiment with co-injection gas was performed on silica sand pack as shown in figure 7.16. The oil saturation initially in the column was 0.36 which is the remaining oil after 6 pore volume waterflooding. The ASP process started with 0.3 pore volume injection with ASP solution (NIP: 0.5% NI blend and 5000 ppm polymer) at 1 ft/day as used for Yates oil. The salinity is 1%NaCl with 1% $Na_2CO_3$. This salinity is chosen because there is more soap in PBB than in the Yates oil so that the optimum injection salinity is lower as shown in the Chapter 6. There is some oil displaced by the ASP solution. However, there is still much oil left and no oil bank formed due to the unfavorable mobility ratio. After 0.3 pore volume, slugs of 0.1 pore volume air and 0.1 pore volume ASP solution were alternately injected at 20 ft/day. Such a high injection rate is to maintain the pressure that can generate strong foam (Yan, 2006). From figure 7.16, it is obvious that much trapped oil was displaced by the alternate injection of air and ASP solution. After 0.8 PV, slugs of 0.1 pore volume air and 0.1 pore volume IOS solution (0.5% IOS, 1% NaCl, 1% $Na_2CO_3$) were alternately injected at 20 ft/day. The IOS solution was chosen because IOS is a strong foamer so that it will show high apparent viscosity and generate good mobility ratio (Yan, 2006). Figure 7.16 indicates that the trapped oil continuously be displaced by the foam drive even without using a polymer drive.

Figure 7.17 shows the oil broke through at 0.6 pore volume. An incremental recovery of 93% of the remaining oil after waterflooding was reached at around 2.0 pore volume. A certain amount of oil solubilized in the aqueous effluent was not measured and not included in this recovery number. The actual recovery might be even higher. Figure 7.18 is the pressure history of this flooding. The highest pressure drop is around 2.5 psi.

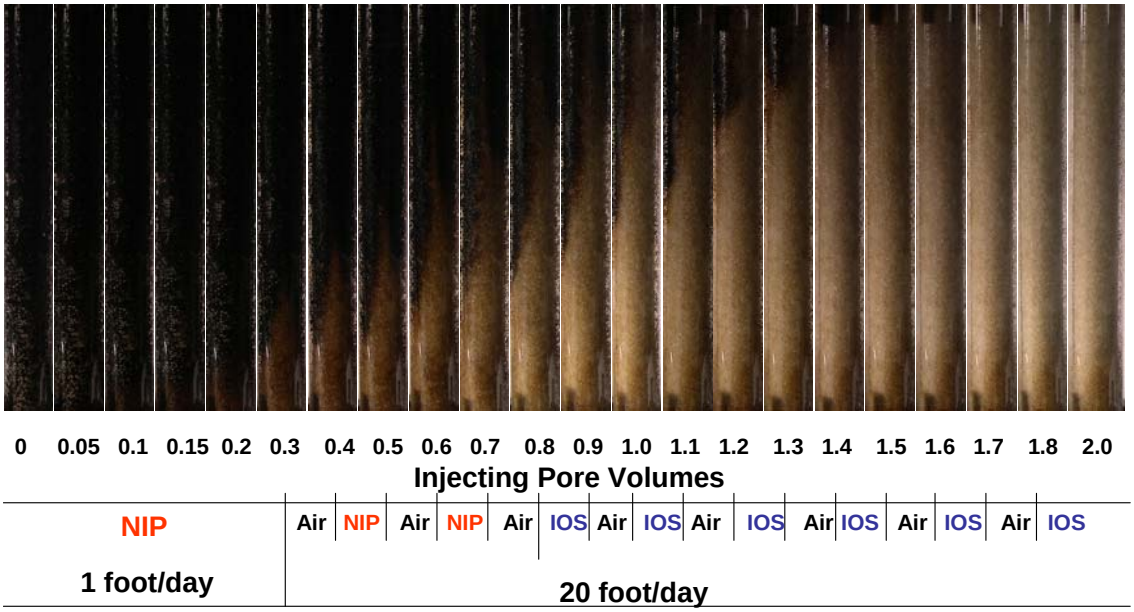


NIP: 0.5% NI, 5000ppm Polymer, 1% NaCl, 1% $Na_2CO_3$
IOS: 0.5% IOS, 1% NaCl, 1% $Na_2CO_3$

**Figure 7.16 Photos of ASP Foam flooding for PBB in silica pack at different injecting pore volumes.**

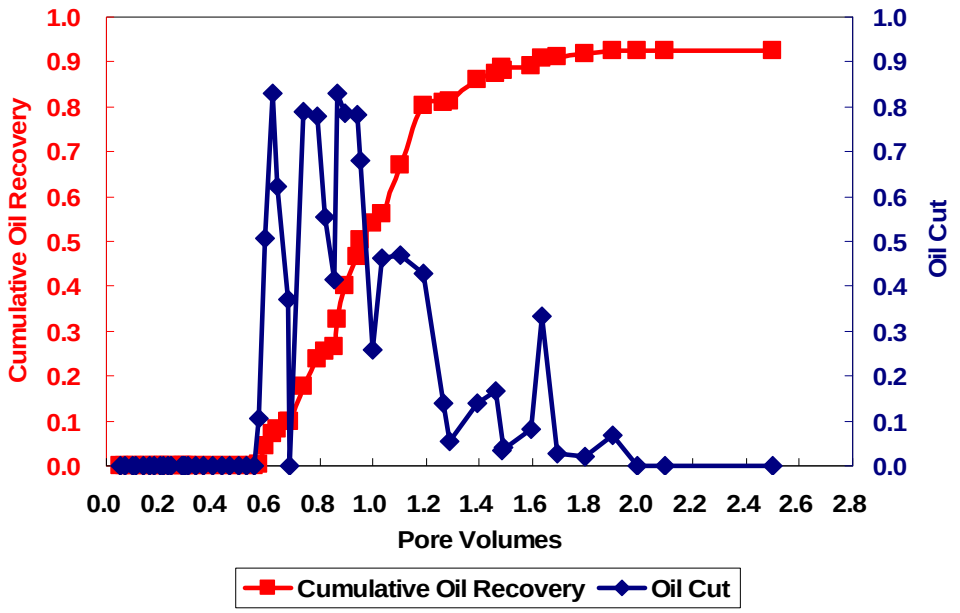


**Figure 7.17 Oil Recovery of ASP Foam Flooding for PBB oil in Silica Sand Pack (ROIP: Residual Oil in place)**

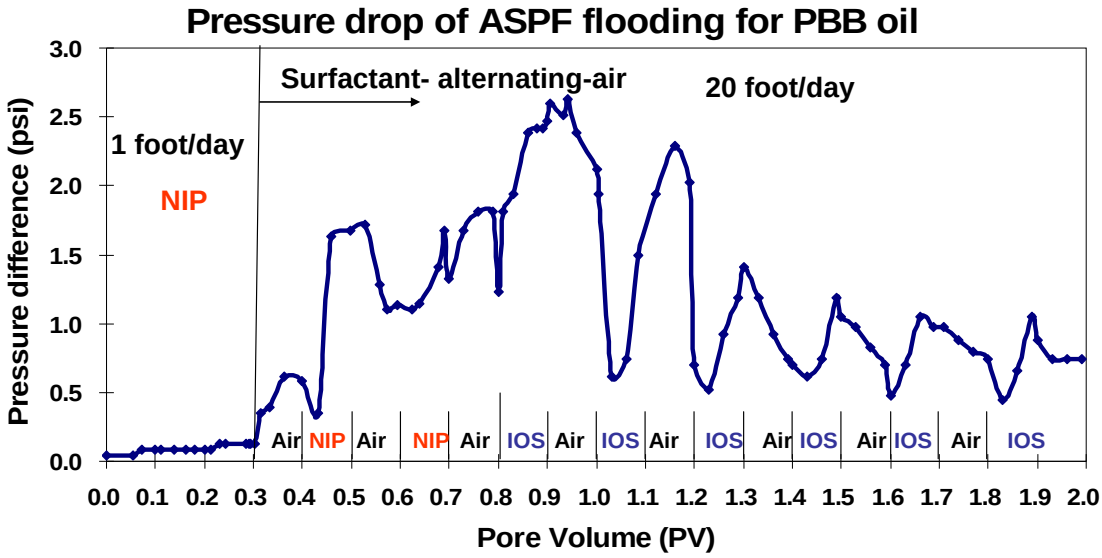


**Figure 7.18 Pressure drop during ASP Foam flood for PBB oil in silica sand pack**

This result shows that alternative injection of ASP solution and gas can recover high viscosity oil that could not be recovered by ASP itself. The mechanisms of this surfactant gas process are still not fully understood and need further study. One speculation for the mechanism is shown at figure 7.19. The local pressure gradient $\nabla P$ at the bubble front may be much greater than the average because the pressure difference in the bubble ($\Delta P_b$) is quite small and the pressure drop along the bubble ($\Delta P_L$) will be concentrated at the bubble front. Also the presence of IOS still significantly reduces the interfacial tension although it is not as good as NI blends. Some foam studies (Yan, 2006, Li, 2006) show that gas saturation can achieve very large values with surfactant than the conditions without presence of surfactant. Since gas saturation becomes larger, it might help to reduce the oil saturation. To verify those mechanisms, more studies are needed.

$$\nabla P \approx \frac{\Delta P_L}{\delta} >> \frac{\Delta P_L}{L}$$

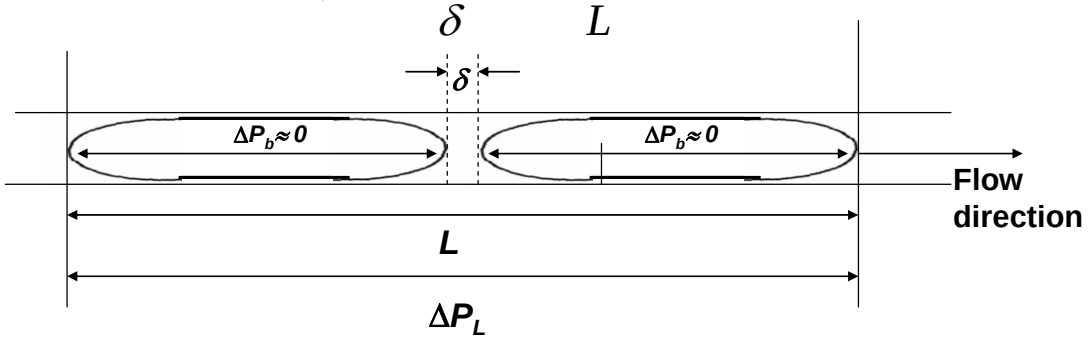


**Figure 7.19 A possible mechanism for ASP foam process**

*Chapter 8*

# Conclusions and Future Work

In this chapter, the conclusions and recommendations for future work are presented.

## 8.1 Conclusions

### 8.1.1 Phase Behaviors of Alkali-Surfactant System (Chapter 3)

Alkali can react with acids in crude oil to form natural soap, which acts as anionic surfactant. However, natural soap usually is too hydrophobic and optimal salinity is very low. The addition of synthetic surfactant can significantly increase the optimum salinity. Alkaline surfactant phase behavior is a function of salinity, surfactant concentration, and water oil ratio (WOR). The optimum salinity depends on soap to surfactant ratio for both low acid number oil (Yates) and high acid number oil (PBB). However, the shape of the optimum salinity curve depends on the oil and surfactant. Different oils and surfactants may have different curves. With the acid number determined by soap extraction with alkali, the mixing rule developed by Bourrel and Schechter for orthoxylene sulfonate mixtures can be used to characterize the alkaline surfactant optimum salinity. This is because soap extraction with alkali only measures the soaps that have surface active properties. From the pure hydrocarbons phase behavior, the optimum salinity is also a

function of refined oil carbon number. Introducing SBA can change the optimum salinity. For NI blend and Yates oil, birefringent material is observed in the microemulsion near optimum salinity. However, it does not affect the viscosity of the microemulsion phase.

### 8.1.2 Interfacial Tension Properties of Alkali Surfactant System (Chapter 4)

Crude oils may be contaminated by emulsion breaker, scale inhibitor, or rust inhibitor. Before any phase behavior or IFT experiments, contaminated oil should be screened out by pendant drop or any other IFT measurement. The IFT of uncontaminated oil and brine should be above 20 mN/m.

For alkaline surfactant system, a spinning drop IFT measurement procedure which can reach the equilibrium IFT quickly was introduced. By using this method, the equilibrium IFT can be reached in less than 60 minutes while the commonly used methods may take as long as 10 hours. In the alkaline surfactant system, the colloidal dispersion plays an important role in producing the low IFT. The colloidal dispersion might be a microemulsion phase with higher ratio of oil to brine than the lower phase so that it behaviors like the middle phase in the classical surfactant behavior. Thus a much wider low tension region can be achieved with the presence of the colloidal dispersion. Experimental IFT measurements show that the alkaline surfactant system investigated here has a wider low IFT region than that for the same system without $Na_2CO_3$.

Huh's correlation can be used to predict IFT of alkali surfactant system from the solubility ratio according the experimental data. Thus, IFT values of those systems for which spinning drop measurement is not easy to conduct can be estimated. It also saves

time and manpower by just making phase behavior samples instead of also conducting spinning drop measurements.

Dynamic measurement for unequilibrated phases provides the IFT only for very large water to oil ratios and does not provide enough information for designing alkali surfactant processes because the optimum condition for alkali surfactant system is a function of water oil ratio. The IFT between pre-equilibrated phases should be used for designing alkali surfactant processes.

### 8.1.3 Chemical Consumption (Chapter 5)

$Na_2CO_3$ substantially reduces adsorption of anionic surfactants (TC blend, NI blend) on carbonate surfaces (calcite, dolomite), especially at low salinities. This is because the carbonate ion is the potential determining ion for carbonate surface that can change the surface charge. To have the surfactant adsorption reduction effect, $Na_2CO_3$ concentration should be larger than 0.1 %. However, hydroxyl ion and/or sulfate ion can not significantly reduce the anionic surfactant adsorption.

When comparing the surfactant adsorption for different systems, adsorption per surface area of porous media should be used although the adsorption per weight of solid is usually used in the field.

Nonionic surfactants have much higher adsorption on sandstone surface than anionic surfactants. But initial experiments indicate that the adsorption of nonionic surfactant on calcite is much lower than that of anionic surfactant without presence of $Na_2CO_3$ and is of the same magnitude of that of anionic surfactant with presence of

$Na_2CO_3$. Thus, nonionic surfactants might be candidates for use in carbonate formations from the adsorption point of view.

Dynamic core flood can measure the surfactant adsorption by comparing the breakthrough curve of surfactant and non-adsorbing tracer. It also shows that the presence of $Na_2CO_3$ reduces surfactant adsorption. The dynamic core flood indicates that the adsorption of surfactants is not an instantaneous process and depends on the flow rate. Thus, a low flow rate (< 1 foot/day) should be used if using dynamic core flood to estimate the equilibrium surfactant adsorption.

If gypsum or anhydrites are present in the reservoir, $Na_2CO_3$ and/or $NaHCO_3$ can not be used as the alkali agent because of precipitation of $CaCO_3$. Other alkali should be considered.

### 8.1.4 Characteristics of Alkali Surfactant Polymer Process (Chapter 6)

A one-dimensional numerical simulator was developed in this work to model the ASP process. Simulation shows that a gradient in soap-to-surfactant ratio develops during the ASP process and propagates through the reservoir. This gradient assures the profile of passing through the optimal condition where the ultra-low IFT is achieved. Furthermore, this gradient makes ASP a robust process because surfactant that moves ahead into the soap-dominant region is retarded and surfactant behind the displacement front travels close to the velocity of the aqueous phase. The soap to surfactant gradient also helps to mitigate the effect of larger dispersion.

The width of the low IFT region is a key factor for ASP recovery. Narrow low IFT region will have less recovery because oil will be trapped again when the IFT increases. When the low IFT region is as wide as the experimental values for Yates oil and NI blend, less oil will be trapped after the low tension region.

The injection solution viscosity has significant effect on recovery. Lower aqueous phase viscosity, i.e., higher mobility ratio, has lower oil recovery even with wide low IFT region. Oil will be trapped again as the low tension region moves ahead.

There is an optimum operation region for ASP process, which can be determined if the initial natural soap content is known. For a certain surfactant concentration, good recovery can be achieved in a range of salinity which follows the relationship of optimum salinity and soap to surfactant ratio.

ASP process could work well either with small surfactant slug or large dispersion.

### 8.1.5 Alkali Surfactant Polymer Flooding (Chapter 7)

Experimental results show that the ASP process with only 0.2% surfactant recovers 98% of the oil that is trapped after water-flooding in both dolomite sand pack and silica sand pack. The simulator can match the experimental data. High salinity can cause the phase separation of injected ASP solutions. This may result in loss of mobility control. For highly viscous oil, e.g. the 260 cp PBB oil, oil recovery is poor due to the poor mobility ratio. It is not economic and difficult to achieve favorable mobility ratio by increasing polymer concentration for viscous oil. Initial experimental results show that

alternative injection of ASP solution and gas, which generates foam, can recover high viscosity oil that could not recovered by ASP itself.

## 8.2 Alkaline Surfactant Polymer Process Design Strategy

The key parameters for designing a good ASP strategy are shown in figure 8.1.

| Key Parameter Required | | Literature Review | Phase behavior Test | Floods | Other Lab tests | Simulation | Pilot Test | Commercial Project |
|---|---|---|---|---|---|---|---|---|
| ASP Chemical Optimization (alkali, surfactant, polymer) | | S | P | S | S[*1] | | | |
| Surfactant consumption | Adsorption | | | S | P[*2] | | | |
| | Phase Trapping | | P | | | S | P | |
| Remaining Oil Saturation for Waterfloods and ASP | | | | S | | S | P | |
| Other Operational Issues[*3] | | | P | | | | P | P |
| Operational Strategy and Economic Estimation | | | | | | P | P | P |

Lab work

Pilot test

Commercial project

P Primary method

S Secondary or Supplemental method

[*1] Other Methods include IFT measurement, natural soap measurements etc.

[*2] Other methods include static adsorption, single phase core flood

[*3] Other operational issues include chemical mixing, produced emulsion treatment etc.

**Figure 8.1 Key parameters for a commercial ASP process**

Based on figure 8.1, the optimization procedure for a successful commercial ASP project is provided as the following steps:

1. By reviewing the literature, alkali, surfactant candidates for the crude oil of interest are chosen for the phase behavior test.

2. By phase behavior test, the formulations with favorable phase behaviors, such as high solubility ratio, high salt tolerance, high compatibility with alkali and polymer, are selected. Meanwhile, the correlation of optimum salinity with soap to surfactant ratio, which is essential information for the ASP simulation, can be obtained by the phase behavior test. The phase behavior also provides the information of over-optimum condition that is related to the phase trapping. Also the phase behavior test can be used as the guide for the operational issues such as surfactant and polymer mixing methods, produced emulsion treatment. The phase behavior tests have been discussed in Chapter 3.

3. Interfacial tension measurement not only testifies whether the low tension is achieved, but also assures that the correlation that will be used in the simulation is correct. Many investigators trust the IFT measurement more than the value estimated from the phase behavior. The special aspects of IFT measurement for alkali surfactant system have been described in detail in Chapter 4.

4. The surfactant consumption can be estimated by both static adsorption test and dynamic adsorption test. The adsorption tests, which are described in Chapter 5, also provide the adsorption parameters for simulation. Steps 2, 3 and 4 are the lab tests for ASP and can be carried out at the same time.

5. With the data collected in steps 2, 3 and 4, the one-dimensional simulation can be conducted to optimize the predicted flood performance and select conditions for flood experiments, as shown in Chapter 6.

6. The flood experiments, which are described in Chapter 7, will verify the flooding capability of the designed formulation. It provides the information about the residual

oil saturation after waterflood and ASP flood. These two values are very important for the future field simulations. The flooding results also help to tune up simulation parameters by matching the history data.

7. The next step will be the pilot test and field simulation before the commercial projects. This part is not included in this thesis. However, several pilots based on the strategies are ongoing now.

## 8.3 Future Work

The phase behavior results in this thesis are at ambient temperature. High temperature phase behavior studies should be conducted for ASP system. More phase behavior experiments should be conducted to test if the relation of optimum salinity and soap to surfactant ratio applies to other crude oils and surfactants.

The colloidal dispersions are observed both in Yates oil and PBB oil. Also wide low IFT regions are found in these two oils by either measuring the IFT or estimating by Huh's correlation. Other alkali surfactant crude oil systems should be investigated to see whether colloidal dispersion and wide IFT are general characteristics of ASP process. The mass transport model for dynamic IFT of fresh oil and alkali surfactant is also an interesting research project that will help people to further understand the ASP process.

$Na_2CO_3$ can significantly reduce the anionic surfactant adsorption on carbonate formation provided gypsum is not present. When gypsum is present, other surfactant adsorption reduction alkalis, such as sodium citrate or sodium metaborate, should be tested.

Three dimensional reservoir simulations for ASP should be investigated. UTChem can be a good platform because it includes many physical and chemical features of surfactant. With three-dimensional reservoir simulator for ASP, the soap to surfactant ratio idea can be tested in the field scale.

The flooding experiments in this thesis are one-dimensional experiments which only show the effects of displacement efficiency. Multi-dimensional flooding will be valuable because the flooding results represent both displacement and sweep efficiency. With the known displacement efficiency from the one-dimensional flooding, the sweep enhanced effect by ASP can be evaluated with multi-dimensional flooding. It is also valuable to conduct the floods with reservoir cores at reservoir conditions such as temperature.

For highly viscous oil, experimental results show foam seems to be a good candidate for mobility control. However, the mechanism of foam in ASP process is not well known yet. More flooding experiments, as well as some mechanism studies of oil displacement by foam, are needed for future ASP foam applications.

# REFERENCES

Adibhatla, B. and Mohanty, K. K., "Oil Recovery from Fractured Carbonates by Surfactant-Aided Gravity Drainage: Laboratory Experiments and Mechanistic Simulations," SPE 99773, presented at SPE/DOE Symposium on Improved Oil Recovery, 22-26 April, Tulsa, Oklahoma

Adamson, A. W., *Physical Chemistry of Surfaces*, 3rd ed., John Wiley & Sons, New York, 1976.

Akstinat, M.H., "Surfactants for EOR Process in High-Salinity Systems: Product Selection and Evaluation," in *Enhanced Oil Recovery*, F.J. Fayers (ed.) New York: Elsevier, 1981.

Al-Hashim, H. S., Obiora, V., Al-Yousef, H. Y., Fernandez, F., and Nofal, W., "Alkaline Surfactant Polymer Formulation for Saudi Arabian Carbonate Reservoirs," SPE 35353, presented at the Tenth Symposium on Improved Oil Recovery, Tulsa, OK, April 1996.

Anderson, G.A., Delshad, M., King C.B., Mohammadi H., and Pope G.A., "Optimization of Chemical Flooding in a Mixed-Wet Dolomite Reservoir," SPE 100082, presented at the SPE/DOE Symposium on Improved Oil Recovery, Tulsa, Oklahoma, April 2006.

Annual Technical Report on Surfactant Based Enhanced Oil Recovery and Foam Mobility Control; prepared for U.S. DOE (DE-FC26-03NT15406), Rice University, Houston, TX (July 2005).

Annual Technical Report on Surfactant Based Enhanced Oil Recovery and Foam Mobility Control; prepared for U.S. DOE (DE-FC26-03NT15406), Rice University, Houston, TX (June 2006).

Aoudia, M., Wade, W. H., and Weerasooriya, V.: "Optimum Microemulsions Formulated with Propoxylated Tridecyl Alcohol Sodium Sulfates," *Journal of Dispersion Science and Technology*, 16(2) 1995, 115-135.

Arihara, N., Yoneyama, Akita, Y., and Lu, X., "Oil Recovery Mechanisms of Alkali-Surfactant-Polymer Flooding," SPE 54330, presented at the 1999 SPE Asia Pacific Oil and Gas Conference and Exhibition, Jakarta, Indonesia, Apr. 1999.

Austad, T., and Milter, J., "Spontaneous Imbibition of Water into Low Permeable Chalk at Different Wettabilities Using Surfactants," SPE 37236 presented at the International Symposium on Oilfield Chemistry, Houston, 1997.

Austad, T., Matre, B., Milter, J., Sævareid, A., and Øyno, L., "Chemical Flooding of Oil Reservoirs 8. Spontaneous Oil Expulsion from Oil- and Water-wet Low Permeable Chalk

Material by Imbibition of Aqueous Surfactant Solutions," *Colloids and Surfaces A.*, **137**, 117-129, 1998.

Austad, T., Strand S., Høgnesen E.J., Zhang P., "Seawater as IOR Fluid in Fractured Chalk," SPE 93000, presented at SPE International Symposium on Oilfield Chemistry, 2-4 February 2005, Woodlands, Texas

Baviere, M., Glenat, P., Plazanet, V., and Labrid, J., "Improved EOR by Use of Chemicals in Combination", *SPERE*, 187-193, Aug. 1995.

Bourrel, M., and Schechter, R. S, *Microemulsions and related systems*, Surfactant Science Series, V. 30, Marcel Dekker, Inc., New York, 1988.

Burauer, S., Belkoura L., Stubenrauch C., Strey R., "Bicontinuous microemulsions revisited," *Colloids and Surfaces A*, 228 (2003) 159–170.

Burk, J. H., "Comparison of Sodium Carbonate, Sodium Hydroxide, and Sodium Orthosilicate for EOR," *SPERE*, 9-16, Feb. 1987.

Celik, M. S., Manev, E. D., and Somasundaran, P., "Sulfonate Precipitation-Redissolution-Reprecipitation in Inorganic Electrolytes," in *Interfacial Phenomena in Enhanced Oil Recovery*, *AIChE* Symposium Series 212, 78, 86-96, 1982.

Chang, H. L., Zhang, Z. Q., Wang, Q. M., Xu, Z. S., Guo, Z. D., Sun, H. Q., Cao, X. L., and Qiao, Q., "Advances in Polymer Flooding and alkaline/Surfactant/Polymer Processes as Developed and Applied in the People's Republic of China," *Journal of Petroleum Technology*, 84-89, February 2006.

Cheng, K. H., "Chemical Consumption During Alkaline Flooding: A Comparative Evaluation," SPE 14944, presented at the 5th Symposium on Enhanced Oil Recovery of the Society Petroleum Engineers and the Department of Energy, Apr. 1986.

Clark, S. R., Pitts, M. J., and Smith, S. M., "Design and Application of an Alkaline-Surfactant-Polymer Recovery System to the West Kiehl Field", SPE 17538 presented at the SPE Rocky Mountain Regional Meeting, Casper, WY, May 1988.

Cooke, C. E., Williams, R. E., and Kolodzie, P. A., "Oil Recovery by Alkaline Waterflooding", *Journal of Petroleum Technology*, 1365-1374, Dec. 1974.

Craig, F. F. Jr., *The Reservoir Engineering Aspects of Waterflooding*, Monograph V. 3 of Henry L. Doherty series, Society of Petroleum Engineers of AIME, Dallas, 1971.

CRC Handbook of Chemistry and Physics, 68th ed., F-315, CRC Press, Boca Raton, FL, 1987.

Delshad, M. *et al*. "Effect of Capillary Number on the Residual Saturation of a Three-Phase Micellar Solution," SPE 14911, Symposium on EOR in Tulsa, OK, April, 1986.

Delshad, M., Han, W., Pope, G.A., Sepehrnoori, K., Wu, W., Yang, R., Zhao, L., "Alkaline/Surfactant/Polymer Flood Predictions for the Karamay Oil Field," SPE 39610, SPE/DOE Improved Oil Recovery Symposium, 19-22 April 1998, Tulsa, Oklahoma

Delshad, M., Asakawa, K., Pope, G. A., Sepehrnoori K., "Simulations of Chemical and Microbial Enhanced Oil Recovery Methods," SPE 75237, presented at SPE/DOE Improved Oil Recovery Symposium, Tulsa, Oklahoma, 13-17 April, 2002.

deZabala, E. F. et al., "A Chemical Theory for Linear Alkaline Flooding," *SPEJ*, 245-258, Apr. 1982.

Ehrlich, R, and Wygal, R. J., "Interrelation of Crude Oil and Rock Properties with the Recovery of Oil by Caustic Waterflooding," *SPEJ*, 263-270, Aug. 1977.

Emery, L. W., Mungan, N., and Nicholson, R. W., "Caustic Slug Injection in the Singleton Field," *Journal of Petroleum Technology*, 1569-1576, Dec. 1970.

Falls, A. H., Thigpen, D. R., Nelson, R. C., et al., "A Field Test of Cosurfactant-Enhanced Alkaline Flooding," SPE 24117, presented at the SPE/DOE 8th Symposium on Enhanced Oil Recovery, Tulsa, OK, 1992.

Fan, T. and Buckley, J. S., "Acid Number Measurements Revisited," SPE 99884, presented at the SPE/DOE Symposium on Improved Oil Recovery in Tulsa, Oklahoma, 22-26 April 2006.

Farmanian, P. A. et al., " Participation of Selective Native Petroleum fractions in Lowering Interfacial Tensions of Aqueous Alkaline System," in *Chemistry of Oil Recovery*, ACS Symposium Series 91, R. T. Johansen and R. L. Berg (eds.), 103-114, Washington, D. C., 1979.

French, T. R., and Burchfield, T. E., " Design and Optimization of Alkaline Flooding Formulations", SPE 20238 presented at the SPE/DOE Seventh Symposium on Enhanced Oil Recovery, Tulsa, OK, 1990.

Gao, S., Li, H., and Li, H., "Laboratory Investigation of Combination of Alkali/Surfactant/Polymer Technology for Daqing EOR", *SPERE*, 194-197, Aug. 1995.

Gao, S., Li, H., Yang, Z., Pitts, M. J., Surkalo, H., and Wyatt, K., "Alkaline/Surfactant/Polymer Pilot Performance of the West Central Saertu, Daqing Oil Field", *SPERE*, 181-188, Aug. 1996.

Glinsmann, G.R., "Surfactant Flooding with Microemulsions Formed in situ- Effect of Oil Characteristics," SPE 8326, 54th Annual Fall Technical Conference and Exhibition of

the Society of Petroleum Engineers of AIME, held in Las Vegas, Nevada, September 23-26, 1979.

Glover, C. J., Puerto, M. C., Maerker, J. M., and Sandvik, E. L., "Surfactant Phase Behavior and Retention in Porous Media," *SPEJ*, 183-193, June, 1979.

Greaser, G. R., and Ortiz J. R., "New Thermal Recovery Technology and Technology Transfer for Successful Heavy Oil Development," SPE 69731, presented at the 2001 SPE International Thermal Operations and Heavy Oil Symposium held in Porlamar, Margarita Island, Venezuela, 12-14 March 2001.

Green, D. W., and Willhite, G. P., *Enhanced Oil Recovery*, SPE Textbook Series Vol. 6, SPE inc., Richardson, TX, 1998.

Grigg, R.B. and Bai B., "Sorption of Surfactant Used in CO2 Flooding onto Five Minerals and Three Porous Media," SPE 93100, SPE International Symposium on Oilfield Chemistry, Woodlands, Texas, 2-4 February, 2005.

Healy, R. N. and Reed, R. L.: "Physicochemical Aspects of Microemulsion Flooding," *SPEJ*, (October 1974), 491-501.

Healy, R. N., Reed, R. L., and Stenmark, D. G., "Multiphase Microemulsion Systems," *SPEJ*, 147-160, 1976.

Healy, R. N., Reed, R. L.: "Immiscible Microemulsion Flooding," *SPEJ,* April 1977, 129-139.

Hill, H. J. and Lake, L. W., "Cation Exchange in Chemical Flooding: Part3-Experimental," *SPEJ*, 18(1978), 445-456.

Hirasaki, G. J., "Ion Exchange with Clays in the Presence of Surfactant," *SPEJ*, 181-191, Apr., 1982.

Hirasaki, G. J., Lawson, J.B., "An Electrostatic Approach to the Association of Sodium and Calcium with Surfactant Micelles," SPE 10921, SPERE, 119-130, Mar., 1986.

Hirasaki, G. J, "The steam-foam process," *Journal of Petroleum Technology,* May1989, 449-456, SPE 19505. (Full-length article is SPE 19518; it is supplement to paper 19505. while not published, this paper passed through peer review with the published paper and is available in SPE e-Library.)

Hirasaki, G. J., Rohan, J. A., Dubey, S. T., and Niko, H., "Wettability Evaluation During Restored-State Core Analysis," SPE 20506, presented at the 65$^{th}$ Annual Tech. Conf. Of SPE, New Orleans, LA, Sept. 1990.

Hirasaki, G.J., van Domselaar, H.R., Koninklijke, Nelson, R.C., "Evaluation of the Salinity Gradient Concept in Surfactant Flooding", SPEJ, 486-500, June, 1983.

Hirasaki, G. J., and Zhang, D. L., "Surface Chemistry of Oil Recovery from Fractured, Oil-Wet, Carbonate Formations," SPE 80988, presented at the SPE International Symposium on Oilfield Chemistry, Houston, TX, Feb. 2003.

Holmberg, K., *Handbook of applied surface and colloid chemistry*, Chichester, New York, Wiley, 2001. Volume 1 & 2.

Huh, C., "Interfacial-Tensions and Solubilizing Ability of a Microemulsion Phase that Coexists with Oil and Brine," *JCIS* 71 (2): 408-426 1979.

Jayanti, S., Britton, L. N., Dwarakanath, V., and Pope, G. A.: "Laboratory Evaluation of Custom Designed Surfactants to Remediate NAPL Source Zones," *Environmental Science and Technology,* (December 2002), 5491.

John, A., Han, C., Delshad, M., Pope, G.A., and Sepehrnoori, K., "A New Generation Chemical-Flooding Simulator," *SPEJ*, 206-216, June 2005.

Koperna G.J., Melzer L.S., and Kuuskraa V.A., "Recovery of Oil Resources From the Residual and Transitional Oil Zones of the Permian Basin," SPE 102972, SPE Annual Technical Conference and Exhibition, San Antonio, Texas, USA. September 2006.

Krumrine, P. H., Falcone, J. S., and Campbell, T. C., "Surfactant Flooding 1: The Effect of Alkaline Additives on IFT, Surfactant Adsorption, and Recovery Efficiency", *SPEJ*, 503-513, Aug. 1982.

Lake, L. W., *Enhanced Oil Recovery*, Prentice-Hall, Englewood Cliffs, NJ, 1989.

Lelanne-Cassou, C., Schechter R. S., *et al*., "Binary Surfactant Mixtures for Minimizing Alcohol Co-solvent Requirements," SPE 12035, ATCE in San Francisco, CA. October, 1983.

Levitt, D.B., Jackson A.C., Heinson C., Britton L.N., Malik T. and Dwarakanath V., and Pope G.A., "Identification and Evaluation of High-Performance EOR Surfactants," SPE 100089, presented at SPE/DOE Symposium on Improved Oil Recovery, 22-26 April 2006, Tulsa, Oklahoma, USA.

Li, B., "Surfactant/foam enhanced aquifer contacting and modeling for aquifer remediation," PhD Thesis, Rice University, 2006.

Li, H., Liao, G., Han, P., Yang, Z., Wu, X., Chen, G., Xu, D., Jin, P., "Alkaline/Surfactant/Polymer (ASP) commercial Flooding Test in central Xing2 Area of Daqing Oilfield," SPE 84896, presented at the SPE International Improved Oil Recovery Conference in asia Pacific in Kuala Lumpur, Malaysia, 20-21 October 2003

Lin, S., and Hwang, H., "Measurement of Low Interfacial Tension by Pendant Drop Digitization", *Langmuir*, **10**, 4703-4709, 1994.

Martin, F. D., and Oxley, J. C., and Lim, H., "Enhanced Recovery of a "J" Sand Crude Oil with a Combination of Surfactant and Alkaline Chemicals", SPE 14293 presented at the 60th Annual Technical Conference and Exhibition of SPE, Las Vegas, NV, Sep. 1985.

Mayer, E. H., Berg, R. L., Carmichael, J. D., and Weinbrandt, R. M., "Alkaline Injection for Enhanced Oil Recovery—A Status Report", *Journal of Petroleum Technology*, 209-221, Jan. 1983.

Miller, C. A., and Neogi, P., *Interfacial Phenomena*, Surfactant Science Series, V. 17, Marcel Dekker, Inc., New York, 1985.

Morrow, N. R., "Wettability and Its Effect on Oil Recovery," *Journal of Petroleum Technology*, 1476-1484, Dec. 1990.

Morrow, N. R. (ed.), *Interfacial Phenomena in Petroleum Recovery*, Marcel Dekker, Inc., New York, 1991.

Nelson, R. C., and Pope, G. A., "Phase Relationships in Chemical Flooding," *SPEJ*, 325-338, 1978.

Nelson, R.C., Lawson, J. B., Thigpen, D. R. and Stegemeier, G. L., "Co-Surfactant Enhanced Alkaline Flooding," SPE 12672, 1984.

Nguyen, Q.P., Alexandrov A. V., Zitha P. L., Currie P. K., "Experimental and Modeling Studies on Foam in Porous Media: A Review," SPE 58799, presented at SPE International Symposium on Formation Damage Control, Lafayette, Louisiana, February 2000.

Olsen, D. K., Hicks, M. D., Hurd, B. G., Sinnokrot, A. A., and Sweigart, C. N., "Design of a Novel Flooding System for an Oil-Wet Central Texas Carbonate Reservoir," SPE20224, presented at the SPE Seventh Symposium on Enhanced Oil Recovery, Tulsa, OK, 1990.

Osterloh, W. T., and Jante, M. J. Jr., "Surfactant Polymer Flooding with Anionic PO/EO Surfactant Microemulsions Containing Polyethylene Glycol Additives," SPE 24151, presented at the Eighth Symposium on Enhanced Oil Recovery, Tulsa, OK, April 1992.

Patton, J. T., Holbrook, S. T., and Hsu, W., "Rheology of Mobility Control Foams," *SPEJ*, June 1983, 456-60

Pitts, M. J., Dowling, P., Wyatt K., Surkalo, H., Adams C., "Alkaline-Surfactant-Polymer Flood of the Tanner Field," SPE 100004, presented at the 2006 SPE/DOE Symposium on Improved Oil Recovery in Tulsa, Oklahoma, 22-26 April 2006.

Pope, G.A., Lake, L.W., Helfferich, F.G., "Cation Exchange in Chemical Flooding: Part 1--Basic Theory Without Dispersion," *SPEJ*, December 1978, 418-434

Pope, G. A., Nelson, R.C., "A Chemical Flooding Compositional Simulator," *SPEJ*, October 1978, 339-354

Pope, G. A., Wu, W., Narayanaswamy, G., Delshad, M., Sharma, M. M. and Wang, P., " Modeling Relative Permeability Effects in Gas-Condensate Reservoirs with a New Trapping Model," *SPERE&E* , 3 (2), 171-178, 2000.

Pratap, M., Gauma M. S., "Field Implementation of Alkaline-Surfactant-Polymer (ASP) Flooding: A maiden effort in India," SPE 88455, presented at the SPE Asia Pacific Oil and Gas Conference and Exhibition in Perth, Australia, 18-20 October 2004.

Puerto, M.C., Gale, W.W., "Estimation of Optimal Salinity and Solubilization Parameters for Alkylorthoxylene Sulfonate Mixtures," *SPEJ*, 193-200, June 1977.

Qiao, Q., Gu, H., Li, D., and Dong, L., "The Pilot Test of ASP Combination Flooding in Karamay Oil Field," SPE 64726 presented at the International Oil and Gas Conference and Exhibition in China, Beijing, China, Nov. 2000.

Qutubuddin, S., Miller, C. A., and Fort, T., Jr. "Phase Behavior of pH-Dependent Microernulsions," *Journal of Colloid and Interface Science*, Vol. 101, No. 1, September 1984.

Ramakrishnan, T. S., and Wasan, D. T., "Alkaline Waterflooding-A Model for interfacial Activity of Acidic Crude Oil/Caustic Systems," SPE 10716, presented at the Third Symposium on Enhanced Oil Recovery of the Society of Petroleum Engineers, Tulsa, Okalahoma, 1982.

Ramakrishnan, T. S., and Wasan, D. T., "A Model for Interfacial Activity of Acidic Crude Oil/Caustic Systems for Alkaline Flooding," *SPEJ*, 602-612, Aug. 1983.

Rao, D. N., "Wettability Effects in Thermal Recovery Operations," *SPERE&E* 2 (5), October 1999.

Reed, R. L., and Healy, R. N., "Contact Angles for Equilibrated Microemulsion Systems," *SPEJ*, 342-350, Jun. 1984.

Rudin, J., and Wasan, D. T., "Mechanisms for Lowering of Interfacial Tension in Alkali/Acidic Oil Systems: Effect of Added Surfactant", *Ind. Eng. Chem. Res*., **31**, 1899-1906, 1992.

Salter, S. J., "Selection of Pseudo-Components in Surfactant-Oil-Brine-Alcohol System," SPE 7056, presented at the 1978 SPE Improved Oil Recovery Symposium, Tulsa, April 16-19.

Sanz, C.A. and Pope, G.A., "Alcohol-Free Chemical Flooding: From Surfactant Screening to Coreflood Design," SPE 28956, Proceedings of the SPE International Symposium on Oilfield Chemistry, San Antonio, TX, February 14-17, (1995).

Scriven, L. E., "Equilibrium Bicontinuous Structure," *Nature*, 263 (5573), 123-125, 1976.

Seethepalli, A., Adibhatla, B., and Mohanty K. K., "Wettability Alteration during Surfactant Flooding of Carbonate Reservoirs," SPE 89423 presented at the SPE/DOE 14th Symposium on Improved Oil Recovery, Tulsa, OK, April 2004.

Seifert, W. K., and Howells, W. G., "Interfacially Active Acids in a California Crude Oil," *Ana. Chem.*, **41** (4), 554-568, 1969.

Shuler, P. J., Kuehne, D. L., and Lerner, R. M., "Improving Chemical Flood Efficiency with Micellar/Alkaline/Polymer Processes," *Journal of Petroleum Technology*, 80-88, Jan. 1989.

Shupe, R. D., "Chemical Stability of Polyacrylamide Polymers," *Journal of Petroleum Technology*, August 1981, 1513-1529.

Sorbie, K. S., *Polymer Improved Oil Recovery*, Blackie and Son Ltd, London, 1991.

Somerton, W.H., and Radke, C.J., "Role of Clays in the Enhanced Recovery of Petroleum from Some California Sands," *Journal of Petroleum Technology*, 643-654, March 1983.

Somasundaran, P., Celik, M., Goyal, A., and Manev, E., "The Role of Surfactant Precipitation and Redissolution in the Adsorption of Sulfonate on Minerals ", SPE 8263, presented at the 54th Annual Technical Conference and Exhibition of the Society of Petroleum Engineers, Las Vegas, Nevada, 1979.

Sorbie, Kenneth, *Polymer Improved Oil Recovery,* Blackie and Son Ltd, Glasgow, 1991.

Spinler, E. A., and Baldwin, B. A., "Surfactant Induced Wettability Alteration in Porous Media", *Surfactants: Fundamentals and Applications in the Petroleum Industry*, Schramm, L. L., ed., Cambridge University Press, Cambridge, 2000.

Standnes, D. C., and Austad, T., "Wettability Alteration in Low-permeable Chalk. Mechanism for Wettability Alteration from Oil-wet to Wet-wet Using Surfactants," 6th International Symposium on Reservoir Wettability and Its Effect on Oil Recovery, Socorro, NM, 2000.

Standnes, D. C., Nogaret, L. A. D., Chen, H. L., and Austad, T., "An Evaluation of Spontaneous Imbibition of Water into Oil-Wet Carbonate Reservoir Cores Using a Nonionic and a Cationic Surfactant," *Energy & Fuels*, **16**, 1557-1564, 2002.

Standnes D. C., Austad T., "Wettability alteration in carbonates - Low-cost ammonium surfactants based on bio-derivatives from the coconut palm as active chemicals to change the wettability form oil-wet to water-wet conditions," *Colloid Surface A* 218 (1-3): 161-173, May, 2003

Thomas, S., Ali, SMF, "Status and assessment of chemical oil recovery methods," *Energy Sources* 21 (1-2): 177-189 JAN-MAR 1999

Thompson, D.W. and Pownall, P.G.: "Surface Electrical Properties of Calcite," *Journal of Colloid and Interface Science* **131**(74), August 1989

Trushenski, S. P., "Micellar Flooding: Sulfonate-Polymer Interaction," in *Improved Oil Recovery by Surfactant and Polymer Flooding*, D. O. Shah and R. S. Schecter New York: Academic Press, 1977.

Vargo, J., Turner, J., Vergnani, B., Pitts, M. J., Wyatt, K., Surkalo, H., and Patterson, D., "Alkaline-Surfactant-Polymer Flooding of the Cambridge Minnelusa Field", *SPERE&E*, **3** (6), 552-557, Dec. 2000.

Wang D., Cheng J., Yang Q., Gong W., Li Q., Chen F., "Viscous-Elastic Polymer Can Increase Microscale Displacement Efficiency in Cores", SPE 63227, SPE Annual Technical Conference and Exhibition, 1-4 October 2000, Dallas, Texas

Wang, D., Zhang, Z., Cheng, J., Yang, J., Gao, S., and Li., L., "Pilot Tests of Alkaline/Surfactant/Polymer Flooding in Daqing Oil Field," *SPERE*, 229-233, Nov., 1997.

Wagner, O. R., and Leach, R. O., "Improving Oil displacement Efficiency by wettability Adjustment", *Petroleum Transactions, AIME*, **216**, 65-72, 1959.

Wardlaw, N. C., "Factors Affecting Oil Recovery from Carbonate Reservoirs and Prediction of Recovery", in Carbonate Reservoir Characterization: A Geologic-Engineering Analysis, Part II, Chilingarian, G. V., Mazzullo, S. J., and Rieke, H. H., ed., Elsevier, New York, 867, 1996.

Wesson, L. L., and Harwell, J. H., "Surfactant Adsorption in Porous Media", *Surfactants: Fundamentals and Applications in the Petroleum Industry*, Schramm, L. L., ed., Cambridge University Press, Cambridge, 2000.

Winsor, P. A., *Solvent Properties of Amphiphilic Compound*, Butterworths, London (1954).

Wu, Y., Shuler, P., Blanco, M., Tang, Y., Goddard, W. A.: "A Study of Branched Alcohol Propoxylate Sulfate Surfactants for Improved Oil Recovery," SPE 95404, presented at the 2005 Annual Technical Conference and Exhibition, Dallas, Texas

Xie, X. and Morrow, N.R.: "Oil Recovery by Spontaneous Imbibition From Weakly Water-Wet Rocks," *Petrophysics*, **42**(4), 313, 2001

Yan, W., "Foam for mobility control in alkaline/surfactant enhanced oil recovery process," Ph. D. Thesis, Rice University, December 2006.

Yang, F., Wang, D., Wang, G., Sui X., Liu W., Kan C., "Study on High Concentration Polymer Flooding to Further Enhance Oil Recovery," SPE 101202, presented at 2006 SPE ATCE in San Antonio, Texas, 24-27 September 2006.

Yang, S. S., "Mechanisms of wettability for crude oil/brine/mica system," PhD Thesis, Rice University, 2000.

Yang, X., Liao, G., Han, P., Yang, Z., Yao, Y., "An Extended field Test Study on Alkaline-surfactant-polymer flooding in Beiyiduanxi of Daqing Oilfield," SPE 80532, presented at the SPE Asia Pacific Oil and Gas Conference and Exhibition in Jakarta, Indonesia, 15-17 April 2003

Zeppieri, S., Rodriguez, J., Lopez de Ramos, A. L., "Interfacial Tension of Alkane + Water Systems", *J. Chem. Eng. Data*, 2001, **46**(5), 1086-1088

Zerpa L. E., Queipo, N. V., Pintos, S., Salager, J., "An Optimization Methodology of Alkaline-Surfactant-Polymer Flooding Processes Using Field Scale Numerical Simulation and Multiple Surrogates," SPE 89387, presented at SPE/DOE Symposium on Improved Oil Recovery, Tulsa, Oklahoma, 17-21 April 2004.

Zhang, D.L., "Surfactant-enhanced oil recovery process for a fractured, oil-wet carbonate reservoir," PhD Thesis, Rice University, 2006.

Zhang, D. L., Liu, S., Puerto, M., Miller, C. A., Hirasaki, J., "Wettability Alteration and Spontaneous Imbibition in Oil-Wet Carbonate Formations," *Journal of Petroleum Science and Engineering*, Volume 52, Issues 1-4, June 2006, 213-226

Zhang, D. L., Liu, S., Yan, W., Puerto, M., Hirasaki, J., Miller, C. A., "Favorable Attributes Of Alkali-Surfactant-Polymer Flooding," SPE 99744, presented at the SPE/DOE Symposium on Improved Oil Recovery in Tulsa, Oklahoma, 22-26 April 2006.

*Appendix A*

# Anionic Surfactant Potentiometric Titration

## A.1 Equipments and Chemicals

**1. Electrode**: pHoenix Surfactant Combination Electrode, from pHoenix Electrode Co. (Cat. No. SUR1502).

**2. Automatic Titrator:** Metrhom Titrino Model 716, from Brinkman Instruments.

**3. Titrant:** Benzethonium Chloride (Hyamine 1622), from Gallord-Schlesinger Industries Inc., standard 0.004 M solution (Cat. No. 192233F), or prepared by crystalline solid (250g, Cat. No. 560162Y).

**4. Standard Anionic Surfactant Solution (for standardizing the titrant):** 0.01 M sodium lauryl sulfate (sodium dodecyl sulfate), from pHoenix Electrode Co. (Cat. No. SURAS02).

**5. Sample Additive (to keeps electrodes clean):** Diluted Triton X-100, from pHoenix Electrode Co. (Cat. No. SURIS01)

**6. Electrode Rinse Solutions:** 0.005 M HCl.

**7. Other Equipments:** 50-100 ml beaker, Magnetic stirrer, Balance

## A.2 Titration Procedure

1. Prepare a solution of benzethonium chloride with approximately 0.004 M (If the standard 0.004 M solution is used, go to step 5). A titrant should be dilute enough to yield a measurable titration volume, about half volume of the titrator burette that stocks the titrant. For a 10 ml burette, the desired titrant volume used is 5 ml.

Titrant consumption should not be less than 1 ml, nor greater than 10 ml. either of which will result in large errors.

2. Weigh about 2 gram standard 0.01M SDS solution into a 100 ml beaker and dilute to approximately 60 ml with deionized water.
3. Immerse the surfactant specific electrode in the solution of analyte. Add one or two drops of a 1% solution of Triton X-100. Commence stirring using a magnetic stirrer. Make sure there is not any air bubble adsorbing to the electrode.
4. Begin adding hyamine solution using the automatic titrator until the maximum rate of voltage change is passed. The titrator will automatically find the end point (inflection point) and stop automatically. Calculate the hyamine concentration as follows (assume the density of the standard SDS solution is 1 g/ml):

$$Nt = \frac{Cs * Ws}{Vt} \qquad \text{(A.1)}$$

Where $Nt$: normality of titrant, M;

$Cs$: concentration of standard SDS solution, 0.01 M;

$Ws$: weight of standard SDS solution, g;

$Vt$: volume of titrant consumed, ml.

5. Weigh enough samples in the 100 ml beaker so that the titrant consumption is about 5 ml.
6. Same as step 3.
7. Same as step 4, but the equation used to calculate sample surfactant concentration is:

$$Csamp = \frac{Nt * Vt}{Wsamp} \qquad \text{(A.2)}$$

Where *Csamp*: sample concentration, M

*Nt*: normality of titrant, M;

*Vt*: volume of titrant consumed, ml.

*Wsamp*: weight of the sample, g;

Here, the volume of the sample is assumed to the same as its weight. If the sample density deviates far from 1 g/ml, then actual volume of the sample should be used instead of its weight.

*Appendix B*

# Simulation Cases Table 1

| Acid | Sor | Acid No. | Soap Conc. (Mol/L) | Surf. conc. (%) | Surfactant conc. (Mol/L) | Surf. Frac. 1 | Soap frac. 1 | Salinity (%NaCl) | recovery eff. (%) | Dimensionless salinity | Store folder | New dimension Less sal | Slug Volume (PV) |
|---|---|---|---|---|---|---|---|---|---|---|---|---|---|
| Low | 0.3 | 0.02 | 3.57E-04 | 1 | 1.50E-02 | 0.99 | 0.01 | 5.50% | 77.12% | 111.11% | Low Acid-1 | 11.0 | ***0.70*** |
| Low | 0.3 | 0.02 | 3.57E-04 | 1 | 1.50E-02 | 0.99 | 0.01 | 5.00% | 100.00% | 100.00% | Low Acid-2 | 10.0 | ***0.70*** |
| Low | 0.3 | 0.02 | 3.57E-04 | 1 | 1.50E-02 | 0.99 | 0.01 | 4.00% | 100.00% | 77.78% | Low Acid-3 | 8.0 | ***0.50*** |
| Low | 0.3 | 0.02 | 3.57E-04 | 1 | 1.50E-02 | 0.99 | 0.01 | 3.00% | 100.00% | 55.56% | Low Acid-4 | 6.0 | ***0.50*** |
| Low | 0.3 | 0.02 | 3.57E-04 | 1 | 1.50E-02 | 0.99 | 0.01 | 2.00% | 76.01% | 33.33% | Low Acid-5 | 4.0 | ***0.50*** |
| Low | 0.3 | 0.02 | 3.57E-04 | 1 | 1.50E-02 | 0.99 | 0.01 | 1.00% | 39.99% | 11.11% | Low Acid-6 | 2.0 | ***0.50*** |
| Low | 0.3 | 0.02 | 3.57E-04 | 1 | 1.50E-02 | 0.99 | 0.01 | 0.50% | 23.52% | 0.00% | Low Acid-7 | 1.0 | ***0.50*** |
| Low | 0.3 | 0.02 | 3.57E-04 | 1 | 1.50E-02 | 0.99 | 0.01 | 0.00% | 13.08% | -11.11% | Low Acid-8 | 0.0 | ***0.50*** |
| Low | 0.3 | 0.02 | 3.57E-04 | 0.1 | 1.50E-03 | 0.91 | 0.09 | 5.50% | 75.34% | 111.11% | Low Acid-9 | 11.0 | ***0.50*** |
| Low | 0.3 | 0.02 | 3.57E-04 | 0.1 | 1.50E-03 | 0.91 | 0.09 | 5.00% | 100.00% | 100.00% | Low Acid-10 | 10.0 | ***0.50*** |
| Low | 0.3 | 0.02 | 3.57E-04 | 0.1 | 1.50E-03 | 0.91 | 0.09 | 4.00% | 100.00% | 77.78% | Low Acid-11 | 8.0 | ***0.50*** |
| Low | 0.3 | 0.02 | 3.57E-04 | 0.07 | 1.05E-03 | 0.87 | 0.13 | 3.00% | 100.00% | 55.56% | Low Acid-12 | 6.0 | ***0.50*** |
| Low | 0.3 | 0.02 | 3.57E-04 | 0.07 | 1.05E-03 | 0.87 | 0.13 | 2.00% | 84.36% | 33.33% | Low Acid-13 | 4.0 | ***0.50*** |
| Low | 0.3 | 0.02 | 3.57E-04 | 0.07 | 1.05E-03 | 0.87 | 0.13 | 1.00% | 78.15% | 11.11% | Low Acid-14 | 2.0 | ***0.50*** |
| Low | 0.3 | 0.02 | 3.57E-04 | 0.07 | 1.05E-03 | 0.87 | 0.13 | 0.50% | 41.14% | 0.00% | Low Acid-15 | 1.0 | ***0.50*** |
| Low | 0.3 | 0.02 | 3.57E-04 | 0.07 | 1.05E-03 | 0.87 | 0.13 | 0.01% | 13.49% | -10.89% | Low Acid-16 | 0.0 | ***0.50*** |
| Low | 0.3 | 0.02 | 3.57E-04 | 0.1 | 1.50E-03 | 0.91 | 0.09 | 3.00% | 99.98% | 55.56% | Low Acid-17 | 6.0 | ***0.50*** |
| Low | 0.3 | 0.02 | 3.57E-04 | 0.1 | 1.50E-03 | 0.91 | 0.09 | 2.00% | 76.59% | 33.33% | Low Acid-18 | 4.0 | ***0.50*** |
| Low | 0.3 | 0.02 | 3.57E-04 | 0.1 | 1.50E-03 | 0.91 | 0.09 | 1.00% | 57.81% | 11.11% | Low Acid-19 | 2.0 | ***0.50*** |
| Low | 0.3 | 0.02 | 3.57E-04 | 0.1 | 1.50E-03 | 0.91 | 0.09 | 0.50% | 43.16% | 0.00% | Low Acid-20 | 1.0 | ***0.50*** |
| | | | | | | | | | | | | | |
| Mid | 0.3 | 0.2 | 3.57E-03 | 0.1 | 1.50E-03 | 0.49 | 0.51 | 2.00% | 98.63% | 33.33% | Mid Acid 1 | 4.0 | ***0.50*** |
| Mid | 0.3 | 0.2 | 3.57E-03 | 0.1 | 1.50E-03 | 0.49 | 0.51 | 1.00% | 93.36% | 11.11% | Mid Acid 2 | 2.0 | ***0.50*** |
| Mid | 0.3 | 0.2 | 3.57E-03 | 0.1 | 1.50E-03 | 0.49 | 0.51 | 0.01% | 13.06% | -11.00% | Mid Acid 3 | 0.0 | ***0.50*** |
| Mid | 0.3 | 0.2 | 3.57E-03 | 0.1 | 1.50E-03 | 0.49 | 0.51 | 5.00% | 53.09% | 100.00% | Mid Acid 4 | 10.0 | ***0.50*** |
| Mid | 0.3 | 0.2 | 3.57E-03 | 0.1 | 1.50E-03 | 0.49 | 0.51 | 5.50% | 25.41% | 111.11% | Mid Acid 5 | 11.0 | ***0.50*** |
| Mid | 0.3 | 0.2 | 3.57E-03 | 0.1 | 1.50E-03 | 0.49 | 0.51 | 4.00% | 100.00% | 77.78% | Mid Acid 6 | 8.0 | ***0.50*** |
| Mid | 0.3 | 0.2 | 3.57E-03 | 0.1 | 1.50E-03 | 0.49 | 0.51 | 0.50% | 89.96% | 0.00% | Mid Acid 7 | 1.0 | ***0.50*** |
| Mid | 0.3 | 0.2 | 3.57E-03 | 0.1 | 1.50E-03 | 0.49 | 0.51 | 3.00% | 100.00% | 55.56% | Mid Acid 8 | 6.0 | ***0.50*** |
| Mid | 0.3 | 0.2 | 3.57E-03 | 0.07 | 1.05E-03 | 0.41 | 0.59 | 1.00% | 95.01% | 11.11% | Mid Acid 9 | 2.0 | ***0.50*** |
| Mid | 0.3 | 0.2 | 3.57E-03 | 0.07 | 1.05E-03 | 0.41 | 0.59 | 0.50% | 94.06% | 0.00% | Mid Acid 10 | 1.0 | ***0.50*** |
| Mid | 0.3 | 0.2 | 3.57E-03 | 0.07 | 1.05E-03 | 0.41 | 0.59 | 0.00% | 13.08% | -11.11% | Mid Acid 11 | 0.0 | ***0.50*** |
| Mid | 0.3 | 0.2 | 3.57E-03 | 0.14 | 2.10E-03 | 0.58 | 0.42 | 2.00% | 98.05% | 33.33% | Mid Acid 12 | 4.0 | ***0.50*** |
| Mid | 0.3 | 0.2 | 3.57E-03 | 0.14 | 2.10E-03 | 0.58 | 0.42 | 3.00% | 100.00% | 55.56% | Mid Acid 13 | 6.0 | ***0.50*** |
| Mid | 0.3 | 0.2 | 3.57E-03 | 0.14 | 2.10E-03 | 0.58 | 0.42 | 4.00% | 100.00% | 77.78% | Mid Acid 14 | 8.0 | ***0.50*** |
| Mid | 0.3 | 0.2 | 3.57E-03 | 0.14 | 2.10E-03 | 0.58 | 0.42 | 5.00% | 88.95% | 100.00% | Mid Acid 15 | 10.0 | ***0.50*** |
| Mid | 0.3 | 0.2 | 3.57E-03 | 0.14 | 2.10E-03 | 0.58 | 0.42 | 5.50% | 33.07% | 111.11% | Mid Acid 16 | 11.0 | ***0.50*** |
| Mid | 0.3 | 0.2 | 3.57E-03 | 1 | 1.50E-02 | 0.91 | 0.09 | 0.01% | 13.08% | -10.89% | Mid Acid 17 | 0.0 | ***0.50*** |
| Mid | 0.3 | 0.2 | 3.57E-03 | 1 | 1.50E-02 | 0.91 | 0.09 | 0.50% | 34.54% | 0.00% | Mid Acid 18 | 1.0 | ***0.50*** |
| Mid | 0.3 | 0.2 | 3.57E-03 | 1 | 1.50E-02 | 0.91 | 0.09 | 1.00% | 52.69% | 11.11% | Mid Acid 19 | 2.0 | ***0.50*** |
| Mid | 0.3 | 0.2 | 3.57E-03 | 1 | 1.50E-02 | 0.91 | 0.09 | 2.00% | 80.72% | 33.33% | Mid Acid 20 | 4.0 | ***0.50*** |
| Mid | 0.3 | 0.2 | 3.57E-03 | 1 | 1.50E-02 | 0.91 | 0.09 | 3.00% | 100.00% | 55.56% | Mid Acid 21 | 6.0 | ***0.50*** |
| Mid | 0.3 | 0.2 | 3.57E-03 | 1 | 1.50E-02 | 0.91 | 0.09 | 4.00% | 100.00% | 77.78% | Mid Acid 22 | 8.0 | ***0.70*** |
| Mid | 0.3 | 0.2 | 3.57E-03 | 1 | 1.50E-02 | 0.91 | 0.09 | 5.00% | 100.00% | 100.00% | Mid Acid 23 | 10.0 | ***0.70*** |
| Mid | 0.3 | 0.2 | 3.57E-03 | 1 | 1.50E-02 | 0.91 | 0.09 | 5.50% | 77.09% | 111.11% | Mid Acid 24 | 11.0 | ***0.70*** |
| | | | | | | | | | | | | | |
| Mid | 0.3 | 0.2 | 3.57E-03 | 0.035 | 5.25E-04 | 0.26 | 0.74 | 0.01% | 12.74% | -10.89% | Mid Acid 25 | 0.0 | ***0.50*** |
| Mid | 0.3 | 0.2 | 3.57E-03 | 0.035 | 5.25E-04 | 0.26 | 0.74 | 0.50% | 97.84% | 0.00% | Mid Acid 26 | 1.0 | ***0.50*** |
| Mid | 0.3 | 0.2 | 3.57E-03 | 0.05 | 7.50E-04 | 0.33 | 0.67 | 1.00% | 97.56% | 11.11% | Mid Acid 27 | 2.0 | ***0.50*** |
| Mid | 0.3 | 0.2 | 3.57E-03 | 0.05 | 7.50E-04 | 0.33 | 0.67 | 2.00% | 99.10% | 33.33% | Mid Acid 28 | 4.0 | ***0.50*** |
| Mid | 0.3 | 0.2 | 3.57E-03 | 0.05 | 7.50E-04 | 0.33 | 0.67 | 3.00% | 100.00% | 55.56% | Mid Acid 29 | 6.0 | ***0.50*** |
| Mid | 0.3 | 0.2 | 3.57E-03 | 0.05 | 7.50E-04 | 0.33 | 0.67 | 4.00% | 57.60% | 77.78% | Mid Acid 30 | 8.0 | ***0.50*** |
| Mid | 0.3 | 0.2 | 3.57E-03 | 0.05 | 7.50E-04 | 0.33 | 0.67 | 5.00% | 20.99% | 100.00% | Mid Acid 31 | 10.0 | ***0.50*** |
| Mid | 0.3 | 0.2 | 3.57E-03 | 0.05 | 7.50E-04 | 0.33 | 0.67 | 5.50% | 16.70% | 111.11% | Mid Acid 32 | 11.0 | ***0.50*** |
| Mid | 0.3 | 0.2 | 3.57E-03 | 0.14 | 2.10E-03 | 0.58 | 0.42 | 1.00% | 89.46% | 11.11% | Mid Acid 33 | 2.0 | ***0.50*** |
| Mid | 0.3 | 0.2 | 3.57E-03 | 0.14 | 2.10E-03 | 0.58 | 0.42 | 0.50% | 80.66% | 0.00% | Mid Acid 34 | 1.0 | ***0.50*** |
| Mid | 0.3 | 0.2 | 3.57E-03 | 0.14 | 2.10E-03 | 0.58 | 0.42 | 0.01% | 13.08% | -10.89% | Mid Acid 35 | 0.0 | ***0.50*** |
| Mid | 0.3 | 0.2 | 3.57E-03 | 0.05 | 7.50E-04 | 0.33 | 0.67 | 0.01% | 12.58% | -10.89% | Mid Acid 36 | 0.0 | ***0.50*** |
| Mid | 0.3 | 0.2 | 3.57E-03 | 0.05 | 7.50E-04 | 0.33 | 0.67 | 0.50% | 95.93% | 0.00% | Mid Acid 37 | 1.0 | ***0.50*** |
| | | | | | | | | | | | | | |
| Mid | 0.3 | 0.2 | 3.57E-03 | 0.14 | 2.10E-03 | 0.58 | 0.42 | 0.01% | 13.08% | -10.89% | Mid Acid 38 | 0.0 | ***0.20*** |
| Mid | 0.3 | 0.2 | 3.57E-03 | 0.14 | 2.10E-03 | 0.58 | 0.42 | 0.50% | 84.44% | 0.00% | Mid Acid 39 | 1.0 | ***0.20*** |
| Mid | 0.3 | 0.2 | 3.57E-03 | 0.14 | 2.10E-03 | 0.58 | 0.42 | 1.00% | 91.42% | 11.11% | Mid Acid 40 | 2.0 | ***0.20*** |
| Mid | 0.3 | 0.2 | 3.57E-03 | 0.14 | 2.10E-03 | 0.58 | 0.42 | 2.00% | 98.39% | 33.33% | Mid Acid 41 | 4.0 | ***0.20*** |
| Mid | 0.3 | 0.2 | 3.57E-03 | 0.14 | 2.10E-03 | 0.58 | 0.42 | 3.00% | 99.54% | 55.56% | Mid Acid 42 | 6.0 | ***0.20*** |
| Mid | 0.3 | 0.2 | 3.57E-03 | 0.14 | 2.10E-03 | 0.58 | 0.42 | 4.00% | 62.57% | 77.78% | Mid Acid 43 | 8.0 | ***0.20*** |
| Mid | 0.3 | 0.2 | 3.57E-03 | 0.14 | 2.10E-03 | 0.58 | 0.42 | 5.00% | 21.44% | 100.00% | Mid Acid 44 | 10.0 | ***0.20*** |
| Mid | 0.3 | 0.2 | 3.57E-03 | 0.14 | 2.10E-03 | 0.58 | 0.42 | 5.50% | 17.33% | 111.11% | Mid Acid 45 | 11.0 | ***0.20*** |

*Appendix B*

# Simulation Cases Table 2

| Acid | Sor | Acid No. | Soap Conc. (Mol/L) | Surf. conc. (%) | Surfactant conc. (Mol/L) | Surf. Frac. 1 | Soap frac. 1 | Salinity (%NaCl) | recovery eff. (%) | Dimensionless salinity | Store folder | New dimension Less sal | Pore Volume |
|---|---|---|---|---|---|---|---|---|---|---|---|---|---|
| High | 0.3 | 1.2 | 2.14E-02 | 0.3 | 4.50E-03 | 0.33 | 0.67 | 0.50% | 93.74% | 0.00% | high acid 8 | 1.0 | 0.50 |
| High | 0.3 | 1.2 | 2.14E-02 | 0.3 | 4.50E-03 | 0.33 | 0.67 | 1.00% | 97.85% | 11.11% | high acid 7 | 2.0 | 0.70 |
| High | 0.3 | 1.2 | 2.14E-02 | 0.3 | 4.50E-03 | 0.33 | 0.67 | 3.00% | 100.00% | 55.56% | high acid 6 | 6.0 | 0.70 |
| High | 0.3 | 1.2 | 2.14E-02 | 0.3 | 4.50E-03 | 0.33 | 0.67 | 4.00% | 69.47% | 77.78% | high acid 5 | 8.0 | 0.70 |
| High | 0.3 | 1.2 | 2.14E-02 | 0.3 | 4.50E-03 | 0.33 | 0.67 | 2.00% | 99.57% | 33.33% | high acid 4 | 4.0 | 0.70 |
| High | 0.3 | 1.2 | 2.14E-02 | 0.3 | 4.50E-03 | 0.33 | 0.67 | 0.01% | 13.08% | -10.89% | high acid 3 | 0.0 | 0.50 |
| High | 0.3 | 1.2 | 2.14E-02 | 0.3 | 4.50E-03 | 0.33 | 0.67 | 5.00% | 36.21% | 100.00% | high acid 2 | 10.0 | 0.70 |
| High | 0.3 | 1.2 | 2.14E-02 | 0.3 | 4.50E-03 | 0.33 | 0.67 | 5.50% | 20.78% | 111.11% | high acid 1 | 11.0 | 0.70 |
| High | 0.3 | 1.2 | 2.14E-02 | 0.08 | 1.20E-03 | 0.12 | 0.88 | 0.01% | 13.08% | -10.89% | high acid-17 | 0.0 | 0.50 |
| High | 0.3 | 1.2 | 2.14E-02 | 0.08 | 1.20E-03 | 0.12 | 0.88 | 0.50% | 99.30% | 0.00% | high acid-18 | 1.0 | 0.50 |
| High | 0.3 | 1.2 | 2.14E-02 | 0.3 | 4.50E-03 | 0.33 | 0.67 | 4.00% | 17.88% | 77.78% | high acid-19 | 8.0 | 0.20 |
| High | 0.3 | 1.2 | 2.14E-02 | 0.3 | 4.50E-03 | 0.33 | 0.67 | 3.00% | 37.14% | 55.56% | high acid-20 | 6.0 | 0.20 |
| High | 0.3 | 1.2 | 2.14E-02 | 0.3 | 4.50E-03 | 0.33 | 0.67 | 1.00% | 97.99% | 11.11% | high acid-21 | 2.0 | 0.20 |
| High | 0.3 | 1.2 | 2.14E-02 | 0.3 | 4.50E-03 | 0.33 | 0.67 | 2.00% | 99.58% | 33.33% | high acid-22 | 4.0 | 0.20 |
| High | 0.3 | 1.2 | 2.14E-02 | 0.3 | 4.50E-03 | 0.33 | 0.67 | 5.00% | 14.41% | 100.00% | high acid-23 | 10.0 | 0.20 |
| High | 0.3 | 1.2 | 2.14E-02 | 0.3 | 4.50E-03 | 0.33 | 0.67 | 5.50% | 14.04% | 111.11% | high acid-24 | 11.0 | 0.20 |
| | | | | | | | | | | | | | |
| High | 0.3 | 1.2 | 2.14E-02 | 1.5 | 2.25E-02 | 0.71 | 0.29 | 0.01% | 13.08% | -10.89% | high acid 9 | 0.0 | 0.50 |
| High | 0.3 | 1.2 | 2.14E-02 | 1.5 | 2.25E-02 | 0.71 | 0.29 | 0.50% | 57.57% | 0.00% | high acid 10 | 1.0 | 0.50 |
| High | 0.3 | 1.2 | 2.14E-02 | 1.5 | 2.25E-02 | 0.71 | 0.29 | 1.00% | 81.93% | 11.11% | high acid 11 | 2.0 | 0.50 |
| High | 0.3 | 1.2 | 2.14E-02 | 1.5 | 2.25E-02 | 0.71 | 0.29 | 2.00% | 95.48% | 33.33% | high acid 12 | 4.0 | 0.50 |
| High | 0.3 | 1.2 | 2.14E-02 | 2.1 | 3.15E-02 | 0.77 | 0.23 | 3.00% | 100.00% | 55.56% | high acid 13 | 6.0 | 0.50 |
| High | 0.3 | 1.2 | 2.14E-02 | 2.1 | 3.15E-02 | 0.77 | 0.23 | 4.00% | 100.00% | 77.78% | high acid 14 | 8.0 | 0.50 |
| High | 0.3 | 1.2 | 2.14E-02 | 2.1 | 3.15E-02 | 0.77 | 0.23 | 5.00% | 100.00% | 100.00% | high acid 15 | 10.0 | 0.50 |
| High | 0.3 | 1.2 | 2.14E-02 | 2.1 | 3.15E-02 | 0.77 | 0.23 | 5.50% | 68.43% | 111.11% | high acid 16 | 11.0 | 0.50 |
| | | | | | | | | | | | | | |
| High | 0.3 | 1.2 | 2.14E-02 | 1.5 | 2.25E-02 | 0.71 | 0.29 | 3.00% | 100.00% | 55.56% | high acid 25 | 6.0 | 0.50 |
| High | 0.3 | 1.2 | 2.14E-02 | 1.5 | 2.25E-02 | 0.71 | 0.29 | 4.00% | 100.00% | 77.78% | high acid 26 | 8.0 | 0.50 |
| High | 0.3 | 1.2 | 2.14E-02 | 1.5 | 2.25E-02 | 0.71 | 0.29 | 5.00% | 100.00% | 100.00% | high acid 27 | 10.0 | 0.50 |
| High | 0.3 | 1.2 | 2.14E-02 | 1.5 | 2.25E-02 | 0.71 | 0.29 | 5.50% | 56.79% | 111.11% | high acid 28 | 11.0 | 0.50 |
| | | | | | | | | | | | | | |
| High | 0.3 | 1.2 | 2.14E-02 | 0.08 | 1.20E-03 | 0.12 | 0.88 | 1.00% | 99.63% | 11.11% | high acid 29 | 2.0 | 0.50 |
| High | 0.3 | 1.2 | 2.14E-02 | 0.08 | 1.20E-03 | 0.12 | 0.88 | 2.00% | 74.03% | 33.33% | high acid 30 | 4.0 | 0.50 |
| High | 0.3 | 1.2 | 2.14E-02 | 0.08 | 1.20E-03 | 0.12 | 0.88 | 3.00% | 21.01% | 55.56% | high acid 31 | 6.0 | 0.50 |
| High | 0.3 | 1.2 | 2.14E-02 | 0.08 | 1.20E-03 | 0.12 | 0.88 | 4.00% | 14.34% | 77.78% | high acid 32 | 8.0 | 0.50 |
| High | 0.3 | 1.2 | 2.14E-02 | 0.08 | 1.20E-03 | 0.12 | 0.88 | 5.00% | 13.62% | 100.00% | high acid 33 | 10.0 | 0.50 |
| High | 0.3 | 1.2 | 2.14E-02 | 0.08 | 1.20E-03 | 0.12 | 0.88 | 5.50% | 13.43% | 111.11% | high acid 34 | 11.0 | 0.50 |
| | | | | | | | | | | | | | |
| High | 0.3 | 1.2 | 2.14E-02 | 2.1 | 3.15E-02 | 0.77 | 0.23 | 0.01% | 13.08% | -10.89% | high acid 35 | 0.0 | 0.50 |
| High | 0.3 | 1.2 | 2.14E-02 | 2.1 | 3.15E-02 | 0.77 | 0.23 | 0.50% | 48.76% | 0.00% | high acid 36 | 1.0 | 0.50 |
| High | 0.3 | 1.2 | 2.14E-02 | 2.1 | 3.15E-02 | 0.77 | 0.23 | 1.00% | 72.87% | 11.11% | high acid 37 | 2.0 | 0.50 |
| High | 0.3 | 1.2 | 2.14E-02 | 2.1 | 3.15E-02 | 0.77 | 0.23 | 2.00% | 92.54% | 33.33% | high acid 38 | 4.0 | 0.50 |
| | | | | | | | | | | | | | |
| High | 0.3 | 1.2 | 2.14E-02 | 0.2 | 3.00E-03 | 0.25 | 0.75 | 0.01% | 13.08% | -10.89% | high acid 39 | 0.0 | 0.50 |
| High | 0.3 | 1.2 | 2.14E-02 | 0.2 | 3.00E-03 | 0.25 | 0.75 | 0.50% | 96.56% | 0.00% | high acid 40 | 1.0 | 0.50 |
| High | 0.3 | 1.2 | 2.14E-02 | 0.2 | 3.00E-03 | 0.25 | 0.75 | 1.00% | 98.91% | 11.11% | high acid 41 | 2.0 | 0.50 |
| High | 0.3 | 1.2 | 2.14E-02 | 0.2 | 3.00E-03 | 0.25 | 0.75 | 2.00% | 99.68% | 33.33% | high acid 42 | 4.0 | 0.50 |
| High | 0.3 | 1.2 | 2.14E-02 | 0.2 | 3.00E-03 | 0.25 | 0.75 | 3.00% | 96.11% | 55.56% | high acid 43 | 6.0 | 0.50 |
| High | 0.3 | 1.2 | 2.14E-02 | 0.2 | 3.00E-03 | 0.25 | 0.75 | 4.00% | 32.64% | 77.78% | high acid 44 | 8.0 | 0.50 |
| High | 0.3 | 1.2 | 2.14E-02 | 0.2 | 3.00E-03 | 0.25 | 0.75 | 5.00% | 16.29% | 100.00% | high acid 45 | 10.0 | 0.50 |
| High | 0.3 | 1.2 | 2.14E-02 | 0.2 | 3.00E-03 | 0.25 | 0.75 | 5.50% | 15.06% | 111.11% | high acid 46 | 11.0 | 0.50 |
| High | 0.3 | 1.2 | 2.14E-02 | 0.3 | 4.50E-03 | 0.33 | 0.67 | 0.50% | 93.75% | 0.00% | high acid 47 | 1.0 | 0.20 |
| High | 0.3 | 1.2 | 2.14E-02 | 0.3 | 4.50E-03 | 0.33 | 0.67 | 0.01% | 13.08% | -10.89% | high acid 48 | 0.0 | 0.20 |
| High | 0.3 | 1.2 | 2.14E-02 | 0.08 | 1.20E-03 | 0.12 | 0.88 | 0.01% | 13.08% | -10.89% | high acid 49 | 0.0 | 0.20 |
| High | 0.3 | 1.2 | 2.14E-02 | 0.08 | 1.20E-03 | 0.12 | 0.88 | 0.50% | 99.30% | 0.00% | high acid 50 | 1.0 | 0.20 |
| High | 0.3 | 1.2 | 2.14E-02 | 0.08 | 1.20E-03 | 0.12 | 0.88 | 1.00% | 99.51% | 11.11% | high acid 51 | 2.0 | 0.20 |
| High | 0.3 | 1.2 | 2.14E-02 | 0.08 | 1.20E-03 | 0.12 | 0.88 | 2.00% | 18.94% | 33.33% | high acid 52 | 4.0 | 0.20 |
| High | 0.3 | 1.2 | 2.14E-02 | 0.08 | 1.20E-03 | 0.12 | 0.88 | 3.00% | 13.83% | 55.56% | high acid 53 | 6.0 | 0.20 |
| High | 0.3 | 1.2 | 2.14E-02 | 0.08 | 1.20E-03 | 0.12 | 0.88 | 4.00% | 13.31% | 77.78% | high acid 54 | 8.0 | 0.20 |
| High | 0.3 | 1.2 | 2.14E-02 | 0.08 | 1.20E-03 | 0.12 | 0.88 | 5.00% | 13.10% | 100.00% | high acid 55 | 10.0 | 0.20 |
| High | 0.3 | 1.2 | 2.14E-02 | 0.08 | 1.20E-03 | 0.12 | 0.88 | 5.50% | 13.05% | 111.11% | high acid 56 | 11.0 | 0.20 |
| High | 0.3 | 1.2 | 2.14E-02 | 2.1 | 3.15E-02 | 0.77 | 0.23 | 0.01% | 13.08% | -10.89% | high acid 57 | 0.0 | 0.20 |
| High | 0.3 | 1.2 | 2.14E-02 | 2.1 | 3.15E-02 | 0.77 | 0.23 | 0.50% | 49.11% | 0.00% | high acid 58 | 1.0 | 0.20 |
| High | 0.3 | 1.2 | 2.14E-02 | 2.1 | 3.15E-02 | 0.77 | 0.23 | 1.00% | 74.07% | 11.11% | high acid 59 | 2.0 | 0.20 |
| High | 0.3 | 1.2 | 2.14E-02 | 2.1 | 3.15E-02 | 0.77 | 0.23 | 2.00% | 93.75% | 33.33% | high acid 60 | 4.0 | 0.20 |
| High | 0.3 | 1.2 | 2.14E-02 | 2.1 | 3.15E-02 | 0.77 | 0.23 | 3.00% | 100.00% | 55.56% | high acid 61 | 6.0 | 0.20 |
| High | 0.3 | 1.2 | 2.14E-02 | 2.1 | 3.15E-02 | 0.77 | 0.23 | 4.00% | 100.00% | 77.78% | high acid 62 | 8.0 | 0.20 |
| High | 0.3 | 1.2 | 2.14E-02 | 2.1 | 3.15E-02 | 0.77 | 0.23 | 5.00% | 70.87% | 100.00% | high acid 63 | 10.0 | 0.20 |
| High | 0.3 | 1.2 | 2.14E-02 | 2.1 | 3.15E-02 | 0.77 | 0.23 | 5.50% | 30.23% | 111.11% | high acid 64 | 11.0 | 0.20 |

*Appendix B*

# Simulation Cases Table 3

| Acid | Sor | Acid No. | Soap Conc. (Mol/L) | Surf. conc. (%) | Surfactant conc. (Mol/L) | Surf. Frac. 1 | Soap frac. 1 | Salinity (%NaCl) | recovery eff. (%) | Dimensionless salinity | Store folder | New dimension Less sal | Pore Volume |
|---|---|---|---|---|---|---|---|---|---|---|---|---|---|
| No Sur | 0.3 | 0.02 | 3.57E-04 | 0 | 0.00E+00 | 0.00 | 1.00 | 0.50% | 70.91% | 0.00% | No Sur-1 | 1.0 | 0.50 |
| No Sur | 0.3 | 0.2 | 3.57E-03 | 0 | 0.00E+00 | 0.00 | 1.00 | 0.50% | 99.73% | 0.00% | No Sur-2 | 1.0 | 0.50 |
| No Sur | 0.3 | 1.2 | 2.14E-02 | 0 | 0.00E+00 | 0.00 | 1.00 | 0.50% | 100.00% | 0.00% | No Sur-3 | 1.0 | 0.50 |
| No Sur | 0.3 | 1.2 | 2.14E-02 | 0 | 0.00E+00 | 0.00 | 1.00 | 1.00% | 33.69% | 11.11% | No Sur-4 | 2.0 | 0.50 |
| No Sur | 0.3 | 1.2 | 2.14E-02 | 0 | 0.00E+00 | 0.00 | 1.00 | 2.00% | 13.04% | 33.33% | No Sur-5 | 4.0 | 0.50 |
| No Sur | 0.3 | 1.2 | 2.14E-02 | 0 | 0.00E+00 | 0.00 | 1.00 | 3.00% | 13.03% | 55.56% | No Sur-6 | 6.0 | 0.50 |
| No Sur | 0.3 | 1.2 | 2.14E-02 | 0 | 0.00E+00 | 0.00 | 1.00 | 5.00% | 13.02% | 100.00% | No Sur-7 | 10.0 | 0.50 |
| No Sur | 0.3 | 1.2 | 2.14E-02 | 0 | 0.00E+00 | 0.00 | 1.00 | 5.50% | 13.02% | 111.11% | No Sur-8 | 11.0 | 0.50 |
| No Sur | 0.3 | 1.2 | 2.14E-02 | 0 | 0.00E+00 | 0.00 | 1.00 | 0.00% | 13.08% | -11.11% | No Sur-9 | 0.0 | 0.50 |
| | | | | | | | | | | | | | |
| No Soap | 0.3 | 0 | 0.00E+00 | 0.2 | 3.00E-03 | 1.00 | 0.00 | 5.00% | 100.00% | 100.00% | No Soap-1 | 10.0 | 0.50 |
| No Soap | 0.3 | 0 | 0.00E+00 | 0.2 | 3.00E-03 | 1.00 | 0.00 | 3.00% | 100.00% | 55.56% | No Soap-2 | 6.0 | 0.50 |
| No Soap | 0.3 | 0 | 0.00E+00 | 0.2 | 3.00E-03 | 1.00 | 0.00 | 2.00% | 75.98% | 33.33% | No Soap-3 | 4.0 | 0.50 |
| No Soap | 0.3 | 0 | 0.00E+00 | 0.2 | 3.00E-03 | 1.00 | 0.00 | 1.00% | 39.98% | 11.11% | No Soap-4 | 2.0 | 0.50 |
| No Soap | 0.3 | 0 | 0.00E+00 | 0.2 | 3.00E-03 | 1.00 | 0.00 | 0.50% | 22.81% | 0.00% | No Soap-5 | 1.0 | 0.50 |
| No Soap | 0.3 | 0 | 0.00E+00 | 0.2 | 3.00E-03 | 1.00 | 0.00 | 5.50% | 77.00% | 111.11% | No Soap-6 | 11.0 | 0.50 |
| No Soap | 0.3 | 0 | 0.00E+00 | 0.2 | 3.00E-03 | 1.00 | 0.00 | 0.00% | 13.08% | -11.11% | No Soap-7 | 0.0 | 0.50 |

Narrow LET with 0.2 PV

| Acid | Sor | Acid No. | Soap Conc. (Mol/L) | Surf. conc. (%) | Surfactant conc. (Mol/L) | Surf. Frac. 1 | Soap frac. 1 | Salinity (%NaCl) | recovery eff. (%) | Dimensionless salinity | Store folder | New dimension Less sal | Pore Volume |
|---|---|---|---|---|---|---|---|---|---|---|---|---|---|
| Mid | 0.3 | 0.2 | 3.57E-03 | 0.14 | 2.10E-03 | 0.58 | 0.42 | 0.01% | 13.08% | -10.89% | Mid Acid 47 | 0.0 | 0.20 |
| Mid | 0.3 | 0.2 | 3.57E-03 | 0.14 | 2.10E-03 | 0.58 | 0.42 | 0.50% | 28.89% | 0.00% | Mid Acid 48 | 1.0 | 0.20 |
| Mid | 0.3 | 0.2 | 3.57E-03 | 0.14 | 2.10E-03 | 0.58 | 0.42 | 1.00% | 57.82% | 11.11% | Mid Acid 49 | 2.0 | 0.20 |
| Mid | 0.3 | 0.2 | 3.57E-03 | 0.14 | 2.10E-03 | 0.58 | 0.42 | 2.00% | 75.16% | 33.33% | Mid Acid 50 | 4.0 | 0.20 |
| Mid | 0.3 | 0.2 | 3.57E-03 | 0.14 | 2.10E-03 | 0.58 | 0.42 | 3.00% | 85.14% | 55.56% | Mid Acid 51 | 6.0 | 0.20 |
| Mid | 0.3 | 0.2 | 3.57E-03 | 0.14 | 2.10E-03 | 0.58 | 0.42 | 4.00% | 80.35% | 77.78% | Mid Acid 52 | 8.0 | 0.20 |
| Mid | 0.3 | 0.2 | 3.57E-03 | 0.14 | 2.10E-03 | 0.58 | 0.42 | 5.00% | 29.29% | 100.00% | Mid Acid 53 | 10.0 | 0.20 |
| Mid | 0.3 | 0.2 | 3.57E-03 | 0.14 | 2.10E-03 | 0.58 | 0.42 | 5.50% | 20.55% | 111.11% | Mid Acid 54 | 11.0 | 0.20 |
| | | | | | | | | | | | | | |
| High | 0.3 | 1.2 | 2.14E-02 | 2.1 | 3.15E-02 | 0.77 | 0.23 | 0.01% | 13.08% | -10.89% | high acid 65 | 0.0 | 0.20 |
| High | 0.3 | 1.2 | 2.14E-02 | 2.1 | 3.15E-02 | 0.77 | 0.23 | 0.50% | 17.36% | 0.00% | high acid 66 | 1.0 | 0.20 |
| High | 0.3 | 1.2 | 2.14E-02 | 2.1 | 3.15E-02 | 0.77 | 0.23 | 1.00% | 28.11% | 11.11% | high acid 67 | 2.0 | 0.20 |
| High | 0.3 | 1.2 | 2.14E-02 | 2.1 | 3.15E-02 | 0.77 | 0.23 | 2.00% | 59.84% | 33.33% | high acid 68 | 4.0 | 0.20 |
| High | 0.3 | 1.2 | 2.14E-02 | 2.1 | 3.15E-02 | 0.77 | 0.23 | 3.00% | 80.55% | 55.56% | high acid 69 | 6.0 | 0.20 |
| High | 0.3 | 1.2 | 2.14E-02 | 2.1 | 3.15E-02 | 0.77 | 0.23 | 4.00% | 89.90% | 77.78% | high acid 70 | 8.0 | 0.20 |
| High | 0.3 | 1.2 | 2.14E-02 | 2.1 | 3.15E-02 | 0.77 | 0.23 | 5.00% | 71.10% | 100.00% | high acid 71 | 10.0 | 0.20 |
| High | 0.3 | 1.2 | 2.14E-02 | 2.1 | 3.15E-02 | 0.77 | 0.23 | 5.50% | 30.22% | 111.11% | high acid 72 | 11.0 | 0.20 |
| | | | | | | | | | | | | | |
| High | 0.3 | 1.2 | 2.14E-02 | 0.3 | 4.50E-03 | 0.33 | 0.67 | 0.01% | 13.08% | -10.89% | high acid 73 | 0.0 | 0.20 |
| High | 0.3 | 1.2 | 2.14E-02 | 0.3 | 4.50E-03 | 0.33 | 0.67 | 0.50% | 42.14% | 0.00% | high acid 74 | 1.0 | 0.20 |
| High | 0.3 | 1.2 | 2.14E-02 | 0.3 | 4.50E-03 | 0.33 | 0.67 | 1.00% | 82.65% | 11.11% | high acid 75 | 2.0 | 0.20 |
| High | 0.3 | 1.2 | 2.14E-02 | 0.3 | 4.50E-03 | 0.33 | 0.67 | 2.00% | 58.81% | 33.33% | high acid 76 | 4.0 | 0.20 |
| High | 0.3 | 1.2 | 2.14E-02 | 0.3 | 4.50E-03 | 0.33 | 0.67 | 3.00% | 26.40% | 55.56% | high acid 77 | 6.0 | 0.20 |
| High | 0.3 | 1.2 | 2.14E-02 | 0.3 | 4.50E-03 | 0.33 | 0.67 | 4.00% | 17.60% | 77.78% | high acid 78 | 8.0 | 0.20 |
| High | 0.3 | 1.2 | 2.14E-02 | 0.3 | 4.50E-03 | 0.33 | 0.67 | 5.00% | 14.41% | 100.00% | high acid 79 | 10.0 | 0.20 |
| High | 0.3 | 1.2 | 2.14E-02 | 0.3 | 4.50E-03 | 0.33 | 0.67 | 5.50% | 14.04% | 111.11% | high acid 80 | 11.0 | 0.20 |
| | | | | | | | | | | | | | |
| High | 0.3 | 1.2 | 2.14E-02 | 0.08 | 1.20E-03 | 0.12 | 0.88 | 0.01% | 13.08% | -10.89% | high acid 81 | 0.0 | 0.20 |
| High | 0.3 | 1.2 | 2.14E-02 | 0.08 | 1.20E-03 | 0.12 | 0.88 | 0.50% | 89.18% | 0.00% | high acid 82 | 1.0 | 0.20 |
| High | 0.3 | 1.2 | 2.14E-02 | 0.08 | 1.20E-03 | 0.12 | 0.88 | 1.00% | 87.76% | 11.11% | high acid 83 | 2.0 | 0.20 |
| High | 0.3 | 1.2 | 2.14E-02 | 0.08 | 1.20E-03 | 0.12 | 0.88 | 2.00% | 17.44% | 33.33% | high acid 84 | 4.0 | 0.20 |
| High | 0.3 | 1.2 | 2.14E-02 | 0.08 | 1.20E-03 | 0.12 | 0.88 | 3.00% | 13.83% | 55.56% | high acid 85 | 6.0 | 0.20 |
| High | 0.3 | 1.2 | 2.14E-02 | 0.08 | 1.20E-03 | 0.12 | 0.88 | 4.00% | 13.31% | 77.78% | high acid 86 | 8.0 | 0.20 |
| High | 0.3 | 1.2 | 2.14E-02 | 0.08 | 1.20E-03 | 0.12 | 0.88 | 5.00% | 13.10% | 100.00% | high acid 87 | 10.0 | 0.20 |
| High | 0.3 | 1.2 | 2.14E-02 | 0.08 | 1.20E-03 | 0.12 | 0.88 | 5.50% | 13.05% | 111.11% | high acid 88 | 11.0 | 0.20 |
| | | | | | | | | | | | | | |
| No Soap | 0.3 | 0 | 0.00E+00 | 0.2 | 3.00E-03 | 1.00 | 0.00 | 0.01% | 13.08% | -10.89% | No Soap 8 | 0.0 | 0.20 |
| No Soap | 0.3 | 0 | 0.00E+00 | 0.2 | 3.00E-03 | 1.00 | 0.00 | 0.50% | 13.06% | 0.00% | No Soap 9 | 1.0 | 0.20 |
| No Soap | 0.3 | 0 | 0.00E+00 | 0.2 | 3.00E-03 | 1.00 | 0.00 | 1.00% | 12.99% | 11.11% | No Soap 10 | 2.0 | 0.20 |
| No Soap | 0.3 | 0 | 0.00E+00 | 0.2 | 3.00E-03 | 1.00 | 0.00 | 2.00% | 26.77% | 33.33% | No Soap 11 | 4.0 | 0.20 |
| No Soap | 0.3 | 0 | 0.00E+00 | 0.2 | 3.00E-03 | 1.00 | 0.00 | 3.00% | 37.42% | 55.56% | No Soap 12 | 6.0 | 0.20 |
| No Soap | 0.3 | 0 | 0.00E+00 | 0.2 | 3.00E-03 | 1.00 | 0.00 | 4.00% | 43.78% | 77.78% | No Soap 13 | 8.0 | 0.20 |
| No Soap | 0.3 | 0 | 0.00E+00 | 0.2 | 3.00E-03 | 1.00 | 0.00 | 5.00% | 100.00% | 100.00% | No Soap 14 | 10.0 | 0.20 |
| No Soap | 0.3 | 0 | 0.00E+00 | 0.2 | 3.00E-03 | 1.00 | 0.00 | 5.50% | 76.43% | 111.11% | No Soap 15 | 11.0 | 0.20 |

*Appendix B*

# Simulation Cases Table 4

Narrow LFT with 0.20 PV

| Acid | Sor | Acid No. | Soap Conc. (Mol/L) | Surf. conc. (%) | Surfactant conc. (Mol/L) | Surf. Frac. 1 | Soap frac. 1 | Salinity (%NaCl) | recovery eff. (%) | Dimensionless salinity | Store folder | New dimension Less sal | Pore Volume |
|---|---|---|---|---|---|---|---|---|---|---|---|---|---|
| No Sur | 0.3 | 1.2 | 2.14E-02 | 0 | 0.00E+00 | 0.00 | 1.00 | 0.01% | 13.10% | -10.89% | No Sur 17 | 0.0 | 0.20 |
| No Sur | 0.3 | 1.2 | 2.14E-02 | 0 | 0.00E+00 | 0.00 | 1.00 | 0.50% | 96.45% | 0.00% | No Sur 16 | 1.0 | 0.20 |
| No Sur | 0.3 | 1.2 | 2.14E-02 | 0 | 0.00E+00 | 0.00 | 1.00 | 1.00% | 33.75% | 11.11% | No Sur 15 | 2.0 | 0.20 |
| No Sur | 0.3 | 1.2 | 2.14E-02 | 0 | 0.00E+00 | 0.00 | 1.00 | 2.00% | 13.04% | 33.33% | No Sur 14 | 4.0 | 0.20 |
| No Sur | 0.3 | 1.2 | 2.14E-02 | 0 | 0.00E+00 | 0.00 | 1.00 | 3.00% | 13.03% | 55.56% | No Sur 13 | 6.0 | 0.20 |
| No Sur | 0.3 | 1.2 | 2.14E-02 | 0 | 0.00E+00 | 0.00 | 1.00 | 4.00% | 13.02% | 77.78% | No Sur 12 | 8.0 | 0.20 |
| No Sur | 0.3 | 1.2 | 2.14E-02 | 0 | 0.00E+00 | 0.00 | 1.00 | 5.00% | 13.02% | 100.00% | No Sur 11 | 10.0 | 0.20 |
| No Sur | 0.3 | 1.2 | 2.14E-02 | 0 | 0.00E+00 | 0.00 | 1.00 | 5.50% | 13.02% | 111.11% | No Sur 10 | 11.0 | 0.20 |
| | | | | | | | | | | | | | |
| Mid | 0.3 | 0.2 | 3.57E-03 | 0.1 | 1.50E-03 | 0.49 | 0.51 | 0.01% | 13.08% | -10.89% | Mid Acid 55 | 0.0 | 0.20 |
| Mid | 0.3 | 0.2 | 3.57E-03 | 0.1 | 1.50E-03 | 0.49 | 0.51 | 0.50% | 42.43% | 0.00% | Mid Acid 56 | 1.0 | 0.20 |
| Mid | 0.3 | 0.2 | 3.57E-03 | 0.1 | 1.50E-03 | 0.49 | 0.51 | 1.00% | 74.41% | 11.11% | Mid Acid 57 | 2.0 | 0.20 |
| Mid | 0.3 | 0.2 | 3.57E-03 | 0.1 | 1.50E-03 | 0.49 | 0.51 | 2.00% | 73.52% | 33.33% | Mid Acid 58 | 4.0 | 0.20 |
| Mid | 0.3 | 0.2 | 3.57E-03 | 0.1 | 1.50E-03 | 0.49 | 0.51 | 3.00% | 47.23% | 55.56% | Mid Acid 59 | 6.0 | 0.20 |
| Mid | 0.3 | 0.2 | 3.57E-03 | 0.1 | 1.50E-03 | 0.49 | 0.51 | 4.00% | 29.47% | 77.78% | Mid Acid 60 | 8.0 | 0.20 |
| Mid | 0.3 | 0.2 | 3.57E-03 | 0.1 | 1.50E-03 | 0.49 | 0.51 | 5.00% | 17.40% | 100.00% | Mid Acid 61 | 10.0 | 0.20 |
| Mid | 0.3 | 0.2 | 3.57E-03 | 0.1 | 1.50E-03 | 0.49 | 0.51 | 5.50% | 15.56% | 111.11% | Mid Acid 62 | 11.0 | 0.20 |
| | | | | | | | | | | | | | |
| Mid | 0.3 | 0.2 | 3.57E-03 | 0.1 | 1.50E-03 | 0.49 | 0.51 | 1.50% | 75.95% | 22.22% | Mid Acid 63 | 3.0 | 0.20 |
| Mid | 0.3 | 0.2 | 3.57E-03 | 0.1 | 1.50E-03 | 0.49 | 0.51 | 1.20% | 74.66% | 15.56% | Mid Acid 64 | 2.4 | 0.20 |
| Mid | 0.3 | 0.2 | 3.57E-03 | 0.1 | 1.50E-03 | 0.49 | 0.51 | 1.80% | 79.09% | 28.89% | Mid Acid 65 | 3.6 | 0.20 |
| Mid | 0.3 | 0.2 | 3.57E-03 | 0.1 | 1.50E-03 | 0.49 | 0.51 | 1.60% | 77.14% | 24.44% | Mid Acid 66 | 3.2 | 0.20 |
| Mid | 0.3 | 0.2 | 3.57E-03 | 0.1 | 1.50E-03 | 0.49 | 0.51 | 1.90% | 77.04% | 31.11% | Mid Acid 67 | 3.8 | 0.20 |
| Mid | 0.3 | 0.2 | 3.57E-03 | 0.1 | 1.50E-03 | 0.49 | 0.51 | 1.90% | 79.26% | 31.11% | Mid Acid 68 | 3.8 | 0.20 |

Narrow LFT 0.5 PV

| Acid | Sor | Acid No. | Soap Conc. (Mol/L) | Surf. conc. (%) | Surfactant conc. (Mol/L) | Surf. Frac. 1 | Soap frac. 1 | Salinity (%NaCl) | recovery eff. (%) | Dimensionless salinity | Store folder | New dimension Less sal | Pore Volume |
|---|---|---|---|---|---|---|---|---|---|---|---|---|---|
| No Soap | 0.3 | 0 | 0.00E+00 | 0.2 | 3.00E-03 | 1.00 | 0.00 | 0.01% | 13.08% | -10.89% | No Soap 16 | 0.0 | 0.50 |
| No Soap | 0.3 | 0 | 0.00E+00 | 0.2 | 3.00E-03 | 1.00 | 0.00 | 0.50% | 13.07% | 0.00% | No Soap 17 | 1.0 | 0.50 |
| No Soap | 0.3 | 0 | 0.00E+00 | 0.2 | 3.00E-03 | 1.00 | 0.00 | 1.00% | 13.04% | 11.11% | No Soap 18 | 2.0 | 0.50 |
| No Soap | 0.3 | 0 | 0.00E+00 | 0.2 | 3.00E-03 | 1.00 | 0.00 | 2.00% | 27.00% | 33.33% | No Soap 19 | 4.0 | 0.50 |
| No Soap | 0.3 | 0 | 0.00E+00 | 0.2 | 3.00E-03 | 1.00 | 0.00 | 3.00% | 37.81% | 55.56% | No Soap 20 | 6.0 | 0.50 |
| No Soap | 0.3 | 0 | 0.00E+00 | 0.2 | 3.00E-03 | 1.00 | 0.00 | 4.00% | 44.27% | 77.78% | No Soap 21 | 8.0 | 0.50 |
| No Soap | 0.3 | 0 | 0.00E+00 | 0.2 | 3.00E-03 | 1.00 | 0.00 | 5.00% | 100.00% | 100.00% | No Soap 22 | 10.0 | 0.50 |
| No Soap | 0.3 | 0 | 0.00E+00 | 0.2 | 3.00E-03 | 1.00 | 0.00 | 5.50% | 77.00% | 111.11% | No Soap 23 | 11.0 | 0.50 |
| | | | | | | | | | | | | | |
| High | 0.3 | 1.2 | 2.14E-02 | 0.08 | 1.20E-03 | 0.12 | 0.88 | 0.01% | 13.08% | -10.89% | high acid 89 | 0.0 | 0.50 |
| High | 0.3 | 1.2 | 2.14E-02 | 0.08 | 1.20E-03 | 0.12 | 0.88 | 0.50% | 89.17% | 0.00% | high acid 90 | 1.0 | 0.50 |
| High | 0.3 | 1.2 | 2.14E-02 | 0.08 | 1.20E-03 | 0.12 | 0.88 | 1.00% | 88.88% | 11.11% | high acid 91 | 2.0 | 0.50 |
| High | 0.3 | 1.2 | 2.14E-02 | 0.08 | 1.20E-03 | 0.12 | 0.88 | 2.00% | 36.11% | 33.33% | high acid 92 | 4.0 | 0.50 |
| High | 0.3 | 1.2 | 2.14E-02 | 0.08 | 1.20E-03 | 0.12 | 0.88 | 3.00% | 19.06% | 55.56% | high acid 93 | 6.0 | 0.50 |
| High | 0.3 | 1.2 | 2.14E-02 | 0.08 | 1.20E-03 | 0.12 | 0.88 | 4.00% | 14.34% | 77.78% | high acid 94 | 8.0 | 0.50 |
| High | 0.3 | 1.2 | 2.14E-02 | 0.08 | 1.20E-03 | 0.12 | 0.88 | 5.00% | 13.63% | 100.00% | high acid 95 | 10.0 | 0.50 |
| High | 0.3 | 1.2 | 2.14E-02 | 0.08 | 1.20E-03 | 0.12 | 0.88 | 5.50% | 13.43% | 111.11% | high acid 96 | 11.0 | 0.50 |
| | | | | | | | | | | | | | |
| High | 0.3 | 1.2 | 2.14E-02 | 2.1 | 3.15E-02 | 0.77 | 0.23 | 0.01% | 13.08% | -10.89% | high acid 97 | 0.0 | 0.50 |
| High | 0.3 | 1.2 | 2.14E-02 | 2.1 | 3.15E-02 | 0.77 | 0.23 | 0.50% | 16.53% | 0.00% | high acid 98 | 1.0 | 0.50 |
| High | 0.3 | 1.2 | 2.14E-02 | 2.1 | 3.15E-02 | 0.77 | 0.23 | 1.00% | 27.74% | 11.11% | high acid 99 | 2.0 | 0.50 |
| High | 0.3 | 1.2 | 2.14E-02 | 2.1 | 3.15E-02 | 0.77 | 0.23 | 2.00% | 57.16% | 33.33% | high acid 100 | 4.0 | 0.50 |
| High | 0.3 | 1.2 | 2.14E-02 | 2.1 | 3.15E-02 | 0.77 | 0.23 | 3.00% | 76.48% | 55.56% | high acid 101 | 6.0 | 0.50 |
| High | 0.3 | 1.2 | 2.14E-02 | 2.1 | 3.15E-02 | 0.77 | 0.23 | 4.00% | 91.76% | 77.78% | high acid 102 | 8.0 | 0.50 |
| High | 0.3 | 1.2 | 2.14E-02 | 2.1 | 3.15E-02 | 0.77 | 0.23 | 5.00% | 100.00% | 100.00% | high acid 103 | 10.0 | 0.50 |
| High | 0.3 | 1.2 | 2.14E-02 | 2.1 | 3.15E-02 | 0.77 | 0.23 | 5.50% | 68.42% | 111.11% | high acid 104 | 11.0 | 0.50 |
| | | | | | | | | | | | | | |
| Mid | 0.3 | 0.2 | 3.57E-03 | 0.14 | 2.10E-03 | 0.58 | 0.42 | 0.01% | 13.08% | -10.89% | Mid Acid 69 | 0.0 | 0.50 |
| Mid | 0.3 | 0.2 | 3.57E-03 | 0.14 | 2.10E-03 | 0.58 | 0.42 | 0.50% | 50.42% | 0.00% | Mid Acid 70 | 1.0 | 0.50 |
| Mid | 0.3 | 0.2 | 3.57E-03 | 0.14 | 2.10E-03 | 0.58 | 0.42 | 1.00% | 65.70% | 11.11% | Mid Acid 71 | 2.0 | 0.50 |
| Mid | 0.3 | 0.2 | 3.57E-03 | 0.14 | 2.10E-03 | 0.58 | 0.42 | 2.00% | 75.44% | 33.33% | Mid Acid 72 | 4.0 | 0.50 |
| Mid | 0.3 | 0.2 | 3.57E-03 | 0.14 | 2.10E-03 | 0.58 | 0.42 | 3.00% | 83.97% | 55.56% | Mid Acid 73 | 6.0 | 0.50 |
| Mid | 0.3 | 0.2 | 3.57E-03 | 0.14 | 2.10E-03 | 0.58 | 0.42 | 4.00% | 93.23% | 77.78% | Mid Acid 74 | 8.0 | 0.50 |
| Mid | 0.3 | 0.2 | 3.57E-03 | 0.14 | 2.10E-03 | 0.58 | 0.42 | 5.00% | 88.92% | 100.00% | Mid Acid 75 | 10.0 | 0.50 |
| Mid | 0.3 | 0.2 | 3.57E-03 | 0.14 | 2.10E-03 | 0.58 | 0.42 | 5.50% | 33.06% | 111.11% | Mid Acid 76 | 11.0 | 0.50 |

*Appendix B*

# Simulation Cases Table 5

Narrow LET 0.5 PV

| Acid | Sor | Acid No. | Soap Conc. (Mol/L) | Surf. conc. (%) | Surfactant conc. (Mol/L) | Surf. Frac. 1 | Soap frac. 1 | Salinity (%NaCl) | recovery eff. (%) | Dimensionless salinity | Store folder | New dimension Less sal | Pore Volume |
|---|---|---|---|---|---|---|---|---|---|---|---|---|---|
| High | 0.3 | 1.2 | 2.14E-02 | 0.3 | 4.50E-03 | 0.33 | 0.67 | 0.01% | 13.08% | -10.89% | high_acid_105 | 0.0 | 0.50 |
| High | 0.3 | 1.2 | 2.14E-02 | 0.3 | 4.50E-03 | 0.33 | 0.67 | 0.50% | 41.00% | 0.00% | high_acid_106 | 1.0 | 0.50 |
| High | 0.3 | 1.2 | 2.14E-02 | 0.3 | 4.50E-03 | 0.33 | 0.67 | 1.00% | 79.77% | 11.11% | high_acid_107 | 2.0 | 0.50 |
| High | 0.3 | 1.2 | 2.14E-02 | 0.3 | 4.50E-03 | 0.33 | 0.67 | 2.00% | 83.32% | 33.33% | high_acid_108 | 4.0 | 0.50 |
| High | 0.3 | 1.2 | 2.14E-02 | 0.3 | 4.50E-03 | 0.33 | 0.67 | 3.00% | 84.90% | 55.56% | high_acid_109 | 6.0 | 0.50 |
| High | 0.3 | 1.2 | 2.14E-02 | 0.3 | 4.50E-03 | 0.33 | 0.67 | 4.00% | 48.00% | 77.78% | high_acid_110 | 8.0 | 0.50 |
| High | 0.3 | 1.2 | 2.14E-02 | 0.3 | 4.50E-03 | 0.33 | 0.67 | 5.00% | 22.40% | 100.00% | high_acid_111 | 10.0 | 0.50 |
| High | 0.3 | 1.2 | 2.14E-02 | 0.3 | 4.50E-03 | 0.33 | 0.67 | 5.50% | 17.09% | 111.11% | high_acid_112 | 11.0 | 0.50 |

* The plotting files plotsmall2.m (including effluent history) and plotsmall3.m (profiles) are stored in the stored folders for each case.

*Appendix C*

# One-dimensional simulator Matlab Code

All the .m files should be in the same folder, and ASP2.m is the main program.

## 1. ASP2.m

```
%Main program
%Index of subscript:
%           1. Water or Aqueous Phase
%           2. Oil      or Oleic Phase
%           3. Synthetic Surfactant
%           4. Natural Soap
%           5. Salinity (%NaCl)
%           6. Alkali
%           7. Polymer
%           8. Naphthenic Acids
%           9. Alkali Consumption factor

%Assumptions:
%            1.KC4=k4k3*KC3, and k4k3=1. Kaver=KC3*(C3/C3+C4)+KC4*C4/(C3+C4),
%           and Kaver is determined by the optimal salinity vs. (C4/C3) curve
%           2.The concentration of surfactant, soap and NaCl... is small and treated as tracer
%           3.Fractional flow is calculated by the IFT
%           4.Surfactant=NI blend.
%           5.Surfactant adsorption parameters comes from the static isotherm. For this system, the % adsorption is
only related to the aqueous phase concentration of surfactant.
%           6.Forward Difference.
%           7.water and salt(salinity) do not dissolve in the oil; and the oil has no solubility in the  % aqueous phase.
%           8.Assume all the components have the same dispersion terms.
%           9.The viscosity depends on the polymer concentration and NaCl
%           concentration.
%           10.non-dimensional


clear all
%Load optimal Ratio to Salinity curve. Surfactant parameters
global optRS Ssoap Ssur CMC k4k3 adsfact3 adsfact4 C3max
load optRS.dat;
Ssoap=interp1(optRS(:,1),optRS(:,2),1e10,'linear','extrap');
Ssur=interp1(optRS(:,1),optRS(:,2),1e-10,'linear','extrap');
CMC=5e-4;                   %Critical Micelle Concentration

%Data loading Area
Sor=0.3;                            %Initial Oil Saturation
Acid_No=0.2;
c42o=Acid_No/56*0.667;          %c42o is the initial condition(Initial soap concentration in the oleic %phase,~=Acid No.*0.667/56).
FBSal=1.65;                     %Formation Brine Salinity(%)
k4k3=1;                             %k4k3=KC4/KC3
dens=2.6;                           %density of substrate:              g/cm3
BETS=0.3;                       %BET surface Area:                  m2/g
adsden3=0.2;            %Adsorption density of surfactant
adsden4=0;              %Adsorption density of soap
SurMol=500;             %molecular weight of Surfactant     g/mol
SoapMol=500;            %molecular weight of Soap            g/mol
adsfact3=5.0;               %adsorption factor for the surfactant
adsfact4=0;             %adsorption factor for the soap
C3max=0.2e-3;
Reactfact=SoapMol/106/2;

%Background Conditions for NX, dx ,dt/dx etc.
NX=100;
```

```
dx=1/NX;
dtdx=0.1;
dt=dtdx*dx;

c31_1=0.001;                    % c31 is the injecting concentration of the surfactant.
T3slug_1=0.00;                  % T3slug_1 define when the finite surfactant slug begins.
c31_2=0.001;
T3slug_2=0.1;                   % T3slug_2 define when the finite surfactant slug turns off.
c31_3=0.001;
T3slug_3=0.2;
T3slug_4=0.5;

c51_1=FBSal;
c51_2=2.0;
c51_3=2.0;
T5slug_1=0.01;          % T5slug_1 define when the finite NaCl slug concentration change
T5slug_2=1.0;           % T5slug_3 define when the drive NaCl slug concentration begins

c61=0.01;
T6slug_1=0.00;          % T6slug define when the finite alkali slug begins.
T6slug_2=3.0;           % T6slug define when the finite alkali slug turns off.
c9=0e-3;                % Alkali consumption factor

c71=0.0032;
T7slug_1=0.00;          % T6slug define when the finite polymer slug begins.
T7slug_2=2.00;          % T6slug define when the finite polymer slug turns off.
c7s=20e-5;              % c7s=10ug/g=0.01mg/g


T=0.1;                  % To get the profile at time N*T
Tfinal=2.0;             % Time to stop the process
NNN=round(Tfinal/dt);
X=[dx/2.:dx:1.0-dx/2.]';        % Coordinate X for plot
Kdis=0.005;             % Disersion term
% End of Input Area


%Initialize variables
C2Old=ones(length(X),1);
C2Old=Sor*C2Old;
F2=C2Old;
F3=F2;
F4=F2;
F5=F2;
F6=F2;
F7=F2;
F8=F2;
IFT=F2;
C3Old=zeros(length(X),1);
c31Old=C3Old;
c32Old=c31Old;
C3Newm=c31Old;
C4Old=ones(length(X),1);
C4Old=C4Old*c42o*Sor;
c41Old=c31Old;
C8Old=C4Old;

if Sor==0
    c42Old=C4Old;
    c82Old=C8Old;
else
    c42Old=C4Old/Sor;
    c82Old=C8Old/Sor;
end

KC3=C3Old;
KC4=KC3;
C5Old=ones(length(X),1)*FBSal*(1-Sor);
c51Old=FBSal*ones(length(X),1);
C6Old=C3Old;
```

```
c61Old=C6Old*0;
C7Old=C3Old;
c71Old=C7Old*0;
C7s=c7s*ones(length(X));

C4Old=0*C4Old;
C9=ones(length(X),1)*c9;

%Initialize IFT profile
for k=1:NX
    IFT(k)=FindIFT (C3Old(k),C4Old(k),c51Old(k));
end

for i=1:NNN %2/dt is to compare with the MOC method
    %differential functions
    for k=1:NX
%           IFT(k)=FindIFT(C3Old(k),C4Old(k),Salinity,optRS,Ssur,Ssoap);
        Muwater=Findvis(c71Old(k),c51Old(k));
        f1(k)=FindFrac(IFT(k),(1-C2Old(k)),Muwater);
        F2(k)=(1-f1(k));
        F3(k)=f1(k)*c31Old(k)+(1-f1(k))*c32Old(k);
        F4(k)=f1(k)*c41Old(k)+(1-f1(k))*c42Old(k);
        F5(k)=f1(k)*c51Old(k);
        F6(k)=f1(k)*c61Old(k);
        F7(k)=f1(k)*c71Old(k);
        F8(k)=F2(k)*c82Old(k);
        if k==1
            if (T3slug_2>=(dt*i) & T3slug_1<=(dt*i))
                C3New(k)=C3Old(k)-dtdx*(F3(k)-c31_1)+Kdis*dtdx/dx*(C3Newm(2)-C3Newm(1));
                %C3New(k)=C3Old(k)-dtdx*(F3(k)-c31)+Kdis*dtdx/dx*(C3Old(2)+c31-2*C3Old(1));
            elseif (T3slug_3>=(dt*i) & T3slug_2<(dt*i))
                C3New(k)=C3Old(k)-dtdx*(F3(k)-c31_2)+Kdis*dtdx/dx*(C3Newm(2)-C3Newm(1));
            elseif (T3slug_4>=(dt*i) & T3slug_3<(dt*i))
                C3New(k)=C3Old(k)-dtdx*(F3(k)-c31_3)+Kdis*dtdx/dx*(C3Newm(2)-C3Newm(1));
            else
                C3New(k)=C3Old(k)-dtdx*(F3(k)-0)+Kdis*dtdx/dx*(C3Newm(2)+0-2*C3Newm(1));
            end
            if (T5slug_1 <= (dt*i) & T5slug_2 >=(dt*i))
                %c51=c51_1+(c51_2-c51_1)*(dt*i/T5slug_1);
                C5New(k)=C5Old(k)-dtdx*(F5(k)-c51_2)+Kdis*dtdx/dx*(C5Old(2)-C5Old(1));
            elseif(T5slug_1 > dt*i)
                C5New(k)=C5Old(k)-dtdx*(F5(k)-c51_1)+Kdis*dtdx/dx*(C5Old(2)-C5Old(1));
            else
                C5New(k)=C5Old(k)-dtdx*(F5(k)-c51_3)+Kdis*dtdx/dx*(C5Old(2)-C5Old(1));
            end
            if (T6slug_2>=(dt*i) & T6slug_1<=(dt*i))
                C6New(k)=C6Old(k)-dtdx*(F6(k)-c61)+Kdis*dtdx/dx*(C6Old(2)-C6Old(1));
            else
                C6New(k)=C6Old(k)-dtdx*(F6(k)-0)+Kdis*dtdx/dx*(C6Old(2)+0-2*C6Old(1));
            end
            if (T7slug_2>=(dt*i) & T7slug_1<=(dt*i))
                C7New(k)=C7Old(k)-dtdx*(F7(k)-c71)+Kdis*dtdx/dx*(C7Old(2)-C7Old(1));
            else
                C7New(k)=C7Old(k)-dtdx*(F7(k)-0)+Kdis*dtdx/dx*(C7Old(2)+0-2*C7Old(1));
            end

            C2New(k)=C2Old(k)-dtdx*(F2(k)-0)+Kdis*dtdx/dx*(C2Old(2)-C2Old(1));
            C4New(k)=C4Old(k)-dtdx*(F4(k)-0)+Kdis*dtdx/dx*(C4Old(2)-C4Old(1));
            C8New(k)=C8Old(k)-dtdx*(F8(k)-0)+Kdis*dtdx/dx*(C8Old(2)-C8Old(1));

        elseif k==NX
            C2New(k)=C2Old(k)-dtdx*(F2(k)-F2(k-1))+Kdis*dtdx/dx*(C2Old(k-1)-C2Old(k));
            C3New(k)=C3Old(k)-dtdx*(F3(k)-F3(k-1))+Kdis*dtdx/dx*(C3Newm(k-1)-C3Newm(k));
            C4New(k)=C4Old(k)-dtdx*(F4(k)-F4(k-1))+Kdis*dtdx/dx*(C4Old(k-1)-C4Old(k));
            C5New(k)=C5Old(k)-dtdx*(F5(k)-F5(k-1))+Kdis*dtdx/dx*(C5Old(k-1)-C5Old(k));
            C6New(k)=C6Old(k)-dtdx*(F6(k)-F6(k-1))+Kdis*dtdx/dx*(C6Old(k-1)-C6Old(k));
            C7New(k)=C7Old(k)-dtdx*(F7(k)-F7(k-1))+Kdis*dtdx/dx*(C7Old(k-1)-C7Old(k));
            C8New(k)=C8Old(k)-dtdx*(F8(k)-F8(k-1))+Kdis*dtdx/dx*(C8Old(k-1)-C8Old(k));
        else
            C2New(k)=C2Old(k)-dtdx*(F2(k)-F2(k-1))+Kdis*dtdx/dx*(C2Old(k-1)+C2Old(k+1)-2*C2Old(k));
```

```
            C3New(k)=C3Old(k)-dtdx*(F3(k)-F3(k-1))+Kdis*dtdx/dx*(C3Newm(k-1)+C3Newm(k+1)-2*C3Newm(k));
            C4New(k)=C4Old(k)-dtdx*(F4(k)-F4(k-1))+Kdis*dtdx/dx*(C4Old(k-1)+C4Old(k+1)-2*C4Old(k));
            C5New(k)=C5Old(k)-dtdx*(F5(k)-F5(k-1))+Kdis*dtdx/dx*(C5Old(k-1)+C5Old(k+1)-2*C5Old(k));
            C6New(k)=C6Old(k)-dtdx*(F6(k)-F6(k-1))+Kdis*dtdx/dx*(C6Old(k-1)+C6Old(k+1)-2*C6Old(k));
            C7New(k)=C7Old(k)-dtdx*(F7(k)-F7(k-1))+Kdis*dtdx/dx*(C7Old(k-1)+C7Old(k+1)-2*C7Old(k));
            C8New(k)=C8Old(k)-dtdx*(F8(k)-F8(k-1))+Kdis*dtdx/dx*(C8Old(k-1)+C8Old(k+1)-2*C8Old(k));
        end
end

%Calculate the equilibrium condition, partition is related to IFT, and
%add the adsorption terms.
%add the reaction of alkali and soap.

for j=1:NX
        c51New(j)=C5New(j)/(1-C2New(j));
        %The reactions---- alkali and soap,alkali comsumption
        if (C6New(j)~=0 & C8New(j)~=0 &C9(j)~=0)
            if (C6New(j) < C9(j))
                C9(j)=C9(j)-C6New(j);
                C6New(j)=0;
            elseif (C6New(j) < (C8New(j)/Reactfact+C9(j)))
                C4New(j)=C4New(j)+Reactfact*(C6New(j)-C9(j));
                C8New(j)=C8New(j)-Reactfact*(C6New(j)-C9(j));
                C6New(j)=0;
                C9(j)=0;
            else
                C6New(j)=C6New(j)-C8New(j)/Reactfact-C9(j);
                C4New(j)=C4New(j)+C8New(j);
                C8New(j)=0;
                C9(j)=0;
            end
        elseif (C9(j)==0)
            if (C6New(j) < C8New(j)/Reactfact)
                C4New(j)=C4New(j)+C6New(j)*Reactfact;
                C8New(j)=C8New(j)-C6New(j)*Reactfact;
                C6New(j)=0;
            else
                C6New(j)=C6New(j)-C8New(j)/Reactfact;
                C4New(j)=C4New(j)+C8New(j);
                C8New(j)=0;
            end
        end
        c61Old(j)=C6New(j)/(1-C2New(j));
        if (C7New(j) >= C7s(j))
            C7New(j)=C7New(j)-C7s(j);
            C7s(j)=0;
        else
            C7s(j)=C7s(j)-C7New(j);
            C7New(j)=0;
        end
        if (C7New(j) < eps)
            C7New(j)=0;
        end
        c71Old(j)=C7New(j)/(1-C2New(j));
        if (C2New(j) > eps)
            c82Old(j)=C8New(j)/C2New(j);
        else
            c82Old(j)=0;
        end
        %if i==10
        %       if j==9
        %               i
        %               j
        %       end
        %end

        if (C2New(j)>eps)
            if (C3New(j)<eps & C4New(j)<eps)
                c31New(j)=0;
                c41New(j)=0;
```

```
                    c32New(j)=0;
                    c42New(j)=0;
                elseif (C3New(j)<eps)
                    c31New(j)=0;
                    c41New(j)=0;
                    c32New(j)=C3New(j)/C2New(j);
                    c42New(j)=C4New(j)/C2New(j);
                elseif (C4New(j)<eps)
                    c31New(j)=C3New(j)/(1-C2New(j));          %This is c31New without adsorption
                    c41New(j)=C4New(j)/(1-C2New(j));
                    bb=c31New(j)-C3max/adsfact3-C3max/(1-C2New(j));
                    c31New(j)=0.5*(bb+(bb^2+4*c31New(j)*C3max/adsfact3)^0.5);    %This is with Langmuir adsorption
                    c32New(j)=0;
                    c42New(j)=0;
                else
                    [KC3(j),          KC4(j),          c31New(j),          c41New(j),          C3ads(j),
C4ads(j)]=FindKads(C2New(j),C3New(j),C4New(j),c51New(j));
                    c32New(j)=c31New(j)*KC3(j);
                    c42New(j)=c41New(j)*KC4(j);
                end
            else
                if adsfact3~=0
                    c31New(j)=0.5*(-(C3max-C3New(j))+sqrt((C3max-C3New(j))^2+4*C3max/adsfact3*C3New(j)));
                else
                    c31New(j)=C3New(j);
                end
                c41New(j)=C4New(j);
                c32New(j)=0;
                c42New(j)=0;
            end
            % Generate new IFT profile
            C3Newm(j)=c31New(j)*(1-C2New(j))+c32New(j)*C2New(j);
            C4Newm(j)=c41New(j)*(1-C2New(j))+c42New(j)*C2New(j);
            IFT(j)=FindIFT (C3Newm(j),C4Newm(j),c51New(j));

        end

        %flowout is to save the effluent history of f
        if i~=0
            flowout2(i,1)=F2(NX);
            flowout5(i,1)=F5(NX);
            flowout6(i,1)=F6(NX);
            flowout7(i,1)=F7(NX);
            if (c31New(NX) == 0 & C2New(NX) ~= 0)
                flowout3(i,1)=c31New(NX)*(1-F2(NX))+C3New(NX)/C2New(NX)*F2(NX);
                flowout4(i,1)=c41New(NX)*(1-F2(NX))+C4New(NX)/C2New(NX)*F2(NX);
            else
                flowout3(i,1)=c31New(NX)*(1-F2(NX))+KC3(NX)*c31New(NX)*F2(NX);
                flowout4(i,1)=c41New(NX)*(1-F2(NX))+KC4(NX)*c41New(NX)*F2(NX);
            end
        end
        CUM2=(sum(C2New)-sum(C2Old))*dx;
        CUM3=(sum(C3New)-sum(C3Old))*dx;
        if (T3slug_4>=(dt*i))
            if (i~=1)
                if (T3slug_2>=(dt*i) & T3slug_1<=(dt*i))
                    TRANS3=(c31_1-flowout3(i-1))*dt;
                elseif (T3slug_3>=(dt*i) & T3slug_2<(dt*i))
                    TRANS3=(c31_2-flowout3(i-1))*dt;
                else
                    TRANS3=(c31_3-flowout3(i-1))*dt;
                end
            else
                TRANS3=c31_1*dt;
            end
        else
            TRANS3=-flowout3(i-1)*dt;
        end
        if CUM3~=0
            RMASS3(i)=TRANS3/CUM3;
```

```
else
      RMASS3(i)=TRANS3-CUM3;
end
%Update all profiles
c31Old=c31New;
c41Old=c41New;
c32Old=c32New;
c42Old=c42New;
c51Old=c51New;
C2Old=C2New;
C3Old=C3New;
C4Old=C4New;
C5Old=C5New;
C6Old=C6New;
C7Old=C7New;
C8Old=C8New;

% Save & Plot profiles at different time
if i==round(T/dt)
    pause
    figure(1)
    [AX,H1,H2] = plotyy (X,c31New,X,c41New);
    title(['Surfactant Concentration Profile      Time=',num2str(T)])
    xlabel('Dimensionless Distance, xD')
    set(get(AX(1),'Ylabel'),'String','c31 (Surfactant Concentration in aqueous phase)','Color','r')
    set(get(AX(2),'Ylabel'),'String','c41 (Soap Concentration in aqueous phase)','Color','b')
    set(AX(1),'YColor','r')
    set(AX(2),'YColor','b')
    set(H1,'Color','r')
    set(H2,'Color','b')
    prof1=[X c31New' c41New' C3New' C4New' C2New' c51New' IFT C6New' C7New'];
    save prof1.dat prof1 /ascii

    figure(2)

    [AX,H1,H2] = plotyy (X,C3New,X,C4New);
    title(['Surfactant Concentration Profile      Time=',num2str(T)])
    xlabel('Dimensionless Distance, xD')
    set(get(AX(1),'Ylabel'),'String','C3 (Overall Surfactant Concentration)','Color','r')
    set(get(AX(2),'Ylabel'),'String','C4 (Overall Soap Concentration)','Color','b')
    set(AX(1),'YColor','r')
    set(AX(2),'YColor','b')
    set(H1,'Color','r')
    set(H2,'Color','b')

    figure(3)
    for i=1:length(c31New)
        if (c31New(i)==0)
            c31New(i)=eps^2;
            C3New(i)=eps;
        end
        if (c41New(i)==0)
            c41New(i)=eps;
        end
    end
    Ratioca=c41New./c31New;
    RatioCT=C4New./C3New;
    [AX,H1,H2] = plotyy (X,IFT,X,RatioCT);
    axis(AX(1),[ 0 1 0 10])
    axis(AX(2),[ 0 1 0 10])
    title(['Soap Surfactant Ratio Profile      Time= 0.1'])
    xlabel('Dimensionless Distance, xD')
    set(get(AX(1),'Ylabel'),'String','IFT','Color','r')
    set(get(AX(2),'Ylabel'),'String','C4/C3','Color','b')
    set(AX(1),'YColor','r','YTickMode','auto')
    set(AX(2),'YColor','b','YTickMode','auto')
    set(H1,'Color','r')
    set(H2,'Color','b')

    figure(4)
```

```
        plot (X,C2New)
        title(['Oil Saturation Profile      Time=',num2str(T)])
        xlabel('Dimensionless Distance, xD')
        ylabel('C2 (Oil Saturation)')
end
if i==round(2*T/dt)
        prof1=[X c31New' c41New' C3New' C4New' C2New' c51New' IFT C6New' C7New'];
        save prof2.dat prof1 /ascii
end
if i==round(3*T/dt)
        prof1=[X c31New' c41New' C3New' C4New' C2New' c51New' IFT C6New' C7New'];
        save prof3.dat prof1 /ascii
end
if i==round(4*T/dt)
        prof1=[X c31New' c41New' C3New' C4New' C2New' c51New' IFT C6New' C7New'];
        save prof4.dat prof1 /ascii
end
if i==round(5*T/dt)
        prof1=[X c31New' c41New' C3New' C4New' C2New' c51New' IFT C6New' C7New'];
        save prof5.dat prof1 /ascii
end
if i==round(6*T/dt)
        prof1=[X c31New' c41New' C3New' C4New' C2New' c51New' IFT C6New' C7New'];
        save prof6.dat prof1 /ascii
end
if i==round(7*T/dt)
        prof1=[X c31New' c41New' C3New' C4New' C2New' c51New' IFT C6New' C7New'];
        save prof7.dat prof1 /ascii
end
if i==round(8*T/dt)
        prof1=[X c31New' c41New' C3New' C4New' C2New' c51New' IFT C6New' C7New'];
        save prof8.dat prof1 /ascii
end
if i==round(9*T/dt)
        prof1=[X c31New' c41New' C3New' C4New' C2New' c51New' IFT C6New' C7New'];
        save prof9.dat prof1 /ascii
end

if i==round(10*T/dt)
        prof1=[X c31New' c41New' C3New' C4New' C2New' c51New' IFT C6New' C7New'];
        save prof10.dat prof1 /ascii
end
if i==round(11*T/dt)
        prof1=[X c31New' c41New' C3New' C4New' C2New' c51New' IFT C6New' C7New'];
        save prof11.dat prof1 /ascii
end
if i==round(12*T/dt)
        prof1=[X c31New' c41New' C3New' C4New' C2New' c51New' IFT C6New' C7New'];
        save prof12.dat prof1 /ascii
end
if i==round(13*T/dt)
        prof1=[X c31New' c41New' C3New' C4New' C2New' c51New' IFT C6New' C7New'];
        save prof13.dat prof1 /ascii
end
if i==round(14*T/dt)
        prof1=[X c31New' c41New' C3New' C4New' C2New' c51New' IFT C6New' C7New'];
        save prof14.dat prof1 /ascii
end
if i==round(15*T/dt)
        prof1=[X c31New' c41New' C3New' C4New' C2New' c51New' IFT C6New' C7New'];
        save prof15.dat prof1 /ascii
end
if i==round(16*T/dt)
        prof1=[X c31New' c41New' C3New' C4New' C2New' c51New' IFT C6New' C7New'];
        save prof16.dat prof1 /ascii
end
if i==round(17*T/dt)
        prof1=[X c31New' c41New' C3New' C4New' C2New' c51New' IFT C6New' C7New'];
        save prof17.dat prof1 /ascii
end
```

```
    if i==round(18*T/dt)
        prof1=[X c31New' c41New' C3New' C4New' C2New' c51New' IFT C6New' C7New'];
        save prof18.dat prof1 /ascii
    end
    if i==round(19*T/dt)
        prof1=[X c31New' c41New' C3New' C4New' C2New' c51New' IFT C6New' C7New'];
        save prof19.dat prof1 /ascii
    end
    if i==round(20*T/dt)
        prof1=[X c31New' c41New' C3New' C4New' C2New' c51New' IFT C6New' C7New'];
        save prof20.dat prof1 /ascii
    end
    if i==round(21*T/dt)
        prof1=[X c31New' c41New' C3New' C4New' C2New' c51New' IFT C6New' C7New'];
        save prof21.dat prof1 /ascii
    end
    if i==round(22*T/dt)
        prof1=[X c31New' c41New' C3New' C4New' C2New' c51New' IFT C6New' C7New'];
        save prof22.dat prof1 /ascii
    end
    if i==round(23*T/dt)
        prof1=[X c31New' c41New' C3New' C4New' C2New' c51New' IFT C6New' C7New'];
        save prof23.dat prof1 /ascii
    end
    if i==round(24*T/dt)
        prof1=[X c31New' c41New' C3New' C4New' C2New' c51New' IFT C6New' C7New'];
        save prof24.dat prof1 /ascii
    end
    if i==round(25*T/dt)
        prof1=[X c31New' c41New' C3New' C4New' C2New' c51New' IFT C6New' C7New'];
        save prof25.dat prof1 /ascii
    end
    if i==round(26*T/dt)
        prof1=[X c31New' c41New' C3New' C4New' C2New' c51New' IFT C6New' C7New'];
        save prof26.dat prof1 /ascii
    end
    if i==round(27*T/dt)
        prof1=[X c31New' c41New' C3New' C4New' C2New' c51New' IFT C6New' C7New'];
        save prof27.dat prof1 /ascii
    end

    if i==round(28*T/dt)
        prof1=[X c31New' c41New' C3New' C4New' C2New' c51New' IFT C6New' C7New'];
        save prof28.dat prof1 /ascii
    end
    if i==round(29*T/dt)
        prof1=[X c31New' c41New' C3New' C4New' C2New' c51New' IFT C6New' C7New'];
        save prof29.dat prof1 /ascii
    end


end
pause
t=[dt:dt:NNN*dt]';
histo=[t flowout3];

figure(5)
[AX,H1,H2] = plotyy (t,flowout3,t,flowout4);
title(['Effluent History'])
xlabel('Dimensionless Time(PV)')
set(get(AX(1),'Ylabel'),'String','Effluent Surfactant Concentration','Color','r')
set(get(AX(2),'Ylabel'),'String','Effluent Soap Concentration','Color','b')
set(AX(1),'YColor','r')
set(AX(2),'YColor','b')
set(H1,'Color','r')
set(H2,'Color','b')

figure (6)
plot(t,flowout2)
```

```
title('Effluent History')
xlabel('Dimensionless Time(PV)')
ylabel('Effluent Oil Saturation')

prof1=[X c31New' c41New' C3New' C4New' C2New' c51New' IFT C6New' C7New'];
save proffinal.dat prof1 /ascii

prod=[t flowout3 flowout4 flowout2 RMASS3' flowout5 flowout6 flowout7];
save prod.dat prod /ascii



%Set up Optimal salinity vs C4/C3 Ratio curve
clear all
%curve shape parameters
Ratio=logspace(-5,5);
Xsoap=Ratio./(1+Ratio);
%NI=Xsoap*0.5+(1-Xsoap)*5.0;
logNI=Xsoap*log(0.5)+(1-Xsoap)*log(5);
optS=exp(logNI);
semilogx(Ratio,optS)
xlabel('Ratio,C4/C3')
ylabel('Optimal Salinity')
optRS=[Ratio' optS'];
save optRS.dat optRS /ascii
```

## 2. Setopt_New.m

```
%Set up Optimal salinity vs C4/C3 Ratio curve
clear all
%curve shape parameters
Ratio=logspace(-5,5);
Xsoap=Ratio./(1+Ratio);
%NI=Xsoap*0.5+(1-Xsoap)*5.0;
logNI=Xsoap*log(0.5)+(1-Xsoap)*log(5);
optS=exp(logNI);
semilogx(Ratio,optS)
xlabel('Ratio,C4/C3')
ylabel('Optimal Salinity')
optRS=[Ratio' optS'];
save optRS.dat optRS /ascii
```

## 3. FindIFT.m

```
%Compute Interfacial Tension from the surfactant/Soap Ratio
function IFT=FindIFT(C3,C4,Sal)
global optRS Ssur Ssoap CMC
IFT0=25;
IFTlow=1e-3;
IFTMAX=25;
IFTMAX_soap=0.5;
if C3==0
      C3=eps^2;
end
R=C4/C3;
if (R>1000)
      R=1000;
end
OptSal=interp1(optRS(:,1),optRS(:,2),R,'linear','extrap');

%Wide IFT at type I region, narrow IFT at type II region
if (OptSal >Sal)
      SalRatio=OptSal/Sal;
      if (SalRatio<2.0)
```

```
            IFT=(10)^(SalRatio)*1e-4;
        elseif (SalRatio<4.0)
            IFT=(3.1623)^(SalRatio)*1e-3;
        else
            IFT=1.2^(SalRatio)*0.0482;
            if IFT>IFTMAX_soap
                IFT=IFTMAX_soap;
            end
        end
else
        SalRatio=Sal/OptSal;
        if (SalRatio<1.0555)
            IFT=(1e18)^(SalRatio)*1e-21;
        elseif (SalRatio<1.2551)
            IFT=(1e5)^(SalRatio)*0.53e-7;
        else
            IFT=2^(SalRatio)*0.0419;
            if IFT>IFTMAX_soap
                IFT=IFTMAX_soap;
            end
        end
end
%if R>100
%       IFT=IFTMAX_soap;
%end
lowbound=CMC/1000; %if C3+C4< low bound , the IFT will be IFTMAX.
if ((C3+C4) < CMC)
        factor1=log10((C3+C4)/lowbound);
        IFT=exp(log(IFTMAX)+1/3*factor1*(log(IFT)-log(IFTMAX)));
end
if (IFT>IFTMAX)
        IFT=IFTMAX;
elseif (IFT<1e-3)
        IFT=1e-3;
end
```

## 4. FindKads.m

```
% From C2, C3, C4, we can get the Kaver and adsorption of surfactant and soap
function [KC3, KC4, c31, c41, C3ads, C4ads]=FindKads(C2,C3,C4,Salinity)
% k4k3=KC4/KC3, we can use this to get KC3 and KC4
%Newton Method for both c3 and c4 are adsorbed
%Return the value of K3,K4,C3ads,C4ads,c31,c41
global optRS Ssoap Ssur CMC k4k3 adsfact3 adsfact4 C3max
% Initial Guess for c31, c41-----c31(1), c31+deltac31,c41+deltac41--------c31(2-5)
delX=1e-3;
c310=0.5*C3/(1-C2);
c410=0.5*C4/(1-C2);
c31=[c310 c310+delX*C3 c310];
c41=[c410 c410 c410+delX*C4];
C3ads=FindC3ads(c31,c41,Salinity);
C4ads=FindC4ads(c31,c41,Salinity);
C3M=C3-C3ads;
C4M=C4-C4ads;
if C3M < eps
        C3M=eps;
end
if C4M <eps
        C4M=eps;
end
Kaver=findK(C3M,C4M,Salinity);
Kaver=Kaver(1);
Kaver0=Kaver;
KC3=Kaver/(1+(k4k3-1)*(C4M/(C3M+C4M)));                    %Kaver=(C3/(C3+C4))*KC3+(C4/(C3+C4))*KC4
KC4=k4k3*KC3;
if (Kaver>100)
```

```
        % When Kaver is larger, adsorption won't affect the calculation much.
        KC3=Kaver/(1+(k4k3-1)*(C4/(C3+C4)));
        KC4=k4k3*KC3;
        c31=C3/(1-C2+C2*KC3);
        c41=C4/(1-C2+C2*KC4);
        C3ads=FindC3ads(c31,c41,adsfact3);
        C4ads=FindC4ads(c31,c41,adsfact4);
        c32=(C3-C3ads-c31*(1-C2))/C2;
        c42=(C4-C4ads-c41*(1-C2))/C2;
        KC3=c32/c31;
        KC4=c42/c41;
else
        %Set up Newton method
        f3=C3-c31*(1-C2)-c31.*KC3*C2-C3ads;
        f4=C4-c41*(1-C2)-c41.*KC4*C2-C4ads;
        F=[f3(1);f4(1)];
        error1=abs(f3(1))+abs(f4(1));
        error2=1;
        Iter=0;
        % Enter the loop
        while (error1 > 1.1e-8 & error2>0 & Iter < 100)
                Kaver0=Kaver;
        %Compute Jacobian
                J(1,1)=(f3(2)-f3(1))/(delX*C3);
                J(1,2)=(f3(3)-f3(1))/(delX*C4);
                J(2,1)=(f4(2)-f4(1))/(delX*C3);
                J(2,2)=(f4(3)-f4(1))/(delX*C4);
                Jinv=inv(J);
                CC=[c31(1);c41(1)]-Jinv*F;
                if (CC(1)<0)
                        CC(1)=0;
                end
            % if (CC(2)<0)
              %       CC(2)=0;
              %end
                c310=c31(1);
                c410=c41(1);
                c31=[CC(1) CC(1)+delX*C3 CC(1)];
                c41=[CC(2) CC(2) CC(2)+delX*C4];
                C3ads=FindC3ads(c31,c41,adsfact3);
                C4ads=FindC4ads(c31,c41,adsfact4);
                C3M=C3-C3ads;
                C4M=C4-C4ads;
                Kaver=findK(C3M,C4M,Salinity);
                KC3=Kaver/(1+(k4k3-1)*(C4M/(C3M+C4M)));
%Kaver=(C3/(C3+C4))*KC3+(C4/(C3+C4))*KC4
                KC4=k4k3*KC3;
                f3=C3-c31*(1-C2)-c31.*KC3*C2-C3ads;
                f4=C4-c41*(1-C2)-c41.*KC4*C2-C4ads;
                F=[f3(1);f4(1)];
                error1=abs(f3(1))+abs(f4(1));
                error2=abs(Kaver-Kaver0);
                Iter=Iter+1;
        end
        c31=c31(1);
        c41=c41(1);
        C3ads=C3ads(1);
        C4ads=C4ads(1);
        % error2=0 means the diffrence of Kaver is small
        if (error2==0)
                if Kaver<1e-3
                        C3ads=FindC3ads(c31,c41,Salinity);
                        C4ads=FindC4ads(c31,c41,Salinity);
                        c31=(C3-C3ads)/(1-C2);
                        c41=(C4-C4ads)/(1-C2);
                        KC3=0;
                        KC4=0;
                elseif Kaver>1e3
                        c31=(C3)/(1-C2+C2*KC3);
                        c41=(C4)/(1-C2+C2*KC4);
```

```
            C3ads=FindC3ads(c31,c41,Salinity);
            C4ads=FindC4ads(c31,c41,Salinity);
        end
    end
    if (Iter >99)
        c31=(c310+c31(1))/2;
        c41=(c410+c41(1))/2;
        C3ads=FindC3ads(c31,c41,Salinity);
        C4ads=FindC4ads(c31,c41,Salinity);
        C3M=C3-C3ads;
        C4M=C4-C4ads;
        KC3=(C3M-c31*(1-C2))/C2/c31;
        KC4=(C4M-c41*(1-C2))/C2/c41;
        Kaver=(C3M/(C3M+C4M))*KC3+(C4M/(C3M+C4M))*KC4;
    end
end
```

## 5. FindK.m

```
%Compute Partition from the surfactant/Soap Ratio
function Kaver=FindK(C3,C4,Sal)
%load optRS.dat;
%Ssoap=interp1(optRS(:,1),optRS(:,2),1e10,'linear','extrap');
%Ssur=interp1(optRS(:,1),optRS(:,2),1e-10,'linear','extrap');
global optRS Ssur Ssoap
if C3==0
    C3=eps^2;
end
R=C4/C3;
if R >100
    R=100;
end
OptSal=interp1(optRS(:,1),optRS(:,2),R,'linear','extrap');
%SalRatio=Sal./OptSal;
if (Sal(1)>OptSal(1))
    SalRatio=Sal./OptSal;
    Kaver=(1e2).^(SalRatio)*0.01;
else
    SalRatio=OptSal./Sal;
    Kaver=1./((1e2).^(SalRatio)*0.01);
end
```

## 6. FindVis.m

```
%Find Viscosity
%Calculate viscosity from the concentration of polymer(Flopaam)
function viscosity=Findvis(c71,Salinity)
N=length(c71);
for i=1:N
    factor=((3.536/(Salinity+0.3443)^2+5)/5)^(c71(i)/0.0015);
    viscosity(i)=factor*(6.119e7*c71(i)^2.523+1);
end
```

## 7. FindFrac.m

```
% Compute the fractional flow from the interfacial tension
function f1=FindFrac(IFT,S1,Muwater)
Swc=0.3;
Sorw=0.3;
nw=1.5;
no=1.5;
```

```
krw0=0.1;
kro0=0.4;
Muoil=19;    % Oil viscosity input
if (IFT>1)
      S1r=Swc;
      S2r=Sorw;
elseif (IFT<0.005)
      S1r=0;
      S2r=0;
      nw=1.0;
      no=1.0;
else
      S1r=Swc*(1+(log10(IFT)/2.3010));
      S2r=Sorw*(1+(log10(IFT)/2.3010));
      nw=1.5+1.0/6*log10(IFT);
      no=nw;
end

if S1<S1r
      SR=0;
elseif S1>(1-S2r)
      SR=1;
else
      SR=(S1-S1r)/(1-S1r-S2r);
end

kr10=krw0+(1-krw0)*(Sorw-S2r)/Sorw;
kr20=kro0+(1-kro0)*(Swc-S1r)/Swc;

if SR==0
      f1=0;
elseif SR==1;
      f1=1;
else
      kr1=kr10*SR^nw;
      kr2=kr20*(1-SR)^no;
      M=kr10*Muoil/(kr20*Muwater);       % Mobility Ratio
      f1=1/(1+1/M*((kr2/kr20)/(kr1/kr10)));
end
```

## 8. Findc3ads.m

```
%Compute the Surfactant Adsorption amount from aqueous phase concentration c31,c41
function c3ads=FindC3ads(c31,c41,Salinty)
global CMC adsfact3 C3max
N=length(c31);
for i=1:N
      c3ads(i)=C3max*c31(i)/(C3max/adsfact3+c31(i));
end
```

## 9. Findc4ads.m

```
%Compute the Soap Adsorption amount from aqueous phase concentration c31,c41
function c4ads=FindC4ads(c31,c41,Salinity)
global CMC adsfact4
N=length(c31);
for i=1:N
      if c41(i)<CMC
            c4ads(i)=adsfact4*c41(i);
      else
            c4ads(i)=adsfact4*CMC;
      end
end
```

## 10. Plotsmall2.m

```
% Plotting program
clear
load prof5.dat
prof=prof5;
load prod.dat
titletime='0.5';
X=prof(:,1);
c31New=prof(:,2);
c41New=prof(:,3);
C3New=prof(:,4);
C4New=prof(:,5);
C2New=prof(:,6);
c51New=prof(:,7);
IFT=prof(:,8);
C6New=prof(:,9);
C7New=prof(:,10);
t=prod(:,1);
flowout3=prod(:,2);
flowout4=prod(:,3);
flowout2=prod(:,4);

load optRS.dat

figure(1)
[AX,H1,H2] = plotyy (X,c31New,X,c41New);
title(['Surfactant Concentration Profile      Time= ', titletime],'FontSize',16)
xlabel('Dimensionless Distance, xD','FontSize',16)
set(get(AX(1),'Ylabel'),'String','c31 (Surfactant Concentration in aqueous phase)','Color','r','FontSize',16)
set(get(AX(2),'Ylabel'),'String','c41 (Soap Concentration in aqueous phase)','Color','b','FontSize',16)
set(AX(1),'YColor','r','YTickMode','auto','yLim',[0 0.005],'FontSize',16)
set(AX(2),'YColor','b','YTickMode','auto','yLim',[0 0.005],'FontSize',16)
set(H1,'Color','r','LineWidth',2)
set(H2,'Color','b','LineWidth',2)

figure(2)
[AX,H1,H2] = plotyy (X,C3New,X,C4New);
title(['Surfactant Concentration Profile      Time= ', titletime],'FontSize',16)
xlabel('Dimensionless Distance, xD','FontSize',16)
set(get(AX(1),'Ylabel'),'String','C3 (Overall Surfactant Concentration)','Color','r','FontSize',16)
set(get(AX(2),'Ylabel'),'String','C4 (Overall Soap Concentration)','Color','b','FontSize',16)
set(AX(1),'yLim',[0 0.009],'YTickMode','auto','YColor','r','FontSize',16)
set(AX(2),'yLim',[0 0.009],'YTickMode','auto','YColor','b','FontSize',16)
set(H1,'Color','r','LineWidth',2)
set(H2,'Color','b','LineWidth',2)

figure(3)
for i=1:length(c31New)
      if (c31New(i)==0)
            c31New(i)=eps^2;
            C3New(i)=eps;
      end
      if (c41New(i)==0)
            c41New(i)=eps;
      end
end
Ratioca=c41New./c31New;
RatioCT=C4New./C3New;
[AX,H1,H2] = plotyy (X,IFT,X,RatioCT);
axis(AX(1),[ 0 1 0 10])
axis(AX(2),[ 0 1 0 10])
title(['Soap Surfactant Ratio Profile      Time= ', titletime],'FontSize',16)
xlabel('Dimensionless Distance, xD','FontSize',16)
set(get(AX(1),'Ylabel'),'String','IFT','Color','r','FontSize',16)
set(get(AX(2),'Ylabel'),'String','C4/C3','Color','b','FontSize',16)
set(AX(1),'YColor','r','yLim',[0.001 1],'YTickMode','auto','YScale','log','FontSize',16)
set(AX(2),'YColor','b','yLim',[0.01 10],'YTickMode','auto','YScale','log','FontSize',16)
```

```
set(H1,'Color','r','LineWidth',2)
set(H2,'Color','b','LineWidth',2)

figure(4)
plot (X,C2New,'LineWidth',2)
title(['Oil Saturation Profile      Time= ', titletime],'FontSize',16)
xlabel('Dimensionless Distance, xD','FontSize',16)
ylabel('C2 (Oil Saturation)','FontSize',16)
set(gca,'FontSize',16)
axis([ 0 1 0 1])

figure(5)
[AX,H1,H2] = plotyy (t,flowout3,t,flowout4);
title(['Effluent History'],'FontSize',16)
xlabel('Dimensionless Time(PV)','FontSize',16)
set(get(AX(1),'Ylabel'),'String','Effluent Surfactant Concentration','Color','r','FontSize',16)
set(get(AX(2),'Ylabel'),'String','Effluent Soap Concentration','Color','b','FontSize',16)
set(AX(1),'YTickMode','auto','YColor','r','FontSize',16)
set(AX(2),'YTickMode','auto','YColor','b','FontSize',16)
set(H1,'Color','r','LineWidth',2)
set(H2,'Color','b','LineWidth',2)

figure (6)
plot(t,flowout2,'LineWidth',2)
title('Effluent History','FontSize',16)
xlabel('Dimensionless Time(PV)','FontSize',16)
ylabel('Effluent Oil Fractional Flow','FontSize',16)
set(gca,'FontSize',16)
axis([ 0 t(length(t)) 0 1])

figure(7)
OptSalPro=interp1(optRS(:,1),optRS(:,2),RatioCT,'linear','extrap');
plot(X,OptSalPro,X,c51New)
title(['Salinity Profile      Time= ', titletime],'FontSize',16)
xlabel('Dimensionless Distance, xD','FontSize',16)
ylabel('Salinity (%)','FontSize',16)
legend('Optimal Salinity Profile', 'Salinity Profile')
set(gca,'FontSize',16)

figure(8)
plot (X,C6New./(1-C2New),'LineWidth',2)
title(['Alkali Concentration Profile    Time= ', titletime],'FontSize',16)
xlabel('Dimensionless Distance, xD','FontSize',16)
ylabel('c61 (Alkali Concentration)','FontSize',16)
set(gca,'FontSize',16)

figure(9)
c71New=C7New./(1-C2New);
for i=1:length(c71New)
      VisProf(i)=Findvis(c71New(i),c51New(i));
end

[AX,H1,H2] = plotyy (X,c71New,X,VisProf);
title(['Polymer Concentration & Aqueous Phase Viscosity Profile      Time= ', titletime],'FontSize',16)
xlabel('Dimensionless Distance, xD','FontSize',16)
set(get(AX(1),'Ylabel'),'String','c71 (Polymer Concentration)','Color','r','FontSize',16)
set(get(AX(2),'Ylabel'),'String','Aqoeous Phase Viscosity (cp)','Color','b','FontSize',16)
set(AX(1),'yLim',[0 0.006],'YTickMode','auto','YColor','r','FontSize',16)
set(AX(2),'yLim',[0 60],'YTickMode','auto','YColor','b','FontSize',16)
set(H1,'Color','r','LineWidth',2)
set(H2,'Color','b','LineWidth',2)

figure(11)
global CMC adsfact3 C3max adsfact4 k4k3
Muoil=19.7;
adsfact3=4.0;
C3max=0.2e-3;
adsfact4=0;
CMC=5e-4;
k4k3=1;
```

```
for i=1:length(C2New)
    Muwater(i)=Findvis(C7New(i)/(1-C2New(i)),c51New(i));

    if (C2New(i)>eps)
        if (C3New(i)<eps & C4New(i)<eps)
            c31New(i)=0;
            c41New(i)=0;
            c32New(i)=0;
            c42New(i)=0;
        elseif (C3New(i)<eps)
            c31New(i)=0;
            c41New(i)=0;
            c32New(i)=C3New(i)/C2New(i);
            c42New(i)=C4New(i)/C2New(i);
        elseif (C4New(i)<eps)
            c31New(i)=C3New(i)/(1-C2New(i));          %This is c31New without adsorption
            c41New(i)=C4New(i)/(1-C2New(i));
            bb=c31New(i)-C3max/adsfact3-C3max/(1-C2New(i));
            c31New(i)=0.5*(bb+(bb^2+4*c31New(i)*C3max/adsfact3)^0.5);    %This is with Langmuir adsorption
            c32New(i)=0;
            c42New(i)=0;
        else
            [KC3(i), KC4(i), c31New(i), c41New(i), C3ads(i), C4ads(i)]=FindKads(C2New(i),C3New(i),C4New(i),c51New(i));
            c32New(i)=c31New(i)*KC3(i);
            c42New(i)=c41New(i)*KC4(i);
        end
    else
        if adsfact3~=0
            c31New(i)=0.5*(-(C3max-C3New(i))+sqrt((C3max-C3New(i))^2+4*C3max/adsfact3*C3New(i)));
        else
            c31New(i)=C3New(i);
        end
        c41New(i)=C4New(i);
        c32New(i)=0;
        c42New(i)=0;
    end
    % Generate new IFT profile
    C3Newm(i)=c31New(i)*(1-C2New(i))+c32New(i)*C2New(i);
    C4Newm(i)=c41New(i)*(1-C2New(i))+c42New(i)*C2New(i);
    IFT(i)=FindIFT(C3Newm(i),C4Newm(i),c51New(i));
    [kr10(i),kr20(i),nw(i),no(i),SR(i)]=Findrelativep(IFT(i),1-C2New(i),Muwater(i));
    Mobility(i)=kr10(i)*SR(i)^nw(i)/Muwater(i)+kr20(i)*(1-SR(i))^no(i)/Muoil;
end

[AX,H1,H2] = plotyy (X,c71New/0.316*0.5,X,Mobility);
title(['Polymer and Mobility Profile Time= ', titletime],'FontSize',16)
xlabel('Dimensionless Distance, xD','FontSize',16)
set(get(AX(1),'Ylabel'),'String','Polymer Concentration','Color','r','FontSize',16)
set(get(AX(2),'Ylabel'),'String','Mobility (krw/Muwater + kro/Muoil)','Color','b','FontSize',16)
set(AX(1),'yLim',[0 0.005],'YTickMode','auto','YColor','r','FontSize',16)
set(AX(2),'yLim',[0 0.2],'YTickMode','auto','YColor','b','FontSize',16)
set(H1,'Color','r','LineWidth',2)
set(H2,'Color','b','LineWidth',2)
```